



University
of Glasgow

<https://theses.gla.ac.uk/>

Theses Digitisation:

<https://www.gla.ac.uk/myglasgow/research/enlighten/theses/digitisation/>

This is a digitised version of the original print thesis.

Copyright and moral rights for this work are retained by the author

A copy can be downloaded for personal non-commercial research or study,
without prior permission or charge

This work cannot be reproduced or quoted extensively from without first
obtaining permission in writing from the author

The content must not be changed in any way or sold commercially in any
format or medium without the formal permission of the author

When referring to this work, full bibliographic details including the author,
title, awarding institution and date of the thesis must be given

Enlighten: Theses

<https://theses.gla.ac.uk/>
research-enlighten@glasgow.ac.uk

flow

THE COMPUTER MODELLING AND VALIDATION OF THE
TRANSWALL PASSIVE SOLAR SYSTEM

by

NTOKOZO SIFISO MTHEMBU

Thesis submitted for the degree of M.Sc.

Department of Mechanical Engineering.

University of Glasgow.

January, 1990.

Glasgow, Scotland.

ProQuest Number: 10970956

All rights reserved

INFORMATION TO ALL USERS

The quality of this reproduction is dependent upon the quality of the copy submitted.

In the unlikely event that the author did not send a complete manuscript and there are missing pages, these will be noted. Also, if material had to be removed, a note will indicate the deletion.



ProQuest 10970956

Published by ProQuest LLC (2018). Copyright of the Dissertation is held by the Author.

All rights reserved.

This work is protected against unauthorized copying under Title 17, United States Code
Microform Edition © ProQuest LLC.

ProQuest LLC.
789 East Eisenhower Parkway
P.O. Box 1346
Ann Arbor, MI 48106 – 1346

DEDICATION

Dedicated to my Family:

Duduzile, my mother

and

Mlamuli-Mthokozisi, Nokubonga-Phiwayinkosi,
Thandwa-Sekamotho and Ntandoyenziwe;
my brothers and sisters.

ACKNOWLEDGEMENTS

I am indebted to Dr. S.K. Nisbet who supervised this work, for his excellent guidance, patience and encouragement that made this work a masterpiece. I also wish to express my sincere thanks to Mr. Ron Kleiser for his assistance in setting up the experimental rig and in taking the measurements.

Thanks are also due to:

Professor B.F. Scott and the Department of Mechanical Engineering, for providing the laboratory facilities.

Dr. Peacock and Mr. Larry McGhee of the Department of Chemistry; Mr. John Denheem, Ms. Yasmine Mather, Mrs. Linda McCormick and Mrs. Carol Carmichael of the University of Glasgow, for their invaluable contribution on certain aspects of this work.

Dr. Debra Nickson and Mr. Alan Birbeck^k who read the manuscript, and for their moral support throughout the programme of this work.

Professor Harold J. Brandon, Department of Mechanical Engineering, Washington University, St. Louis, MO., and Professor Bruce W. Richards, Department of Physics, Oberlin College, OH., who acted as my referees.

The United Nations Educational Training Programme for Southern Africa (UNETPSA) for providing financial assistance.

My family and friends for their moral support throughout my education.

Finally, I wish to sincerely thank Messrs. Computype who typed this thesis for their patience and understanding.

TABLE OF CONTENTS

Nomenclature	viii
Abstract	x
Introduction	1
CHAPTER 1. PASSIVE SOLAR SYSTEMS	9
1.1 Introduction	9
1.2 Direct Gain Systems	10
1.2.1 Windows	10
1.2.2 Conservatories/Sun spaces	11
1.3 Thermal Storage Walls and Roofs	13
1.3.1 Trombe Wall	14
1.3.2 Water Walls	15
1.3.3 Water Roofs	17
1.3.4 The Transwall	19
1.4 Conclusions	32
 CHAPTER 2. THE DEVELOPMENT AND VALIDATION OF THE ONE-DIMENSIONAL COMPUTER MODEL OF THE TRANSWALL	 33
2.1 Introduction	33
2.2 Water Circulation in the Transwall	33
2.3 The One-Dimensional Computer Model of the Temperature Distribution Within the Transwall Module	38
2.3.1 The Concept of Effective Conductivity	38
2.3.2 The One-Dimensional Explicit Finite Difference Method: Surface Contact Resistance Model	40

2.3.3	The One-Dimensional Explicit Finite Difference Equations for the Transwall Module	41
2.4	The One-Dimensional Computer Model of the Irradiation Absorption in the Transwall Module	49
2.4.1	Outer Glass Slabs (Window side)	51
2.4.2	Inner Glass Slabs (Room side)	53
2.4.3	Water Slabs	54
2.5	Experiments and Model Development	57
2.5.1	The Solar Simulator	57
2.5.2	The Small Transwall Module	59
2.6	Ambient Temperature Variations	66
2.7	Comparison: Experiment with the Computer Models	67
2.7.1	Computer Model 1	67
2.7.2	Computer Model 2	69
2.7.3	Computer Model 3	70
2.8	Conclusions	73

CHAPTER 3.	THE DEVELOPMENT AND VALIDATION OF THE TWO-DIMENSIONAL COMPUTER MODEL OF THE TRANSWALL	75
3.1	Introduction	75
3.2	The Two-Dimensional Absorption Analysis: Greveniotis' Computer Model	77
3.2.1	Introduction	77

3.2.2	Refractive Altitude and Azimuth Angles	77
3.2.3	Lid Shading and Reflections at the Bottom Glass (Base)	78
3.2.4	Beam Irradiation	79
3.2.5	Diffuse Irradiation	80
3.2.6	Treatment of Backward Irradiation from Room	80
3.3	The Modification of the Computer Two-Dimensional Absorption Model of the Transwall	82
3.3.1	Introduction	82
3.3.2	Outer Glass Slabs (Window side)	84
3.3.3	Inner Glass Slabs (Room side)	86
3.3.4	Water Slabs	89
3.4	The Two-Dimensional Explicit Finite Difference Analysis: Surface Contact Resistance Computer Model Development of the Transwall Temperature	97
3.4.1	Water Slabs	102
3.4.2	Front Glass Slabs	107
3.4.3	Rear Glass Slabs	
3.4.4	Horizontal End Surfaces	110
3.5	Experimental Validation of the Two- Dimensional Computer Model of the Transwall	111
3.5.1	The Full Size Transwall Module	111
3.5.2	Solar Irradiation Measurements	113
3.5.3	Transwall Temperature Measurements	114

3.5.4	Collection of Data: Methodology	114
3.5.5	Heat Transfer Coefficient Measurements	116
3.6	Comparison: Experiment with the Two- Dimensional Computer Model of the Transwall	117
3.6.1	Introduction	117
3.6.2	Results	118
3.7	Stratification Effects: Computer Predicted Vertical Temperature Profiles vs. Experimental Plots	123
3.8	Conclusions	125
CHAPTER 4.	APPLICATION OF THE TRANSWALL MODELS	127
4.1	Introduction	127
4.2	The House	127
4.3	The Heat Load	130
4.4	The Simulation Model	131
4.5	Derivation of the Glazing and Air Gap Temperature	132
4.6	Results of the Computer Simulation	137
4.6.1	Optimum Dye Concentration and Water Thickness	137
4.6.2	Comparison of MERA and Ames Transwalls	138
4.6.3	Effect of Air Circulation	141
4.6.4	Annual Energy Savings	142
4.7	Conclusions	144

CHAPTER 5.	FUTURE WORK, SUMMARY AND CONCLUSIONS	145
5.1	Introduction	145
5.2	Future Work	145
5.2.1	Concept: The Partial Redistribution of the Enthalpy Rise in the Transwall	146
5.2.2	Correlation Factors for Stratification	149
5.2.3	Summary of Improvements to the Experimental Apparatus	152
5.3	Summary of the Achievements of this Programme of Work	153
5.4	Conclusions	155
APPENDICES		159
A	Glasgow University Transwall Design	159
B	Procedure for the Alignment of the Solar Simulator	160
C	Experiments with the Small Transwall Module: Investigating the 13% Discrepancy in Transmission	163
D	The Calibration of the Transwall Thermocouples	168
E	The Two-Dimensional Absorption Analysis: Greveviotis' Model, Illustrations	173
F	The Specification of the Design House	
G	The Spectral Extinction Coefficients	
REFERENCES		185

Nomenclature

A	=	surface area (m^2)
AF	=	acceptance factor
a	=	azimuth angle (radians)
a	=	water slab horizontal direction thickness (m)
a	=	constant
B	=	volumetric expansion coefficient ($/K$)
b	=	water slab vertical direction thickness (m)
b	=	constant
c	=	specific heat capacity at constant pressure ($J/kg.K$)
D	=	distance between vertical walls (m)
F	=	Fourier number
Gr	=	Grashof number
g	=	glass thickness (m)
g	=	glass path length (m)
H	=	height of the vertical enclosure/slot (m)
h	=	convective heat transfer coefficient ($W/m^2.K$)
I^i	=	incident irradiation per unit area of window surface (W/m^2)
I	=	solar irradiation absorbed per unit area of transwall surface (W/m^2)
$I\alpha$	=	incident irradiation falling on the transwall after passing through glazing per unit area of transwall surface (W/m^2)
K	=	extinction coefficient (m^{-1})
k	=	thermal conductivity ($W/m.K$)
L	=	depth of water (m)
L	=	distance between plates (m)
L	=	path length (m)
M	=	total number of vertical direction slabs
m_a	=	mass flow rate (kg/s)
N	=	total number of all 1/2-slabs (glass & water), and 5 water full-slabs
Nu	=	Nusselt number
n	=	the n^{th} slab, where $\sum n = N$
Pr	=	Prandtl number
q	=	heat flux (W/m^2)
Ra	=	Rayleigh number
r	=	refractive angle (radians)
r	=	vertical effective conductivity factor
S_t	=	Stratification number
SF	=	shading factor
s	=	vertical temperature gradient ($^{\circ}C/m$)
T	=	temperature ($^{\circ}C$)
\bar{T}	=	mean enclosure temperature ($^{\circ}C$)
Δt	=	vertical temperature difference over length L ($^{\circ}C/m$)
t_g	=	temperature gradient ($^{\circ}C/m$)
V_F	=	view factor
α	=	absorptivity
α	=	refractive altitude

y = vertical direction (m)
 δt = time interval (s)
 λ = wavelength (μm)
 ρ = density (kg/m^3)
 ρ = reflectance
 γ = stratification parameter
 τ = transmittance
 ν = kinematic viscosity (m^2/s)

SUBSCRIPTS

a = air
 amb = combined convection & radiation outer glazing to ambient
 α = absorbed
 b = base, bottom, boundary
 c = cold
 $i-c$ = 'contact' inner glass to water
 $o-c$ = 'contact' outer glass to water
 e = effective conductivity
 f = front
 g = glass, gap, gradient
 ga = convective, between air, transwall and glazing surfaces with air circulation

 i = inner, station i
 k = convective, across air gap without air circulation based on temperature difference ($T_o - T_{gi}$)

 kg = convective, across air gap without air circulation between glazing sheets

 L = height
 o = outer
 p = pressure, time station
 r = room
 s = solar
 sr = refractive solar
 t = top
 w = wall, water, width, window

Abstract

Abstract

The object of this thesis was to develop a two-dimensional computer model of the transwall passive solar system. The methodology employed an explicit finite difference solution together with the concept of effective conductivity to account for circulation phenomena.

A small transwall module irradiated by a solar simulator was used to establish a basic one-dimensional computer model. This was the basis for the development of the one-dimensional and two-dimensional computer programs for predicting the temperature distributions within the full size transwall^{module} and its heat transfer with the environment.

The transmission of irradiance measured through the small transwall module was found to agree with that predicted to 3% for pure water and 2% for a water/dye solution, Lissamine Red 3GX. Various one-dimensional computer models were tested against experimental results for the small transwall module. Variations included models with, and without boundary layer, full glass and multi-glass slabs, full water and half water slabs. The third model which involves the boundary layer gave good agreement between theory and experiment, and consequently it was used to develop two dimensional computer models that apply to a full size transwall module tested in a solar test cell.

The two-dimensional model was found to predict the horizontal temperature distributions within the transwall reasonably well, but it does not reproduce as well the vertical temperature gradients. The validation experimentation in the solar test cell suggests that the effective conductivity approach of itself cannot reproduce well the effects of stratification. Two alternative approaches are suggested for further investigation.

The one-dimensional computer program was applied as a design tool to a house designed on passive solar principles, including a transwall. The simulated performance of the transwall shows that the version developed in the University of Glasgow is superior to the water-gel type used by Ames Research Laboratory of Iowa University, the optimum parameters of water thickness (0.15m) and Lissamine Red 3GX dye concentration (10-20 ppm) are determined, the performance insensitivity to free air circulation established, and the fraction of the heat load met by the transwall quantified, including direct gain through the transwall, 12% in Winter, and 30% in Spring/Autumn.

Introduction

Introduction

Passive solar heating has become increasingly important and a new passive solar heating system called the 'Transwall' is currently under development. Most of the initial work on Transwalls has been undertaken by the Ames Research Laboratory of Iowa University, U.S.A.

The transwall is a visually transparent thermal storage wall which is placed in building areas that receive direct solar irradiation. It has a unique feature in that it incorporates the aspects of both the direct gain and Trombe wall systems. A typical transwall is made of modules (1.2 m x 0.6 m x 0.18 m) of water filled glass, or plastic, tanks held within a framework behind the glazing window as Figure (1) illustrates. Of the incident solar irradiation falling on the transwall after passing through the window (glazing) about half is absorbed, one sixth is transmitted as direct gain, and the rest is reflected by the supporting structure.

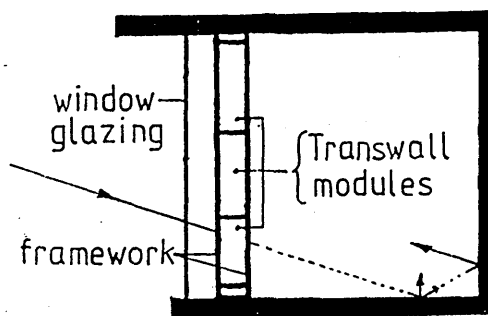


Figure 1 The TRANSWALL

The room is illuminated by the transmitted fraction of solar energy, as in the direct gain system. This fraction can be made small enough to eliminate overheating, glare and photodegradation of the interior

furnishings, which are undesirable characteristics of conventional direct gain systems, while still allowing good visual transmission. These aspects make the transwall system to be more architecturally appealing than the completely absorbing Trombe wall system.

The aim of the present work was to develop and validate a computer model to predict the temperature distributions in the transwall, and hence its heat transfer in the environment. This was achieved by first developing a one-dimensional computer model using a small transwall module irradiated by a solar simulator in a temperature controlled laboratory. The results of the small transwall analysis were used as a guide to the development of the one-dimensional and two-dimensional computer models applicable to the full size transwall module.

This thesis starts with the description of the conventional passive solar systems that are rivals or complementary systems to the transwall, together with a general review of transwall development. There follows a critical evaluation of the transwall designs pioneered by the Ames Research Laboratory of Iowa University, and the merits attributed to the transwall developed by the Mechanical Engineering Research Annexe (MERA) of Glasgow University.

The second chapter is devoted to the development and experimental validation of one-dimensional computer models of the transwall temperature distribution. The

computer models in general are based on the concept of 'effective conductivity' because experience at the University of Glasgow has shown that the running time of a computer program modelling transwall temperatures and velocities using the fundamental approach of balancing volumetric energy, momentum, mass, was too long even on a mainframe computer. The boundary layer at the glass/water interface is accounted for by a form of 'contact resistance', while still recognizing that there is no factual temperature drop at the inter surface plane. Thus the transwall is treated essentially as a semi-transparent solid with spectral absorption as an important feature. The equations for the temperature distribution in the transwall are solved by a finite difference method. The explicit method was chosen over implicit because it is better able to handle the potentially large number of equations.

The chapter goes on to describe experiments involving the small transwall module. The module was irradiated by a solar simulator and it was used to develop the initial one-dimensional models because the laboratory conditions are controlled, and in particular irradiation is unidirectional and appropriate to the one-dimensional system, i.e. there is little diffuse irradiation or shading. A number of one-dimensional computer models were then developed and tested against experimental results for the small transwall module. These include models with and without boundary layer,

full glass and multi-glass slabs, full water and half water slabs. The model which incorporates the boundary layer was chosen as the most representative of observed phenomena, and thus it was used to develop the one-dimensional and two-dimensional computer models of the full size transwall module.

Some experimental problems were encountered, particularly with the solar simulator and the effects of laboratory temperature fluctuations. The simulator irradiance depends on voltage, and the fractional energies of the spectral wavebands were not as originally expected. The second chapter then continues to recount how uncertainties in the extinction coefficients of the glass and water-dye were resolved. Finally, the chapter describes how the laboratory temperature fluctuations were tackled. Basically the boundary conditions of the computer models clearly depend on the heat transfer coefficients transwall surface to air and on the laboratory temperature in the region of the transwall. The former were determined by selective insulation of the module surfaces and 'back-calculating' the heat transfer coefficients to match the observed reduction in temperatures while the module cooled. The inadequate laboratory temperature control proved to be a rather intractable problem, and eventually recourse was made to fitting draught screens which only partially ameliorated the problem.

Chapter three starts by giving a synopsis of the two

dimensional computer model of the absorption in a transwall developed by Greveniotis [20]. This is followed by a detailed description of the modifications adopted to improve the model, the development of the two-dimensional temperature prediction program, the experiments with the full size transwall in the solar test cell, and finally the comparison of the computer model with experimental results.

In general, the two dimensional computer model of the absorption acknowledges that shading within and without the transwall occurs, including reflections from the bottom glass, and then sets about calculating absorption in various slabs into which the transwall is divided. The computer model of the absorption was extensively modified. Firstly, it was translated from BASIC to FORTRAN in order to run it on the IBM P/S Microcomputers. Secondly, it was modified to accommodate the model of surface contact resistance in the boundary layer, and finally, it was incorporated into the temperature subroutine program that employs the concept of effective conductivity to account for "circulation phenomena using the method of finite differences.

Despite the poor summer of 1988 experiments were carried out in a solar test cell using the full size transwall to collect data, viz solar irradiation and temperature distributions in the transwall. The heat transfer coefficients transwall to air, were calculated

in a similar manner, 'back-calculating' described in the second chapter. The measured values of the heat transfer coefficients were compared to those predicted by the temperature subroutine program. Results indicate that the two dimensional model is insensitive to vertical variations of the heat transfer coefficients, transwall to air.

The third chapter then concludes by giving a detailed account of the comparison of the two dimensional computer model with experiments. The model was found to yield a fairly reasonable agreement with experimental horizontal temperature distributions in the transwall. However, the two dimensional computer model could not reproduce as well vertical temperature gradients. A possible suspect is that the circulation pattern in the transwall is more complex than originally anticipated, and hence the effective conductivity of itself is inadequate to quantify stratification effects. Two alternatives are suggested in the final chapter on future work.

The penultimate chapter is devoted to the application of the Glasgow transwall simulation model to determine the optimum parameters for the transwall when built in a house designed on solar engineering principles and located in the West of Scotland. The one-dimensional computer model was chosen to study the performance of the Glasgow University water-dye transwall against the water-gel version developed by the

Ames Research Laboratory of Iowa University. Not unnaturally the Glasgow transwall was found to be superior to the Ames version. The Glasgow transwall optimum parameters were determined, i.e. the water thickness, and the Lissamine Red 3GX dye concentration. The performance was found to be insensitive to free air circulation unlike the Trombe wall. The fractional heat load provided by the transwall, including its component of direct gain, is 30% in Spring/Autumn and 12% in Winter.

The last chapter begins by an appraisal of future work that could be undertaken to improve the performance of the computer models, with emphasis on better quantifying stratification. Two suggestions are offered, namely the two dimensional approach involving the partial redistribution of the enthalpy rise in the first water half-slabs to the upper 1 1/2-slabs, and a one-dimensional analysis in which the transwall is divided into halves, the upper and the lower, and then linking the temperatures of both halves by a dimensionless correlation. The chapter then goes on to give a summary of improvements to the experimental apparatus associated with both the small and the full size transwalls. It concludes by giving a summary of the achievements attained in this work, together with the conclusions reached.

Finally, the work reported in this thesis is the author's own with the following exceptions. The solar

simulator was designed and commissioned by Paparsenos. [26]. The solar test cell was designed and mainly instrumented by Nisbet [7], but modified by the author. The two dimensional absorption program was written originally in BASIC by Greveniotis [20]. The author rewrote the program in FORTRAN and then extensively modified it. The heat load program for the solar house of chapter 4 was written by Ham [47], and the stress analysis/design of the transwall frame by Francis [48]. The author's one-dimensional computer program replaced Ham's lumped system approach in determining the heat release from the transwall.

Chapter 1

Chapter 1

Passive Solar Systems.

1.1 Introduction.

Passive solar systems are distinguished from active systems by the fact that they do not require mechanical systems such as pumps, fans, blowers to collect and transport heat energy. Instead, heat transfer is by free convection, conduction and radiation [1,2]. However, in practice, the distinction becomes blurred because systems involving small air circulation fans and/or air distribution systems are often classified as passive. It is a matter of degree. Passive systems can be subdivided into direct gain, thermal storage systems, and hybrid systems involving both classifications e.g. the transwall defined in the introduction.

This chapter describes passive solar systems which are rivals to the transwall; namely direct gain, conservatory, (sunspaces), Trombe wall, water wall, and water roof. Transwall systems are then described followed by comparisons with competitive systems. Finally there is a critical appraisal of the transwall designs developed by the Ames Research Laboratory and the advantages claimed for the version developed by the Mechanical Engineering Research Annexe (MERA) of Glasgow University.

1.2 Direct Gain Systems.

Direct gain systems use solar irradiance transmitted through glazing to warm up the surfaces and thus the space of a building. Such systems employ windows, clerestories and conservatories to collect heat energy.

1.2.1 Windows.

The direct gain of energy through windows meets part of the building heating load, but it is estimated that only a small percentage (circa 5%) of the heat load of an average domestic house is met by the solar gain [2]. In a modern design of a highly insulated house, with most (circa 80%) of its windows to the south, the percentage rises to 30%. The principal drawback of an enhanced window area in a solar energy system is that the windows also provide a path for heat losses. This leads to the concept of the "Effective U-Value" (EUV), which is the average heat loss less the solar gain. South facing windows [1,2], single glazed have a high EUV of $3.0 \text{ W/(m}^2\text{.K)}$ (U-value of $5.6 \text{ W/(m}^2\text{.K)}$) compared to an EUV for double glazing of $0.8 \text{ W/(m}^2\text{.K)}$, or Kappafloat⁺ double glazing of $0.2 \text{ W/(m}^2\text{.K)}$. Clearly an improved thermal performance requires an

+ Kappafloat is a Pilkington trade name for a double glazed window with a long wavelength reflective coating on an inner surface.

increase in capital outlay e.g. Kappafloat glazing costs 40% more than double glazing.

Clerestories are high windows in a building which allows solar irradiance to penetrate to the internal north face. Obviously such buildings have to be open plan in design and frequently incorporate a gallery. A house utilizing this principle is described in Section 1.2.2.

1.2.2 Conservatories (Sun spaces).

Conservatories, or sun spaces, are used increasingly as energy saving units in buildings where their function is to preheat air prior to circulation through the house, and they can also incorporate a large mass of thermal storage. Previously conservatories have been used as sunny lounge areas with plenty of vegetation, a "greenhouse", and their potential as energy savers was never acknowledged [1].

Conservatories have a tendency to overheat if not carefully designed and a ventilation system is essential. In winter, the conservatory can also become a heating liability and this can be prevented by thermally decoupling the conservatory from the building. A double glazed conservatory will stay above the 13°C habitability limit for 37% of the heating season and 90% of the daylight hours [1,2].

Conservatories are often single glazed structures, but double glazing normally is preferred because it

extends substantially its operational season. A typical conservatory for a building is shown in Figure 1.1(a) and Figure 1.1(b). The south facing conservatory captures the available solar gain, and when its temperature is above that of the middle zone the glazed doors can be opened to admit the warmer air. The concrete floors in the conservatory and in the middle zone absorb and store direct solar irradiance, the sun's rays reaching into the middle zone through the roof and the glazed wall. Overheating is controlled by manually operated reflecting blinds that hang internally and cover the windows and the roof of the conservatory. The shutters between the middle zone and the conservatory are reflective so that they shade the middle zone. Ventilation is achieved by opening a roof window at the top of the sun space and cross ventilation is achieved in summer by opening the sun space doors, the middle zone windows and the north zone windows. In winter, heat transfer is prevented from the middle zone into the sun space by insulating shutters as Figure 1.1(b) shows.

The conservatory can reduce energy consumption to 62% of that of a standard house built under a strict Danish energy saving code [4]. The cost of a conservatory/sunspace is about £350/m² if single glazed without base, £570/m² if double glazed without base, and £1200/m² if double glazed with base and with low part wall. The payback period can be long in a building designed for low energy cost. As an

Heating Season with Sun - Summer

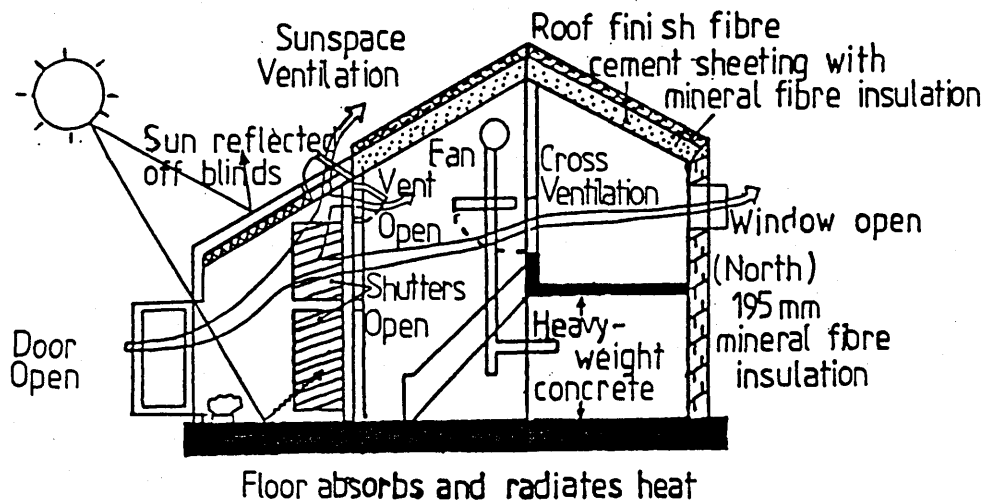


Figure 1.1(a) A typical domestic house during heating season with single glazed sunspace, insulating shutters and internal folding blinds [1].

Heating Season with No Sun

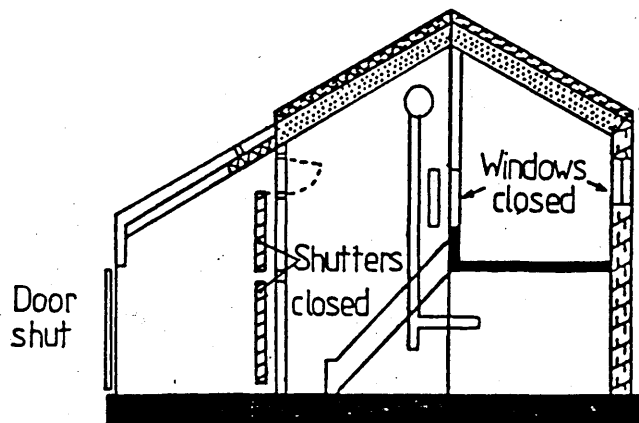


Figure 1.1(b) The solar gain system in a domestic house during no heating season [1].

illustration a conservatory for the Danish building illustrated in Figure 1.1 costs from 90 000 Kroner, to 150 000 Kroner (£7500 - £12500) depending on size.

Conservatories, sun spaces, are generally well liked by their owners, but more for the pleasant environment created than for the energy savings promised. Experience has shown, [5,6], that conservatories are generally not operated correctly by the occupants. Instead of thermally decoupling the system the space is used throughout the year and energy savings in practice are minimal. Another, perhaps more subtle, example of mal operation is to cram the conservatory with plants not realizing that their evapotranspiration will reduce the sensible heat rise by roughly half, [7].

1.3 Thermal Storage Walls and Roofs

Thermal storage walls/roofs are distinguished from direct gain systems by the fact that they employ a thermal mass which is placed between the glazed solar collection area and the interior spaces of the building. The thermal storage wall then absorbs the solar irradiance and distributes heat energy to the interior of the building by conduction, convection and radiation [1,2]. There are four common types of storage walls/roofs, namely Trombe walls, water walls, water roofs and transwalls. The transwall is still under development.

1.3.1 The Trombe Wall.

The Trombe wall is so far the best known passive solar storage system in which solar irradiance is absorbed in a massive black painted south facing wall located behind the glazing. Some Trombe walls are made from glazed built-on structures and some are an integral part of the building [1]. Such storage walls are typically 0.3 m - 0.45 m thick [1,2,3].

The heat transport from the storage medium into the interior of the room, or building, is by radiation and convection from the interior surface of the thermal storage wall and convection of room air through the gap between the exterior face of the wall and the outside glazing, via the ventilation ports at the top and bottom of the thermal storage wall. The ventilation ports are sized to about $0.06 \text{ m}^2/\text{vent port/m run of wall}$ [1]. A typical Trombe wall is shown in Figure 1.2. Trombe found that roughly two thirds of the heat transfer to the room is by conduction through the wall, and one third is by air circulation [2,8]. The long term 'collector efficiency' is around one third in the heating season and less in the off-season [2].

Thermal losses incurred during the night can be reduced by using either double glazing or single glazing with thermal panels. An optimum coupling exists of storage to space volume. Too small storage capacity results in high storage temperatures and corresponding heat losses, and yet too large a storage capacity gives

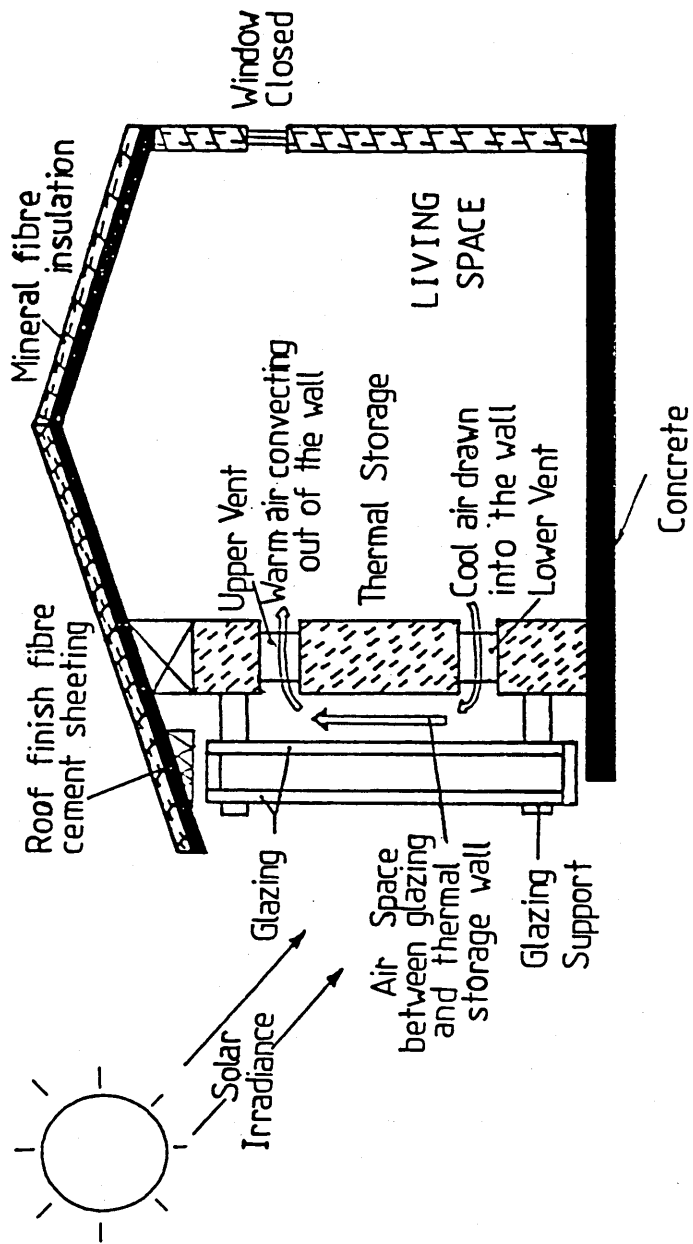


Figure 1.2 A Trombe thermal storage wall with ventilation ports and double exterior glazing. (X-sectional view)

lower wall temperatures but results in the room overheating [2,8]. Overheating in summer can be curbed by the use of overhangs, shutters, cross-ventilation and a large thermal mass. But even so passive systems generally require tolerance of higher temperature swings in the living space than is normal with a conventional system [2].

The vents at the top and bottom of the wall increase the overall performance of the wall. However, it is essential that vent flaps prevent reverse flow otherwise the overall performance will be less than if the vents were not used at all [8].

The Trombe wall has some fundamental disadvantages aside from having to form part of the building structure. Trombe wall buildings are often ugly because it is difficult to make attractive a large stretch of black painted wall, and window penetration to the south is necessarily minimal. Finally the highest temperatures are generated at the surface facing the window and so heat losses are maximized.

1.3.2 Water Walls.

Passive solar systems using water walls for storage are among the most effective and economical installations for natural heating and ventilation [9,10,11,12,13,14,15].

The water passive solar system is conceptually similar to the Trombe wall, except that it uses enclosed

water instead of masonry or concrete. Water is usually contained in metal tanks or glass tanks (transwall-like), metal culverts, metal cans or in oil drums [9]. The heat transfer into the interior of the building is by radiation, convection, and circulation within the tank yields a high effective conductivity. Water is almost three times more efficient than masonry for thermal storage per unit volume (the thermal capacity of water is about 2 1/2 times, that of concrete). It will typically costs only two thirds as much as masonry for an equivalent storage.

The drawback of a water wall compared to a concrete Trombe wall is that heat is lost evenly on both the interior and exterior sides [10]. It is claimed that the heat losses can be alleviated by using a selective surface coating on the exterior of the thermal mass. A selective surface coating [10] is a coating whose absorptance for solar irradiation is high (0.90 - 0.95) while its emittance for converted long wave radiation is low (0.05 - 0.10). Such a surface is useful in solar applications because there is very little overlap in the wavelength rays between incoming solar irradiance and emitted long wave radiation. A typical water wall - retrofitted domestic house is shown in Figure 1.3. A standard house with a Bainbridge water tank [9] can achieve a very good performance. Therefore, for the house in question with 10% of the floor area of a standard frame house in south facing windows and 19 to

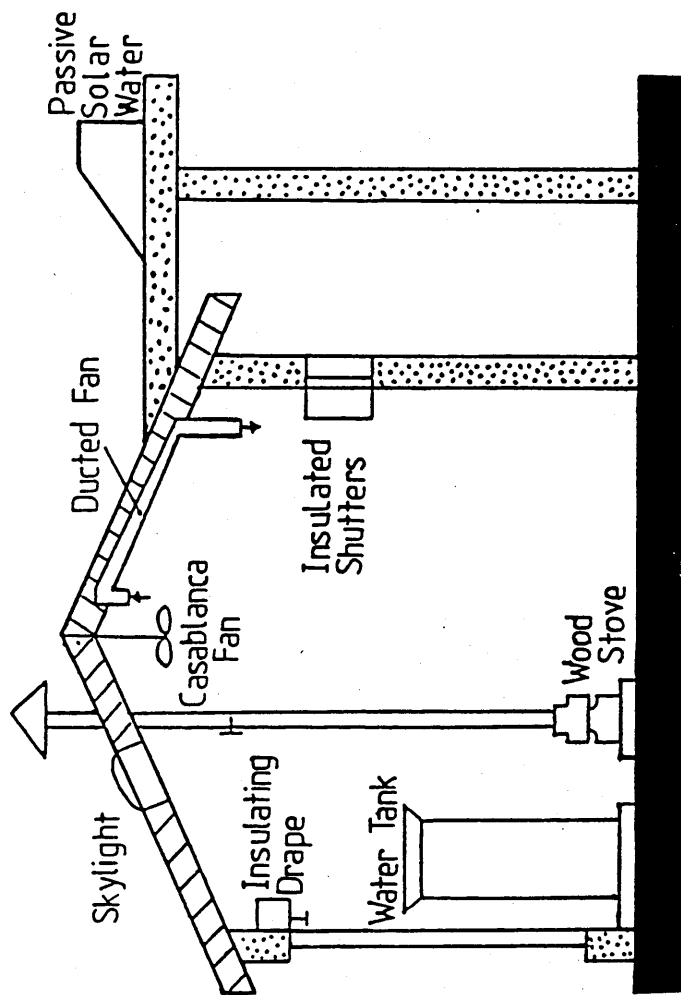


Figure 1.3 The Bainbridge Water Tank: Passive Solar House in Davis, California, U.S.A. [9].

23 litres of water/square metre of south glass, full cooling and up to 90% natural heating can be achieved [9].

Water walls work best if the water containers are placed directly in the sun behind a south facing window. The tank should be painted flat black or very dark brown or blue. The water wall may use a tank which can be textured and painted to match the walls so it becomes almost invisible. Rust is not likely to be a problem for walls in most areas, but a water tank magnesium anode, or appropriate inhibitors, can be added to ensure that rust problems will not occur [9]. The low temperature, lack of oxygen, and lack of water flow in the sealed tank tend to limit corrosion.

1.3.3 Water Roofs.

Water roofs operate on the same principles as the collector wall except that solar energy transfer into the room is primarily by radiation from the storage ceiling [16,17,18,19,20]. A roof carries a shallow water filled pond, about 0.2 m deep, either in tanks or in plastic bags in thermal contact with a strong and highly conductive flat roof and ceiling structure [1,20]. Water bags sealed in clear polyvinyl chloride are sometimes preferred.

Solar energy is stored in the water which in turn heats up the ceiling. It is also necessary to insulate the pond at night to prevent excessive heat loss, as

illustrated in Figure 1.4(a) for a winter heating operating mode. Alternatively, the system can operate as a passive cooling system in which water is exposed to the sky by night and covered by day to shield it from solar irradiation, while it absorbs heat transfer from the room below. Figure 1.4(b) shows the system for a summer cooling operating mode. Clearly a suitable climate is required which has hot days and cold nights. This is more likely to be found in inland or desert areas than in coastal regions. The water roof is more suitable for low latitude regions in which case the collector aperture per unit volume of a single story house is high and impressive energy savings can be achieved.

An example of a passive solar system based on the principle of roof ponds, is the Cool Pool shown in Figure 1.4(c). The Cool Pool [17] located in Winters, California, U.S.A., is a passive cooling system consisting of a shaded evaporating roof pond which thermosiphons cool water into the columns located within a building [18]. The thermosiphoning Cool Pool does not require moveable insulation and allows the roof pond to be physically isolated from the building interior. Also it does not introduce any additional water vapour into the interior space, noting that evaporation is the method of heat rejection [17].

Experiments performed to monitor the performance of the Cool Pool showed that it is a powerful passive

Winter Heating Mode

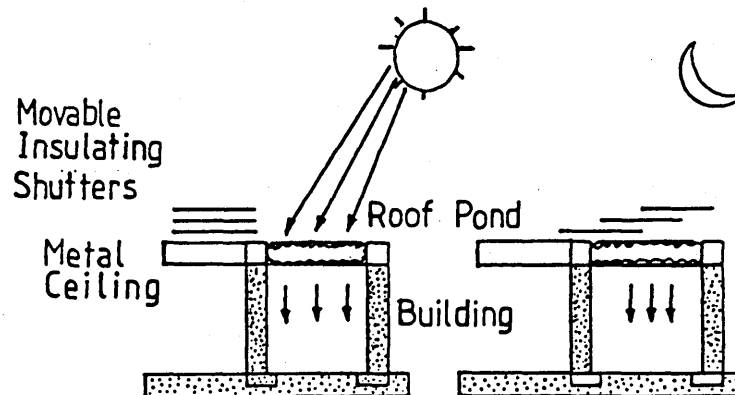


Figure 1.4(a) A house naturally heated by use of roof ponds during the winter heating season for both day and night situations [2].

Summer Cooling Mode

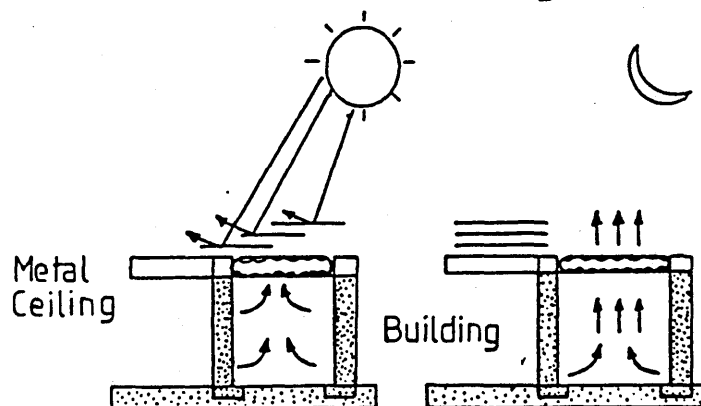


Figure 1.4(b) A house naturally cooled by use of roof ponds during the summer cooling season for both day and night situations [2].

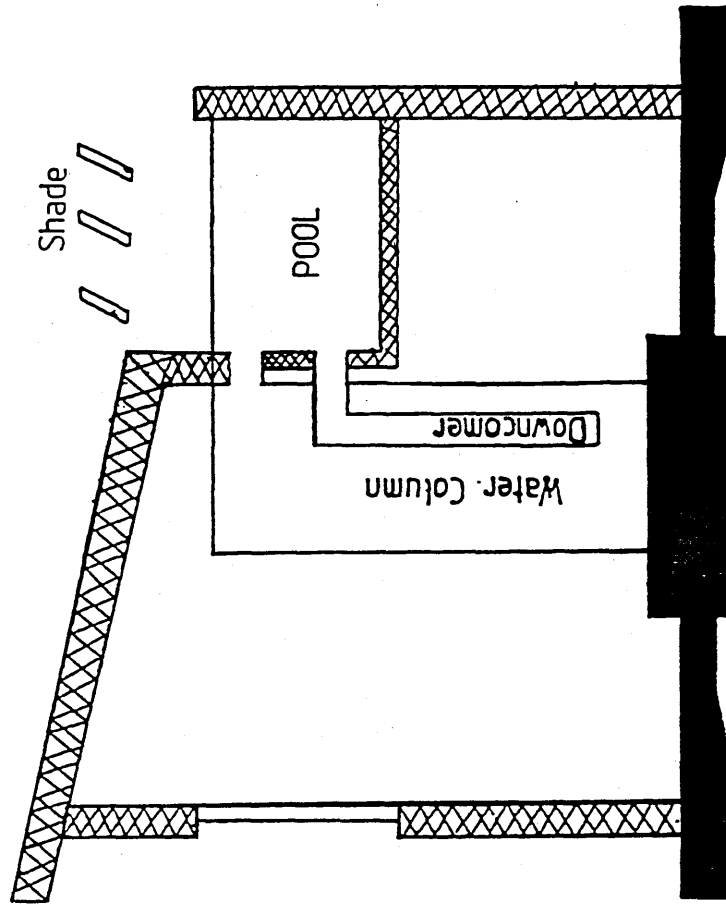


Figure 1.4(c) The Thermosiphoning Cool Pool Building [17].

cooling system that is capable of providing 100% of the cooling needs of a building in many parts of the U.S.A. [17]. The system does not require daily attention and operates without any supplementary power. The cylinders (culverts) used for the Cool Pool during summer can also be used as thermal mass for a solar heating system during the winter.

1.3.4. The Transwall.

The transwall is a visually transparent thermal storage water wall which is placed in building areas that receive direct solar irradiation. The wall consists of modules of water filled glass, or plastic, tanks held within a framework. Typically each module is roughly 1 m long by 0.6 m high by 0.1-0.2 m thick and has the appearance of a thin aquarium tank.

The transwall has a unique feature in that it incorporates the aspects of both direct gain and storage wall systems [21,25]. This hybrid phenomenon is illustrated schematically in Figure 1.5. Typically 50% of the incident solar irradiation is absorbed in the transwall, 10-20% is transmitted as direct gain into the room, and the remainder is absorbed or reflected by the glazing and the frame structure. The absorption of the solar irradiation through the water wall can be enhanced by various means. A central "high iron" glass absorbing

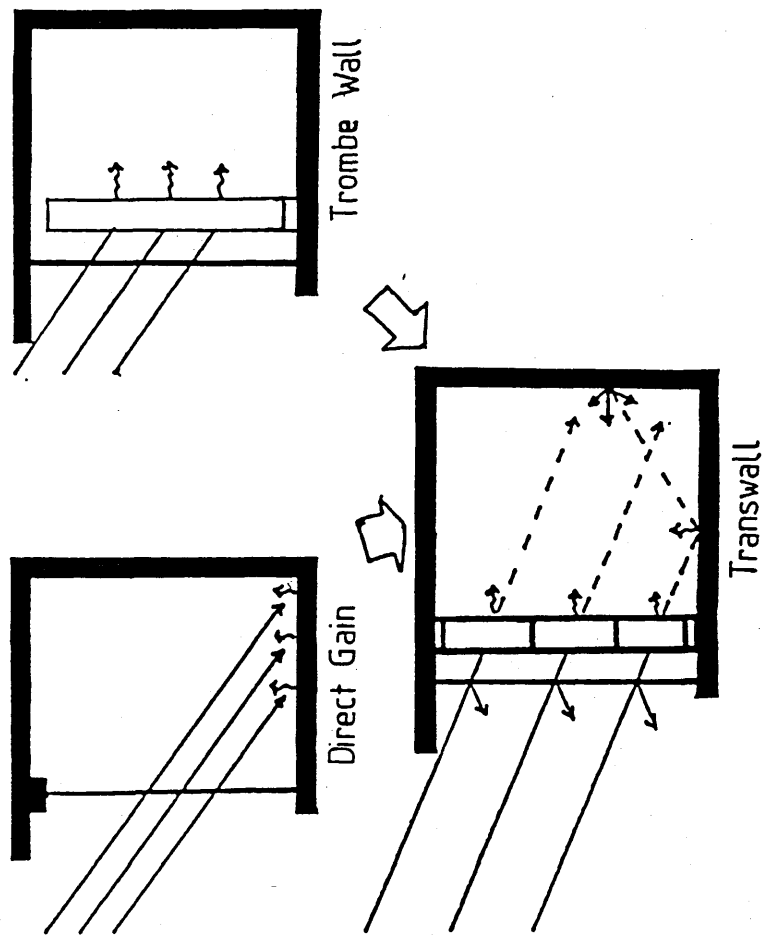


Figure 1.5 The Transwall system combines the characteristics of both direct gain and Trombe wall systems for passive solar heating of interiors.

plate is used in some Ames⁺ designs [22,23,24,25]. The addition of a "heat mirror" on the exterior facing transwall module walls will reduce radiative heat losses and enhance absorption. The advantage of a heat mirror over the doubling glazing glass is that the solar energy is reflected in the coating rather than heating up the glazing.

The MERA design utilizes a water-dye to increase absorption. The colour is not important thermally but most work has been done using a dye, Lissamine Red 3GX, which produces a pale magenta transwall.

Sometimes algae growth becomes a problem, and in such cases the problem is eliminated by the addition of 100 ppm CuSO_4 , a common algicide, and 150 ppm disodium ethylenediamine tetracetate (EDTA), a chelating compound [25]. A copper sulphide solution, Copersafe, has been successfully used in the MERA design.

In the MERA design, the transwall modules are formed into a wall by locating them in a framework constructed from 40 mm square mild steel box section. The modules are secured in place by 75 mm wide facing strips and each module can be removed separately. However, this should not be a frequent necessity because the modules are filled and emptied by a pipe system hidden by the

+ Ames Research Laboratories, United States Department of Energy, Iowa University, Iowa U.S.A.

facing strips and controlled by concealed valves at the base of the wall. Details are given in Appendix A.

The length and height of the modules is a compromise between weight, stress and a desire to minimise visual obstruction. It is believed that an empty mass of 50 kg is the maximum which can be reasonably handled by two persons, the height is limited to 0.6-0.7 m by the glass stresses, and the thickness by thermal consideration. This results in a length of 1.2 m.

1.3.4.1 Transwall Review.

Research on the transwall passive solar system has been carried out over the past decade by researchers on both sides of the Atlantic. Most of this work has been undertaken at Ames Research Laboratory - United States Department of Energy (USDOE), of Iowa University, Iowa, U.S.A. [21-25].

J.R. Hull and J.F. McClelland and co-workers [21] used a mathematical model of few nodes to study the effect of Ames design parameter changes on the performance of a transwall passive solar heating system for different climates. The Ames transwall design parameters varied are: collector area to building load ratio, transwall thickness, transmittance of the absorber plate, and the amount of internal mass. Their results suggest that module thickness and absorber plate transmission can be varied substantially without significantly compromising the system's thermal

performance. Their preliminary estimates of the Nusselt number of the free circulating water in the module suggest that vertical temperature stratification tends to reduce the horizontal convective heat transfer within the transwall. An increase in water thickness beyond 10 cm gains very little in the Solar Savings Fraction (SSF)⁺ and their model was found to be relatively insensitive to the Nusselt number of the water cavity. Their analysis was based on a Nusselt number of 2.5. However, the results by Paparsenos [26] for a continuous radiation input of about 400 to 500 W/m² showed a higher effective conductivity which was compatible with a Nusselt number of 20. This is supported by the work of this thesis.

Preliminary analytical results by Fuchs and McClelland [22,23] indicated that the thermal performance of an Ames transwall can be improved by the use of baffles and/or a gelling compound to eliminate the internal convective heat transfer. This conclusion is based on the argument that if internal convection is eliminated, and solar absorption confined largely to the centre of the wall, or to the interior wall, the temperatures of the exterior facing wall will be minimised and thus a major source of heat loss reduced.

+ The SSF is defined as:-

$$SSF = 1 - \frac{\text{auxilliary heat required with solar}}{\text{heat required without solar}}$$

Paparsenos [26] on the other hand reckoned that the use of baffles is a difficult and uneconomical venture, and instead recommended the use of gelling agents such as Courtaulds Courlose F1000G and Celanese Celanol HA7 150000S.

These compounds have been tested at the Mechanical Engineering Research Annexe (MERA) of the University of Glasgow and showed the former compound to have an advantage over the latter because of clarity. However, there are problems associated with the use of these compounds. They encourage the growth of micro-organisms, and the long chain molecules in weak solutions have been observed to contract over several weeks, leaving the lower regions somewhat opaque. Paparsenos [26] suggested that solutions stronger than 0.5% (kg of agent/kg of water) tested might alleviate this problem, but unavoidably at the expense of visual clarity and additional cost to the system.

Subsequently it has been found that a 0.05% solution of Carbopol 941 (Goodrich Chemicals) eliminates water circulation and does not impare visual clarity. However, its long term performance under strong irradiation has yet to be determined. It is emphasized that the prevention of water circulation is important to the Ames design of transwall, whereas in the MERA version of the transwall using a water-dye solution water circulation is not inhibited.

McClelland, Mercer et al. used a computer model [25]

to investigate the use of a transmitting selective coating, dubbed a "heat mirror" on the exterior face of the transwall modules to reduce radiative heat losses, and also the effect of moving the absorber plate from the centre to the inside tank wall. The latter design's main objective was to simplify the tank design, lower the cost and hence improve the transwall appearance. Their investigations revealed that the change in location of the absorber plate marginally improved (1%) the transwall thermal performance. However, the addition of the selective coating reduced the auxilliary building heating required by 50% with double glazing, but could not compensate for the replacement of single outside glazing for double glazing. In addition, the heat mirror produced a higher predicted performance improvement than moveable night insulation or the glazing.

R.Fuchs and J.F.McClelland of Ames [22] using a thermal network model compared the thermal performance of transwalls to that of Trombe walls and direct gain systems. They found that the transwall thermal performance can be very close to, or exceeds that of Trombe wall and direct gain systems when operating under similar conditions.

Sodha et al. [27] used a periodic analysis method, rather than finite difference, to examine the performance of a transwall which contained methyl methacrylate as the absorbing material. The use of

methyl methacrylate by Sodha et al. is surprising because it would diffuse into the water, but a (poly)methyl methacrylate on the other hand would be understandable. Their conclusion for winter operation was that the (poly)methyl methacrylate, Perspex, should be 9 cm thick if it formed, in effect, the outer face of the transwall, and if it was located in the water cavity then it should be positioned closer to the outer rather than the inner face of the wall. The cost of such a slab of Perspex must be considerable.

Nisbet and Kwan [7] of Glasgow University used a computer model to analyse the energy savings resulting from the use of plastic film transwalls in horticultural glasshouses. They found that energy cost savings of 15-20% could be achieved depending on the uncertain effects of evapotranspiration. The payback period is predicted to be about 2 1/2 years to 5 years for the west of Scotland, and 4 to 8 years for the southeast of England. The range of payback times depends on whether the modules were self constructed or purchased.

Greveniotis [20] analysed the performance of a transwall module using a lumped system approach (infinite conductivity). His conclusions were that the lumped system can predict the temperature rise within an error of approximately 20% for a glass transwall, and with an error probably substantially lower for the plastic film transwall developed by Nisbet and Kwan [7] for glasshouse installations. Greveniotis further

developed and validated a computer programme for the two-dimensional absorption of irradiation in the transwall. This forms part of a larger programme that models the phenomena within the transwall using the finite difference method and the concept of effective conductivity, the thrust of this current research.

1.3.4.2 Ames Transwall versus MERA Transwall.

This discussion would be incomplete without reference to the differences between the transwall prototypes pioneered by the Ames Research Laboratory of Iowa University, and that used by the Mechanical Engineering Research Annexe (MERA) of Glasgow University.

The Ames computer models were limited to one-dimensional analysis, few nodes and constant absorption, i.e. the absorption did not vary with solar position. At MERA, both the one-dimensional and two-dimensional analyses with a considerable number of nodes have been used. The absorption is taken to vary with solar position.

Both designs use modules of roughly similar size, 1.2 m long x 0.6 m high x 0.15-0.18 m overall thickness. The physical differences as shown in Figure 1.6 are that the Ames transwall modules use either a solar absorbing glass plate at the centre or forming the rear wall to absorb a fraction of incident solar energy, and store the heat energy in the surrounding water. The absorber plate, or wall, is a 3.2 mm, or 6 mm, thick

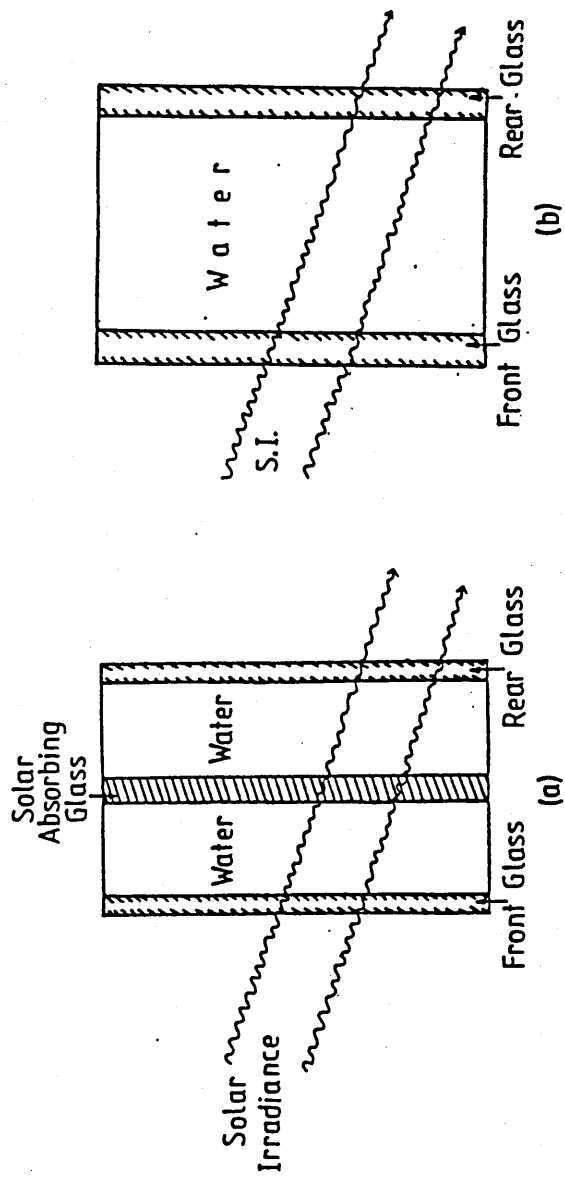


Figure 1.6 (a) The Ames Transwall Prototype ; (b) The MERA Transwall Version.

grey tinted high iron glass [21-25]. The MERA transwall, on the other hand, is more simple. It uses plain 10 mm glass plates forming the front, the rear and side walls of the transwall module, and uses a water-dye solution to enhance absorption. The 10 mm glass thickness of the MERA module is considered the minimum for reasons of safety if the tank is not to be reinforced with a lid or upper cross strapping. The final Ames version uses 6 mm glass with a reinforcing lid which must always be fitted when the tank is filled. This may be acceptable in a laboratory situation but it is not for domestic employment. The original MERA module was constructed from 6 mm glass and in a safety test it was filled without its reinforcing lid. The resulting bowing of glass when half full caused the test to be abandoned abruptly. An aquarium manufacturer claims that a 10 mm tank is considered "child proof", and a 10 mm transwall module in a test cell at MERA survived a vehicle impact which moved the substantial cell 0.2 m rearwards.

The Ames transwalls sometimes use the transparent baffles to inhibit circulation in order to increase their performance. Inhibiting water circulation will not improve the performance of the MERA water-dye modules because the bulk of the absorption is in the first few centimetres of the water. A disadvantage of the Ames method of enhancing absorption is that it is fixed i.e. the transmission is 12% in summer and

winter. This is too low for a dull winter's day. The MERA system of using a water-dye is more flexible in principle because the transmission can be varied from 50%, clear water, to zero if necessary. The colour is not important thermally, only the transmission. However, some colours are best avoided, e.g. green gives a bilious effect and it is unsuitable for plants. Magenta transmits the wavelengths required for plant growth and generates a warm feeling, blue imparts a feeling of coolness. Even a tartan transwall is technically feasible and it might have advertising merit.

Most of the transwall modelling work undertaken by Ames uses a 'quenched' transwall i.e. a model in which there is no air circulation in the air gap between the outside window and the front glass plate of the transwall. The Ames researches reckon that preventing circulation over the transwall increases the Solar Savings Fraction (SSF) from 76% unquenched to 88% when quenched [22,23]. Because the Ames transwalls have either a central absorbing plate or a high solar absorbing plate forming the room side of the transwall, Ames claims that with this arrangement the window side temperature is reduced and consequently the heat loss to the window is also reduced. This argument is regarded with skepticism at MERA because of the high absorption of infra red radiation in the first few mm of the water path length. Ames later improved their system by

removing the central absorbing plate and replacing the inner transwall glass by a high absorbing glass. While this arrangement of Ames gives a 10% higher heat release to the room than the MERA version because of the reduced heat loss to the window, computer simulation runs carried out at MERA indicate that the heat release 6 pm to midnight is actually 30% less with the Ames system than with MERA system. The merits of air and water circulation are elaborated in Chapter 4.

The Ames transwalls are more expensive than the MERA version. The typical Ames transwall costs, about £150/m² (\$270/m² by 1981 estimates) for a transwall made from 6 mm glass. The purchase cost of a MERA transwall module in 1988 was £35 imported glass which leads to a cost/m², including the frame, of £75. Estimating the U.K. cost of an Ames type transwall is complicated by the fact that imported cheap clear 10 mm glass is readily available but solar absorbing glass less so. Based on the relative costs of 10 mm Pilkington float glass, £32/m² clear, £60/m² Antisun Grey, then the Ames design will increase module material costs by about one third. Hence, the MERA is cheaper than Ames prototype.

1.3.4.3 Transwall compared with other Systems.

(a) Direct Gain Systems.

Aside from enhanced heat losses, direct gain systems suffer from two further disadvantages; excessive

irradiation penetrating the building and the lack of a storage medium other than the building fabric. The occupants of such systems tend to fit blinds to reduce the glare and photodegradation of the fabric and, of course, by so doing circumvent the system's operational principle. The lack of thermal storage leads to overheating by day, and this problem is exacerbated by the current trend towards lightweight building construction. In contrast, the MERA version of the transwall allows a variable transmission of light, 10-50%, into the building interior with an almost total absence of photodegrading UV irradiation because it has to pass through a total of 32 mm of glass. The transwall's thermal capacity is relatively high, equivalent to a 40 cm concrete wall, and so day time overheating is avoided. Thus the transwall has the advantages of a direct gain system, good views, light airy feeling etc. without its attendant disadvantages.

It is possible to instal a transwall in a conservatory with the purposes of providing extra, or alternative, thermal storage and reducing glare. However, the thermal decoupling of the conservatory in winter would make this a dubious economic prospect.

(b) Storage Walls

Trombe Wall.

It has been noted [21] that the most important difference, in terms of thermal performance, between the

transwall and the Trombe wall, is that in the former case most of the solar energy is absorbed within the wall, not at the front surface facing windows which leads to higher heat losses. Further, the room is also heated directly and illuminated by the transmitted fraction of solar energy, 12-40% as in direct gain systems. The transwall is lighter, transparent and more architecturally appealing than a large stretch of black painted massive wall - the Trombe wall system.

Water Wall.

The lower cost of the containment and structure gives an economic edge to the water wall over the Trombe wall and transwall. Like the Trombe wall the water wall suffers from not being visually transparent and difficulty in making it an attractive feature. Disguising the water wall as Doric columns was not found to be cost effective because their thermal mass was small compared to that of the house [28].

Water Roof.

The transwall and the water roof should be seen as mutually exclusive systems rather than as rivals i.e. use the transwall for higher latitudes, the water roof for lower. If the site is in middle latitudes, the building is of single story construction and the climate is suitable, then the water roof is likely to outperform the transwall because of its superior thermal capacity

to space volume ratio and its superior capacity for cooling.

1.4 Conclusion.

The Transwall passive solar system overcomes a number of drawbacks associated with conventional passive solar systems such as Trombe wall and direct gain systems, in that, it admits light to the room and allows the occupants to see through the window with minimum glare, photodegradation and overheating problems.

It is believed that the MERA version is superior to that of Ames on the grounds of superior performance when most required, low cost and flexibility in light transmission.

It remains to be seen whether the Transwall will compete successfully in the market place against already established conventional systems. The transwall cost, its overall performance and durability will be the deciding factors.

Chapter 2

Chapter 2

The Development and Validation of the One-Dimensional Computer Model of the Transwall.

2.1 Introduction

The chapter is concerned with the development of one-dimensional computer models of the temperature distribution in the transwall. These were used as a basis for the two-dimensional model. The models apply to a full size transwall module, solar irradiated, and to a smaller module irradiated by a solar simulator. An outline of the computer models is given and the means by which water circulation and boundary layers are represented.

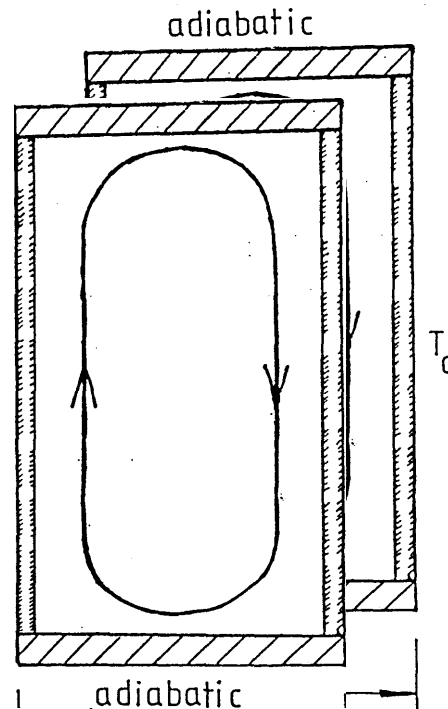
The solar simulator is described together with the way in which some of the problems associated with spectral emittance from the lamps was tackled. The various experimental runs involving the small transwall modules are detailed and compared to the predictions of the computer models. Some experimental details are consigned to the appendices; solar simulator, B, transwall irradiation absorption, C, and thermocouple calibration, D.

2.2 Water Circulation in the Transwall.

Heat transfer within the transwall falls into the category of free convection in enclosed spaces, a

general classification rich in papers. Unfortunately, many of these apply to heat transfer between isothermal hot and cold walls which is not the situation for a two-dimensional transwall. Most reported work has much higher temperature differences between the walls than applies in the transwall case, and few reports take into account the driving force of radiation absorption throughout the circulating medium. No papers have been found whose analysis can be applied with confidence to the specific case of the transwall.

In a conventional vertically enclosed volume in which heat transfer occurs between an isothermal opaque hot surface, temperature, T_h , and an isothermal opaque cold surface, T_c , the possible flow regimes up and down the vertical walls can be divided into five classifications; conduction, asymptotic flow, laminar boundary layer flow, transitional, and finally turbulent boundary layer flow.



The bounds of these regimes are set by either the Grashof number or the Rayleigh number.

$$Gr_L = \frac{gB (T_h - T_c)L^3}{\nu^2}, \text{ and } Ra_L = Gr_L \times Pr$$

where Gr_L = local Grashof number
 g = gravitational acceleration
 L = distance between plates
 T_h = temperature of isothermal hot surface
 T_c = temperature of isothermal cold surface
 ν = kinematic viscosity
 B = volume expansion coefficient
 Ra_L = local Rayleigh number
 Pr = Prandtl number

The bounding limits suggested by various experiments are:-

Conduction Regime

$Ra < 10^3$ Holman [29]
 $Ra_w^* < 10^3$ MacGregor and Emery [30]

Asymptotic

$Ra = 10^3 - 3 \times 10^4$ Holman [29]
 $10^3 < Ra_w$ MacGregor and Emery [30]
 $4 \times 10^4 < Gr < 3 \times 10^6$ Newell and Schmidt [31]

Laminar

$Ra < 10^6$ Holman, $Ra < 10^6$ White [29]
 $3 \times 10^4 < Ra < 3 \times 10^6$ MacGregor and Emery [30]

* Ra_w where subscript, w, denotes the width of the cell.

Transitional

$Ra < 10^6 - 10^7$ Holman, $Ra = 10^7$ White [29,32]
 $3 \times 10^6 < Ra_w < 10^7$ MacGregor and Emery [30]
 $Ra \ 1.3 \times 10^5 - 2.2 \times 10^5$ Landis discussion in
Dropkin and Somerscales [33]

Turbulent Regime

$Ra > 10^7$ Holman, 10^7 White [29,42]
 $Ra > 10^7$ MacGregor and Emery [30]
 $Ra > 10^7$ Emery and Chu [34]
 $Ra > 5 \times 10^9$ Lankhorst [35]
 $5 \times 10^4 < Ra$ Dropkin and Somerscales [33]
(non enclosure)

On the evidence presented in the above papers it is likely that the scatter in regime limits is due mainly to excluding the effect of the aspect ratio of the enclosure in the Rayleigh number. A secondary source of scatter may be the inclusion of high Prandtl number fluids in the correlation. This is unlikely to affect the transwall water with its Prandtl number of around 7.

Webb and Viskanta [36] have examined by computation and experiment radiation induced buoyancy driven flow in a rectangular enclosure $4.8 \times 14.5 \times 4.1$ cm wide which is much smaller than even the small transwall modules. The cell contained water and was irradiated by quartz halogen lamps through glass vertical walls. The wall temperatures were similar to that experienced in the transwall. Interferometer measurements showed that the

boundary layer at the cooled wall was very thin, much less than expected. The circulation was modelled by the conventional mass, momentum, energy balance and the Patankar technique [37]. Difficulty was experienced in modelling water temperatures close to the glass because of the limitation on the number of nodes. It was found that most of the heat transfer within the cell takes place at the top of the cooler wall, where the warm fluid first meets the wall, and heat transfer is low at the bottom of this wall. Thus heat transfer at the cooler face is a distinctly two-dimensional affair. The aspect ratio of the cavity seemed to have little effect on the final result. It was noted that radiation induced buoyancy flow does not exhibit some of the characteristics of hot wall induced flow. In particular the flow loses completely the centrosymmetry characteristic of the latter flow.

Lauriat [38] carried out a numerical analysis of irradiated gray gas trapped between hot and cold isothermal walls. His results were compared with published experimental data. Like Webb and Viskanta [36] he found that the classical centrosymmetry of non-irradiated flow is destroyed by irradiation and the aspect ratio has little effect. He reports that the radiation delays the onset of instability in a slot.

The flow regimes in a transwall have been examined by injecting small quantities of milk into the boundary layer. Milk has the advantage of a density close to

that of water and it does not diffuse as rapidly as some dyes. It will, of course, absorb more radiant energy than the surrounding water. The movement of the milk streaks suggests that the boundary layer is laminar and evidence of turbulence was not observed. The down flow on the rear wall tends to migrate very slowly to the centre showing that the normal core of a non-irradiated enclosure is destroyed. The Rayleigh number for the transwall based on the thickness, 0.16 m, and the glass wall temperature difference, is in the region of 10^8 . This places the boundary layer flow for a non-irradiated enclosure in the transitional/turbulent regime. However, the observed laminar flow seems to confirm Lauriat's contention that irradiation delays the onset of instability. As a consequence correlations for the Nusselt number required to model the temperature drop across the boundary layers in the transwall have been chosen as appropriate to a laminar flow regime.

2.3 The One-Dimensional Computer Model of The Temperature Distribution in a Transwall Module.

2.3.1. The Concept of Effective Conductivity.

It was found that the running time of the computer program modelling transwall velocities and temperatures developed by Paparsenos [26], employing the fundamental approach of balancing energy, momentum, mass, was excessive when run on a mainframe computer to the extent

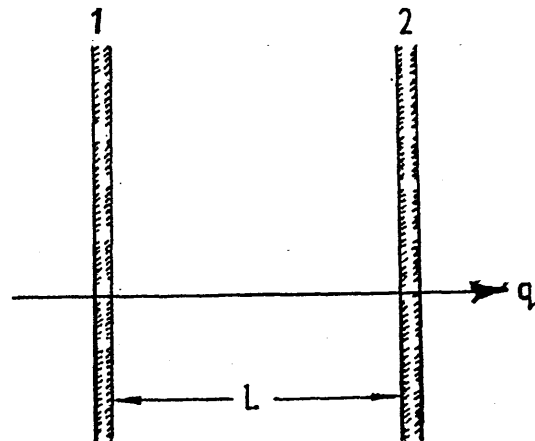
that 1 second real time took 200 seconds computer time. Therefore, it was believed that the problem could be solved by using the concept of effective conductivity; i.e. the normal thermal conductivity of the water is increased by some factor to represent circulation and the water, or water/dye solution, is taken to be at rest. The Fourier equation can now be applied to this situation and the temperature distribution found by solving the equation by the method of finite differences.

The Nusselt number represents the ratio of convective to conductive heat transfer and hence, the effective conductivity between two walls 1 and 2 separated by a fluid can be expressed as a Nusselt number as follows:

$$Nu = \frac{hL}{k_e}$$

$$\begin{aligned} \text{and } q &= h A (T_1 - T_2) \\ &= k_e \frac{A(T_1 - T_2)}{L} \end{aligned}$$

$$\text{Therefore, } k_e = h L = Nu k_w$$



where

h = convective heat
transfer coefficient,
wall-fluid

A = surface area

k_e = effective
conductivity

k_w = water thermal
conductivity.

The Nusselt number can vary between 2 and 30, depending on such factors as stratification, absorptivity and aspect ratio. The effective conductivity correlations adopted for the present transwall situation are those given by MacGregor and Emery [30] as:-

$$Nu = 0.42 Ra^{1/4} Pr^{0.012} (H/L)^{-1/3}$$

where Nu = Nusselt number

Ra = Rayleigh number

Pr = Prandtl number

H/L = aspect ratio

This correlation was chosen because it was believed to model most closely the behaviour of the transwall situation.

2.3.2 The One-Dimensional Explicit Finite Difference Method: Surface Contact Resistance Model.

The one-dimensional explicit finite difference

method of treating the Fourier equation was used to develop a computer program to calculate the one-dimensional temperature distribution within the small transwall module. The program also had to cover the case of the full size module solar irradiated through the window of a solar test cell. It is the latter case for which the method is developed here. The explicit method of finite differences is preferred here to the implicit method because it is better able to handle the potentially large number of equations [39,40], and so reduce the computer running time. It is believed that this factor is more important than the larger time interval permitted by the implicit solution. The explicit time interval used was 25 seconds which gives a short computer running time.

2.3.3 The One-Dimensional Explicit Finite Difference Equations for the Transwall Module

Consider the transwall module with the following slab divisions: 4 x half-glass slabs, 2 x half-water slabs near the glass/water interface, and 5-full water slabs in between the water half-slabs as shown in Figure 2.1. This arrangement constitutes 8 full slabs; 6 water slabs and 2 full glass slabs.

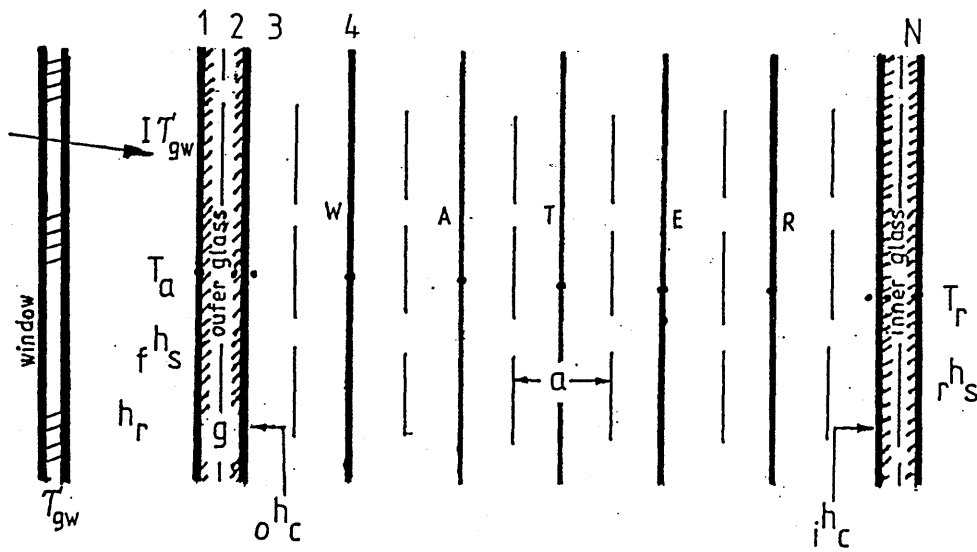


Figure 2.1 The vertical direction slab division of the Transwall Module.

Nomenclature:-

T_a	=	air temperature in window/glass gap
T_r	=	room temperature
T_{gz}	=	window/glazing temperature
$f h_s$	=	convective heat transfer coefficient, front glass to window
$r h_s$	=	heat transfer coefficient, rear glass to room, convection and radiation.
$o h_c$	=	surface contact heat transfer coefficient, outer glass to water.
$i h_c$	=	surface contact heat transfer coefficient, inner glass to water.
h_r	=	linearized radiation heat transfer coefficient
a	=	water slab thickness.
α	=	fractional absorption, nth slab
$I_{\lambda\tau_{gw}}$	=	incident irradiation after passing through glazing - window/unit area of transwall surface.

The governing Fourier equation is given by;

$$\frac{\partial T}{\partial t} = \frac{k}{\rho c} \left[\frac{\partial^2 T}{\partial x^2} + \frac{\partial^2 T}{\partial y^2} + \frac{\partial^2 T}{\partial z^2} \right] + \frac{q_g}{\rho c}$$

For a one - dimensional system, the following conditions apply:

(i) uniform temperature in the vertical z-direction,

$$\therefore \frac{\partial^2 T}{\partial z^2} = 0$$

(ii) uniform temperature in the y-direction,

$$\therefore \frac{\partial^2 T}{\partial y^2} = 0$$

Therefore,

$$\frac{\partial T}{\partial t} = \frac{k}{\rho c} \left(\frac{\partial^2 T}{\partial x^2} \right) + \frac{q_g}{\rho c}$$

and

$$\frac{\partial^2 T}{\partial x^2} = \frac{p^{T_{n+1}} + p^{T_{n-1}} - 2p^{T_n}}{a^2}$$

The volumetric heat generation, q_g , becomes the volumetric irradiation absorption, evaluated in Section 2.4.

(1) Water Slabs.

(i) Consider n-full water slabs; Node (n^{th}), $n=4,5,\dots,N-3$

$$\begin{aligned} \frac{p_{+1}T_n - pT_n}{\delta t} &= \frac{k_e}{\rho_w c_w} \frac{\partial^2 T}{\partial x^2} + \frac{I_{\lambda} \tau g_w \alpha_n \cdot 1}{a \cdot 1 \cdot \rho_w c_w} \\ &= \frac{k_e}{a^2 \rho_w c_w} (pT_{n+1} + pT_{n-1} - 2pT_n) + \frac{I_{\lambda} \tau g_w \alpha_n}{a \rho_w c_w} \\ \therefore p_{+1}T_n &= F_{wx} \left[pT_{n+1} + pT_{n-1} + \left\{ \frac{1}{F_{wx}} - 2 \right\} pT_n + \frac{a}{k_e} I_{\lambda} \tau g_w \alpha_n \right] \end{aligned}$$

..... (2.1)

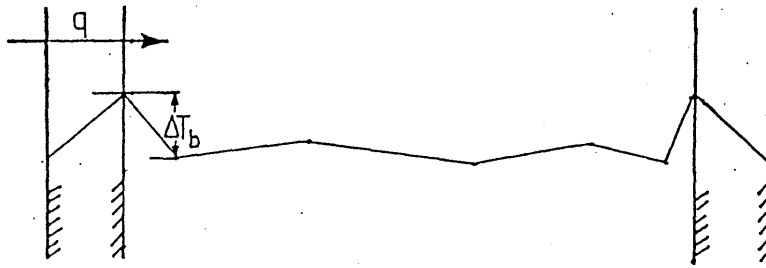
where $F_{wx} = \frac{k_e \delta t}{a^2 \rho_w c_w}$, the Fourier Number.

The stability criterion for the explicit method requires that the function of the current temperature remains positive, i.e.

$$\left[\frac{1}{F_{wx}} - 2 \right] \geq 0$$

This stability criterion is noted but not recorded for the other equations developed.

ii) Water 1/2 - Slabs



It was observed that the experimental temperature distribution had the above form. In order to represent the temperature change, ΔT_b , over the boundary layer which is relatively thin (circa 7-8 mm) it was decided to represent ΔT_b change as a form of 'contact resistance', though recognizing that there is no factual temperature drop at the water surface plane.

$$\Delta T_b = \frac{q}{h_c}$$

where q = heat flux across the boundary/m²

h_c = surface 'contact' heat transfer coefficient

The correlation for the surface heat transfer is

given by Bayley et al.[41], and can be expressed as:-

$$Nu_x = 0.508 Pr^{1/2} (0.952 + Pr)^{-1/4} Gr_x^{1/4}$$

where Nu_x = local Nusselt number at midpoint

Pr = Prandtl number

Gr_x = local Grashof number

In the case of the present study it was found that the surface contact heat transfer correlation to the 1/4-power gave better results than the 1/3-power suggested by other researchers [33,42] under slightly different conditions. This confirms that the flow regime in the boundary layer is laminar.

(iii) 1st Water 1/2-Slab; Node (3).

$$\frac{p_{+1}T_3 - pT_3}{\delta t} = \frac{2k_e}{a^2\rho_w c_w} \left[\frac{a}{k_e} (pT_2 - pT_3) - (pT_3 - pT_4) \right] + \frac{I_{\lambda} \tau g_w \alpha_3}{\rho_w c_w a/2}$$

$$\therefore p_{+1}T_3 = 2F_{wx} \left[\left(\frac{a}{k_e} \right) pT_2 + pT_4 + \left\{ \frac{1}{2F_{wx}} - \frac{a}{k_e} - 1 \right\} pT_3 \right]$$

$$+ \frac{a}{k_e} I_{\lambda} \tau g_w \alpha_3 \quad \dots\dots\dots (2.2)$$

Similarly,

(iv) 2nd Water 1/2-Slab; Node(N-2).

$$\begin{aligned}
 p_{+1}T_{N-2} = 2F_{wx} \left[\left(\frac{a}{k_e} \right) p_{T_{N-1}} + p_{T_{N-3}} + \left\{ \frac{1}{2F_{wx}} - \frac{a}{k_e} - 1 \right\} p_{T_{N-2}} \right. \\
 \left. + \frac{a}{k_e} I_{\lambda} \tau g_w \alpha_{N-2} \right] \dots\dots\dots (2.3)
 \end{aligned}$$

(2) Front Glass Slabs.

(i) 1st Glass 1/2-Slab; Node (1).

$$\begin{aligned}
 \frac{p_{+1}T_1 - p_{T_1}}{\delta t} = \frac{2k_g}{g^2 \rho_g c_g} \left\{ \frac{g f h_s}{k_g} (p_{T_1} - p_{T_a}) - (p_{T_1} - p_{T_2}) + \frac{g}{k_g} h_r (p_{T_{gw}} - p_{T_1}) \right\} \\
 + \frac{I_{\lambda} \tau g_w \alpha_1}{\rho_g c_g g/2} \\
 p_{+1}T_1 = 2F_{gx} \left[\left(\frac{g f h_s}{k_g} \right) p_{T_a} + \left(\frac{g h_r}{k_g} \right) p_{T_{gw}} + p_{T_2} + \left\{ \frac{1}{2F_{gx}} - \frac{g f h_r}{k_g} - \frac{g h_r}{k_g} \right. \right. \\
 \left. \left. - 1 \right\} p_{T_1} + \frac{g}{k_g} I_{\lambda} \tau g_w \alpha_1 \right] \dots\dots\dots (2.4)
 \end{aligned}$$

where $F_{gx} = \frac{k_g \delta t}{g^2 \rho_g c_w}$, the Fourier Number.

Similarly,

(ii) 2nd Glass 1/2-Slab; Node (2).

$$\begin{aligned}
 {}_{p+1}T_2 = 2F_{gx} \left[\left(\frac{g_{ohc}}{k_g} \right) {}_pT_3 + {}_pT_1 + \left\{ \frac{1}{2F_{gx}} - \frac{g_{ohc}}{k_g} - 1 \right\} {}_pT_2 \right. \\
 \left. + \frac{g}{k_g} I_{\lambda} \tau_{gw} \alpha_2 \right] \dots\dots\dots (2.5)
 \end{aligned}$$

(3) Rear Glass 1/2-Slab; Node.

(i) 3rd Glass 1/2-Slab; Node (N-1).

$$\begin{aligned}
 {}_{p+1}T_{N-1} = 2F_{gx} \left[\left(\frac{g_{ihc}}{k_g} \right) {}_pT_{N-2} + {}_pT_N + \left\{ \frac{1}{2F_{gx}} - \frac{g_{ihc}}{k_g} - 1 \right\} {}_pT_{N-1} \right. \\
 \left. + \frac{g}{k_g} I_{\lambda} \tau_{gw} \alpha_{N-1} \right] \dots\dots\dots (2.6)
 \end{aligned}$$

and,

(ii) 4th Glass 1/2-Slab; Node (N).

$$\begin{aligned}
 {}_{p+1}T_N = 2F_{gx} \left[\left(\frac{g_{rh_s}}{k_g} \right) {}_pT_r + {}_pT_{N-1} + \left\{ \frac{1}{2F_{gx}} - \frac{g_{rh_s}}{k_g} - 1 \right\} {}_pT_N \right. \\
 \left. + \frac{g}{k_g} I_{\lambda} \tau_{gw} \alpha_N \right] \dots\dots\dots (2.7)
 \end{aligned}$$

2.4 The One-Dimensional Computer Model of the Irradiation Absorption In the Transwall Module.

Consider the full size transwall module divided as shown in Figure 2.2. The incident irradiation is divided into wavebands;

0.3 - 0.35, 0.35 - 0.4, 0.4 - 0.6,
 0.6 - 0.75, 0.75 - 0.9, 0.9 - 1.2,
 1.2 - 2.1, 2.1 - 4.1 μm .

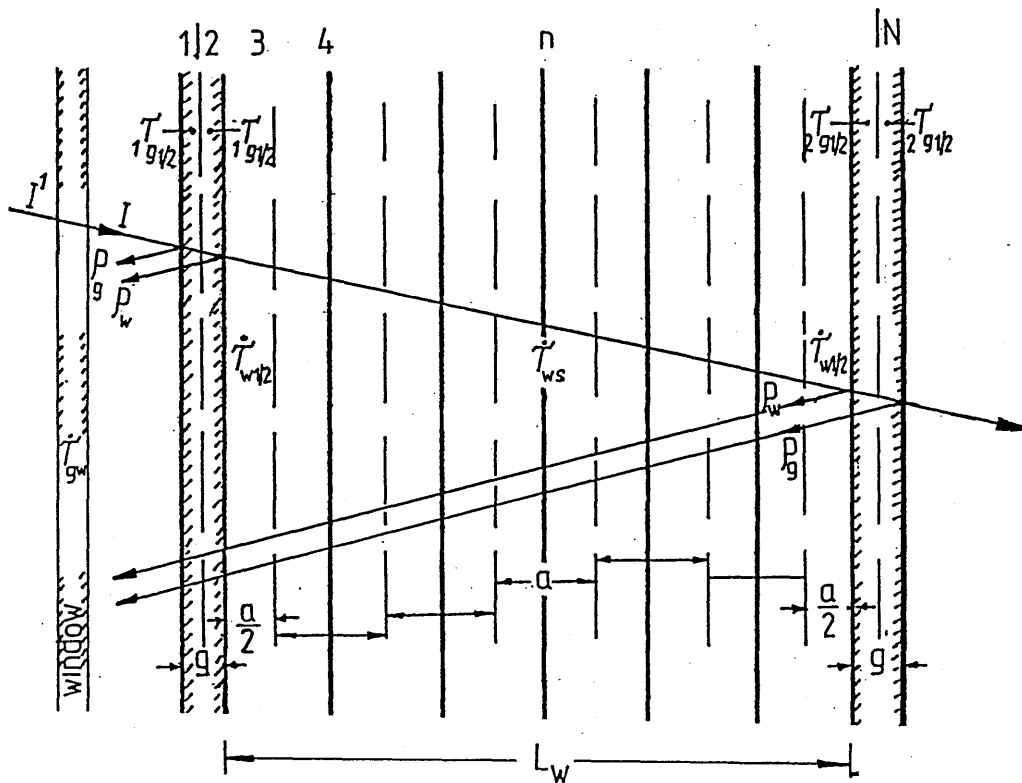


Figure 2.2 The Transwall Slab Divisions.

Nomenclature:

Note, all extinction coefficients apply to one waveband.

$$\tau_{g\frac{1}{2}} = e^{-K_g g/2} = \text{transmittance of glass } \frac{1}{2}\text{-slab}$$

where K_g = extinction coefficient of glass,

and g = path length (glass)

τ_{gw} = transmittance of window/glazing

$$\tau_w = e^{-K_w L_w} = \text{transmittance of water}$$

where K_w = extinction coefficient of water

L_w = path length (water)

ρ_g = reflectance, air/glass

ρ_w = reflectance, water/glass

I^1 = incident irradiation

I = $I^1(1-\rho)^2 \tau_{gw}$, beam irradiation falling on the transwall after passing through window.

n = the n^{th} slab where $\sum n = N$

N = the total number of all $\frac{1}{2}$ -slabs (glass and water), and 5 full water slabs considered here.

2.4.1 Outer Glass Slabs (Window Side).

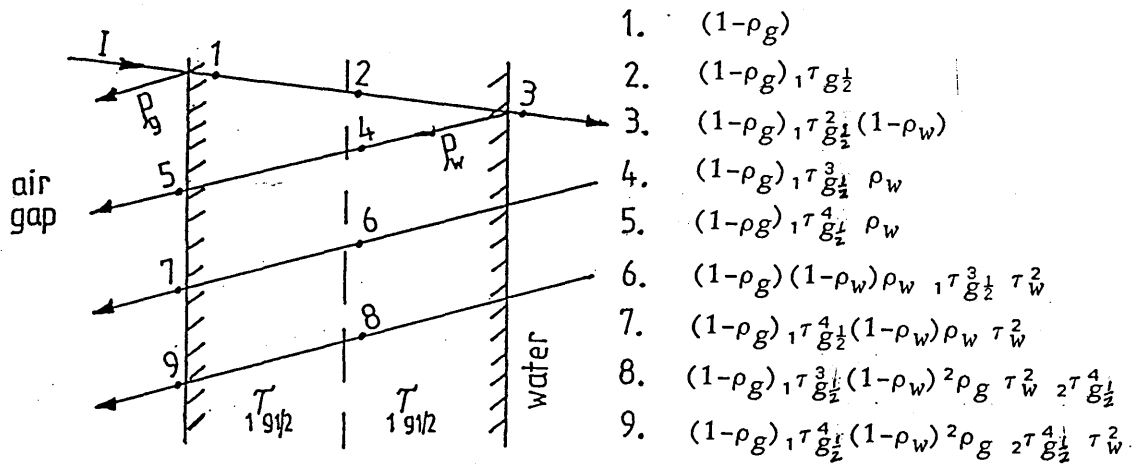


Figure 2.3 Outer glass $\frac{1}{2}$ -slabs, window side.

$$\begin{array}{lcl} \text{Irradiation} & & \text{Radiation Energy} \\ \text{Absorbed in Slab} & = & \text{Input} - \text{Output} \end{array}$$

(a) Beam Irradiation Absorbed By 1st Glass Outer $\frac{1}{2}$ -Slab.

$$\begin{aligned} \left. \begin{array}{l} \text{Irrad.} \\ \text{absorbed} \end{array} \right\} &= I [1 - \rho_g - (1 - \rho_g) \tau_{g\frac{1}{2}} + (1 - \rho_g) \tau_{g\frac{1}{2}}^3 \rho_w (1 - \tau_{g\frac{1}{2}}) \\ &\quad + (1 - \rho_g) \tau_{g\frac{1}{2}}^3 (1 - \rho_w) \rho_w \tau_w^2 (1 - \tau_{g\frac{1}{2}}) \\ &\quad + (1 - \rho_g) \tau_{g\frac{1}{2}}^3 (1 - \rho_w)^2 \tau_{g\frac{1}{2}}^4 \rho_g \tau_w^2 (1 - \tau_{g\frac{1}{2}})] \end{aligned}$$

Rearranging,

$$\begin{aligned} \left. \begin{array}{l} \text{Irrad.} \\ \text{absorbed} \end{array} \right\} &= I (1 - \rho_g) (1 - \tau_{g\frac{1}{2}}) [1 + \tau_{g\frac{1}{2}}^2 \{ \rho_w \tau_{g\frac{1}{2}} + (1 - \rho_w) \rho_w \tau_w^2 \tau_{g\frac{1}{2}} \\ &\quad + \tau_{g\frac{1}{2}} (1 - \rho_w)^2 \rho_g \tau_w^2 \tau_{g\frac{1}{2}}^4 \}] \\ &\dots\dots\dots (2.8) \end{aligned}$$

(b) Beam Irradiation Absorbed By 2nd Outer Glass 1/2-Slab.

$$\begin{aligned}
 \left. \begin{array}{l} \text{Irrad.} \\ \text{absorbed} \end{array} \right\} &= I \left[(1-\rho_g) {}_1\tau_{g\frac{1}{2}} - (1-\rho_g) {}_1\tau_{g\frac{1}{2}}^2 (1-\rho_w) - (1-\rho_g) {}_1\tau_{g\frac{1}{2}}^3 \rho_w \right. \\
 &\quad + (1-\rho_g) {}_1\tau_{g\frac{1}{2}}^2 (1-\rho_w) \rho_w \tau_w^2 (1-{}_1\tau_{g\frac{1}{2}}) \\
 &\quad \left. + (1-\rho_g) {}_1\tau_{g\frac{1}{2}}^2 (1-\rho_w)^2 \rho_g \tau_w^2 {}_2\tau_{g\frac{1}{2}}^4 (1-{}_1\tau_{g\frac{1}{2}}) \right]
 \end{aligned}$$

Rearranging,

$$\begin{aligned}
 \left. \begin{array}{l} \text{Irrad.} \\ \text{absorbed} \end{array} \right\} &= I (1-\rho_g) {}_1\tau_{g\frac{1}{2}} \left[1-\rho_w {}_1\tau_{g\frac{1}{2}}^2 - (1-\rho_w) {}_1\tau_{g\frac{1}{2}} \right. \\
 &\quad \left. + (1-\rho_w) (1-{}_1\tau_{g\frac{1}{2}}) {}_1\tau_{g\frac{1}{2}} \tau_w^2 \{ \rho_w + (1-\rho_w) \rho_g {}_2\tau_{g\frac{1}{2}}^4 \} \right] \\
 &\quad \dots\dots\dots (2.9)
 \end{aligned}$$

2.4.2 Inner Glass Slabs (Room Side).

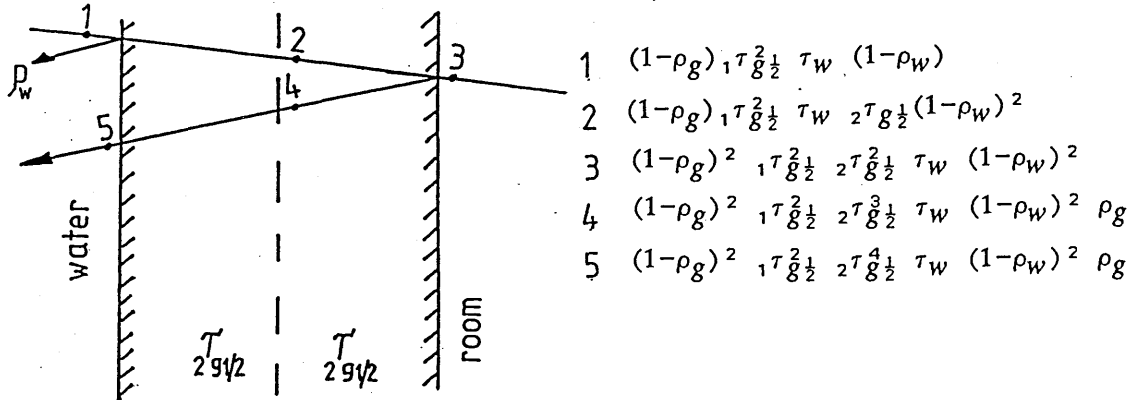


Figure 2.4 Inner glass $\frac{1}{2}$ -slabs, room side.

(a) Beam Irradiation Absorbed By 1st Inner Glass 1/2-Slab.

$$\left. \begin{array}{l} \text{Irrad.} \\ \text{absorbed} \end{array} \right\} = I(1-\rho_g)_1 \tau_{g\frac{1}{2}}^2 (1-\rho_w) \tau_w [(1-\rho_w) - {}_2\tau_{g\frac{1}{2}} (1-\rho_w) \\ + \rho_g {}_2\tau_{g\frac{1}{2}}^3 (1-\rho_w) (1-{}_2\tau_{g\frac{1}{2}})]$$

Rearranging,

$$\left. \begin{array}{l} \text{Irrad.} \\ \text{absorbed} \end{array} \right\} = I(1-\rho_g)_1 \tau_{g\frac{1}{2}}^2 (1-\rho_w)^2 \tau_w [1 - {}_2\tau_{g\frac{1}{2}} + \rho_g {}_2\tau_{g\frac{1}{2}}^3 (1-{}_2\tau_{g\frac{1}{2}})]$$

.....(2.10)

(b) Beam Irradiation Absorbed By 2nd Inner Glass 1/2-Slab.

$$\left. \begin{array}{l} \text{Irrad.} \\ \text{absorbed} \end{array} \right\} = I(1-\rho_g)_1 \tau_{g\frac{1}{2}}^2 (1-\rho_w) \tau_w [{}_2\tau_{g\frac{1}{2}} - (1-\rho_g) {}_2\tau_{g\frac{1}{2}}^2 \\ - \rho_g {}_2\tau_{g\frac{1}{2}}^3] (1-\rho_w)$$

Rearranging,

$$\left. \begin{array}{l} \text{Irrad.} \\ \text{absorbed} \end{array} \right\} = I(1-\rho_g)_1 \tau_{g\frac{1}{2}}^2 (1-\rho_w)^2 {}_2\tau_{g\frac{1}{2}} \tau_w [1 - (1-\rho_g) {}_2\tau_{g\frac{1}{2}} - \rho_g {}_2\tau_{g\frac{1}{2}}^2]$$

..... (2.11)

2.4.3 Water Slabs.

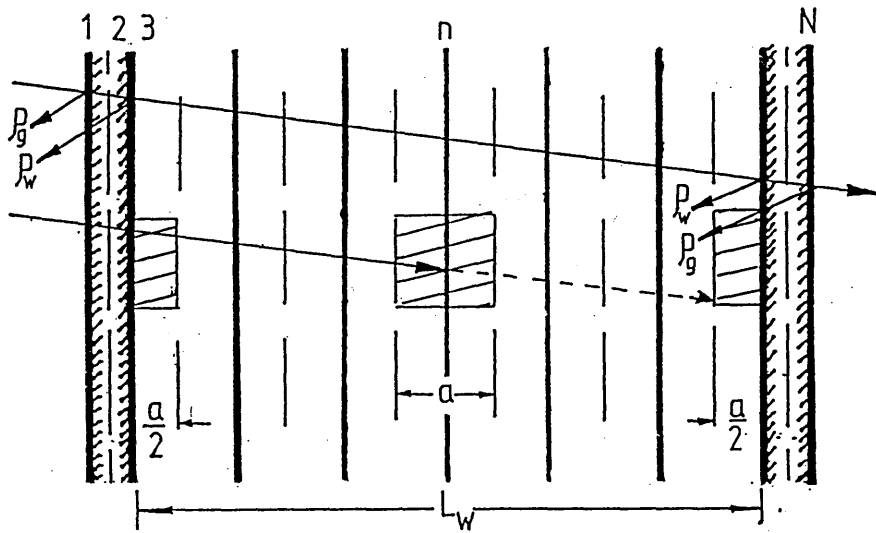


Figure 2.5 Water Slabs. $\tau_w = e^{-K_w L_w}$

(a) Beam Irradiation Absorbed By 1st Water 1/2-Slab.

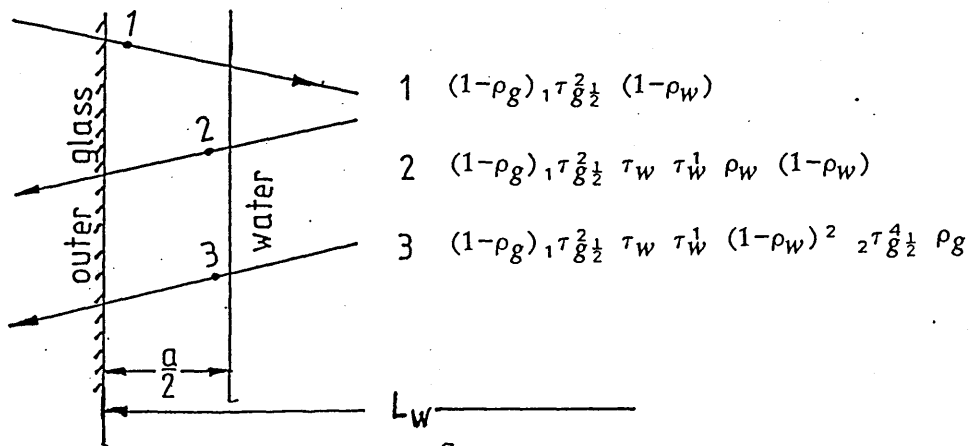


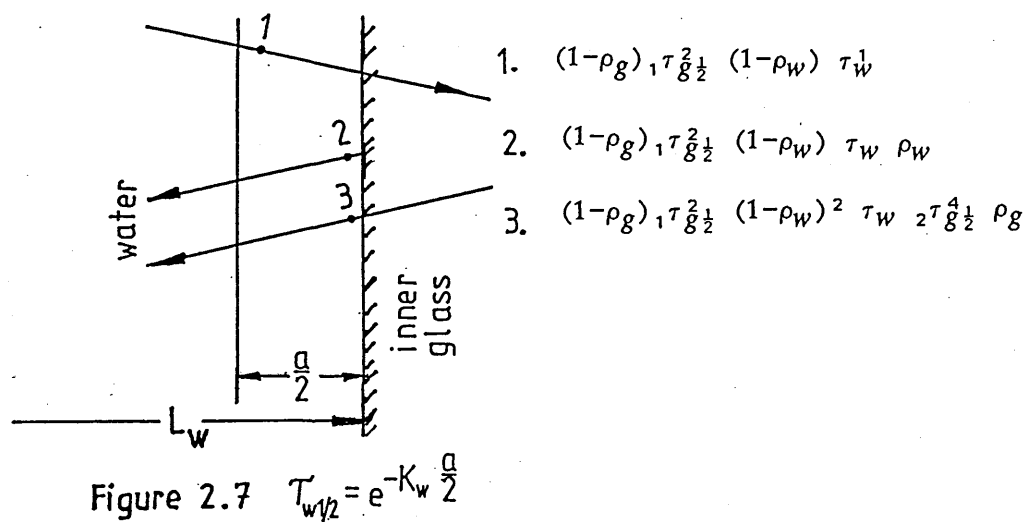
Figure 2.6 $\tau_w^1 = e^{-K_w (L_w - \frac{a}{2})}$ & $\tau_{w\frac{1}{2}} = e^{-K_w \frac{a}{2}}$

$$\begin{aligned}
 \left. \begin{array}{l} \text{Irrad.} \\ \text{absorbed} \end{array} \right\} &= I \left[(1-\rho_g)_1 \tau_{g\frac{1}{2}}^2 (1-\rho_w) \{1-\tau_{w\frac{1}{2}}\} \right. \\
 &\quad + (1-\rho_g)_1 \tau_{g\frac{1}{2}}^2 (1-\rho_w) \tau_w \tau_w^1 \rho_w \{1-\tau_{w\frac{1}{2}}\} \\
 &\quad \left. + (1-\rho_g)_1 \tau_{g\frac{1}{2}}^2 (1-\rho_w)^2 \tau_w \tau_w^1 \rho_g {}_2\tau_{g\frac{1}{2}}^4 \{1-\tau_{w\frac{1}{2}}\} \right]
 \end{aligned}$$

Rearranging,

$$\left. \begin{array}{l} \text{Irrad.} \\ \text{absorbed} \end{array} \right\} = I(1-\rho_g)_1 \tau_{g\frac{1}{2}}^2 (1-\rho_w)(1-\tau_{w\frac{1}{2}}) [1 + \tau_w \tau_w^1 \{\rho_w + \rho_g(1-\rho_w)_2 \tau_{g\frac{1}{2}}^4\}] \dots (2.12)$$

(b) Beam Irradiation Absorbed By 2nd Water 1/2-Slab.



$$\left. \begin{array}{l} \text{Irrad.} \\ \text{absorbed} \end{array} \right\} = I[(1-\rho_g)_1 \tau_{g\frac{1}{2}}^2 (1-\rho_w) \tau_w^1 \{1-\tau_{w\frac{1}{2}}\} + (1-\rho_g)_1 \tau_{g\frac{1}{2}}^2 (1-\rho_w) \tau_w \rho_w \{1-\tau_{w\frac{1}{2}}\} + (1-\rho_g)_1 \tau_{g\frac{1}{2}}^2 (1-\rho_w)^2 \tau_w \rho_g 2\tau_{g\frac{1}{2}}^4 \{1-\tau_{w\frac{1}{2}}\}]$$

Rearranging,

$$\left. \begin{array}{l} \text{Irrad.} \\ \text{absorbed} \end{array} \right\} = I(1-\rho_g)_1 \tau_{g\frac{1}{2}}^2 (1-\rho_w)(1-\tau_{w\frac{1}{2}}) [\tau_w^1 + \tau_w \{ \rho_w + (1-\rho_w) \rho_g 2\tau_{g\frac{1}{2}}^4 \}] \dots (2.13)$$

(c) Beam Irradiation Absorbed By n-Full Water Slabs.

Consider the n^{th} slab below;

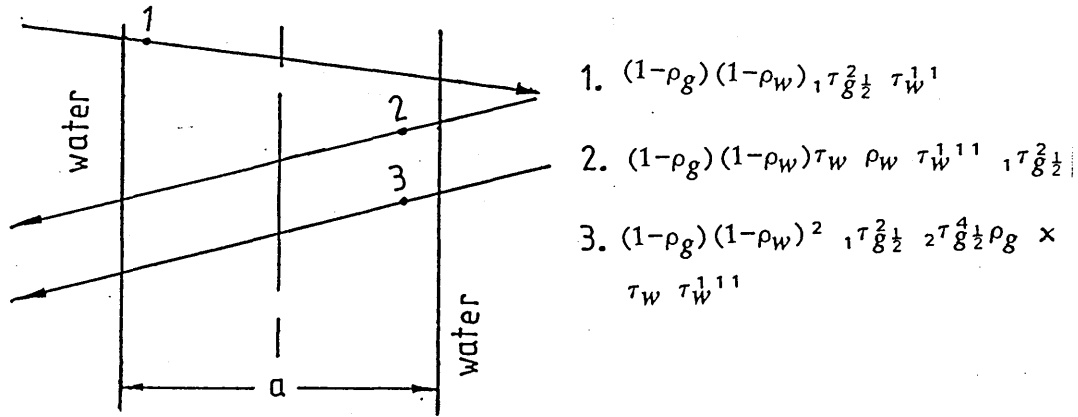


Figure 2.8 $\tau_{wi}^{11} = e^{-K_w(n-3.5)a}$; $\tau_{wi}^{111} = e^{-K_w(N-n-2.5)a}$
and $\tau_{ws} = e^{-K_w a}$

$$\left. \begin{array}{l} \text{Irrad.} \\ \text{absorbed} \end{array} \right\} = I \left[(1-\rho_g) {}_1\tau_{g\frac{1}{2}}^2 (1-\rho_w) \tau_w^{11} \{1-\tau_{ws}\} \right. \\ \left. + (1-\rho_g) {}_1\tau_{g\frac{1}{2}}^2 (1-\rho_w) \tau_w^{111} \rho_w \tau_w \{1-\tau_{ws}\} \right. \\ \left. + (1-\rho_g) {}_1\tau_{g\frac{1}{2}}^2 (1-\rho_w)^2 \tau_w^{111} \tau_w \rho_g {}_2\tau_{g\frac{1}{2}}^4 \{1-\tau_{ws}\} \right]$$

Rearranging,

$$\left. \begin{array}{l} \text{Irrad.} \\ \text{absorbed} \end{array} \right\} = I (1-\rho_g) {}_1\tau_{g\frac{1}{2}}^2 (1-\rho_w) (1-\tau_{ws}) \left[\tau_w^{11} + \tau_w \tau_w^{111} \{ \rho_w \right. \\ \left. + \rho_g (1-\rho_w) {}_2\tau_{g\frac{1}{2}}^4 \} \right] \quad \dots\dots (2.14)$$

2.5 Experiments and Model Development.

Experiments involving the solar simulator and the small transwall module were carried out as tools to develop the main computer model. The simulator was used to irradiate the small transwall and consequently it was necessary to check the uniformity of the simulator irradiance. The details of experiments are discussed in this section.

2.5.1 The Solar Simulator.

(a) The Simulator Description.

The ability to control the experimental parameters, particularly irradiation, proved to be invaluable in developing the computer model. To this end a solar simulator was used to irradiate the small transwall module (24.5 x 19 x 7.5 cm) in a temperature controlled laboratory. The solar simulator at MERA was constructed by Paparsenos [26] according to the suggestions given by Yass et al. in NASA Report N74-27719 [43].

The simulator is shown in Figure 2.9. It consists of twelve 120 V ELH Quartzline tungsten-halogen projector lamps with dichroic reflectors behind corresponding twelve Fresnel lenses. The lamps are mounted on an 0.3 cm aluminium sheet, 75.9 x 75.9 cm with a 4.4 cm diameter holes for the lamps. The hexagonal fresnel lenses are mounted on a 1.8 cm plywood board, 75 cm by 75 cm. The mounting sheet and board are

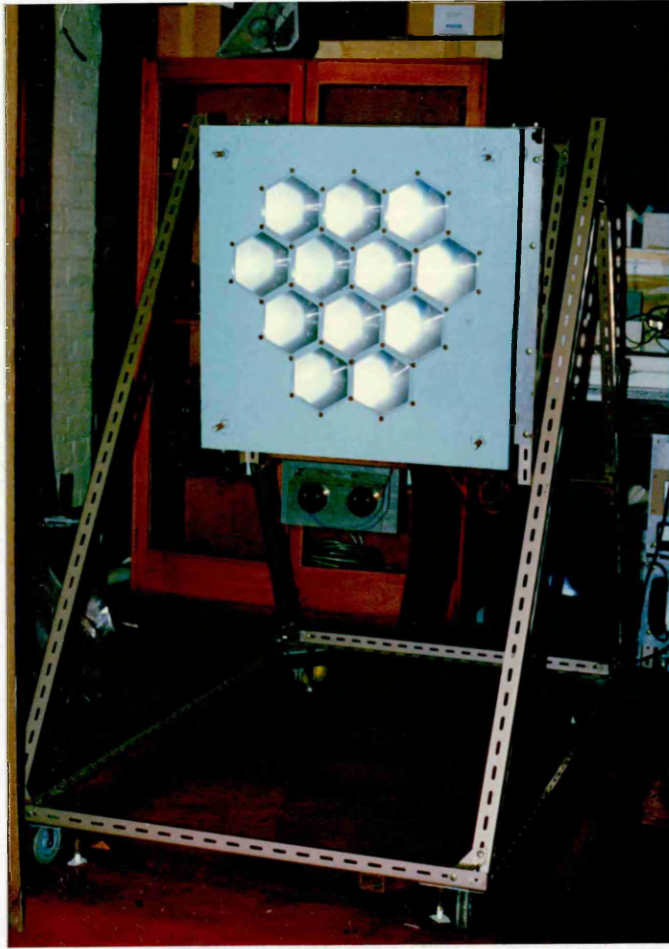


Figure 2.9 The Solar Simulator.

parallel to each other and can be varied by four threaded rods with accompanying washers and nuts. The distance between the lamps and the lenses was 27.6 cm in order to produce a reasonably parallel beam from the lenses. The lamp mounting sheet is held on a Handy Angle frame by two threaded rods of 1.9 cm diameter which allow the lamp-lens mounting sheet/board to pivot on the frame. This enables the simulator to irradiate at various angles of incidence. The Handy Angle frame is equipped with four wheels to enable it to be moved from one position to another. It can also be secured in position by means of four jacks.

(b) Power to the Solar Simulator

The power to the lamp unit of the solar simulator is supplied by a triple-ganged Variac transformer. The transformer output is kept between 105 and 120 volts. The lamps are cooled during operation by an air supply provided by two 0.5 hp centrifugal blowers through a distributor over the back of the lamps.

The transformer is essential for starting up. The resistance of the lamps is very low when cold, and if the full 120 V were suddenly applied the lamps would explode. It also allows different voltages as a secondary task and it improves the life of the lamps. The lamp life is given as 35 hours at 120 V, but well over 100 hours can be achieved by running at 105 V. The lower voltage, however, substantially changes the

spectral energy distribution of the simulator. In practice, lower voltages tend to shift the maximum spectral irradiance to the infrared. ($>1\mu\text{m}$). Figure 2.10 shows the 90-, 105-, and 120-V spectral curves [43] which are normalized so that the areas under the curves are equal (75.7 mW/cm^2). Inspection of the curves confirms the expected spectral irradiance shift.

(c) The Lamps/Lenses Arrangement

The lamps/lenses are located in an asymmetrical arrangement of 3 working lamp/lenses forming a triangle surrounded by 9 guards, Figure 2.11. The working area of the simulator beam is 25 cm x 20 cm with a uniformity of irradiance of $\pm 5\%$. The solar simulator is designed to produce a spectral irradiance approximating to air mass 2.

2.5.2. The Small Transwall Module

(a) The Module Description.

The module is made from 6 mm Pilkington clear float glass and has dimensions of 24.5 cm by 19 cm by 7.5 cm internal thickness. The photograph in Figure 2.12 shows the module sitting on its stand on a Handy Angle Frame. The sides are insulated by double glazing in order to be visually transparent, the bottom by perspex and polystyrene, and the free water surface by a carefully fitted double layer of plastic bubble film. The glass temperatures are measured by thermocouples coiled onto

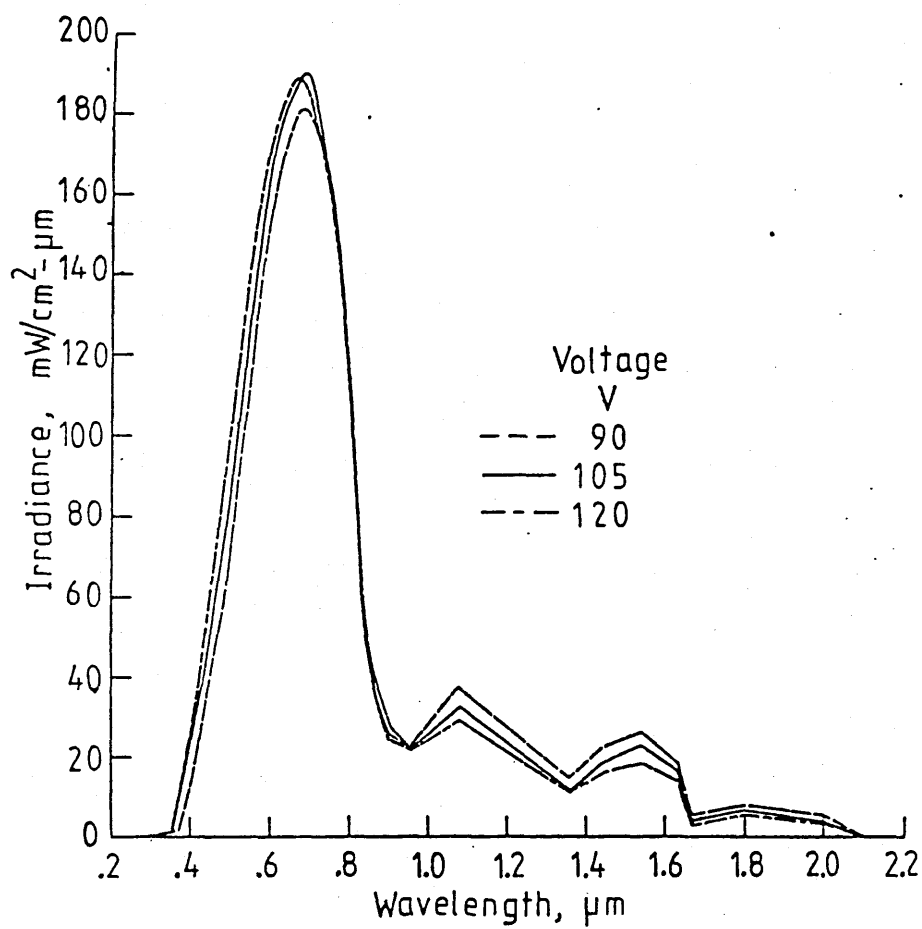


Figure 2.10 Variation of spectral irradiance with wavelength at three voltages [Yass et al., 1974].

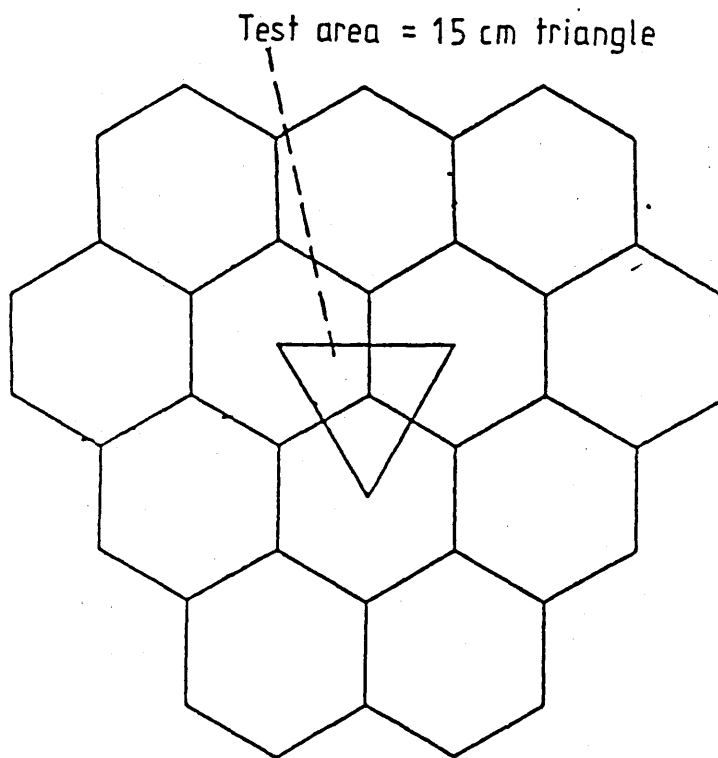


Figure 2.11 -12- Lamp lens array [Yass et al., 1974].

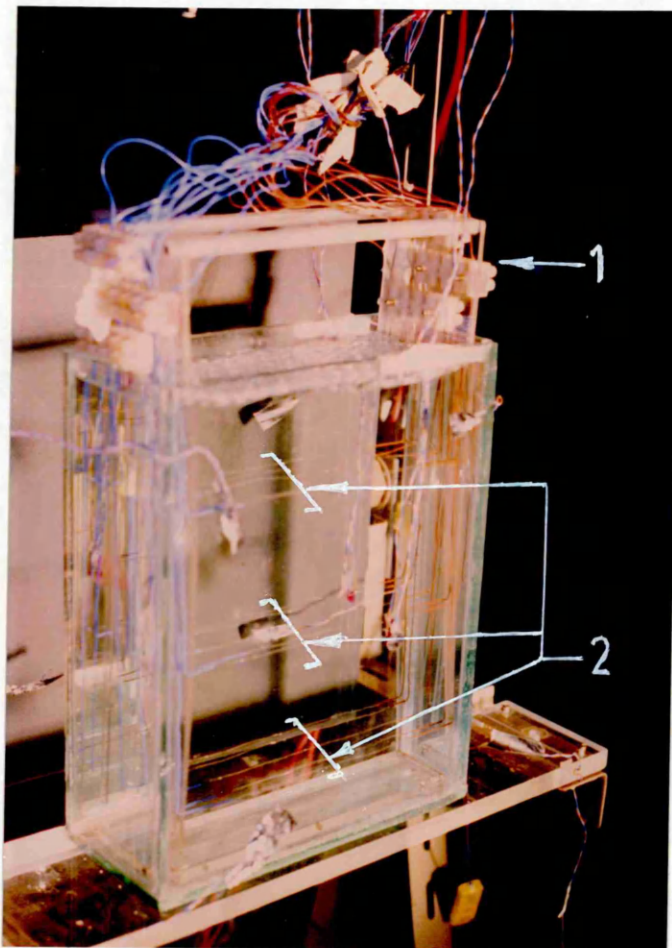


Figure 2.12 The Small Transwall Module on a Handy Angle frame, with the thermocouple grid support, (1). Position (2) shows three horizontal planes of five thermocouple rows.

the glass and secured by silicon adhesive. The coil length is 5 mm and the 50 to 1 ratio of length to diameter minimises conduction errors. The water temperature is measured by a grid of 15 thermocouples (section 2.5.2(b)).

(b) Irradiation and Temperature Measurements

The small transwall module was irradiated by the solar simulator operating at 120 volts, for 2 hours, and the solar irradiation was measured by a Kipp and Zonen CM3 solarimeter connected to a 7045 Solartron digital multimeter. The solarimeter dome was placed 3 cm behind the module.

Chromel-alumel thermocouples were used to measure water and glass temperatures within the small cell. These were mounted in a grid support and arranged in three horizontal planes of five thermocouple rows from front to rear end of the support, Figure 2.12. The front row thermocouples were about 1.6 mm from the interior face of the front transwall glass while the back row thermocouples were about 5 mm from the interior face of the rear glass. Each row is formed by stretching the thermocouple wires between the grid supports so that the hot junctions are central. The grid support system is used because it keeps the thermocouples in the same position and hence makes it easiest to locate. Chromel-alumel thermocouples, diameter 0.2 mm, were preferred to the more stable

copper-constantan variety because of their superior strength. The chromel-alumel thermocouples were calibrated against a platinum resistance thermometer coupled to a 6 decade AC Bridge. Details are given in Appendix D. The results showed that the transwall temperatures were measured to within $\pm 0.15^{\circ}\text{C}$, which is reasonable for the chromel-alumel thermocouples used.

(c) Absorption Measurement.

A difference was found between the measured transmission through the small transwall and that predicted from the spectral extinction coefficients measured by the spectrophotometer, a Perkin-Elmer Lambda 9 UV/VIS/NIR, of the Chemistry Department at Glasgow University.

Initially, this was thought due to difficulty in measuring the absorption of the glass and/or dye and/or water. In addition, the extinction coefficients of the original glass was in doubt because it was not certain that the glass was truly of Pilkington manufacturer as requested on the order. Another cell was constructed with off-cuts provided so that the extinction coefficients could be measured. However, careful rechecking (Appendix B) improved the value of various extinction coefficients, but a difference of 13% in transmission still remained. Examination then turned to the spectrum of the solar simulator and its variation with voltage.

Table 2.1 Fractional Energies in wavebands for Solar Simulator Lamp Spectrum at 120V compared to Air Mass 2 Fractional Energies in same wavebands.

Waveband (μm)	Fraction Energy Solar Simulator Lamp Spectrum	Fraction Energy Air Mass 2
0.3 - 0.35	0.001	0.007
0.35 - 0.4	0.008	0.024
0.4 - 0.6	0.265	0.282
0.6 - 0.75	0.349	0.218
0.75 - 0.9	0.162	0.140
0.9 - 1.2	0.098	0.146
1.2 - 2.1	0.117	0.146
2.1 - 4.1	0.0	0.040

The fractional energies in the 8 wavebands 0.3 - 4.1 μm , Table 2.1, above, emitted by the solar^{simulator} at 120 volts were calculated using the spectrum of the ELH 120 volts, 300 watt lamps, supplied by the manufacturer, Thorn Lighting Limited. Lanarkshire, U.K.. The plot points from the Thorn ENX-1 curve claimed to be "theoretically very similar" to the ELH lamp [Thorn Ltd], are shown in Fig. 2.13(a) superimposed on the NASA curves by Yass et al. and gave good agreement. However, the manufacturer's claim that the curve is bell-shaped stopping at 1 micron is clearly incorrect. Figure 2.13 (b) shows the curve, an 82C, 360W ENX-1 supplied by the manufacturer.

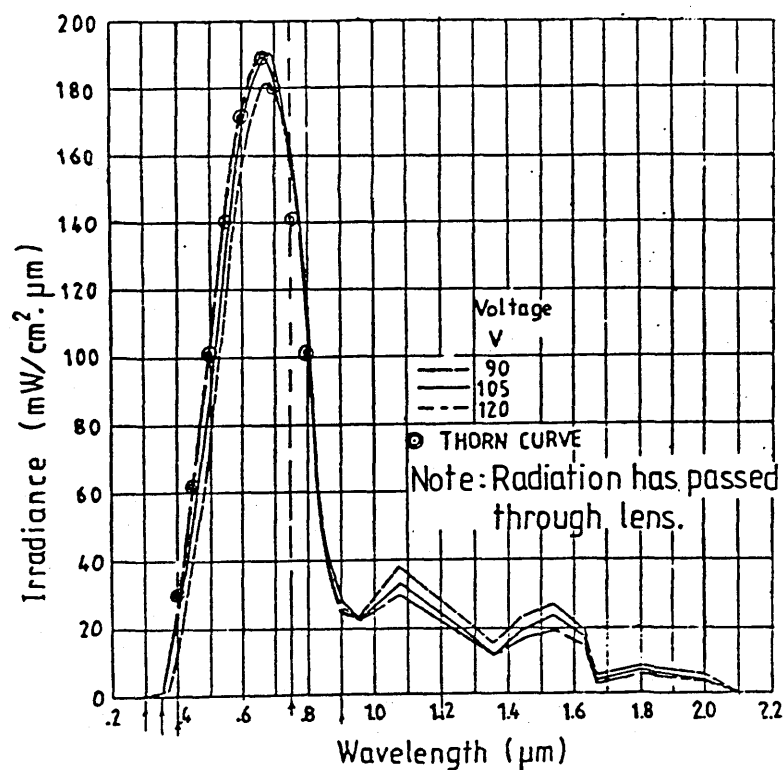


Figure 2.13(a) The THORN curve superimposed on the NASA curves by Yass et al., 1974.

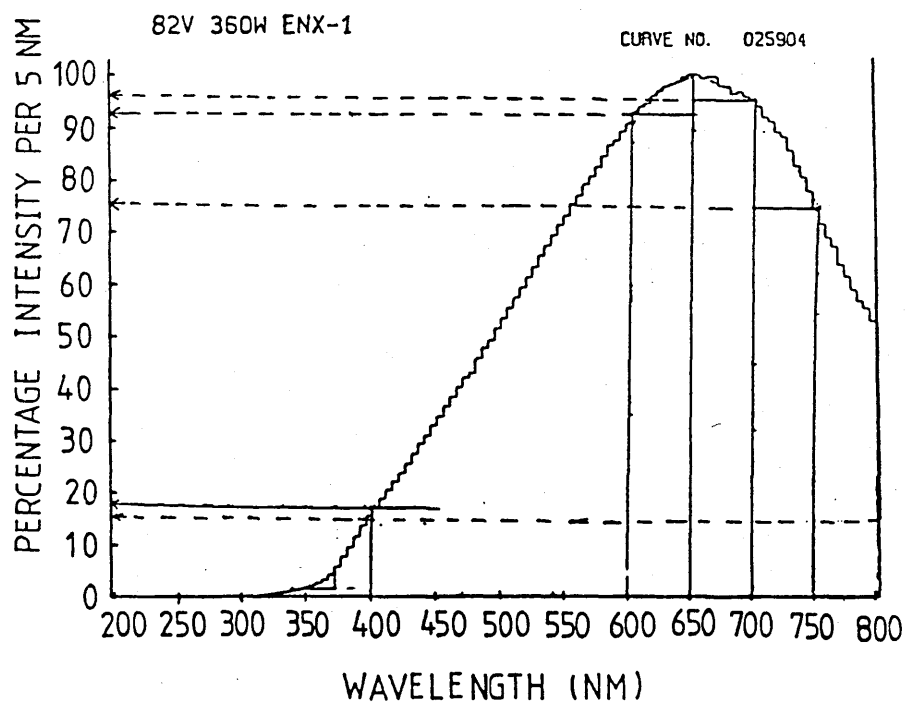


Figure 2.13(b) An 82V 360W ENX-1 spectral irradiance curve for the Solar Simulator lamp spectrum [Thorn Ltd, 1988].

The fractional energy in the wavebands are shown in Table 2.1 together with A.M.2 fractional for solar irradiation in Glasgow calculated by Greveniotis, 1986. The disparity is clear. When the absorption of irradiation within the small transwall module was calculated using the new values of the solar simulator fractional waveband energies, and the extinction coefficients calculated from the glass, water, water/dye transmission curves (Appendix B), the measured transmission and that predicted differed by 3% for clear water, and 2% for Lissamine Red 3GX water/dye solution.

A problem remained in that better results are achieved with higher lamp voltages and this shortens the life of the bulbs which cost around £11 each and 12 bulbs are involved. Uniform irradiation over a larger area would be obtained by adding another 5 bulbs with their fresnel lenses [43], but the cost in bulb replacement will be considerable, and increasing the number of bulbs increases the probability of a run being aborted because of a bulb failure. A substantial increase in the simulator working area will require a new lamp system.

(d) Heat Transfer Coefficients; Module/Laboratory

The one-dimensional computer models require the values for the heat transfer coefficients between the front and back module surfaces and the room. These were calculated from a cooling test.

The module was irradiated for 2 hrs by the solar simulator at 120 V, and then allowed to cool without irradiation for 2 hours with only the surface under test (front or rear surface) uninsulated. The sides, bottom, top and one surface of the module had increased insulation. A variation was to have the free water surface (top) uninsulated together with the module surface being tested. The sides, the bottom and the module surfaces were insulated by a 5 cm thick polystyrene, and the top end or free water surface was insulated by a double layer of plastic bubble film. Stable ambient temperatures were maintained by the laboratory cooling system, a chiller unit over which is blown a vigorous air flow.

The experimental values of the calculated heat transfer coefficients are shown in Table 2.2. An average value of the combined heat transfer coefficient of $11.8 \text{ W/(m}^2\text{.K)}$ was found for both the front and rear surfaces to room. When the top free surface was uninsulated during the cooling test, a much higher average value of $16.4 \text{ W/(m}^2\text{.K)}$ was found.

Table 2.2 Experimental Measurements of the Combined Convection and Radiation Heat Transfer Coefficient, h , for a Small Transwall Module, Surface to Laboratory Ambient. :

Condition of Heat Loss Test	Period of Cooling Test Hr	h (Average) $W/(m^2K)$	
Heat Loss through the Front Face	2	12.2	} 11.8
Heat Loss through the Rear Face	2	11.5	
Heat Loss through the Front Face and the Top End	$\frac{1}{2}$	15.5	} 16.4
Heat Loss through the Rear Face and the Top End	1	17.3	

2.6 Ambient Temperature Variations

Various attempts were made to reduce temperature variations in the small transwall environment in the laboratory. The solar simulator generates 3.6 KW of power in the laboratory which is countered by the laboratory cooling system consisting of a chiller unit supplying a cold air flow. An on/off thermostat system copes inadequately with the room temperature after about 60 minutes but it was too costly to replace it. The air flow produces eddies and consequent temperature fluctuations at the transwall module. Screens were erected at each side of the solar simulator which reduced these fluctuations by a factor of 3. The long term solution will be to partition the laboratory and isolate the simulator behind a glass screen. Figure 2.14 shows the average ambient temperature difference between start and finish for a 2-hour run, before the screens were erected (Curve 1), and after the use of screens (Curve 2).

The improvement can be clearly seen in Curve 2. However, a scatter of ambient temperature values from the start to the end of a run still remained. The shielded ambient temperature thermocouples, 4 close to each face of the small transwall, placed near each corner so that they do not interfere with the solar simulator beam irradiation, were recording different values of the ambient temperature. Consequently it was uncertain how to combine the reading to give the true

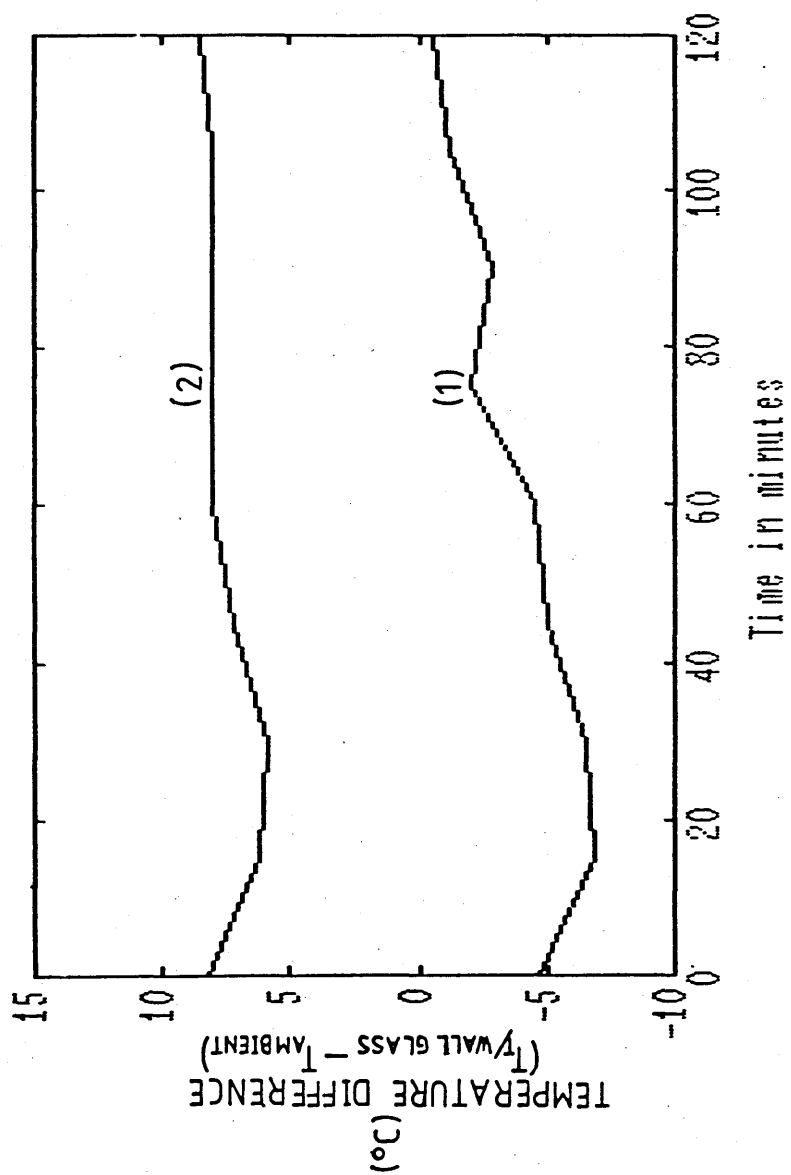


Figure 2.14 The average ambient temperature differences from transwall glass before the use of screens, Curve(1), and after the screens were employed, Curve (2).

ambient temperatures. An average of these values was taken, and the computer models were evaluated at the lowest minimum value possible, $T_a, \text{min.}$, and at the highest maximum value possible, $T_a, \text{max.}$ Clearly, the true curve lies in between the two extremes. The computer model 1 was not evaluated using this approach.

2.7 Comparison: Experiment With the Computer Models.

The temperature distribution in the small transwall module was measured (Section 2.5.2(b)) and compared with predicted values for three computer models using clear water, and a water/dye solution (20 ppm Lissamine Red 3GX). The computer models differ from each other by the way in which either a glass slab or a water slab, and/or both glass and water slabs were divided.

The experimental start temperatures, top to bottom, were fairly uniform. The mean vertical temperature gradient for water inside the transwall was about 0.50°C at the start, and about 2.5°C at the end of a 2-hour run. Therefore, the middle plane thermocouples were chosen to represent the average temperature of the small transwall module, and hence used to test the computer models discussed in Sections 2.7.1 - 2.7.3.

2.7.1 Computer Model 1 - Comparison with Experiment

The slab divisions for Model 1 are shown below. The model assumes that the glass slab thickness of about 6

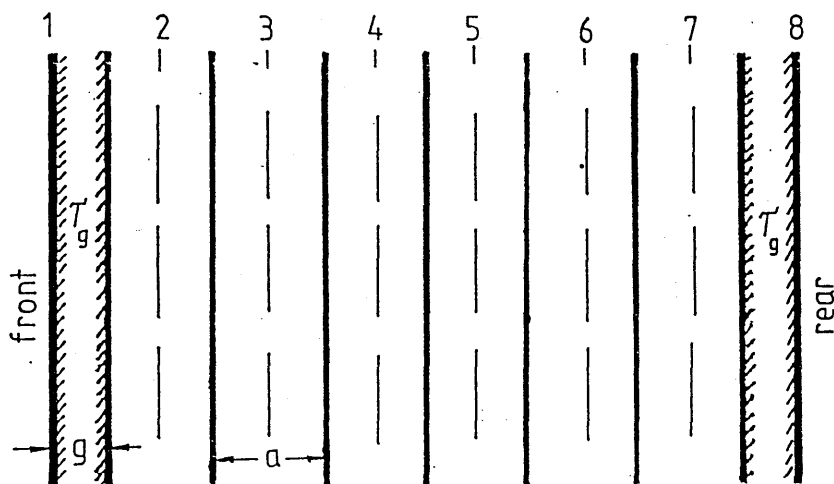


Figure 2.15 $g = 6 \text{ mm}$ and $a = 12.5 \text{ mm}$

mm is half the size of the water slab thickness, 12.5 mm. In all, there are 6 full water slabs, and 2 glass slabs.

The plots of the computer Model 1 and experiment are shown in Figures 2.16(a) - 2.16(d) for both clear water and a water/dye solution, a 20 ppm Lissamine Red 3GX. Figures 2.16(c) and 2.16(d) show the cases for clear water when the effective conductivity factor given by the Nusselt number, Nu , was kept constant, and also when it was allowed to vary according to the correlation given by McGregor and Emery [30], respectively. The Nusselt number was constant at 9.2 and allowed to vary, ranging from 8.9 to 9.4 for clear water, and from 9.4 to 9.8 for Lissamine Red 3GX. Clearly, the effective conductivity is fairly constant, and thus its sensitivity does not play a role here. The computer model 1 overpredicts the mean temperature rise by 12%

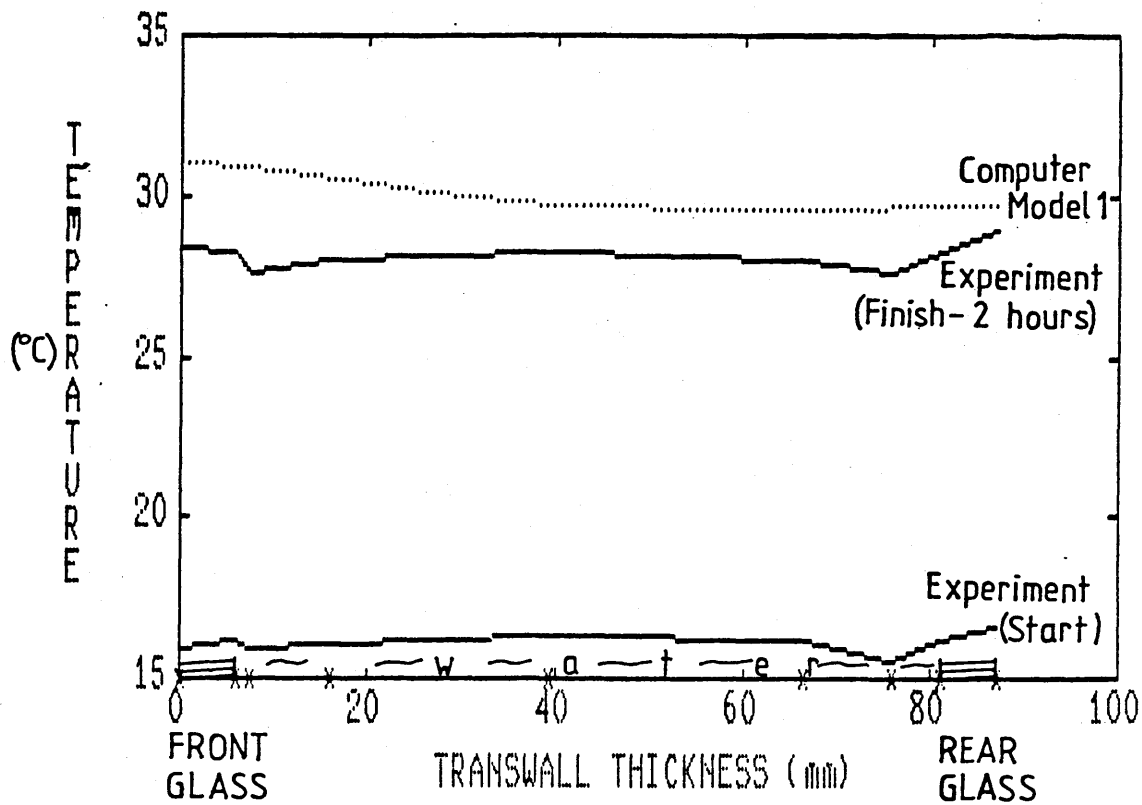


Figure 2.16(a) The temperature profiles for clear water with effective conductivity factor constant, i.e. $Nu = 9.2$.

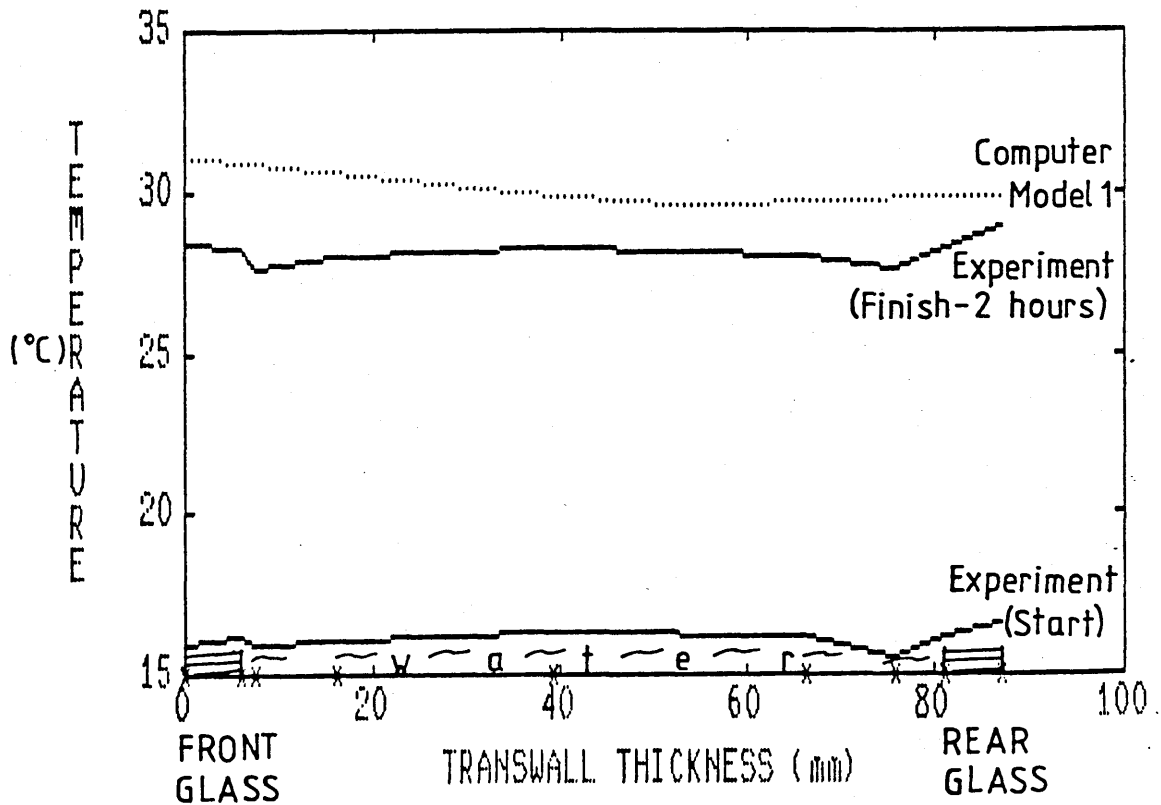


Figure 2.16(b) The temperature profiles for clear water with effective conductivity factor, ecf, varying from 8.9 to 9.4. The ecf varies according to the correlation given by MacGregor et al. [30].

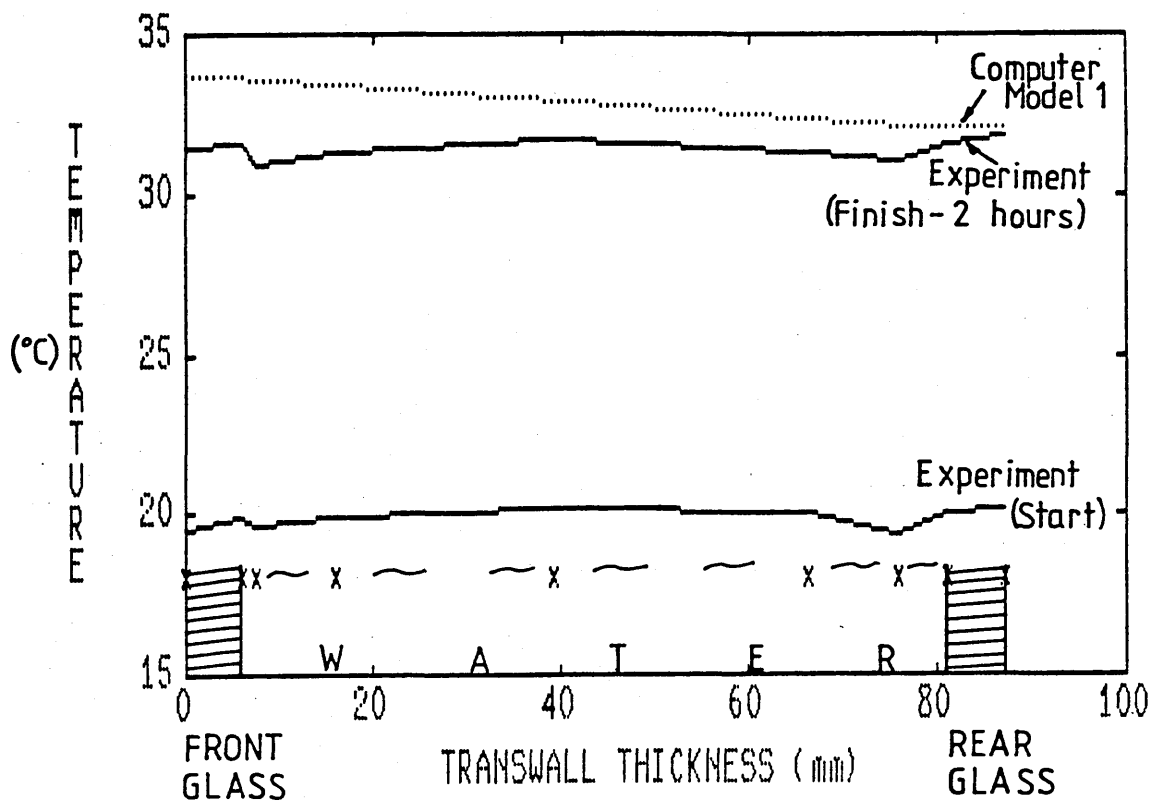


Figure 2.16(c) The temperature profiles for a water-dye, 20 ppm Lissamine Red BGX, with constant effective conductivity factor, i.e. $Nu = 9.2$.

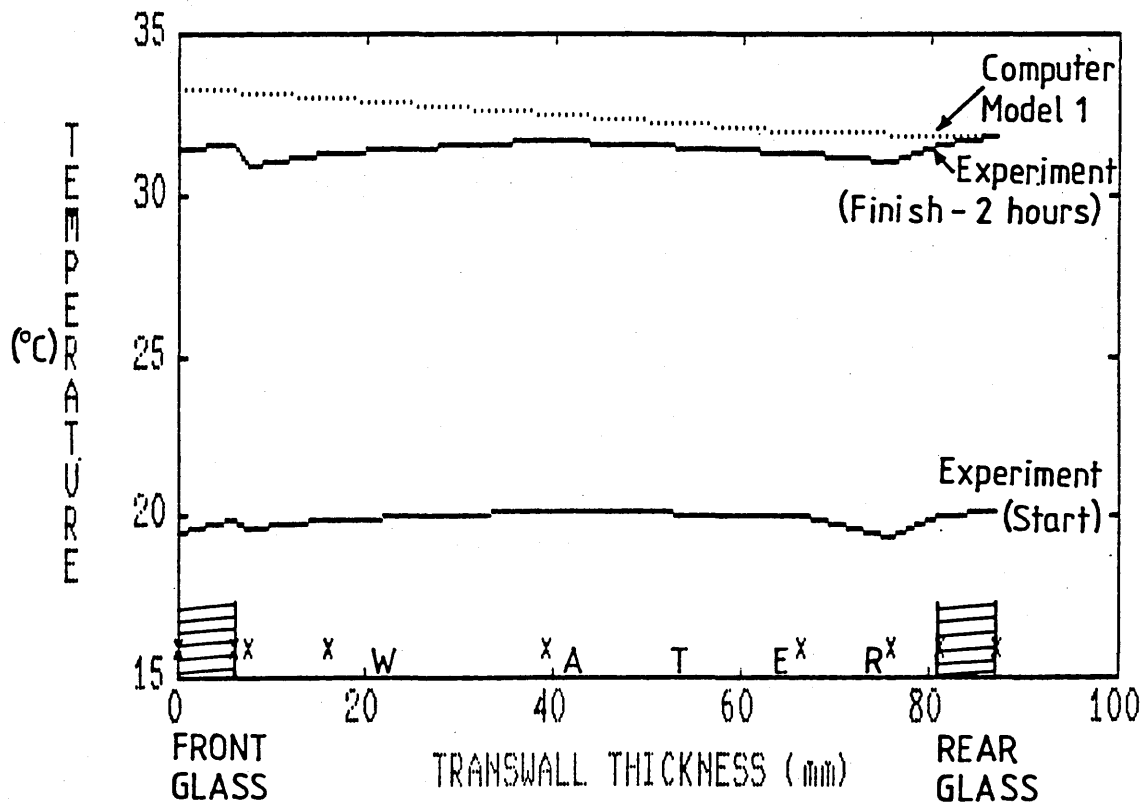


Figure 2.16(d) The temperature profiles for a water-dye, 20 ppm LR3GX, with effective conductivity factor varying from 9.4 to 9.8. The ecf varies according to the correlation given by MacGregor et al. [30]

for clear water, and by 6% for Lissamine Red 3GX.

The shapes of both curves (water and water/dye) do not resemble the experimental curve at the glass ends, but merely flatten out in a straight line. The behaviour of the computer model at the glass ends is considered important in the analysis, because the glass surface temperature is a controlling factor in the heat release from the wall. It is thus concluded that the computer Model 1 does not adequately represent the phenomenon in the small transwall module.

2.7.2 Computer Model 2 - Comparison with Experiment

The Model 2 slab divisions are similar to those of Model 1, at least in the case of the glass slabs. The only difference is the water slab divisions as shown:-

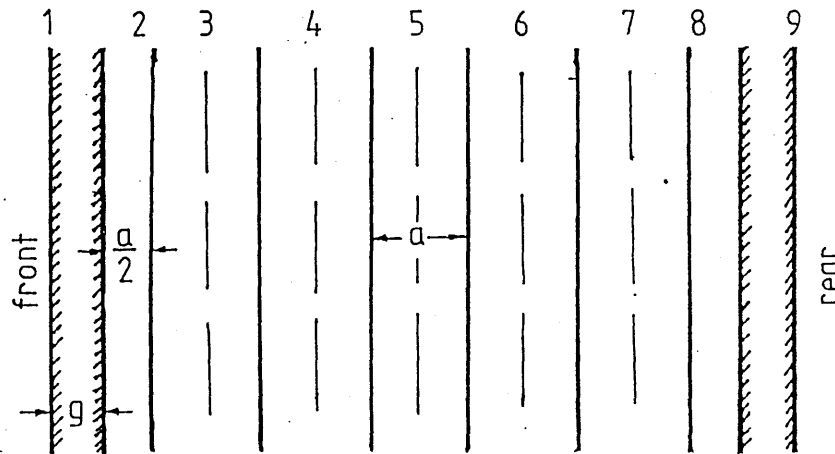


Figure 2.17 $g=6\text{ mm}$ and $a=12.5\text{ mm}$

The water slabs were divided into 1/2-water slabs, in the immediate glass/water interface vicinity, and 5 full water slabs in between. The computer Model 2

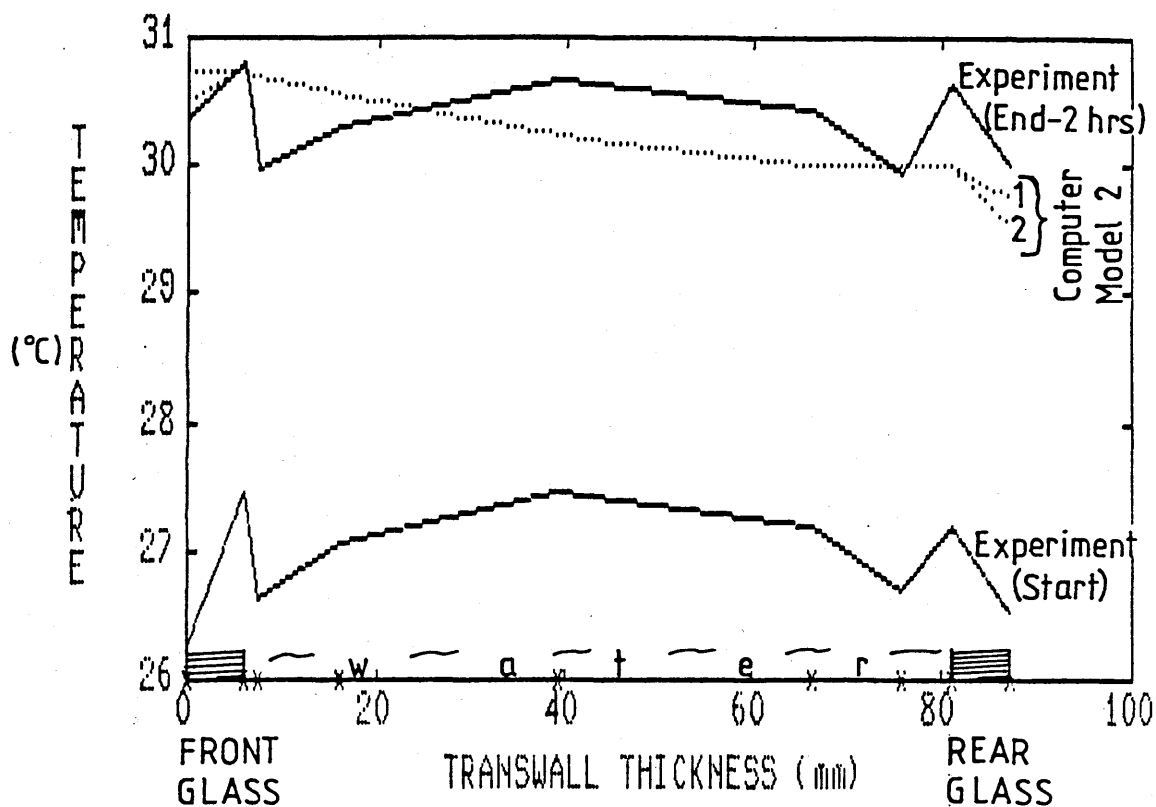


Figure 2.18(a) The temperature profiles for clear water with computer model 2, i.e. no boundary layer at the glass/water interface. The model was evaluated at $T_{a,max.}$, Curve(1), and at $T_{a,min.}$, Curve(2). (see section 2.6 for $T_{a,max.}$ & $T_{a,min.}$).

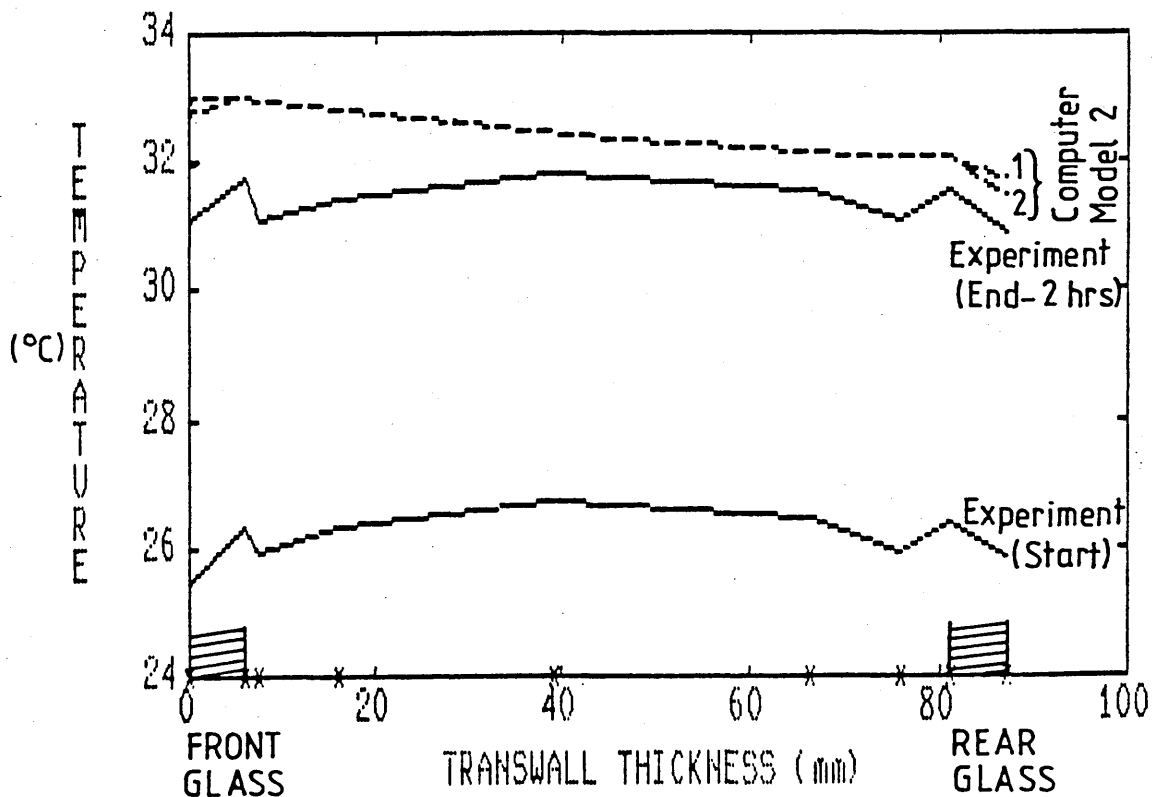


Figure 2.18(b) The temperature profiles for a 20 ppm LR3GX with computer model 2, i.e. no boundary layer at the glass/water interface. The model was evaluated at $T_{a,max.}$, Curve(1), and at $T_{a,min.}$, Curve(2). (see section 2.6 for $T_{a,max.}$ & $T_{a,min.}$).

assumed that there was no temperature drop between the glass and the bulk temperature of the water 1/2-slab. In reality, there is no temperature difference surface to water at the surface. However, there is a temperature difference between the surface and the fluid outside of the boundary layer.

The computer Model 2 was found to agree reasonably well with experiment for both clear water, (Figure 2.18 (a)), and 20 ppm Lissamine Red 3GX, (Figure 2.18(b)). The computer model underpredicts the mean water temperature rise of the small transwall by 15%, while it overpredicts the mean water/dye temperature rise by about 11%.

The shape of both curves resemble the experimental curve at the glass ends when the computer Model 2 was evaluated at $T_{a, \min}$. However, both curves deviate from the experimental curve at the front glass end when the model was evaluated at $T_{a, \max}$. The curves merely form a straight line.

2.7.3 Computer Model 3 - Comparison with Experiment.

The model treated each glass as a 1/2-slab and retained the 1/2-water slab in the immediate water/glass interface region (as in Model 2) together with 5 water full-slabs in between the 1/2-slabs. In total, this arrangement produced 4 glass half-slabs, 2 water half-slabs and 5 water full-slabs. The Model 3 replaced the boundary layer of Model 2 with surface

contact resistances at the glass/water boundary (at nodes 2,3. and 9,10 in the slab division arrangement below).

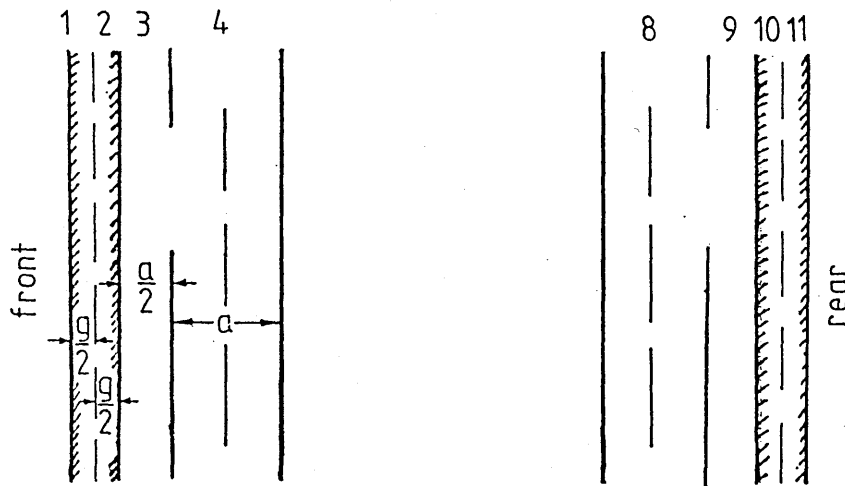


Figure 2.19

The plots of the computer Model 3 are shown in Figure 2.20(a), for clear water, and Figure 2.20(b), for 20 ppm Lissamine Red 3GX. The computer model agrees reasonably well with experiment for both water and dye. It underpredicts the mean water temperature rise by 18% when the model was evaluated at $T_{a, \text{min}}$, and only by 3% when it was evaluated at $T_{a, \text{max}}$. The true curve predicted by the model lies in between the two extremes. For the case of a water/dye solution, the computer model underpredicts the mean water/dye temperature rise by 16% when it was evaluated at $T_{a, \text{max}}$.

The shapes of both curves resemble their experimental counterparts at both glass ends. Because the small transwall is at a higher temperature than the surroundings it loses heat energy into the environment.

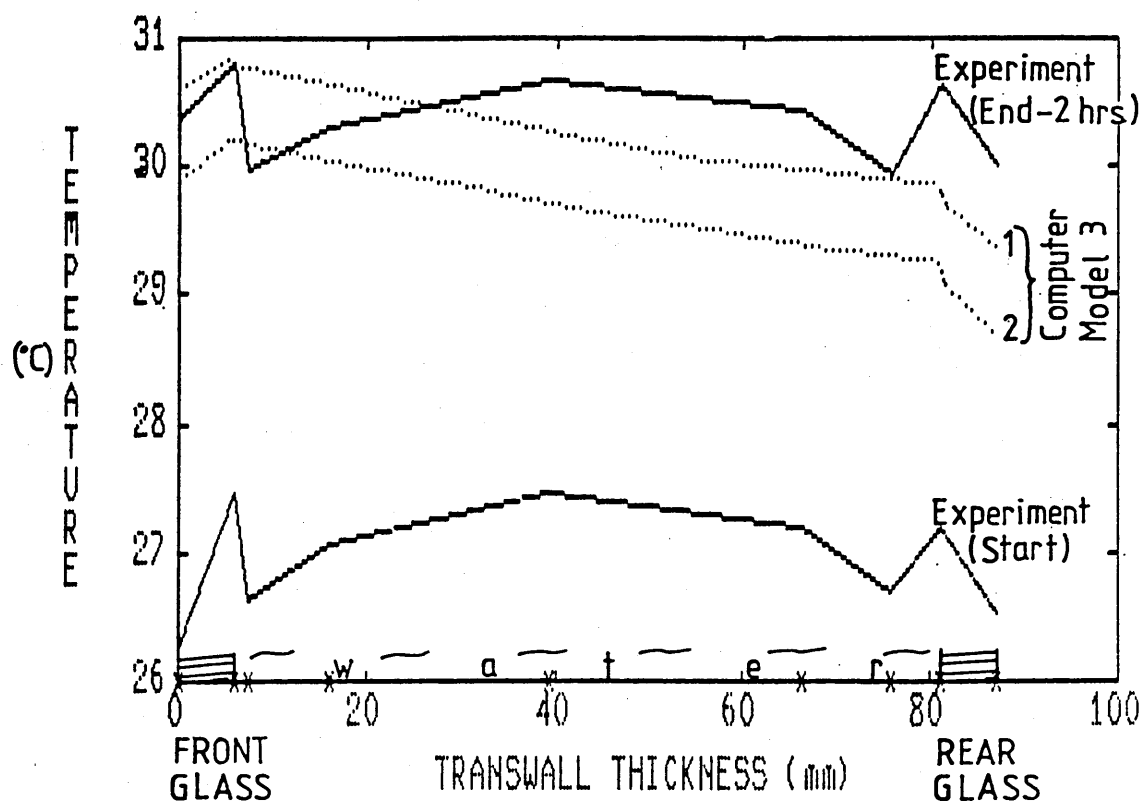


Figure 2.20(a) The temperature profiles for clear water with computer model 3, i.e. surface contact resistance model at the glass/water interface. The model was evaluated at $T_{a,max}$, Curve (1), and at $T_{a,min}$, Curve (2).

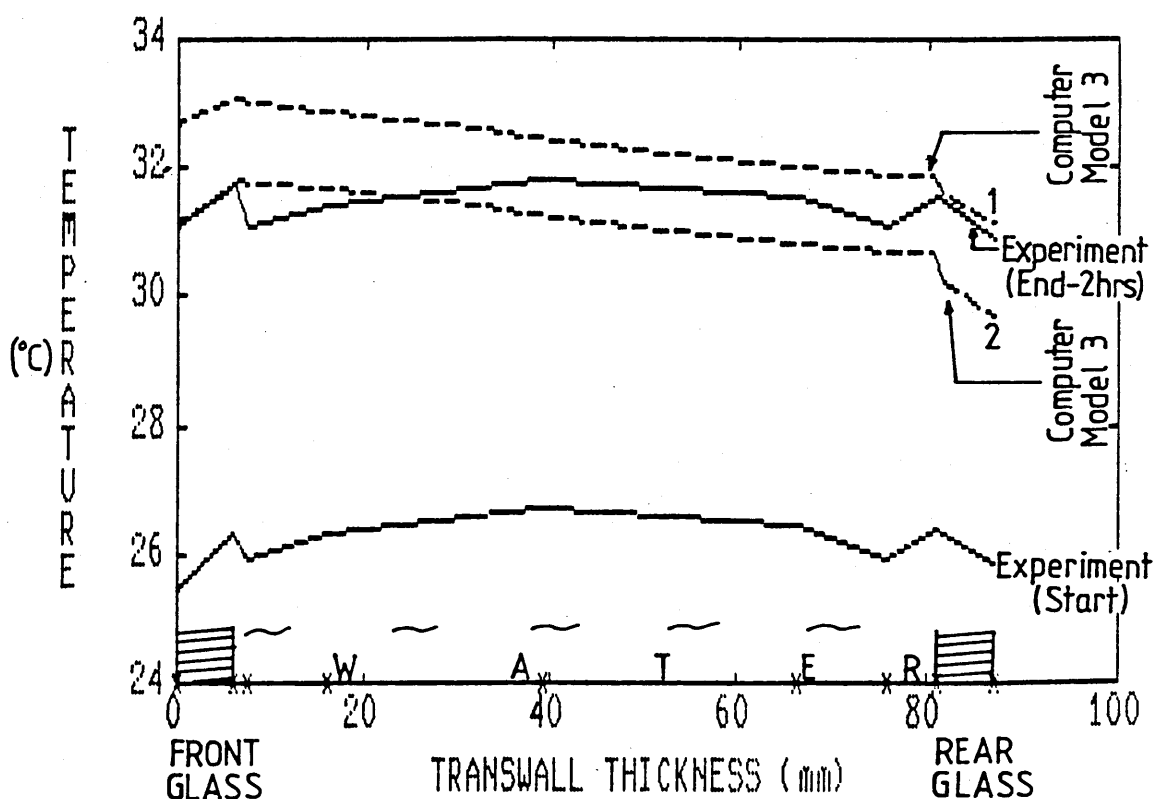


Figure 2.20(b) The temperature profiles for a 20 ppm Lissamine Red 3GX with computer model 3, i.e. surface contact resistance at glass/water interface. The model was evaluated at $T_{a,max}$, Curve (1), and at $T_{a,min}$, Curve (2).

This is clearly shown by the steep gradients from the inner glass to the outer glass ends of the experimental plots despite irradiation.

The computer Model 3 mimicks the experimental plots very well in this case. The Model, however, does not show the effect of surface contact resistance at the front glass/water interface as well as it does at the rear glass/water interface.

The computer Model 3 proved to be sensitive to the surface heat transfer coefficients, especially in the rear glass end of the small transwall module. The behaviour of the model is shown in Figure 2.20(c), for the case of clear water only. The surface heat transfer was made to vary according to the correlation suggested by Bayley et al. [41], (see Figure 2.20(c)), and kept constant at $50 \text{ W/(m}^2\text{.K)}$.

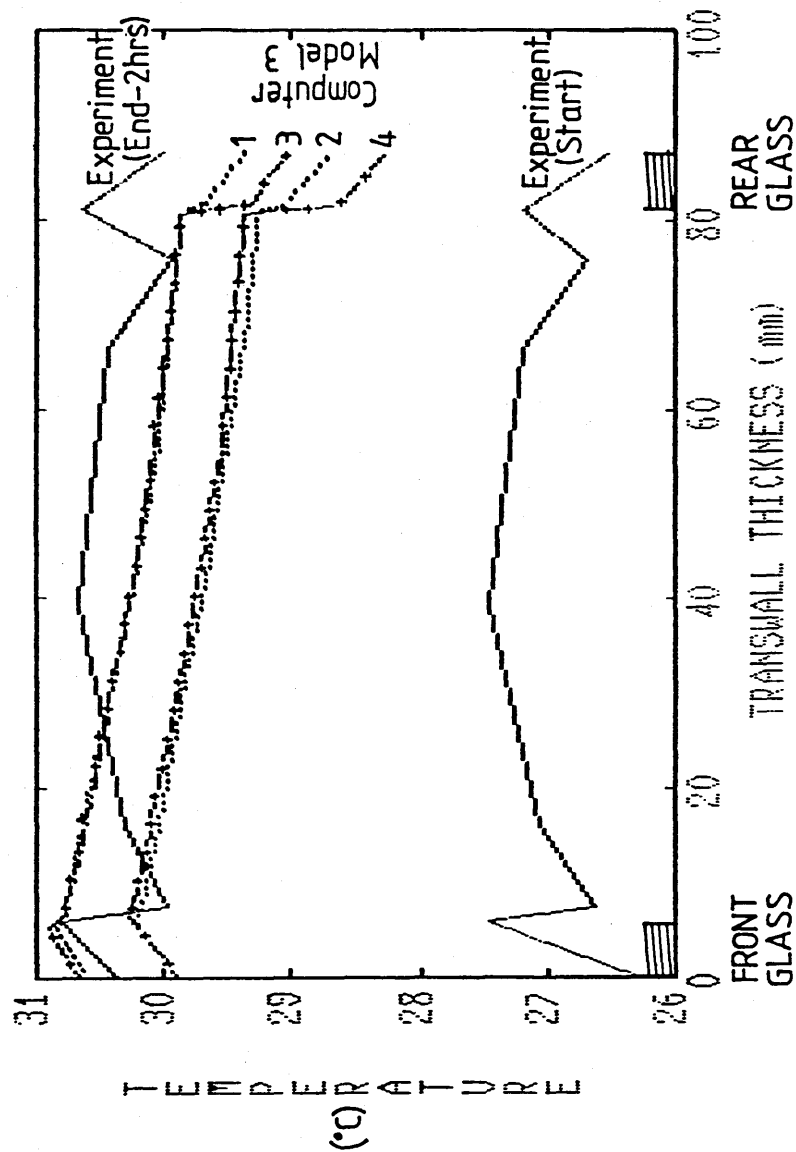


Figure 2.20(c) The computer model 3 is shown with the surface heat transfer coefficients constant, i.e. $h_c = h_{c0} = 50 \text{ W/m}^2\text{K}$, Curves (3) & (4), and with the s.h.t. coeffs varying according to the correlation by Bayley et al. [41], from $h_c = 174.3 - 191.4 \text{ W/(m}^2\text{K)}$ and $h_c = 171.5 - 153.9 \text{ W/(m}^2\text{K)}$ at T_a , min., Curve (2); & $h_c = 162.8 - 186.5 \text{ W/(m}^2\text{K)}$ and $h_c = 181.0 - 163.6 \text{ W/(m}^2\text{K)}$ at T_a , max., Curve (1).

2.8 Conclusion

The following conclusions were arrived at from the tests on the smaller transwall module.

- 1) The 3rd computer model is the best of the three. It can predict the mean temperature rise in the small transwall module to within a maximum error of 18%, and to within 13% based on mean ambient temperatures. Various reasons could be advanced for the modest discrepancy between the computed and the experimental values of the transwall temperature, aside from experimental errors and uncertainties. Clearly, the application of one-dimensional treatment to a three-dimensional problem is likely to produce error. The uncertainty in ambient temperatures and glass/air heat transfer coefficients compound this problem. Finally the water circulation, and its associated mass and heat transfer, is complex and difficult to model accurately by the concept of effective conductivity. It is contended that the loss in accuracy is more than compensated by the simplicity and utility of this model when compared to the complexity and computing power required to model transwall phenomena using the fundamental Patankar approach of volumetric balancing of mass, momentum, energy.

- 2) The experimental and theoretical transmissions through the smaller transwall module agree. It is important that due account be taken of the spectral energy distribution of the simulator lamps and its dependence on voltage.
- 3) The laboratory temperature requires better control, such as isolating the simulator cooling system from the transwall environment.

Chapter 3

Chapter 3

The Development and Validation of the Two-Dimensional Computer Model of the Transwall.

3.1 Introduction.

The chapter gives an outline of a two-dimensional computer model of the absorption in a transwall developed by Greveniotis [20]. This is followed by a detailed development of the modification necessary to this model, and then the two-dimensional temperature prediction program employing the finite difference method and effective conductivities is presented. The solar test cell and apparatus used in the model validation are described. The chapter is closed by discussing a comparison between experimental results and those predicted by the two-dimensional computer model of the temperature distribution within the transwall.

A crucial factor in analyzing radiation induced thermal stratification in water is the direction in which the water is irradiated. If the water is in the form of a pond, say a roof pond, and irradiated from overhead by the sun then the temperature distribution can be found by performing a one-dimensional finite difference analysis, using effective conductivity ($Nu=5$) and volumetric spectral absorption, to give a good match with experiment [44]. In this case the water is stably stratified.

The warmer water settles on top and there is no

drive mechanism to displace it. However, in the case of the transwall the water is irradiated from the side and buoyancy forces cause a flow up the irradiated wall, which must be replaced by cooler water from the bottom which has (mostly) flowed down the cooler rear wall. Thus the degree of stratification is compounded by circulation, and in turn as the temperature stratification increases then there is probably a reduction in circulation.

Because the finite difference method with effective conductivity had been so successful in predicting the roof pond temperature gradient it was thought that it might, with modification, be capable of reflecting the vertical transwall temperature distribution. Factors affecting vertical temperature differences which can be accommodated by this two-dimensional treatment are:-

- (a) varying the effective conductivity in the horizontal and vertical planes;
- (b) allowing for heat transfer across the upper and lower horizontal surfaces;
- (c) varying the air boundary layer thickness on the glass walls and therefore the heat transfer;
- (d) finally incorporating the vertical test cell temperature distribution into the program.

Measured vertical temperature distributions in the transwall are only 2 to 4°C/m, and consequently it was thought that the above factors could produce a temperature gradient of this magnitude although the shape of the gradient might differ.

3. The Two-Dimensional Absorption Analysis Greveniotis' Computer Model

3.2.1 Introduction

The role of volumetric irradiation absorption in determining the temperature distribution within the transwall has been established in Chapter 2.

The computer model accepts that shading within and without the transwall occurs and sets about calculating absorption in the various volumes into which the transwall is divided. Obviously the choice of volumes is dependent on the model chosen for the temperature distribution. This had not been determined when Greveniotis developed his program and consequently modifications were required. The transwall is taken to be long and the method is strictly two-dimensional i.e. the absorption is allowed to vary in the x-y plane, but uniform in the z-direction. The three-dimensional nature of beam irradiation is retained. The orientation of the transwall is due south (MERA situation), and hence in applying the equations in other orientations the wall azimuth angle, a_w , is deducted from the solar azimuth, a_s , term, i.e. replace $\cos a_s$ with $\cos (a_s - a_w)$.

3.2.2 Refractive Altitude and Azimuth Angles.

The incident ray is bent within a transwall, and the altitude and solar azimuth angles calculated in air do

not apply. It is necessary, therefore, to calculate "effective altitude and solar azimuth angles" for each material of different refractive index. The refracted solar azimuth and altitude angles are used when calculating shadow factors and acceptance factors, defined later, because it is important to determine where the limiting beam vector strikes the horizontal and vertical planes of the various slabs. It is important to note that the incident and refracted rays lie in the same plane. The refractive solar azimuth angle, a_{sr} , is given as:-

$$a_{sr} = \tan^{-1} (\tan r \cos \theta),$$

and the refracted altitude angle, α_r , is given as

$$\alpha_r = \sin^{-1} (\sin r \cos \theta)$$

where r = refractive angle

θ = inclination angle of the incident plane.

Details are given in Appendix E1.

3.2.3 Lid Shading and Reflections at the Bottom Glass (Base).

The inner glass slabs will, in addition to receiving beam irradiation directly, have their upper slabs shaded by the lid and their lower slabs irradiated by reflected irradiation from below (Appendix E) as shown in Figure 3.1(a). In the case of a MERA transwall, only the top 1/2 slabs of the 5 slabs vertical, Figure 3.1 (b), will be in shadow for latitude 56° . The limited height to receive irradiation reflected from the glass/air

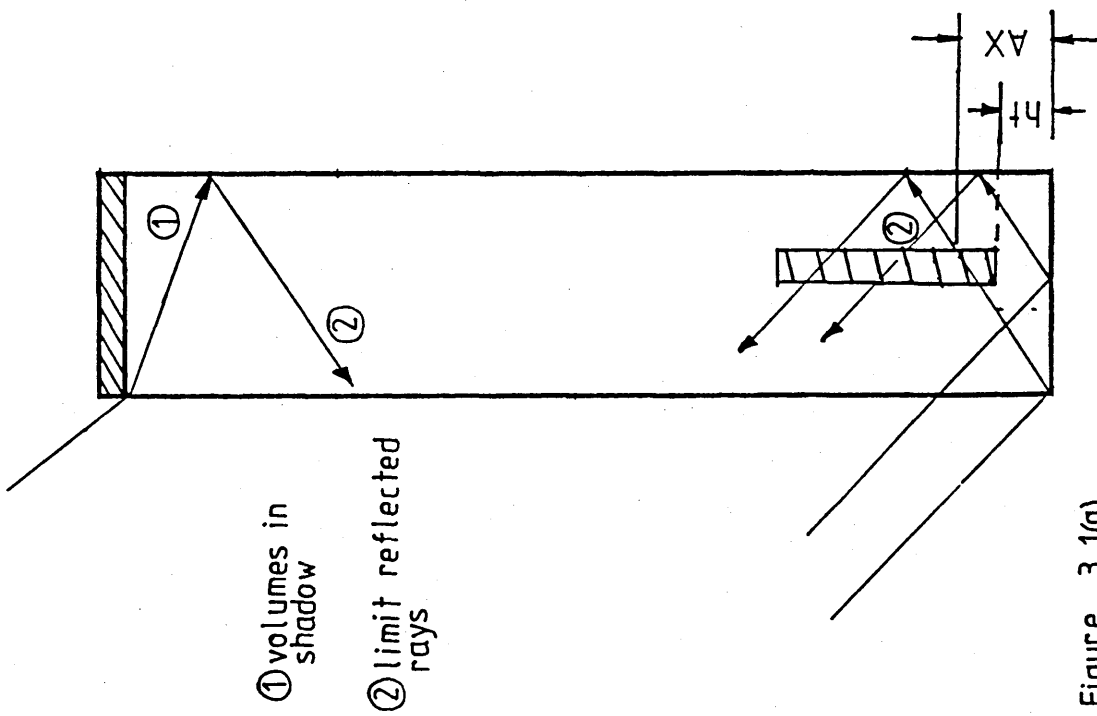


Figure 3.1(a)

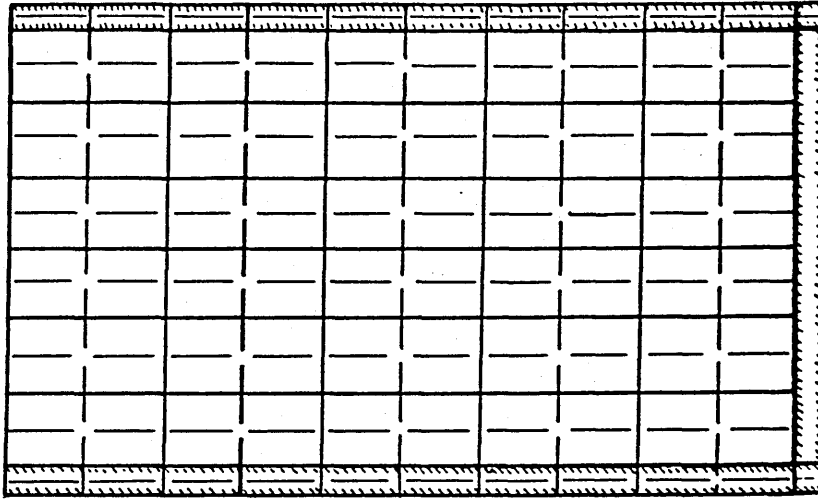


Figure 3.1(b) Transwall Slab Arrangement.

interface at the bottom is given by:-

$$AX = t_w \frac{\tan \alpha_{r2}}{\cos a_{sr2}}, \quad (\text{Appendix E2})$$

where t_w = water thickness

α_{r2} = altitude of refracted ray

a_{sr2} = solar azimuth angle of refracted ray.

An Acceptance Factor, $AF(j)$, is defined so that for slabs completely above the limiting ray i.e. ht. greater than AX , then $AF(j)$ is zero; for slabs completely below, $AF(j)$ equals unity; and for the slab hit by the limiting ray, $AF(j)$ varies between zero and unity, i.e. (0-1).

3.2.4 Beam Irradiation

In calculating beam irradiation, each volume of the transwall has to be associated with its own shading and acceptance factors (Appendix E3). The shadow factors for beam irradiation are considered as follows: if the slab does not receive any irradiation reflected or otherwise, the shadow factor, SF , equals zero; if all of the slab receives reflected irradiation, the shadow factor equals unity; and if part of the slab receives irradiation, the shadow factor varies from zero to unity (0-1). Acceptance factors have a similar role to shadow factors where reflected rays are involved. Only one reflection is considered because the energy in a double reflection is small and the slight increase in accuracy

does not justify the extra complication.

3.2.5 Diffuse Irradiation.

The following assumptions apply when treating diffuse irradiation:-

- i) The path lengths are all appropriate to an effective incidence angle of 60° as suggested by Beckman and Brandemeuhl, 1980, [45].
- ii) No shadow factors are involved because irradiation is considered isotropic, but view factors are considered.

A problem arises in summing diffuse irradiation over the wavelengths and ^{waveband} intervals because reflected irradiation is composed of part beam part diffuse, and the fractional energy per waveband is different for both cases. This can be accomplished by fixing a ratio between beam and diffuse irradiation, IR , (see Appendix E4.1). In addition, the transwall will not see a complete quarter-sphere of the sky dome because of shading of the roof (see Appendix E4.2). The maximum effective sky dome angle, β , was measured to be 101° for the MERA transwall.

3.2.6 Treatment of Backward Irradiation from Room.

The room reflected irradiation onto the back of the transwall is small (measured circa 5%) of the incident irradiation on the front of the transwall so that the treatment assumes that the spectrum of room reflected

irradiation is that of diffuse irradiation and is simply added to the diffuse irradiation from the inner transwall glass/air interface.

3.2.7 Computer Program for Absorption.

The two-dimensional program developed by Greveniotis had to be modified in order to incorporate the surface contact resistance model (Section 2.2.1). First, it had to be translated from BASIC to FORTRAN with an intention to run it on the IBM PS Microcomputers. The translated version proved to be too big to run on the Mircrosoft FORTRAN compiler. The program was then extensively modified and is now running successfully on the Ryan-McFarland FORTRAN PS/2 Personal Systems, and on the VAX 750/VMS Mainframe computer.

Greveniotis' absorption model program divided the transwall into vertical and horizontal slabs. The horizontal direction glass slabs were each treated as a full slab, and the horizontal direction water slabs were divided into six equal full slabs. The vertical direction slabs were divided into five slabs, two equal half slabs at the top and bottom and four full slabs in between, Figure 3.2, Section 3.3.1. The 5-slab number was chosen as a compromise between accuracy and computer running time. Too many slabs, say 10, would produce more accurate results, but the computer running time would be substantial because of the increased number of equations.

The translated program was then incorporated into the two-dimensional explicit finite difference program employing the concept of effective conductivity to account for circulation within the transwall. The two-dimensional temperature subroutine was the simple model, Computer Model 1 (Section 2.5.1). When the program was run it was found to overpredict the temperature distribution in the transwall by about 30%. The temperature subroutine was then modified along the lines of Computer Model 3 (Section 2.5.3) to employ the model of surface contact resistance at the glass/water interface. This modification called upon the absorption subroutine program to be modified as well. The discussion that follows gives details of modifications to the absorption and temperature computer models of the transwall.

3.3 The Modification of the Computer Two-Dimensional Absorption Model of the Transwall.

3.3.1 Introduction

The computer two-dimensional absorption model was modified by treating each transwall glass plate as two half slabs, and also taking the water slabs in the vicinity of the glass/water interface as half slabs. The remaining water slabs were retained as full slabs. This slab arrangement shown in Figure 3.2. produced four

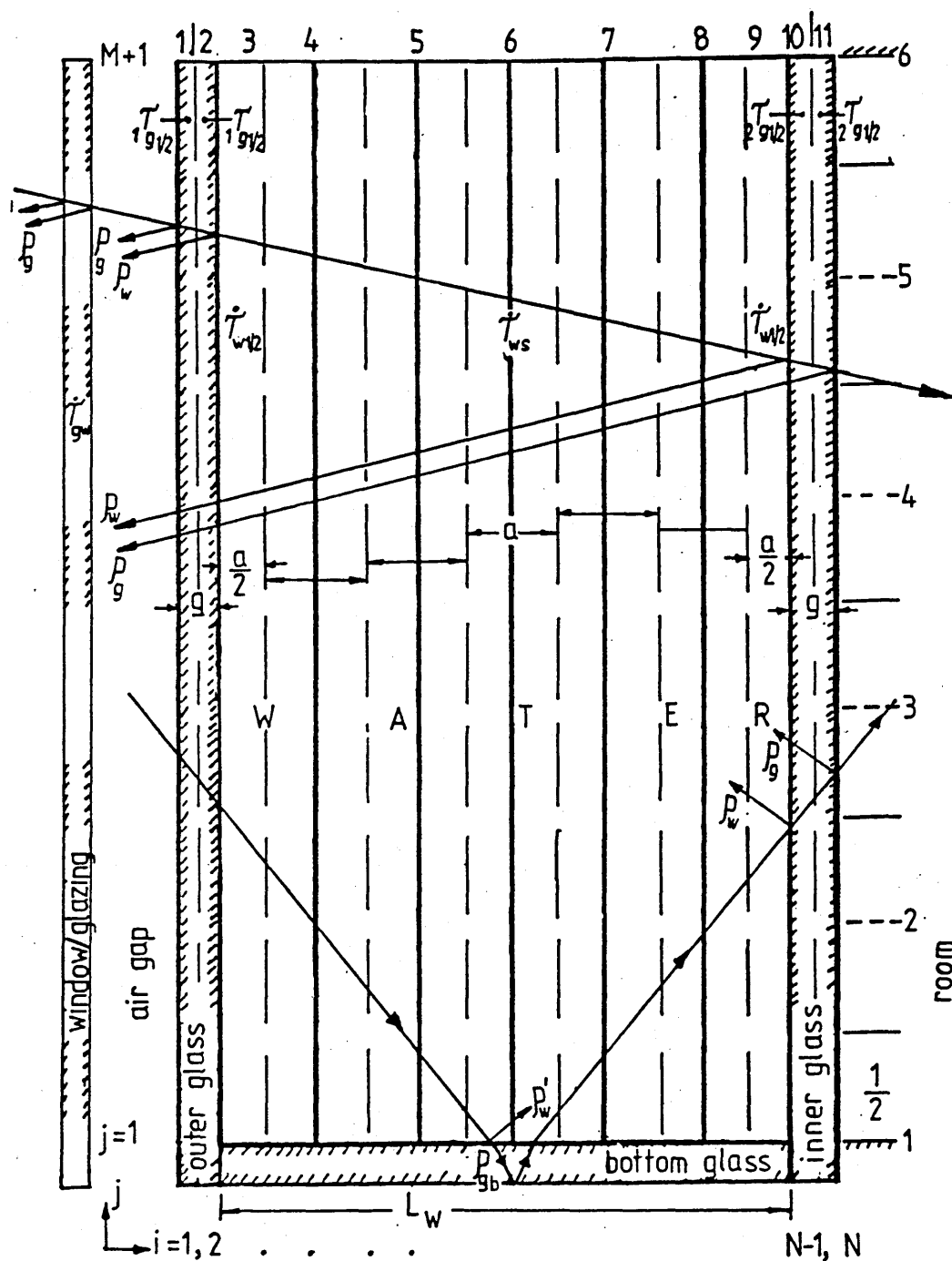


Figure 3.2 The Transwall Slab Arrangement for the Absorption Model

glass half-slabs, two water half-slabs and five water full-slabs, giving a total of 11 horizontal direction slabs. The vertical direction slabs were kept at 5, with half slabs on either end, top and bottom.

Consider the transwall horizontal and vertical direction slab divisions as shown in Figure 3.2. The shadow view and acceptance factors are incorporated according to the suggestions outlined in Greveniotis' model. The major changes considered here are those due to the attenuation of solar irradiation in the half-slabs of both glass and water materials. The treatment of irradiation through the five full water slabs is inevitably affected by the preceding alterations in the glass/water half-slabs.

3.3.2 Outer Glass Slabs (Window Side).

$$oI_b = (1-\rho_g)^2 \tau_{gw}$$

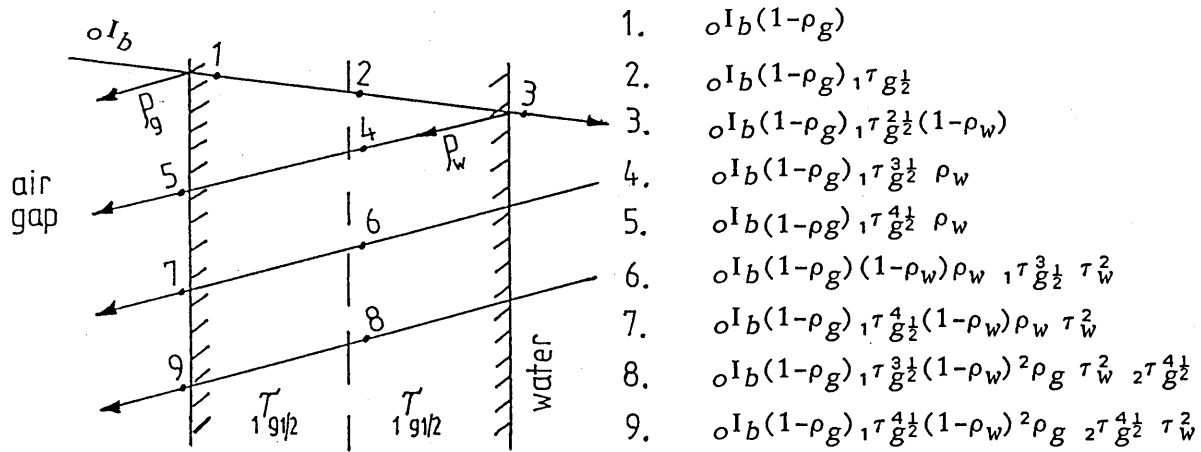


Figure 3.3 Outer glass $\frac{1}{2}$ -slabs, window side.

(a) Beam Irradiation Absorbed By 1st Outer Glass $\frac{1}{2}$ -Slab.

$$\left. \begin{array}{l} \text{Beam} \\ \text{absorbed} \end{array} \right\} = oI_b[(1-\rho_g)-(1-\rho_g)_1\tau_{g\frac{1}{2}}+(1-\rho_g)_1\tau_{g\frac{1}{2}}^3\rho_w(1-\tau_{g\frac{1}{2}})$$

$$+ SF_1(j) \times (1-\rho_g)_1\tau_{g\frac{1}{2}}^3(1-\rho_w)\rho_w\tau_w^2(1-\tau_{g\frac{1}{2}})$$

$$+ SF_1(j) \times (1-\rho_g)_1\tau_{g\frac{1}{2}}^3(1-\rho_w)^2\rho_g\tau_w^2_2\tau_{g\frac{1}{2}}^4(1-\tau_{g\frac{1}{2}})]$$

Rearranging,

$$\left. \begin{array}{l} \text{Beam} \\ \text{absorbed} \end{array} \right\} = oI_b(1-\rho_g)(1-\tau_{g\frac{1}{2}})[1+\tau_{g\frac{1}{2}}^3\{\rho_w+SF_1(j)\tau_w^2[\rho_w(1-\rho_w)$$

$$+\rho_g(1-\rho_w)^2_2\tau_{g\frac{1}{2}}^4]\}]$$

..... (3.1)

Similarly,

(b) Diffuse Irradiation Absorbed By 1st Outer Glass 1/2-Slab.

$$\left. \begin{array}{l} \text{Diffuse} \\ \text{absorbed} \end{array} \right\} = oI_d \times VF_1(j) (1-\rho_g)(1-\tau_{g\frac{1}{2}}) [1 + \tau_{g\frac{1}{2}}^3 \{ \rho_w + \tau_w^2 [\rho_w(1-\rho_w) + \rho_g(1-\rho_w)^2 \tau_{g\frac{1}{2}}^4] \}]$$

..... (3.2)

(c) Beam Irradiation Absorbed By 2nd Outer Glass 1/2-Slab.

$$\left. \begin{array}{l} \text{Beam} \\ \text{absorbed} \end{array} \right\} = oI_b [(1-\rho_g) \tau_{g\frac{1}{2}} - (1-\rho_g)(1-\rho_w) \tau_{g\frac{1}{2}}^2 - (1-\rho_g) \rho_w \tau_{g\frac{1}{2}}^3 + SF_1(j) \times (1-\rho_g) \tau_{g\frac{1}{2}}^3 (1-\rho_w) \rho_w \tau_w^2 (1-\tau_{g\frac{1}{2}}) + SF_1(j) \times (1-\rho_g) \tau_{g\frac{1}{2}}^3 (1-\rho_w)^2 \rho_g \tau_w^2 \tau_{g\frac{1}{2}}^4 (1-\tau_{g\frac{1}{2}})]$$

Rearranging,

$$\left. \begin{array}{l} \text{Beam} \\ \text{absorbed} \end{array} \right\} = oI_b (1-\rho_g) \tau_{g\frac{1}{2}} [1 - \tau_{g\frac{1}{2}} \{ (1-\rho_w) + \rho_w \tau_{g\frac{1}{2}} - SF_1(j) \times (1-\rho_w) \tau_w^2 (1-\tau_{g\frac{1}{2}}) [\rho_w + \rho_g(1-\rho_w) \tau_{g\frac{1}{2}}^4] \}]$$

..... (3.3)

Similarly,

(d) Diffuse Irradiation Absorbed By 2nd Outer Glass 1/2-Slab.

$$\left. \begin{array}{l} \text{Diffuse} \\ \text{absorbed} \end{array} \right\} = oI_d \times VF_1(j) \times (1-\rho_g) \tau_{g\frac{1}{2}} [1 - \tau_{g\frac{1}{2}} \{ (1-\rho_w) + \rho_w \tau_{g\frac{1}{2}} - (1-\rho_w) \tau_w^2 (1-\tau_{g\frac{1}{2}}) [\rho_w + \rho_g(1-\rho_w) \tau_{g\frac{1}{2}}^4] \}]$$

..... (3.4)

3.3.3 Inner Glass Slabs (Room side).

(i) The Reflection at the Bottom Glass (Base) End.

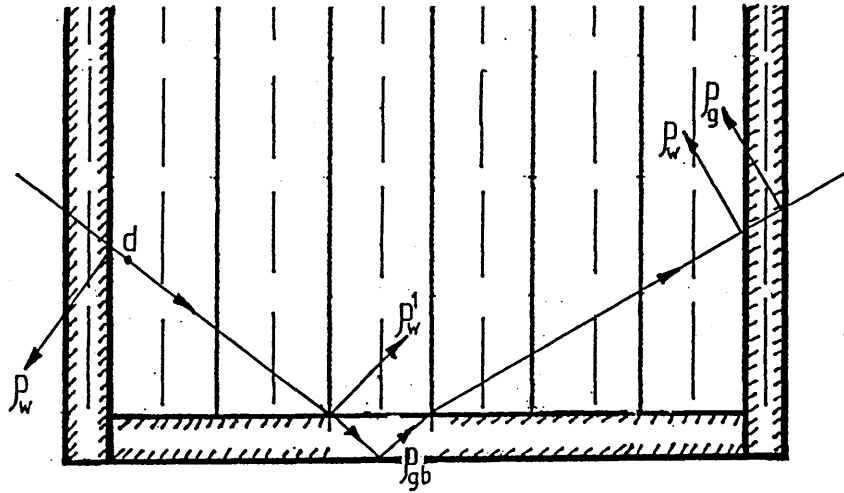


Figure 3.4 $d = \frac{I_b}{I_g} (1 - \rho_g) \frac{T_g^2 (1 - \rho_w)}{1 - \rho_w^2}$; $T_{wb} = e^{-K_w \rho_{wb}}$ & $T_{gb} = e^{-K_g \rho_{gb}}$

where ρ_{wb} = path length through water of reflected beam

ρ_{gb} = path length in bottom glass

(ii) let $c = d \tau_w$

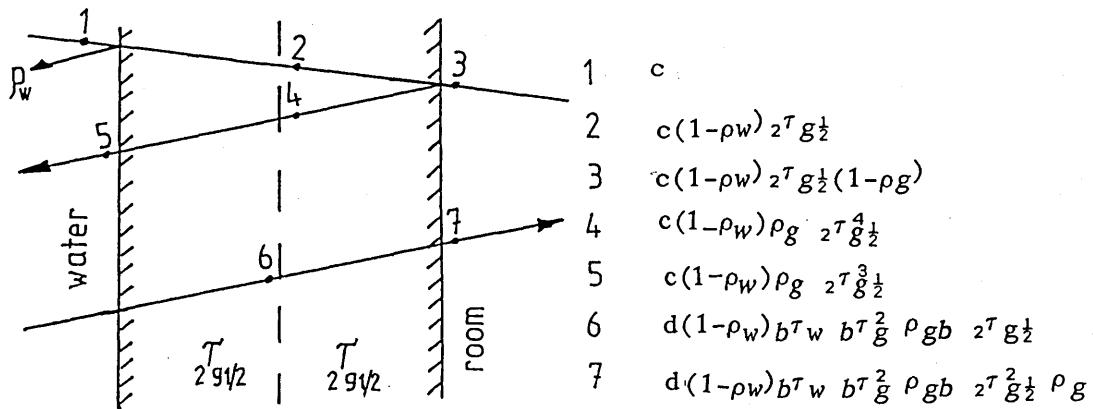


Figure 3.5 Inner glass $\frac{1}{2}$ -slabs, room side.

(a) Beam Irradiation Absorbed By 1st Inner Glass 1/2-Slab.

The reflected beam off the bottom is weak relative to the direct beam and the reflection, ρ_w^1 , Figure 3.4, is ignored.

$$\left. \begin{array}{l} \text{Beam} \\ \text{absorbed} \end{array} \right\} = oI_b [SF_2(j) \times (1-\rho_g)_1 \tau_{g\frac{1}{2}}^2 (1-\rho_w)^2 \tau_w \\ - SF_2(j) \times (1-\rho_g)_1 \tau_{g\frac{1}{2}}^2 (1-\rho_w)^2 \tau_w {}_2\tau_{g\frac{1}{2}} \\ + SF_2(j) \times (1-\rho_g)_1 \tau_{g\frac{1}{2}}^2 (1-\rho_w)^2 \rho_g \tau_w {}_2\tau_{g\frac{1}{2}}^3 (1-{}_2\tau_{g\frac{1}{2}}) \\ + AF(j) \times (1-\rho_g)_1 \tau_{g\frac{1}{2}}^2 (1-\rho_w)^2 b\tau_w b\tau_g^2 \rho_{gb} (1-{}_2\tau_{g\frac{1}{2}})]$$

Rearranging,

$$\left. \begin{array}{l} \text{Beam} \\ \text{absorbed} \end{array} \right\} = oI_b (1-\rho_g)_1 \tau_{g\frac{1}{2}}^2 (1-\rho_w)^2 (1-{}_2\tau_{g\frac{1}{2}}) [SF_2(j) \tau_w \{1+\rho_g {}_2\tau_{g\frac{1}{2}}^3\} \\ + AF(j) b\tau_w b\tau_g^2 \rho_{gb}] \\ \dots\dots\dots (3.5)$$

Similarly,

(b) Diffuse Irradiation Absorbed By 1st Inner Glass 1/2-Slab.

$$\left. \begin{array}{l} \text{Diffuse} \\ \text{absorbed} \end{array} \right\} = oI_d \times VF_2(j) \times (1-\rho_g)_1 \tau_{g\frac{1}{2}}^2 (1-\rho_w)^2 (1-{}_2\tau_{g\frac{1}{2}}) [\tau_w \\ \{1+\rho_g {}_2\tau_{g\frac{1}{2}}^3\} + AD(j) b\tau_w \rho_{gb} b\tau_{g\frac{1}{2}}^2] \\ \dots\dots\dots (3.6)$$

where $AD(j)$ = factor which is 1 for 1/2-slab.

(c) Beam Irradiation Absorbed By 2nd Inner Glass 1/2-Slab.

$$\begin{aligned}
 \left. \begin{array}{l} \text{Beam} \\ \text{absorbed} \end{array} \right\} &= oI_b [SF_2(j) \times (1-\rho_g) {}_1\tau_{g\frac{1}{2}}^2 (1-\rho_w)^2 {}_2\tau_{g\frac{1}{2}} \tau_w \\
 &\quad - SF_2(j) \times (1-\rho_g)^2 {}_1\tau_{g\frac{1}{2}}^2 (1-\rho_w)^2 \tau_w {}_2\tau_{g\frac{1}{2}}^2 \\
 &\quad - SF_2(j) \times (1-\rho_g)^2 {}_1\tau_{g\frac{1}{2}}^2 (1-\rho_w)^2 \tau_w \rho_g {}_2\tau_{g\frac{1}{2}}^3 \\
 &\quad + AF(j) \times (1-\rho_g) {}_1\tau_{g\frac{1}{2}}^2 (1-\rho_w)^2 b\tau_w b\tau_g^2 \rho_{gb} {}_2\tau_{g\frac{1}{2}} (1-{}_2\tau_{g\frac{1}{2}})]
 \end{aligned}$$

Rearranging,

$$\begin{aligned}
 \left. \begin{array}{l} \text{Beam} \\ \text{absorbed} \end{array} \right\} &= oI_b (1-\rho_g) {}_1\tau_{g\frac{1}{2}}^2 (1-\rho_w)^2 [SF_2(j) {}_2\tau_{g\frac{1}{2}} \tau_w \{ 1 - (1-\rho_g) {}_2\tau_{g\frac{1}{2}} \\
 &\quad - \rho_g {}_2\tau_{g\frac{1}{2}}^2 \} + AF(j) b\tau_w b\tau_g^2 \rho_{gb} {}_2\tau_{g\frac{1}{2}} \{ 1 - {}_2\tau_{g\frac{1}{2}} \} \\
 &\quad \dots\dots\dots (3.7)
 \end{aligned}$$

Similarly,

(d) Diffuse Irradiation Absorbed By 2nd Inner Glass 1/2-Slab.

$$\begin{aligned}
 \left. \begin{array}{l} \text{Diffuse} \\ \text{absorbed} \end{array} \right\} &= oI_d \times VF_2(j) \times (1-\rho_g) {}_1\tau_{g\frac{1}{2}}^2 (1-\rho_w)^2 [{}_2\tau_{g\frac{1}{2}} \tau_w \{ 1 - (1-\rho_g) \\
 &\quad {}_2\tau_{g\frac{1}{2}} - \rho_g {}_2\tau_{g\frac{1}{2}}^2 \} + AF(j) b\tau_w b\tau_g^2 \rho_{gb} {}_2\tau_{g\frac{1}{2}} \{ 1 - {}_2\tau_{g\frac{1}{2}} \}] \\
 &\quad \dots\dots\dots (3.8)
 \end{aligned}$$

3.3.4 Water Slabs.

The water slab divisions, the two $\frac{1}{2}$ -slabs near the glass/water boundaries, and the five full-slabs are outlined as shown in Figure 3.6.

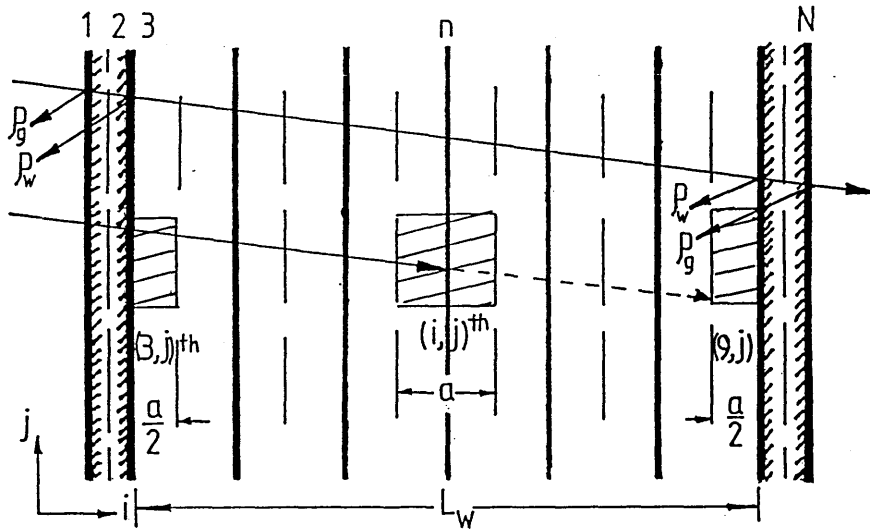


Figure 3.6 Water Slabs. $\tau_w = e^{-K_w L_w}$

(a) First Water 1/2-Slab: [Slab (3,j)]

$$d = o I_b (1 - \rho_g) {}_1 \tau_{g \frac{1}{2}}^2 (1 - \rho_w)$$

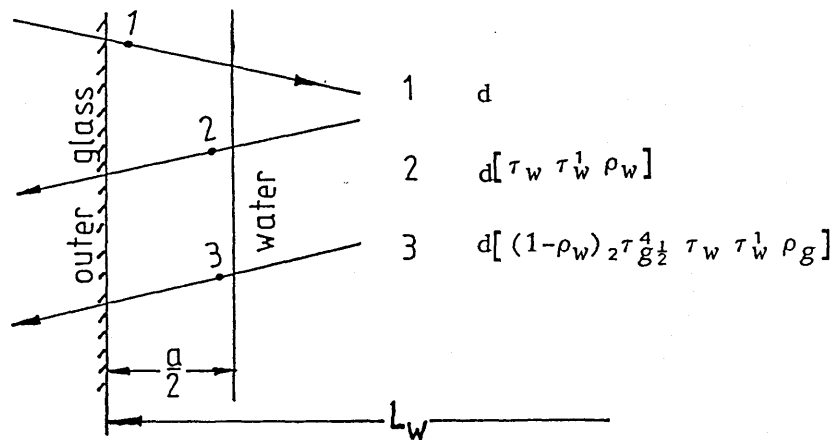


Figure 3.7 $\tau_w^1 = e^{-K_w (L_w - \frac{a}{2})}$ & $\tau_{w1/2} = e^{-K_w \frac{a}{2}}$

(i) Beam Irradiation Absorbed By 1st Water 1/2-Slab.

$$\left. \begin{array}{l} \text{Beam} \\ \text{absorbed} \end{array} \right\} = oI_b [(1-\rho_g)_1 \tau_{g\frac{1}{2}}^2 (1-\rho_w) \{1-\tau_{w\frac{1}{2}}\} \\ + SF_3(3,j) \times (1-\rho_g)_1 \tau_{g\frac{1}{2}}^2 (1-\rho_w) \tau_w \tau_w^1 \rho_w \{1-\tau_{w\frac{1}{2}}\} \\ + SF_4(3,j) \times (1-\rho_g)_1 \tau_{g\frac{1}{2}}^2 (1-\rho_w)^2 {}_2\tau_{g\frac{1}{2}}^4 \tau_w \tau_w^1 \\ \rho_g \{1-\tau_{w\frac{1}{2}}\}]$$

Rearranging,

$$\left. \begin{array}{l} \text{Beam} \\ \text{absorbed} \end{array} \right\} = oI_b (1-\rho_g)_1 \tau_{g\frac{1}{2}}^2 (1-\rho_w) (1-\tau_{w\frac{1}{2}}) [1 + \tau_w \tau_w^1 \{ SF_3(3,j) \times \rho_w \\ + SF_4(3,j) \times \rho_g (1-\rho_w) {}_2\tau_{g\frac{1}{2}}^4 \}] \\ \dots\dots\dots (3.9)$$

In this case the thicker water slabs, relative to the glass $\frac{1}{2}$ -slab require two shadow factors for the reflected ray.

Similarly,

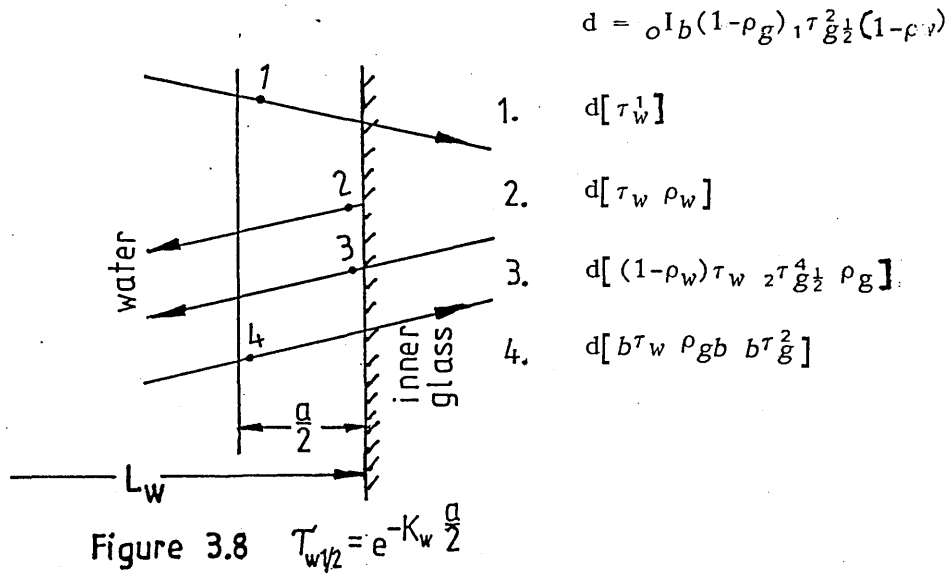
(ii) Diffuse Irradiation Absorbed By 1st Water 1/2-Slab.

$$\left. \begin{array}{l} \text{Diffuse} \\ \text{absorbed} \end{array} \right\} = oI_d \times (1-\rho_g)_1 \tau_{g\frac{1}{2}}^2 (1-\rho_w) (1-\tau_{w\frac{1}{2}}) [VF_3(3,j) \\ + \tau_w \tau_w^1 \times \{ VF_2(j) [\rho_w + \rho_g (1-\rho_w) {}_2\tau_{g\frac{1}{2}}^4] \}] \\ \dots\dots\dots (3.10)$$

where $VF_2(j)$ = view factor of back glass

$VF_3(j)$ = view factor for diffuse irradiation, not off
tank bottom.

(b) Second Water 1/2-Slab, [Slab (9,j)-th]



(i) Beam Irradiation Absorbed By 2nd Water 1/2-Slab.

$$\left. \begin{array}{l} \text{Beam} \\ \text{absorbed} \end{array} \right\} = {}_oI_b[SF_3(9,j) \times (1-\rho_g) {}_1\tau_{g\frac{1}{2}}^2 (1-\rho_w) \tau_w^1 \{1-\tau_{w\frac{1}{2}}\} \\ + SF_4(9,j) \times (1-\rho_g) {}_1\tau_{g\frac{1}{2}}^2 (1-\rho_w) \tau_w \rho_g \{1-\tau_{w\frac{1}{2}}\} \\ + SF_4(9,j) \times (1-\rho_g) {}_1\tau_{g\frac{1}{2}}^2 (1-\rho_w)^2 \tau_w \rho_g {}_2\tau_{g\frac{1}{2}}^4 \{1-\tau_{w\frac{1}{2}}\} \\ + AF(9,j) \times (1-\rho_g) {}_1\tau_{g\frac{1}{2}}^2 (1-\rho_w) b\tau_w b\tau_g^2 \rho_{gb} \{1-\tau_{w\frac{1}{2}}\}]$$

Rearranging,

$$\left. \begin{array}{l} \text{Beam} \\ \text{absorbed} \end{array} \right\} = {}_oI_b(1-\rho_g) {}_1\tau_{g\frac{1}{2}}^2 (1-\rho_w) (1-\tau_{w\frac{1}{2}}) [SF_3(9,j) \times \tau_w^1 \\ + SF_4(9,j) \times \tau_w \{\rho_w + (1-\rho_w) \rho_g {}_2\tau_{g\frac{1}{2}}^4\} \\ + AF(9,j) \times b\tau_w \rho_{gb} b\tau_g^2] \\ \dots\dots\dots (3.11)$$

Similarly,

(ii) Diffuse Irradiation Absorbed By 2nd Water 1/2-Slab.

$$\begin{aligned}
 \left. \begin{array}{l} \text{Diffuse} \\ \text{absorbed} \end{array} \right\} &= oI_d \times (1-\rho_g)_1 \tau_{g\frac{1}{2}}^2 (1-\rho_w) (1-\tau_{w\frac{1}{2}}) [VF_3(3,j) \tau_w^1 \\
 &+ VF_2(j) \times \tau_w \{ \rho_w + (1-\rho_w) \rho_g \tau_{g\frac{1}{2}}^4 \} \\
 &+ VF_{f1,2} \times AD(j) b\tau_w \rho_{gb} b\tau_g^2] \\
 &\dots\dots\dots (3.12)
 \end{aligned}$$

where $AD(j)$ = factor 1 for 1 1/2 slabs, and 0 for higher,
 VF_{f1} = view factor of the bottom 1/2 slab, slab 1
 VF_{f2} = view factor slab 2

(e) Full Water Slabs; Slab (i,j)-th.

$$d = oI_b(1-\rho_g)_1 \tau_{g\frac{1}{2}}^2 (1-\rho_w)$$

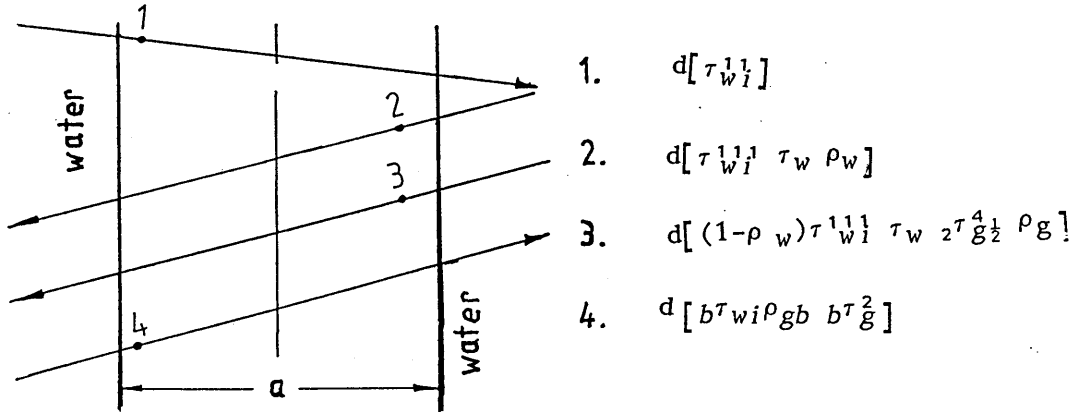


Figure 3.9 $\tau_{wi}^{II} = e^{-K_w(n-3.5)a}$ $\tau_{wi}^{III} = e^{-K_w(N-n-2.5)a}$
 and $\tau_{ws} = e^{-K_w a}$

(i) Beam Irradiation Absorbed By n-full Water Slabs.

$$\begin{aligned}
 \left. \begin{array}{l} \text{Beam} \\ \text{absorbed} \end{array} \right\} &= oI_b [SF_3(i, j) \times (1-\rho_g)_1 \tau_{g\frac{1}{2}}^2 (1-\rho_w) \tau_{wi}^{11} \{1-\tau_{ws}\} \\
 &+ SF_4(i, j) \times (1-\rho_g)_1 \tau_{g\frac{1}{2}}^2 (1-\rho_w) \tau_{wi}^{111} \rho_w \tau_w \{1-\tau_{ws}\} \\
 &+ SF_4(i, j) \times (1-\rho_g)_1 \tau_{g\frac{1}{2}}^2 (1-\rho_w)^2 \tau_{wi}^{111} \tau_w \rho_g \tau_{g\frac{1}{2}}^4 \{1-\tau_{ws}\} \\
 &+ AF(i, j) \times (1-\rho_g)_1 \tau_{g\frac{1}{2}}^2 (1-\rho_w) b\tau_{wi} \rho_{gb} b\tau_{gb}^2 \{1-\tau_{ws}\}
 \end{aligned}$$

where $b\tau_{wi}$ will vary from slab to slab.

Rearranging,

$$\begin{aligned}
 \left. \begin{array}{l} \text{Beam} \\ \text{absorbed} \end{array} \right\} &= oI_b (1-\rho_g)_1 \tau_{g\frac{1}{2}}^2 (1-\rho_w) (1-\tau_{ws}) [SF_3(i, j) \tau_{wi}^{11} \\
 &+ SF_4(i, j) \tau_w \tau_{wi}^{111} \{ \rho_w + \rho_g (1-\rho_w) \tau_{g\frac{1}{2}}^4 \} \\
 &+ AF(i, j) b\tau_{wi} \rho_{gb} \tau_{gb}^2]
 \end{aligned}$$

.....(3.13)

Similarly,

(ii) Diffuse Irradiation Absorbed By n-full Water Slabs.

$$\begin{aligned}
 \left. \begin{array}{l} \text{Diffuse} \\ \text{absorbed} \end{array} \right\} &= {}_0I_d \times (1-\rho_g) \tau_{g\frac{1}{2}}^2 (1-\rho_w) (1-\tau_{ws}) [VF_3(i,j) \tau_{wi}^{11} \\
 &+ VF_2(j) \tau_w \tau_{wi}^{11} \{ \rho_w + \rho_g (1-\rho_g) \tau_{g\frac{1}{2}}^4 \} \\
 &+ VF_{f1,2} \times AD(j) \tau_{wi} \rho_{gb} \tau_{gb}^2] \\
 &\dots\dots\dots(3.14)
 \end{aligned}$$

3.4 The Two-Dimensional Explicit Finite Difference Analysis: Surface Contact Resistance Computer Model Development of the Transwall Temperature

It is believed that because the transwall is wide compared to its height and thickness, the three-dimensional approach will contribute very little to the accuracy, and therefore, the two-dimensional solution is outlined as shown in Figure 3.10

Nomenclature

$fh_{s,j}$ = combined convective and radiation heat transfer coefficient, front glass to window opposite slab j.

$rh_{s,j}$ = combined convective and radiation heat transfer coefficient, rear glass to room opposite slab j.

$oh_{c,j}$ = surface "contact" heat transfer coefficient at the (front) outer glass/water interface opposite slab j.

$ih_{c,j}$ = surface contact heat transfer coefficient at the (rear) inner glass/water interface opposite slab j.

h_r = linearized radiation heat transfer coefficient.

h_b	=	combined convective and radiation heat transfer coefficient, base end of transwall to ambient.
h_t	=	combined convective and radiation heat transfer coefficient, top end of transwall to ambient.
$T_{a,j}$	=	air gap temperature opposite slab j
$T_{r,j}$	=	room temperature opposite slab j
$T_{gw,j}$	=	window glass temperature opposite slab j
T_b	=	base end of transwall temperature
T_t	=	top end of transwall temperature
k_g	=	thermal conductivity glass
k_w	=	thermal conductivity water
k_e	=	effective conductivity, horizontal
F_g	=	Fourier number for glass
F_w	=	Fourier number for water
δt	=	time interval
g	=	glass thickness
b	=	horizontal direction slab thickness
a	=	vertical direction slab thickness
α_{ij}	=	fractional absorption in slab (i,j)
$I_{\lambda\tau gw}$	=	incident irradiation after passing through window/m ² transwall surface.

The development of nodes in both glass and water slabs is governed by the Fourier equation.

$$\frac{\partial T}{\partial t} = \frac{k}{\rho c} \left[\frac{\partial^2 T}{\partial x^2} + \frac{\partial^2 T}{\partial y^2} + \frac{\partial^2 T}{\partial z^2} \right] + \frac{q_g}{\rho c}$$

assuming (i) $\frac{\partial^2 T}{\partial z^2} = 0$

Therefore,
$$\frac{\partial T}{\partial t} = \frac{k}{\rho c} \left[\frac{\partial^2 T}{\partial x^2} + \frac{\partial^2 T}{\partial y^2} \right] + \frac{q_g}{\rho c}$$

This can be written as a finite difference relation in the same way as for a one-dimensional approach.

For (i,j)-th slab, Figure 3.10,

$$\frac{\partial^2 T}{\partial x^2} = \frac{p^{T_{i+1}} + p^{T_{i-1}} - 2 p^{T_i}}{a^2}$$

and
$$\frac{\partial^2 T}{\partial y^2} = \frac{p^{T_{j+1}} + p^{T_{j-1}} - 2 p^{T_j}}{b^2}$$

3.4.1 Water Slabs.

In order to allow for vertical stratification it was decided to investigate the concept of anisotropic effective conductivities i.e. having different conductivities for the *i* and *j* directions. In effect this is similar to pyrolysed graphite which has a thermal conductivity in one direction 200 times that in a perpendicular plane.

$$\text{let } r = \frac{k_e \text{ vertical}}{k_e \text{ horizontal}}$$

where $k_e = \text{Nu} \cdot k_w$

(a) Full Water Slabs; Node (i, j) $i = 4, 5, \dots, N-3$
 $j = 2, 3, \dots, M$

$$\begin{aligned}
 \frac{p_{i+1}T_{i,j} - p_{i,j}}{\delta t} &= \frac{k_e}{\rho_w c_w a^2} \frac{\partial^2 T}{\partial x^2} + \frac{rk_e}{\rho_w c_w} \frac{\partial^2 T}{\partial y^2} + \frac{I_{\lambda} \tau_{gw} \alpha_i}{ab.1. \rho_w c_w} \\
 &= \frac{k_e}{\rho_w c_w a^2} (p_{i+1,j} + p_{i-1,j} - 2 p_{i,j}) \\
 &\quad + \frac{rk_e}{\rho_w c_w b^2} (p_{i,j+1} + p_{i,j-1} - 2 p_{i,j}) + \frac{I_{\lambda} \tau_{gw} \alpha_i}{a \rho_w c_w} \\
 p_{i+1}T_{i,j} &= F_{wx} \left[p_{i+1,j} + p_{i-1,j} + \left\{ \frac{1}{F_{wx}} - 2 \frac{ra^2}{b^2} - 2 \right\} p_{i,j} \right. \\
 &\quad \left. + \frac{ra^2}{b^2} (p_{i,j+1} + p_{i,j-1}) + \frac{a}{k_e} (I_{\lambda} \tau_{gw} \alpha_i) \right] \\
 &\dots\dots\dots(3.15)
 \end{aligned}$$

where $F_{wx} = \frac{k_e \delta t}{\rho_w c_w a^2}$, the Fourier Number.

The stability criterion for the explicit method required that function of the current temperature remains positive, i.e.

$$\left[\frac{1}{F_{wx}} - 2 \frac{ra^2}{b^2} - 2 \right] \geq 0$$

This stability is not repeated for other equations developed.

All of the equations are checked against one dimensional equations by putting $b = \infty$ as shown below. This check is shown below as an example and is not repeated.

$$b = \infty$$

$$p_{+1}T_i = F_{wx} \left[pT_{i+1} + pT_{i-1} + \left\{ \frac{1}{F_{wx}} - 2 \right\} pT_{i,j} + \frac{a}{k_e} (I_{\lambda} \tau_{gw} \alpha) \right]$$

(b) 1st Water 1/2-Slab.

(i) Bottom Slab; Node (3,1).

$$\begin{aligned} \frac{p_{+1}T_{3,1} - pT_{3,1}}{\delta t} &= \frac{4k_e}{\rho_w c_w a^2} \left\{ \frac{a}{2k_e} o h_{c,1} (pT_{2,1} - pT_{3,1}) - \right. \\ &\quad \left. - \frac{1}{2} (pT_{3,1} - pT_{4,1}) \right\} + \frac{4rk_e}{\rho_w c_w b^2} \left\{ \frac{b}{2rk_e} h_b (pT_b - pT_{3,1}) \right. \\ &\quad \left. - \frac{1}{2} (pT_{3,1} - pT_{3,2}) \right\} + \frac{I_{\lambda} \tau_{gw} \alpha_{3,1}}{\rho_w c_w a/2} \end{aligned}$$

Rearranging,

$$\begin{aligned} p_{+1}T_{3,1} &= 4F_{wx} \left[\left(\frac{a}{2k_e} o h_{c,1} \right) pT_{2,1} + \left(\frac{ra^2}{2b^2} \right) pT_{3,2} + \left(\frac{a^2 h_b}{2bk_e} \right) pT_b + \right. \\ &\quad \left. + \frac{1}{2} pT_{4,1} + \left\{ \frac{1}{4F_{wx}} - \frac{a}{2k_e} o h_{c,1} - \frac{ra^2}{2b^2} - \frac{a^2 h_b}{2bk_e} - \frac{1}{2} \right\} pT_{3,1} \right. \\ &\quad \left. + \frac{a}{2k_e} I_{\lambda} \tau_{gw} \alpha_{3,1} \right] \end{aligned} \quad \dots\dots\dots (3.16)$$

Similarly,

(ii) Top Slab; Node (3,M+1).

$$\begin{aligned}
 p_{+1}T_{3,M+1} = & 4F_{wx} \left[\left(\frac{a}{2k_e} \right) p_{T_2,M+1} + \left(\frac{ra^2}{2b^2} \right) p_{T_3,M} + \left(\frac{ah_t}{2bk_e} \right) p_{T_t} \right. \\
 & + \frac{1}{2} p_{T_4,M+1} + \left\{ \frac{1}{F_{wx}} - \frac{a}{2k_e} - \frac{ra^2}{2b^2} - \frac{a^2h_t}{2bk_e} - \frac{1}{2} \right\} p_{T_3,M+1} \\
 & \left. + \frac{a}{2k_e} I_{\lambda\tau} g_w \alpha_{3,M+1} \right] \quad \dots\dots\dots (3.17)
 \end{aligned}$$

(ii) Middle Slab; Node (3,j) ; j=2,3,\dots\dots M

$$\begin{aligned}
 \frac{p_{+1}T_{3,j} - p_{T_3,j}}{\delta t} = & \frac{2k_e}{\rho_w c_w a^2} \left\{ \frac{a}{k_e} oh_{c,j} (p_{T_2,j} - p_{T_3,j}) - (p_{T_3,j} - p_{T_4,j}) \right\} \\
 & + \frac{2k_e}{\rho_w c_w b^2} \left\{ \frac{1}{2} \left[(p_{T_3,j+1} - p_{T_3,j}) + (p_{T_3,j} - p_{T_3,j-1}) \right] \right\} \\
 & + \frac{I_{\lambda\tau} g_w \alpha_{3,j}}{\rho_w c_w a}
 \end{aligned}$$

Rearranging,

$$\begin{aligned}
 p_{+1}T_{3,j} = & 2F_{wx} \left[\left(\frac{a}{k_e} \right) p_{T_2,j} + p_{T_4,j} + \frac{ra^2}{2b^2} (p_{T_3,j-1} + p_{T_3,j+1}) \right. \\
 & + \left\{ \frac{1}{2F_{wx}} - \frac{a}{k_e} - \frac{ra^2}{b^2} - 1 \right\} p_{T_3,j} + \frac{a}{k_e} I_{\lambda\tau} g_w \alpha_{3,j} \left. \right] \quad \dots\dots\dots (3.18)
 \end{aligned}$$

Similarly,

(c) 2nd Water 1/2-Slab.

(i) Bottom Slab; Node(N-2,1).

$$\begin{aligned}
 p_{+1}T_{N-2,1} = & 4F_{wx} \left[\left(\frac{a_i h_{c,1}}{2k_e} \right) p_{T_{N-1,1}} + \left(\frac{ra^2}{2b^2} \right) p_{T_{N-2,2}} + \left(\frac{a^2 h_b}{2bk_e} \right) p_{T_b} \right. \\
 & + \frac{1}{2} p_{T_{N-3,1}} + \left\{ \frac{1}{4F_{wx}} - \frac{a_i h_{c,1}}{2k_e} - \frac{ra^2}{2b^2} - \frac{a^2 h_b}{2bk_e} - \frac{1}{2} \right\} p_{T_{N-2,1}} \\
 & \left. + \frac{a}{2k_e} I_{\lambda} \tau_{gw} \alpha_{N-2,1} \right] \dots\dots\dots (3.19)
 \end{aligned}$$

(ii) Top Slab; Node (N-2,M+1).

$$\begin{aligned}
 p_{+1}T_{N-2,M+1} = & 4F_{wx} \left[\left(\frac{a_i h_{c,M+1}}{2k_e} \right) p_{T_{N-1,M+1}} + \left(\frac{ra^2}{2b^2} \right) p_{T_{N-2,M}} \right. \\
 & + \left(\frac{a^2 h_t}{2bk_e} \right) p_{T_t} + \frac{1}{2} p_{T_{N-4,M+1}} + \left\{ \frac{1}{4F_{wx}} - \frac{a_i h_{c,M+1}}{2k_e} - \frac{ra^2}{2b^2} \right. \\
 & \left. \left. - \frac{a^2 h_t}{2bk_e} - \frac{1}{2} \right\} p_{T_{N-2,M+1}} + \frac{a}{2k_e} I_{\lambda} \tau_{gw} \alpha_{N-2,M+1} \right] \dots\dots\dots (3.20)
 \end{aligned}$$

(iii) Middle Slab; Node (N-2,j); j=2,3,...,M

$$\begin{aligned}
 {}^{p+1}T_{N-2,j} = & 2F_{wx} \left[\left(\frac{a}{k_e} h_{c,j} \right) {}^pT_{N-2,j} + {}^pT_{N-3,j} + \frac{ra^2}{2b^2} ({}^pT_{N-2,j-1} \right. \\
 & \left. + {}^pT_{N-2,j+1}) + \left\{ \frac{1}{2F_{wx}} - \frac{a}{k_e} h_{c,j} - \frac{ra^2}{b^2} - 1 \right\} {}^pT_{N-2,j} \right. \\
 & \left. + \frac{a}{k_e} I_{\lambda} \tau_{gw} \alpha_{N-2,j} \right] \quad \dots\dots\dots(3.21)
 \end{aligned}$$

3.4.2 Front Glass Slabs.

(a) 1st Glass 1/2-Slab.

(i) Bottom Slab; Node (1,1).

$$\begin{aligned}
 \frac{{}^{p+1}T_{1,1} - {}^pT_{1,1}}{\delta t} = & \frac{4k_g}{g^2 \rho_g c_g} \left\{ \frac{g}{2k_g} f h_{s,1} ({}^pT_{a,1} - {}^pT_{1,1}) - \frac{1}{2} ({}^pT_{1,1} - {}^pT_{2,1}) \right. \\
 & \left. + \frac{g h_{r,1}}{2k_g} ({}^pT_{gw,1} - {}^pT_{1,1}) \right\} + \frac{4k_g}{b^2 \rho_g c_g} \left\{ \frac{b h_b}{2k_g} ({}^pT_b - {}^pT_{1,1}) \right. \\
 & \left. - \frac{1}{2} ({}^pT_{1,1} - {}^pT_{1,2}) \right\} + \frac{I_{\lambda} \tau_{gw} \alpha_{1,1}}{\rho_g c_g g/2}
 \end{aligned}$$

Rearranging,

$$\begin{aligned}
 p_{+1}T_{1,1} = 4F_{gx} \left[\left(\frac{g f h_{s,1}}{2k_g} \right) p_{Ta,1} + \left(\frac{g h_{r,1}}{2k_g} \right) p_{Tgw,1} + \frac{1}{2} p_{T2,1} \right. \\
 \left. + \left(\frac{g^2}{2b^2} \right) p_{T1,2} + \left(\frac{g^2 h_b}{2bk_g} \right) p_{Tb} + \left\{ \frac{1}{4F_{gx}} - \frac{g f h_{s,1}}{2k_g} - \frac{g^2}{2b^2} - \frac{g h_{r,1}}{2k_g} \right. \right. \\
 \left. \left. - \frac{g^2 h_b}{2bk_g} - \frac{1}{2} \right\} p_{T1,1} + \frac{g}{2k_g} I_{\lambda^{\tau} gw} \alpha_{1,1} \right]
 \end{aligned}
 \dots\dots\dots(3.22)$$

where $F_{gx} = \frac{k_g \delta t}{g^2 \rho_g c_g}$, the Fourier Number.

Similarly

(ii) Top Slab; Node(1,M+1).

$$\begin{aligned}
 p_{+1}T_{1,M+1} = 4F_{gx} \left[\left(\frac{g f h_{s,M+1}}{2k_g} \right) p_{Ta,M+1} + \left(\frac{g h_{r,M+1}}{2k_g} \right) p_{Tgw,M+1} \right. \\
 \left. + \frac{1}{2} p_{T2,M+1} + \left(\frac{g^2}{2b^2} \right) p_{T1,M} + \left(\frac{g^2 h_t}{2bk_g} \right) p_{Tt} + \left\{ \frac{1}{4F_{gx}} - \frac{g f h_{r,M+1}}{2k_g} \right. \right. \\
 \left. \left. - \frac{g^2}{2b^2} - \frac{g h_{r,M+1}}{2k_g} - \frac{g^2 h_b}{2bk_g} - \frac{1}{2} \right\} p_{T1,M+1} + \frac{g}{2k_g} I_{\lambda^{\tau} gw} \alpha_{1,M+1} \right]
 \end{aligned}
 \dots\dots\dots(3.23)$$

(iii) Middle Slab; Node (1,j); j=2.3,...M

$$\begin{aligned} \frac{p_{+1}T_{1,j} - pT_{1,j}}{\delta t} = & \frac{2k_g}{g^2 \rho_g c_g} \left\{ \frac{g}{k_g} f h_{s,j} (pT_{a,j} - pT_{1,j}) - (pT_{1,j} - pT_{2,j}) \right. \\ & + \frac{g}{k_g} h_{r,j} (pT_{gw,j} - pT_{1,j}) \left. \right\} + \frac{2k_g}{b^2 \rho_g c_g} \left\{ \frac{1}{2} [(pT_{1,j+1} - pT_{1,j}) \right. \\ & \left. - (pT_{1,j} - pT_{1,j-1})] \right\} + \frac{I_{\lambda} \tau_{gw} \alpha_{1,j}}{\rho_g c_g g/2} \end{aligned}$$

Rearranging,

$$\begin{aligned} p_{+1}T_{1,j} = & 2F_{gx} \left[\left(\frac{g}{k_g} f h_{s,j} \right) pT_{a,j} + \left(\frac{g h_{r,j}}{k_g} \right) pT_{gw,j} + pT_{2,j} \right. \\ & + \frac{g^2}{2b^2} (pT_{1,j+1} + pT_{1,j-1}) + \left\{ \frac{1}{2F_{gx}} - \frac{g h_{r,j}}{2k_g} - \frac{g f h_{s,j}}{k_g} \right. \\ & \left. \left. - \frac{g^2}{b^2} - 1 \right\} pT_{1,j} + \frac{g}{k_g} I_{\lambda} \tau_{gw} \alpha_{1,j} \right] \end{aligned} \quad \dots\dots\dots (3.24)$$

(b) 2nd Glass 1/2-Slab.

(i) Bottom Slab; Node (2,1).

$$\begin{aligned} \frac{p_{+1}T_{2,1} - pT_{2,1}}{\delta t} &= \frac{4k_g}{g^2 \rho_g c_g} \left\{ \frac{g o h_{c,1}}{2k_g} (pT_{3,1} - pT_{2,1}) \right. \\ &\quad \left. - \frac{1}{2} (pT_{2,1} - pT_{1,1}) \right\} + \frac{4k_g}{b^2 \rho_g c_g} \left\{ \frac{bh_b}{2k_g} (pT_b - pT_{2,1}) \right. \\ &\quad \left. - \frac{1}{2} (pT_{2,1} - pT_{2,2}) \right\} + \frac{I_{\lambda} \tau g_w \alpha_{2,1}}{\rho_g c_g g/2} \end{aligned}$$

Rearranging,

$$\begin{aligned} p_{+1}T_{2,1} &= 4F_{gx} \left[\left(\frac{g o h_{c,1}}{2k_g} \right) pT_{3,1} + \frac{1}{2} pT_{1,1} + \left(\frac{g^2}{2b^2} \right) pT_{2,2} \right. \\ &\quad \left. + \left(\frac{g^2 h_b}{2b} \right) pT_b + \left\{ \frac{1}{4F_{gx}} - \frac{g o h_{c,1}}{2k_g} - \frac{g^2}{b^2} - \frac{g^2 h_b}{2b} - \frac{1}{2} \right\} pT_{2,1} \right. \\ &\quad \left. + \frac{g}{2k_g} I_{\lambda} \tau g_w \alpha_{2,1} \right] \end{aligned} \quad \dots\dots\dots (3.25)$$

Similarly,

(ii) Top Slab; Node (2,M+1).

$$\begin{aligned}
 p_{+1}T_{2,M+1} = & 4F_{gx} \left[\left(\frac{g}{2k_g} o h_{c,M+1} \right) pT_{3,M+1} + \frac{1}{2} pT_{1,M+1} + \left(\frac{g^2}{2b^2} \right) pT_{2,M} \right. \\
 & + \left(\frac{g^2 h_t}{2b} \right) pT_t + \left\{ \frac{1}{4F_{gx}} - \frac{g}{2k_g} o h_{c,M+1} - \frac{g^2}{b^2} - \frac{g^2 h_t}{2b} - \frac{1}{2} \right\} pT_{2,M+1} \\
 & \left. + \frac{g}{2k_g} I_{\lambda} \tau g w^{\alpha_2, M+1} \right] \quad \dots\dots\dots (3.26)
 \end{aligned}$$

(iii) Middle Slab; Node (2,j). j=2,3,...M

$$\begin{aligned}
 \frac{p_{+1}T_{2,j} - pT_{2,j}}{\delta t} = & \frac{2k_g}{g^2 \rho_g c_g} \left\{ \frac{g}{k_g} o h_{c,j} (pT_{3,j} - pT_{2,j}) - (pT_{2,j} - pT_{1,j}) \right\} \\
 & + \frac{2k_g}{b^2 \rho_g c_g} \left\{ \frac{1}{2} [(pT_{2,j+1} - pT_{2,j}) - (pT_{2,j} - pT_{2,j-1})] \right\} \\
 & + \frac{I_{\lambda} \tau g w^{\alpha_2, j}}{\rho_g c_g g/2}
 \end{aligned}$$

Rearranging,

$$\begin{aligned}
 p_{+1}T_{2,j} = & 2F_{gx} \left[\left(\frac{g}{k_g} o h_{c,j} \right) pT_{3,j} + pT_{1,j} + \frac{g^2}{2b^2} (pT_{2,j+1} + pT_{2,j-1}) \right. \\
 & + \left\{ \frac{1}{2F_g} - \frac{g}{k_g} o h_{c,j} - \frac{g^2}{b^2} - 1 \right\} pT_{2,j} + \frac{g}{k_g} I_{\lambda} \tau g w^{\alpha_2, j} \left. \right] \\
 & \dots\dots\dots (3.27)
 \end{aligned}$$

Similarly,

3.4.3 Rear Glass Slabs.

(a) 3rd Glass 1/2-Slab.

(i) Bottom Slab; Node (N-1,1)

$$\begin{aligned}
 p_{+1}T_{N-1,1} = & 4F_{gx} \left[\left(\frac{g}{2k_g} i h_{c,1} \right) p_{T_{N-2,1}} + \frac{1}{2} p_{T_{N,1}} + \left(\frac{g^2}{2b^2} \right) p_{T_{N-1,2}} \right. \\
 & + \left(\frac{g^2 h_b}{2b} \right) p_{T_b} + \left\{ \frac{1}{4F_{gx}} - \frac{g}{2k_g} i h_{c,1} - \frac{g^2}{2b^2} - \frac{g^2 h_b}{2b} - \frac{1}{2} \right\} p_{T_{N-1,1}} \\
 & \left. + \frac{g}{2k_g} I_{\lambda\tau} g w^{\alpha_{N-1,1}} \right] \quad \dots\dots\dots (3.28)
 \end{aligned}$$

(ii) Top Slab; Node (N-1,M+1).

$$\begin{aligned}
 p_{+1}T_{N-1,M+1} = & 4F_{gx} \left[\left(\frac{g}{2k_g} i h_{c,M+1} \right) p_{T_{N-2,M+1}} + \frac{1}{2} p_{T_{N,M+1}} \right. \\
 & + \left(\frac{g^2}{2b^2} \right) p_{T_{N-1,M}} + \left(\frac{g^2 h_t}{2b} \right) p_{T_t} + \left\{ \frac{1}{4F_{gx}} - \frac{g}{2k_g} i h_{c,M+1} - \frac{g^2}{2b^2} \right. \\
 & \left. \left. - \frac{g^2 h_t}{2b} - \frac{1}{2} \right\} p_{T_{N-1,M+1}} + \frac{g}{2k_g} I_{\lambda\tau} g w^{\alpha_{N-1,M+1}} \right] \quad \dots\dots\dots (3.29)
 \end{aligned}$$

(iii) Middle Slab; Node(N-1, j); j=2, 3, ..., M.

$$\begin{aligned}
 p_{+1}T_{N-1,j} = & 2F_{gx} \left[\left(\frac{g}{k_g} h_{c,j} \right) p_{T_{N-2,j}} + p_{T_{N,j}} + \frac{g^2}{2b^2} (p_{T_{N-1,j+1}} \right. \\
 & + p_{T_{N-1,j-1}}) + \left\{ \frac{1}{2F_{gx}} - \frac{g}{k_g} h_{c,j} - \frac{g^2}{b^2} - 1 \right\} p_{T_{N-1,j}} \\
 & \left. + \frac{g}{k_g} I_{\lambda} \tau_{gw} \alpha_{2,j} \right] \quad \dots\dots\dots (3.30)
 \end{aligned}$$

(b) 4th Glass 1/2-Slab.

(i) Bottom Slab; Node (N,1).

$$\begin{aligned}
 p_{+1}T_{N,1} = & 4F_{gx} \left[\left(\frac{g}{2k_g} r_{s,1} \right) p_{T_{r,1}} + \frac{1}{2} p_{T_{N-1,1}} + \left(\frac{g^2}{2b^2} \right) p_{T_{N,2}} \right. \\
 & + \left(\frac{g^2 h_b}{2bk_g} \right) p_{T_b} + \left\{ \frac{1}{4F_{gx}} - \frac{g}{2k_g} r_{s,1} - \frac{g^2}{2b^2} - \frac{g^2 h_b}{2bk_g} - \frac{1}{2} \right\} p_{T_{N,1}} \\
 & \left. + \frac{g}{2k_g} I_{\lambda} \tau_{gw} \alpha_{N,1} \right] \quad \dots\dots\dots (3.31)
 \end{aligned}$$

(ii) Top Slab; Node (N,M+1).

$$\begin{aligned}
 p_{+1}T_{N,M+1} = & 4F_{gx} \left[\left(\frac{g \text{ } rh_{S,M+1}}{2k_g} \right) p_{Tr,M+1} + \frac{1}{2} p_{TN-1,M+1} \right. \\
 & + \left(\frac{g^2}{2b^2} \right) p_{TN,M} + \left(\frac{g^2 h_t}{2bk_g} \right) p_{Tt} + \left\{ \frac{1}{4F_{gx}} - \frac{g \text{ } rh_{S,M+1}}{2k_g} - \frac{g}{2b^2} \right. \\
 & \left. \left. - \frac{g^2 h_t}{2bk_g} - \frac{1}{2} \right\} p_{TN,M+1} + \frac{g}{2k_g} I_{\lambda^{\tau}} g w^{\alpha_{N,M+1}} \right] \\
 & \dots\dots\dots (3.32)
 \end{aligned}$$

(iii) Middle Slab; Node (N,j) ; j=2,3,....M

$$\begin{aligned}
 p_{+1}T_{N,j} = & 2F_{gx} \left[\left(\frac{g \text{ } rh_{S,j}}{k_g} \right) p_{Tr,j} + p_{TN-1,j} + \frac{g^2}{2b^2} (p_{TN,j+1} + p_{TN,j-1}) \right. \\
 & \left. + \left\{ \frac{1}{2F_{gx}} - \frac{g \text{ } rh_{S,j}}{k_g} - \frac{g^2}{b^2} - 1 \right\} p_{TN,j} + \frac{g}{k_g} I_{\lambda^{\tau}} g w^{\alpha_{N,j}} \right] \\
 & \dots\dots\dots (3.33)
 \end{aligned}$$

3.4.4 Horizontal End Surfaces.

(a) Bottom End Nodes (i,1); i=4,5,.....N-3

$$\begin{aligned} \frac{p_{+1}T_{i,1} - p_{-1}T_{i,1}}{\delta t} &= \frac{2k_e}{a^2\rho_w c_w} \left\{ \frac{1}{2} (p_{-1}T_{i-1,1} - p_{-1}T_{i,1}) - \frac{1}{2} (p_{+1}T_{i,1} - p_{+1}T_{i+1,1}) \right\} \\ &+ \frac{2rk_e}{b^2\rho_w c_w} \left\{ \frac{b}{rk_e} h_b (p_{-1}T_{b,-1} - p_{-1}T_{i,1}) - (p_{+1}T_{i,1} - p_{+1}T_{i,2}) \right\} \\ &+ \frac{I_{\lambda\tau} g_w \alpha_{i,1}}{\rho_w c_w a/2} \end{aligned}$$

Rearranging,

$$\begin{aligned} p_{+1}T_{i,1} &= 2F_{wx} \left[\frac{1}{2} (p_{+1}T_{i+1,1} + p_{-1}T_{i-1,1}) + \left(\frac{ra^2}{b^2}\right) p_{+1}T_{i,2} + \left(\frac{a^2 h_b}{bk_e}\right) p_{-1}T_b \right. \\ &\left. + \left\{ \frac{1}{2F_{wx}} - \frac{a^2 h_b}{bk_e} - \frac{ra^2}{b^2} - 1 \right\} p_{+1}T_{i,1} + \frac{a}{2k_e} I_{\lambda\tau} g_w \alpha_{i,1} \right] \\ &\dots\dots (3.34) \end{aligned}$$

Similarly

(b) Top End Nodes (i,M+1); i=4,5,.....N-3

$$\begin{aligned}
 p_{i+1}T_{i,M+1} = & 2F_{wx} \left[\frac{1}{2} (p_{i+1}^{T,M+1} + p_{i-1}^{T,M+1}) + \left(\frac{ra^2}{b^2} \right) p_{i,M} \right. \\
 & + \left(\frac{a^2 h_t}{bk_e} \right) p_{i,t} + \left\{ \frac{1}{2F_{wx}} - \frac{a^2 h_t}{bk_e} - \frac{ra^2}{b^2} - 1 \right\} p_{i,M+1} \\
 & \left. + \frac{a}{2k_e} I_{\lambda^T} g_w^{\alpha_i, M+1} \right] \quad \dots\dots\dots (3.35)
 \end{aligned}$$

The two-dimensional computer model time interval dependence was examined by running the model using different time intervals, δt , from the lowest to the

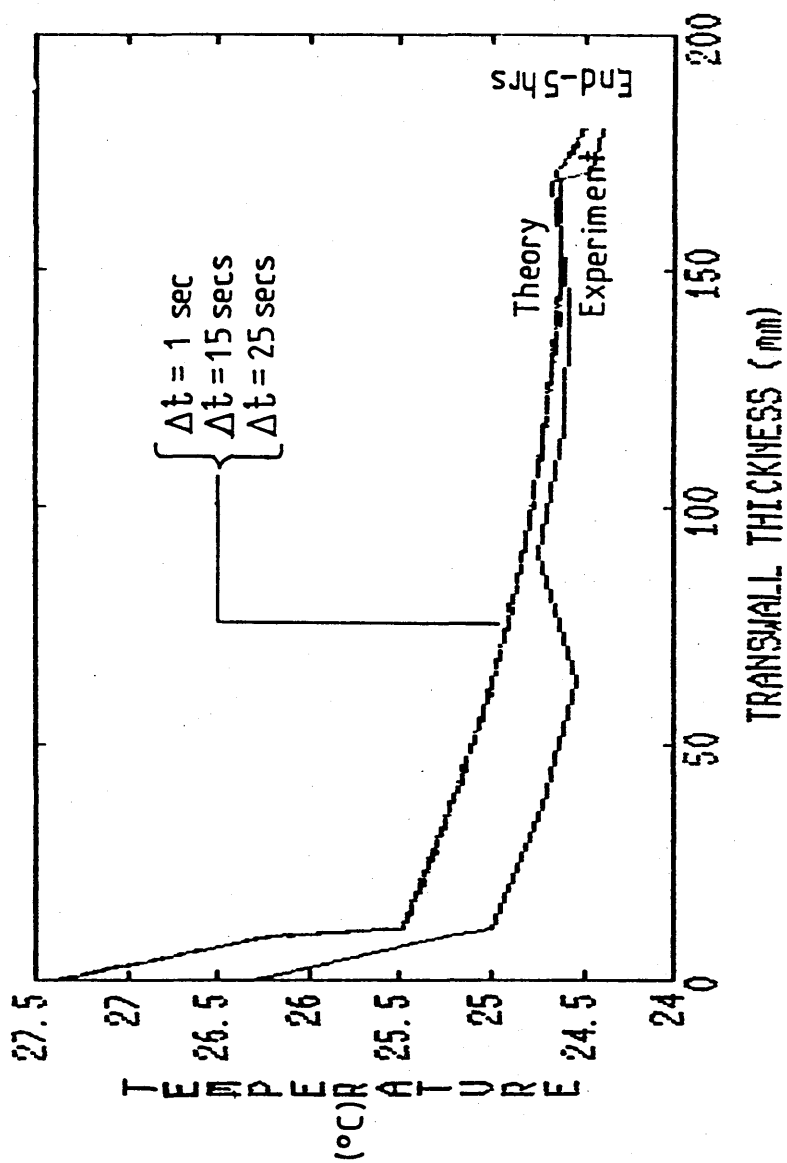


Figure 3.11 The 2-D computer model showing different time intervals to test time interval dependence criterion. The transwall temperature is higher than the surroundings, and one horizontal plane is shown.

highest. The lowest δt was 1 second and the highest δt was 25 seconds.

The model showed no significant dependence. There was no difference in predicted temperatures when the lowest and highest time intervals were used. Figure 3.11 shows the curve for the three time intervals tested, i.e. $\delta t = 1$ sec, $\delta t = 15$ secs, and for $\delta t = 25$ secs, and show that the curves overlap. This is for a case in which the transwall temperature is higher than the surroundings. Similar results were found for the other case in which the transwall temperature was lower than the surroundings. However, as expected with an explicit solution, the two-dimensional model was found to be unstable for values of time interval greater than 25 seconds.

3.5 Experimental Validation of the Two-Dimensional Temperature Distribution Program.

3.5.1 The Full Size Transwall Module

The full size transwall module dimensioned 1.2 m by 0.6 m by 0.16 m internal thickness was located in a solar test cell. The cell shown in Figure 3.12 is of wooden tongued and grooved construction and is located at the Mechanical Engineering Research Annexe (MERA). It has a south facing 6 mm single glazed window of 1.6 m by 1.7 m and is fitted with night insulation consisting

of an aluminium cover backed by 50 mm of expanded polystyrene. The test cell is divided by a partition into a test space of 2 m by 2 m by 1.4 m and a logging/working space of 2 m by 1.8 m by 1 m. The test space is air cooled by a low mounted fan drawing in outside air and exhausting it through controlled vents at the top or bottom of the partition. The test cell is fitted with three calibrated Kipp and Zonen solarimeters - global, diffuse and global vertically mounted. Reflected solar irradiation within the test cell is measured by silicon cells. The environmental parameters and data from the system were recorded using a Solartron-Schlumberger 3530 Orion Data logging system.

3.5.2 Solar Irradiation Measurements.

Solar irradiation falling into the full size transwall was measured by three Kipp and Zonen solarimeters - global, diffuse and global vertical shown in Figure 3.12. The global and diffuse solarimeters, C.M.5.s, were fitted on the outside roof of the solar test cell. A C.M.3 model was mounted vertically on top of the transwall module facing the south window in order to measure the diffuse irradiation falling on the transwall. The shading ring of the diffuse solarimeter was regularly checked to ensure continuous recording of diffuse irradiation with changing declination angle. Reflected irradiation within the test cell was measured by three silicon cells. The solarimeters and silicon

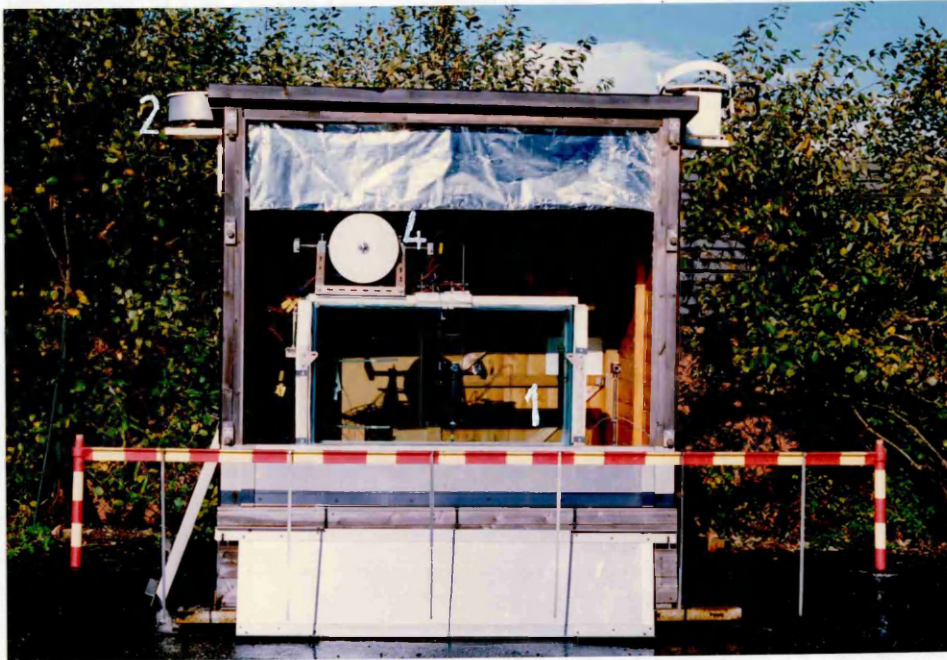


Figure 3.12 The Solar Test Cell showing the full size transwall module, (1), and the Kipp & Zonen solarimeters - global, (2), diffuse, (3), global vertical, (4).

cells were connected to the Solartron-Schlumberger data logger that was programmed to record the irradiation data every 6 seconds and average these over 15-minute intervals.

3.5.3 Transwall Temperature Measurements

The temperature distribution within the full size transwall module was measured using chromel-alumel thermocouples, Figure 3.13. The PTFE insulated thermocouples, diameter 0.2 mm are arranged as 4 sets of five thermocouple "fingers" lying on a horizontal plane. The thermocouple wire protrudes 20 mm from a 1.8 mm o.d. hypodermic tubing. The fingers are attached to vertical hypodermic tubes that can be raised, lowered or rotated by clamps outside the transwall. The full size transwall thermocouples, were calibrated twice against an NPL certificated P.R.T. (platinum resistance thermometer). The results showed that the transwall temperature was measured to within $\pm 0.15^{\circ}\text{C}$. The discussion on the calibration of the full size transwall thermocouples is given in Appendix D. The transwall thermocouples were connected to the data logger which was programmed to record the temperature rise every 15 minutes.

3.5.4 Collection of Data: Methodology

Despite the very poor summer of 1988 some runs were achieved using the programme outlined below:-

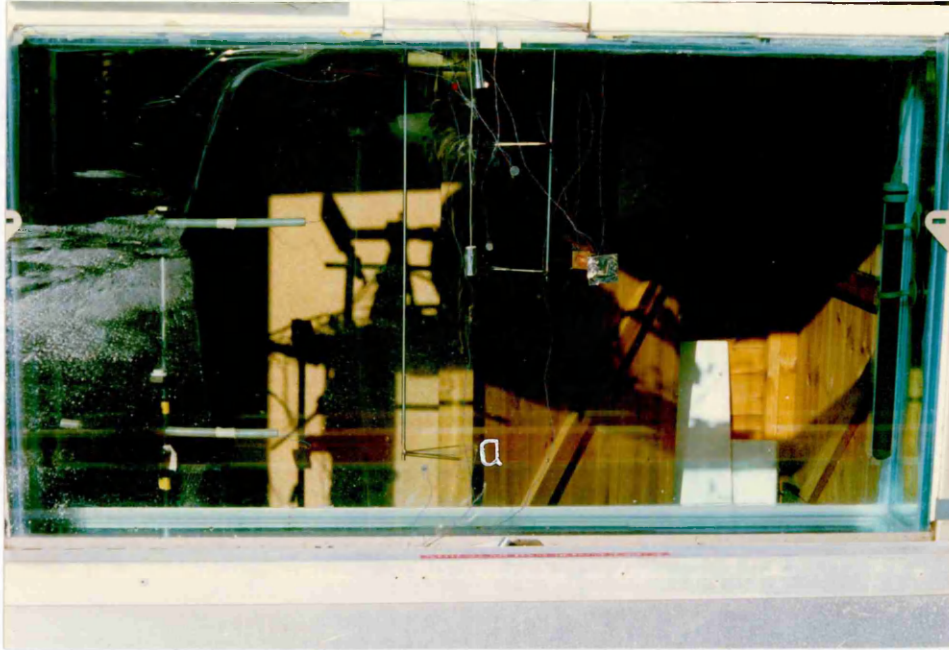


Figure 3.13 The PTFE insulated thermocouples arranged in 4 sets of five thermocouple fingers, (a).

- (a) The runs were made with clear water, and a water/dye solution, 20 ppm Lissamine Red 3GX.
- (b) Air stratification within the test cell was varied for clear water and 20 ppm Lissamine Red 3GX by,
 - i) directing the fan upwards and opening bottom exhaust vents. The opening of the bottom vents was intended to reduce air stratification;
 - ii) directing the fan down and opening top vents.
- (c) The runs were undertaken with one dye concentration and varying sky conditions, i.e. clear, cloud, overcast. This exercise proved difficult to achieve because of its complete dependency on capricious weather conditions.
- (d) The transwall temperatures were changed for the start of each run by using an aquarium water heater attached to the E-facing side of the transwall. One run was done with the water heater left off, in which case the room temperature would soon rise above the transwall; and another with the heater left on overnight. When the heater was switched off after running overnight the water was stirred for about 30 minutes before starting a run in order to reduce normal water stratification gradients. Readings were logged for 30 minutes before a start, and the night insulation then removed immediately after a logged reading.
- (e) The runs were generally made from 10 a.m. to 4 p.m.

3.5.5 Heat Transfer Coefficients Measurements

The two-dimensional computer program, temperature subroutine, calculates the heat transfer coefficients front glass to air gap, and rear glass to room as a function of transwall module height using the correlation suggested by Bayley et al. [41]. However, it was considered essential to the transwall analysis to obtain experimental values of the heat transfer coefficients for both module surfaces as a check on the theoretical values.

The coefficients had to be determined in situ because the fan and the venting arrangements were thought to have a major effect on the values. Accordingly the heat transfer coefficients were estimated from tests in which the transwall was allowed to cool with all but the test face insulated with 50 mm of expanded polystyrene. The fan was kept blowing and its orientation was interchanged in each case, allowing the fan to run normally, i.e. facing upwards, with bottom vents at the partition wall of the solar test cell open. The procedure was then reversed, allowing the fan to run facing downwards with the top vents open.

The experimental values of the heat transfer coefficients, front glass to air gap, and rear glass to room are shown in Table 3.1 for the case in which the transwall surfaces were insulated (except the surface under test). The heat transfer coefficients at the top and bottom horizontal surfaces of the transwall module

Table 3.1 Experimental Measurements of the Heat Transfer Coefficient, h , for a full size insulated Transwall Module, Surface to Solar Test Cell Ambient.

Condition of Fan	Type of Transwall Face	Heat Transfer Coefficient h	
		Measured $W/m^2.K$	Predicted ⁽¹⁾ $W/m^2.K$
Normal-Up position, Bottom vents open	North/Rear	6.1	8.8 - 7.2 ⁽²⁾
	South/Front	7.7	7.6 - 6.6 ⁽²⁾
	Top	5.4	
	Bottom	5.2	
Downward position, Top vents open	North/Rear	11.1	
	South/Front	15.4	
	Top	3.1	
	Bottom	5.4	

1) Transwall surface temperature higher than surroundings.

2) Transwall height-dependent heat transfer values, from bottom to top of transwall surface.

were also calculated for the case in which the module surfaces were insulated. The heat transfer coefficients calculated represent the overall coefficients combining radiation and convection.

3.6 Comparison : Experiment with the Two-Dimensional Computer Model of the Transwall

3.6.1 Introduction

The experimental start temperatures were not uniform as in the case of the small transwall module. The average vertical temperature gradient for water inside the transwall from top to bottom was about $1^{\circ}\text{C}/\text{m}$ at the start, and about $2^{\circ}\text{C}/\text{m}$ at the end of a 5-hour run, for the case in which the transwall temperature was higher than the surroundings. A similar situation was found for the case in which the transwall temperature was lower than the surroundings. The plots of the four planes of transwall thermocouples (transwall higher than surroundings) are shown in Figure 3.14(a) The end transwall temperatures predicted by the two-dimensional computer model are shown compared with experimental end temperatures, in Figure 3.14(b). The two-dimensional computer temperatures form two bands that lie in between the two experimental extremes, the top and bottom end temperature planes.

The top plane temperatures predicted by the two-dimensional computer model, Curve(6), are much lower

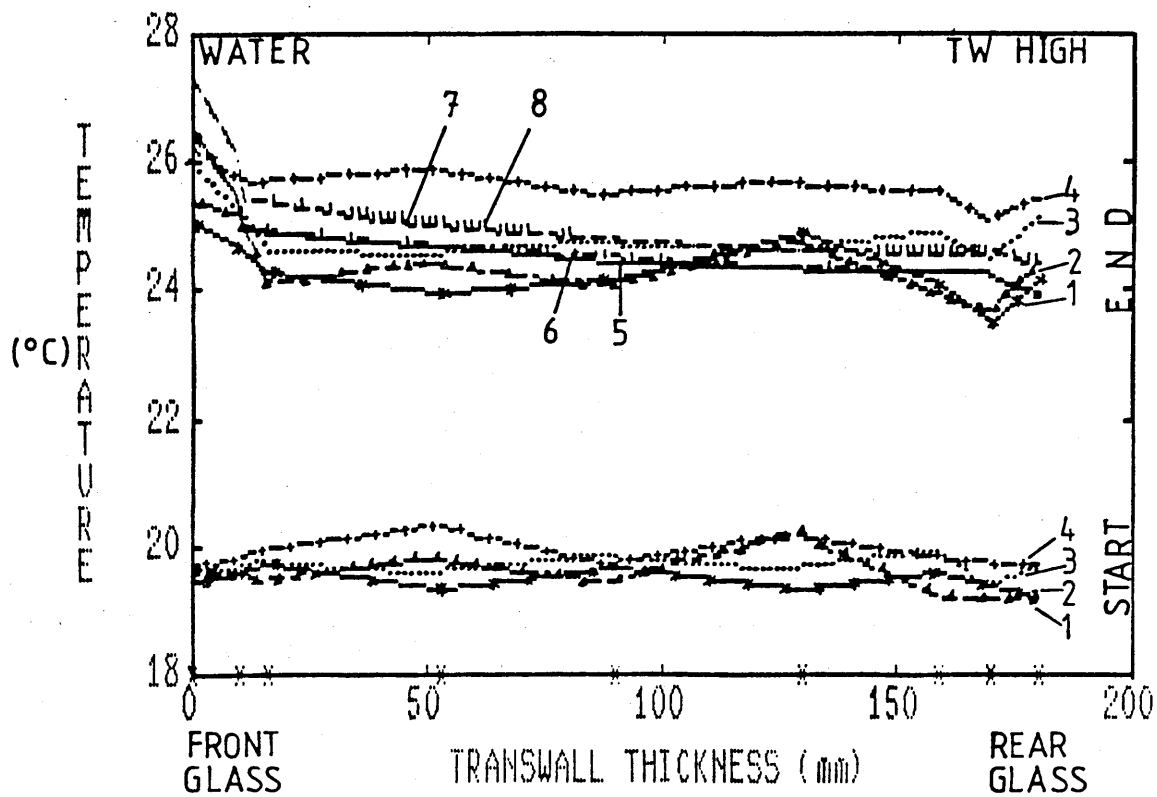


Figure 3.14(a) The plots of the 4 planes of transwall thermocouple 'fingers'. Curves (1,2,3&4) show measured temperatures and Curves (5,6,7&8) predicted values (see Fig. 3.14(b) below for details).

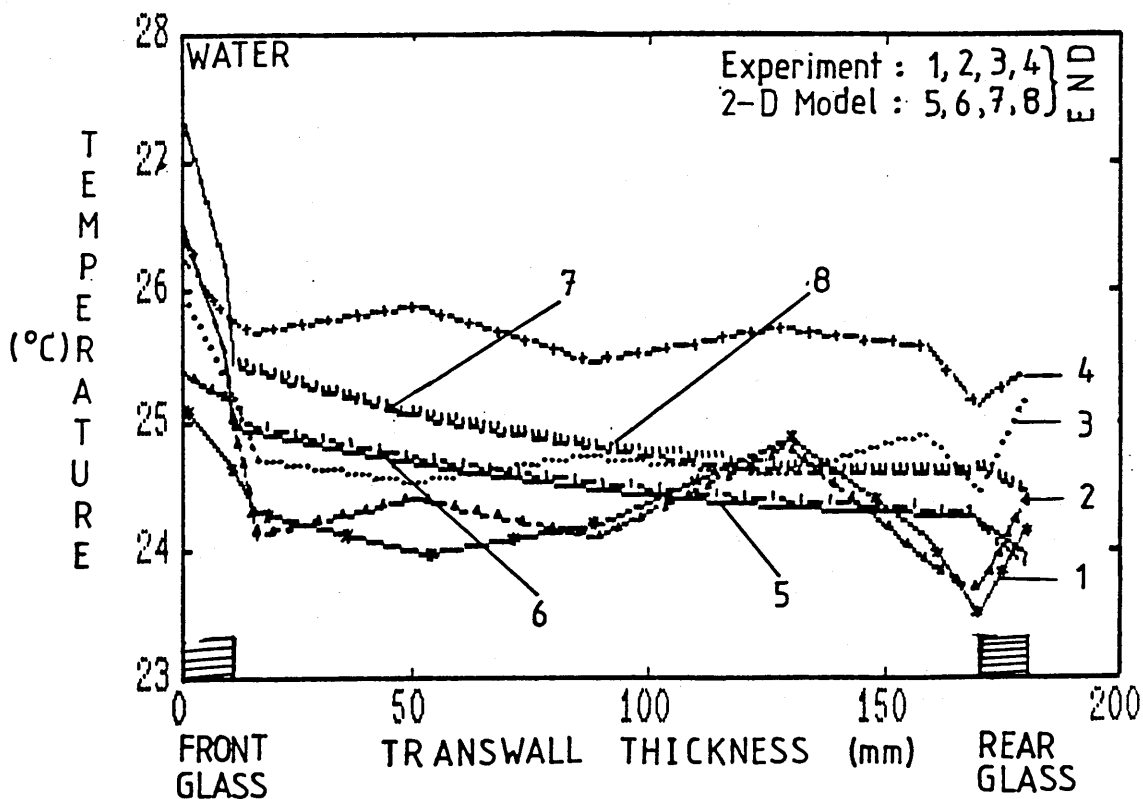


Figure 3.14(b) The plots of the transwall final temperature planes, experiment vs 2-D Model. Transwall is higher than surroundings. Curves (1&5)–bottom; Curves (2&8)–mid lower; Curves (3&7)–mid upper and Curves (4&6)–top plane.

than their experimental counterparts. The likely reasons for this under prediction are the inability of the effective conductivity approach by itself to represent adequately stratification and the uncertainty in the actual heat transfer coefficients at the top and bottom surfaces. This matter is dealt with more fully in section 3.7. The plot of the four planes of temperature is cluttered and confusing. It is believed that the mid-upper thermocouple plane is the best compromise of the transwall temperature distributions between the top and bottom extremes and this single plane is plotted hereafter.

3.6.2 Results.

(a) Case 1: Transwall Temperature Higher than Surroundings.

(i) Water.

The two-dimensional computer model was found to agree reasonably well with experiment when using water without a dye in the transwall. The two-dimensional model slightly overpredicts the mid upper level transwall temperature rise by 7%. The one-dimensional model, on the other hand, seems to perform better than the two-dimensional model because it overpredicts by 2% relative to the mid upper temperature. This is considered fortuitous because the one-dimensional

computer model does not take into account the vertical ambient temperature gradients that have been found to be significant in the computer modelling (Section 3.6.1). Also the one-dimensional program will underpredict the absorption relative to the two-dimensional because the former ignores shading and reflection off the bottom. The effect on the temperature distribution of water circulation is shown in Figure 3.15(a) in which the Nusselt number is put to unity. The shapes of both curves (one-dimensional and two-dimensional) show that the net effect of circulation is to flatten the curves substantially.

The shape of the curves at the front glass end is similar to the experimental plot. However, the experimental plot shows an unusual dip at the rear end of the glass (inside glass temperature). This is possibly due to cooler water entrained into the boundary layer at this surface. Otherwise, the shapes of the computer model curves are reasonably similar to that of their experimental counterpart. The effect of a surface contact resistance modelling the boundary layer is clearly visible in both model curves, and the shape in that region is very similar to the experiment.

The sensitivity of the variation or otherwise, of the overall heat transfer coefficients glass to air is examined in Figure 3.15(b). They varied in this case from 7.6, bottom, to 6.6 W/(m².K), top, for the room side, and from 8.8, bottom, to 7.2 W/(m².K), top, for

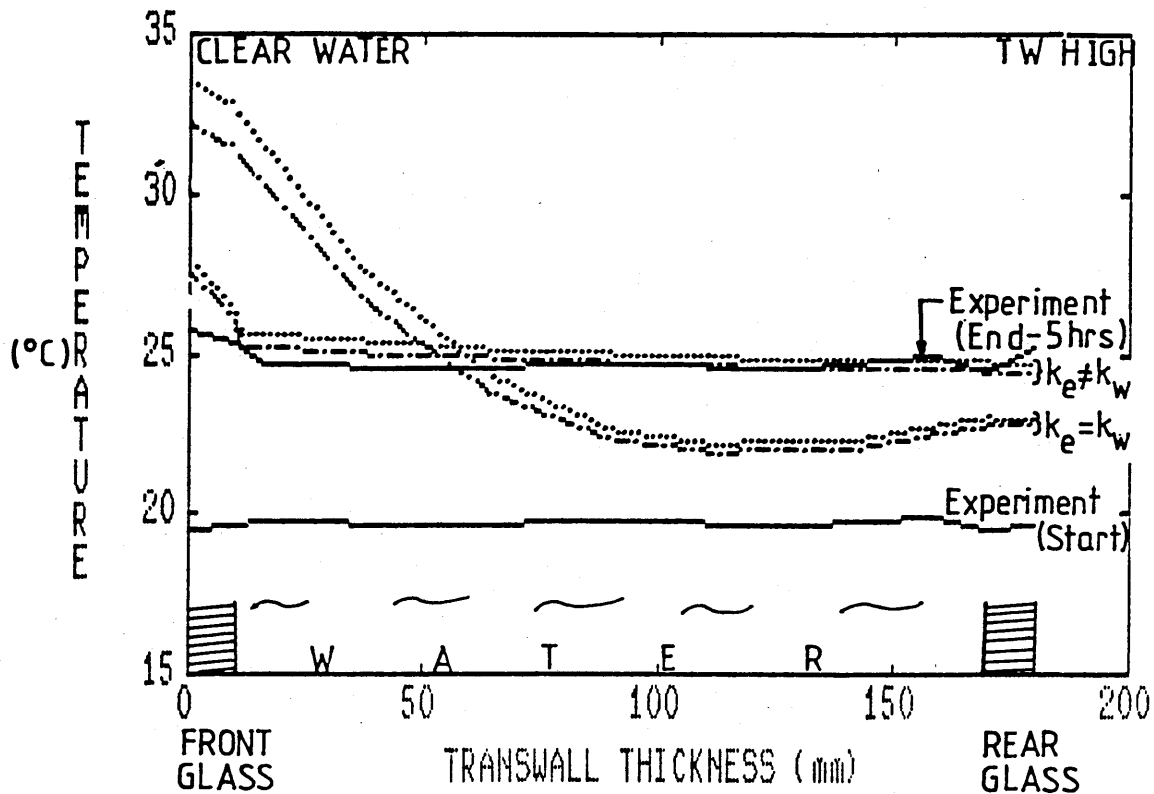


Figure 3.15(a) The 2-D vs 1-D computer models showing clear water for the case in which the Transwall temperature is higher than the surroundings. (..... 2-D Model & ---- 1-D Model).

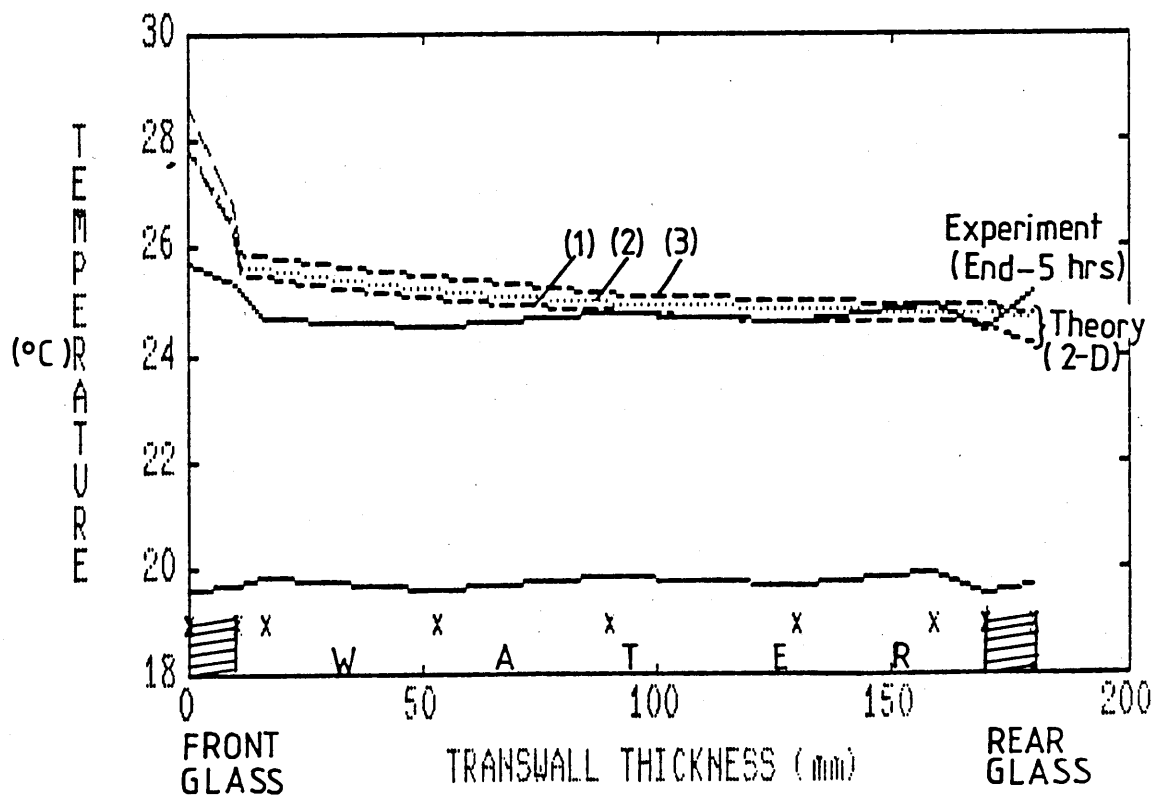


Figure 3.15(b) The effect of keeping the convective heat transfer coefficients constant or varying with transwall height for a 2-D computer model. 'curve code p120'

the window side. The effect of using measured mean values of the overall heat transfer coefficients, for the case in which the fan was running normal, i.e. facing upwards with bottom vents open, are shown compared with predicted values, height dependent, in Figure 3.15(b). The measured values are $6.1 \text{ W/(m}^2\text{.K)}$, room side, and $7.7 \text{ W/(m}^2\text{.K)}$, window side, Curve (1). Curve (2) represents height varying predicted values of overall heat transfer coefficients. Curve (3) examines the effects of using $15 \text{ W/(m}^2\text{.K)}$ for the window side, and $8 \text{ W/(m}^2\text{.K)}$, for the room side. It is clear that the computer model is not unduly sensitive to the variation with height of surface/air heat transfer coefficients, or indeed to their value within limits. This, of course, depends on their being normal temperature differences between the surfaces and air, 30°C room side, 40°C window side in this case.

ii) Lissamine Red 3GX (Water/dye solution)

When a 20 ppm Lissamine Red 3GX water/dye solution was used in the transwall the two-dimensional computer model, Figure 3.15(c) overpredicted the average transwall temperature rise by 0.6°C , based on the upper thermocouple plane, Curve (2) and by 1.4°C based on the bottom thermocouple plane, Curve (1). Hence, the two-dimensional computer model does not perform so well in this case, and the reason is unclear. A possible suspect was the absorption program. But a check of

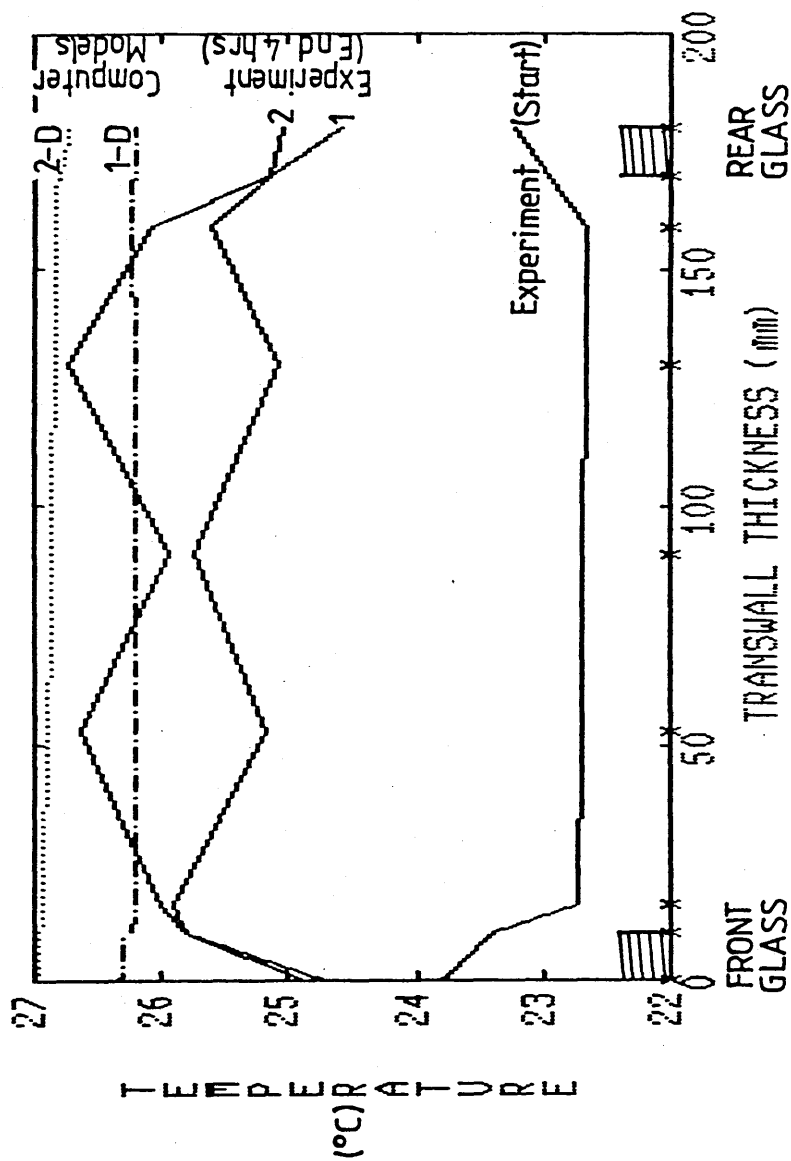


Figure 3.15(c) The 2-D vs 1-D computer models showing a water-dye solution, 20 ppm Lissamine Red 3GX, for the case in which the transwall temperature is higher than the surroundings. Curve (1) represents the bottom temperature plane, and Curve (2) the top temperature plane.

measured transmission through the transwall with Lissamine Red 3GX showed reasonable agreement, 2%, with the program. The dye does fade to some extent over a few weeks and this would account for some level of overprediction. Another factor is the increased stratification arising from the enhanced absorption compared to that of water. It has been reported [36] that heat transfer coefficients liquid to surface in an irradiated enclosure are higher than if irradiation is not present. This factor will also mitigate the overprediction.

The one-dimensional computer model, on the other hand performed better than the two-dimensional model. It overpredicted the temperature rise in the transwall by 0.7°C , based on the bottom thermocouple plane, and it underpredicted by 0.1°C , based on the upper thermocouple plane. This is perhaps due to the fact that the one-dimensional computer model does not consider the stratification effects as does the two-dimensional model. Both models do not exhibit the "saw-tooth" like, [20], shape of their experimental counterpart at the end of the run. This is a classic feature of circulation within an enclosed space.

(b) Case 2: Transwall Temperature Lower than Surroundings.

(i) Water.

The two-dimensional computer model did not perform quite so favourably when the transwall temperatures were lower than surroundings. The model underpredicts the temperatures by 20% as shown in Figure 3.15(d). The one-dimensional model, however, was found to overpredict the transwall temperature rise by 10%. Clearly, there is a contradiction. This is perhaps due to the complex air circulation pattern that exists over the transwall when the system's operation is reversed, i.e. the transwall surfaces are relatively cool. The one-dimensional model ignores stratification, ambient temperature variations, and performs better in this case. Another contributing factor is that the actual overall heat transfer coefficients surface /air could be much higher than predicted by the two-dimensional computer model, or measured from experiment, Table 3.1, which was undertaken with the transwall temperature well above that of the room. The computer predicted values of overall heat transfer coefficients varied in this case from 8.6, bottom, 7.1 W/(m².K), for the room side, and from 8.8, bottom, to 7.3 W/(m².K), top, for the window side.

The shape of both curves (two-dimensional and one-dimensional) resemble the experimental plot on the

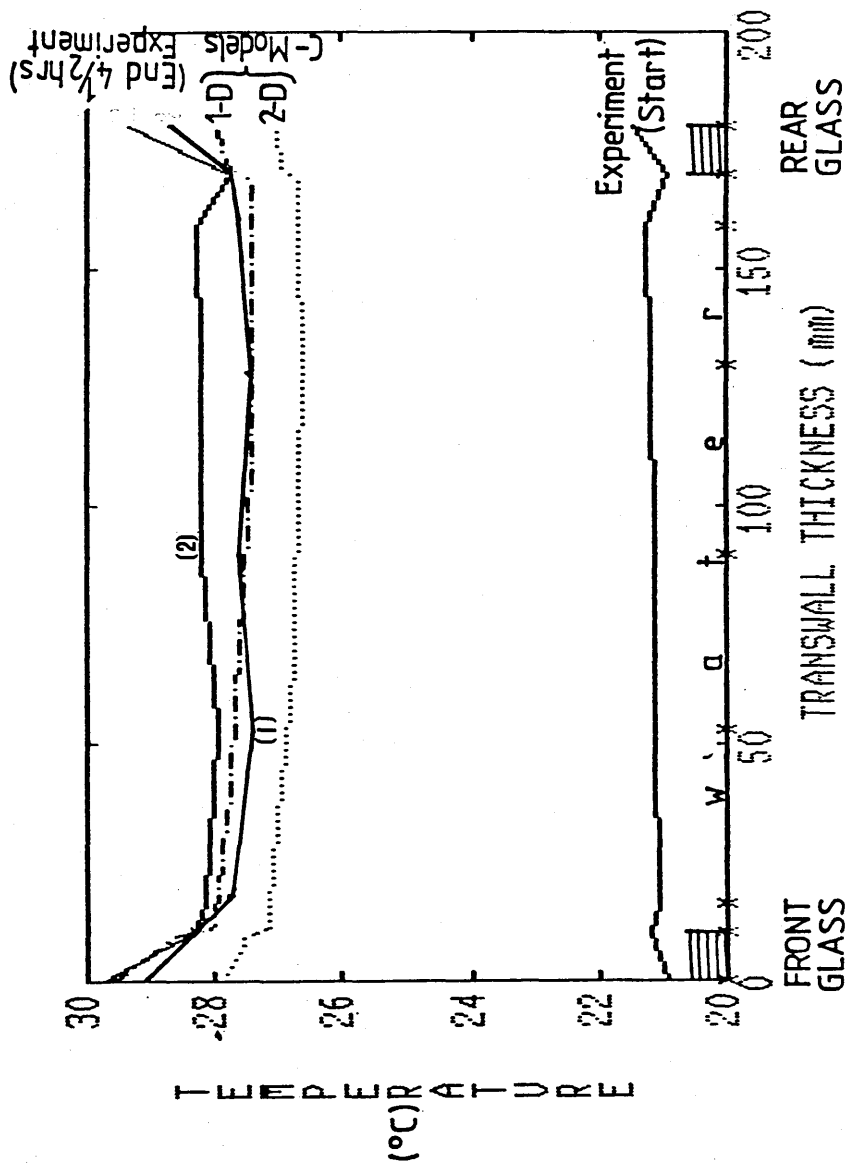


Figure 3.15(d) The 2-D vs 1-D computer models showing clear water for the case in which the transwall temperature is lower than surroundings. Curve (1) shows the bottom temperature plane, and Curve (2) the mid upper temperature plane.

window side. However, the dip in the experimental plot on the room side (inside glass temperature) is again possibly due to circulation phenomenon. Otherwise, the shapes are also reasonably similar to the experimental plot on the rear side as well. The effect of the "surface contact resistance" i.e. boundary layer on both model curves is pronounced.

ii) Lissamine Red 3GX (Water/dye solution)

When the two-dimensional computer model was applied to the case with a lower transwall temperature and with a water/dye solution, 20 ppm Lissamine Red 3GX, the model was found to overpredict the average transwall temperature rise by 34%, while the one-dimensional computer model seemed to perform better by underpredicting the transwall temperature rise by 15%. The computer-predicted plots of the two models are shown in Figure 3.15(e). The two-dimensional model is more consistent than the one-dimensional in the sense that it overpredicts irrespective of the direction of the heat transfer transwall surface to air.

The shape of the two-dimensional model curve is consistent at both ends with the experimental plot, while the one-dimensional model curve shows a slightly steeper gradient from outer glass surface to the inner glass surface at the front side of the transwall. This is strange for a lower transwall temperature that is receiving heat transfer from the surroundings.

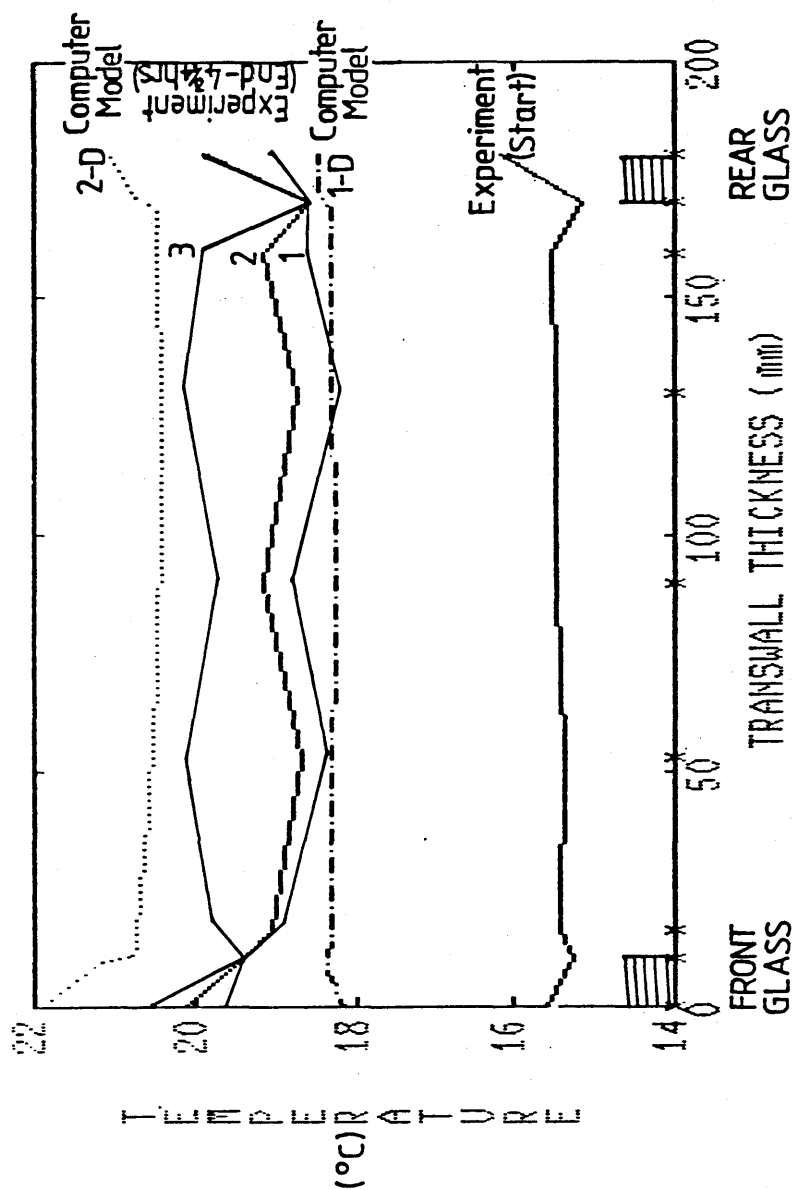


Figure 3,15(e) The 2-D vs 1-D computer models showing a water-dye solution, 20 ppm Lissamine Red 3GX, for the case in which the transwall temperature is lower than the surroundings. Curve (1) - bottom temperature plane, Curve (2) - mid upper temperature plane, & Curve (3) - top temperature plane.

3.7 Stratification Effects: Computer Predicted Vertical Temperature Profiles vs. Experimental Plots.

The plots of the computer predicted vertical temperature gradients compared with experimental plots are shown in Figures 3.16(a-e). Figure 3.16(a) shows the gradients for the case in which the transwall surface temperature was higher than the surroundings. The effect of varying vertical effective conductivity factor (ratio vertical to horizontal effective conductivity) from 0.1 to 1 is shown in Figure 3.16(b). Similarly, Figures 3.16(c) and 3.16(d) show the case for the transwall surface lower than the surroundings.

The case for a water/dye solution, 20 ppm Lissamine Red, is shown in Figure 3.16(e), for the surface transwall temperature higher than the surroundings. The experimental gradient here indicates higher temperatures at the top and bottom, which suggests circulation drive because of enhanced volumetric absorption by the dye. The central core, on the other hand, is much cooler. Clearly, the circulation pattern is much more complex.

In conclusion, it appears that the computed vertical temperature gradient is adequate for the bottom third, Figures 3.16(a-d), but too small for the remainder, and cannot on this evidence, provide a reliable gradient.

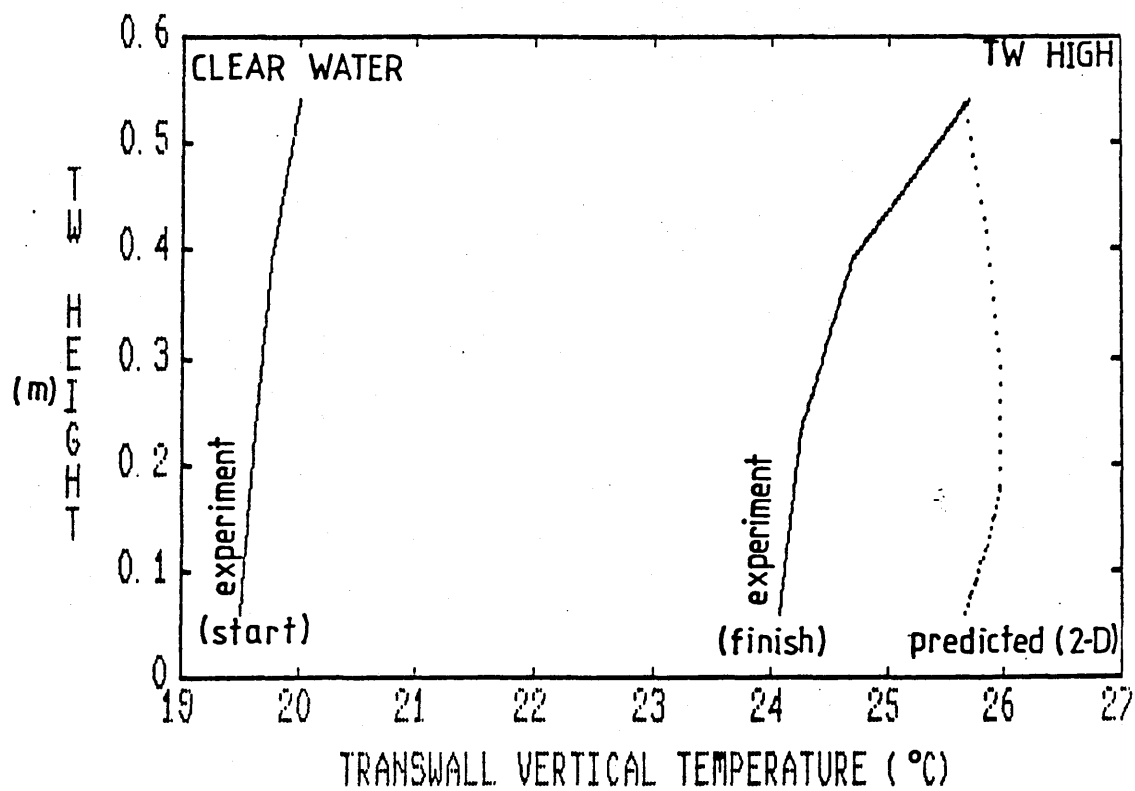


Figure 3.16(a) The transwall vertical temperature profiles. Surface temperature of transwall is HIGHER than the surroundings. Vertical effective conductivity factor, r , equals unity.

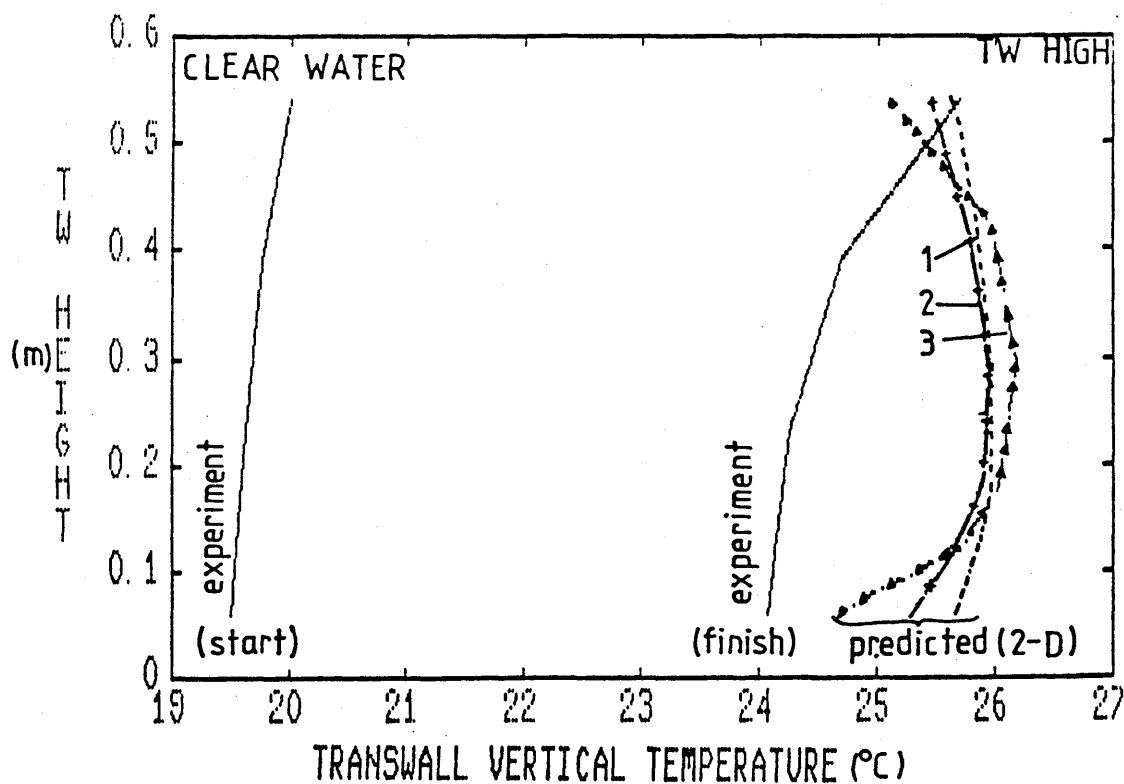


Figure 3.16(b) The transwall vertical temperature profiles. Surface temperature of transwall is HIGHER than the surroundings. Vertical effective conductivity factor equals 1, Curve (1); 0.5, Curve (2), and 0.1, Curve (3).

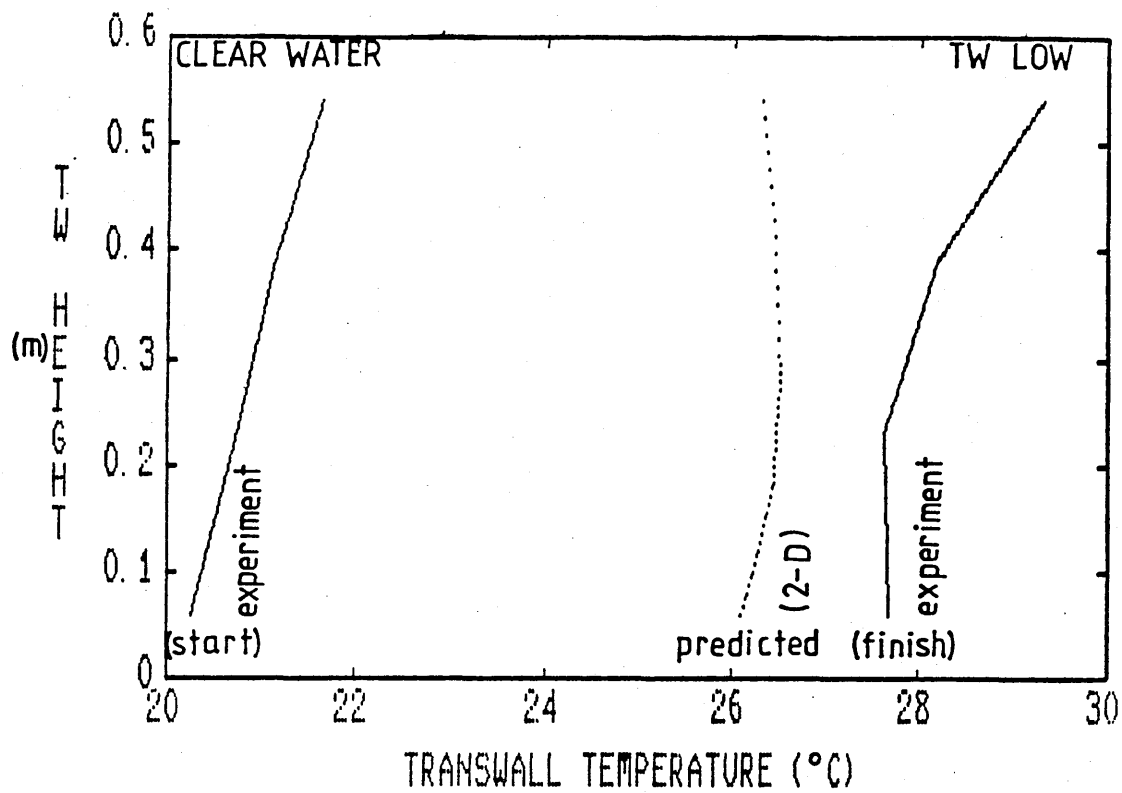


Figure 3.16(c) The transwall vertical temperature profiles. Surface temperature of transwall is LOWER than the surroundings. Vertical effective conductivity factor equals unity.

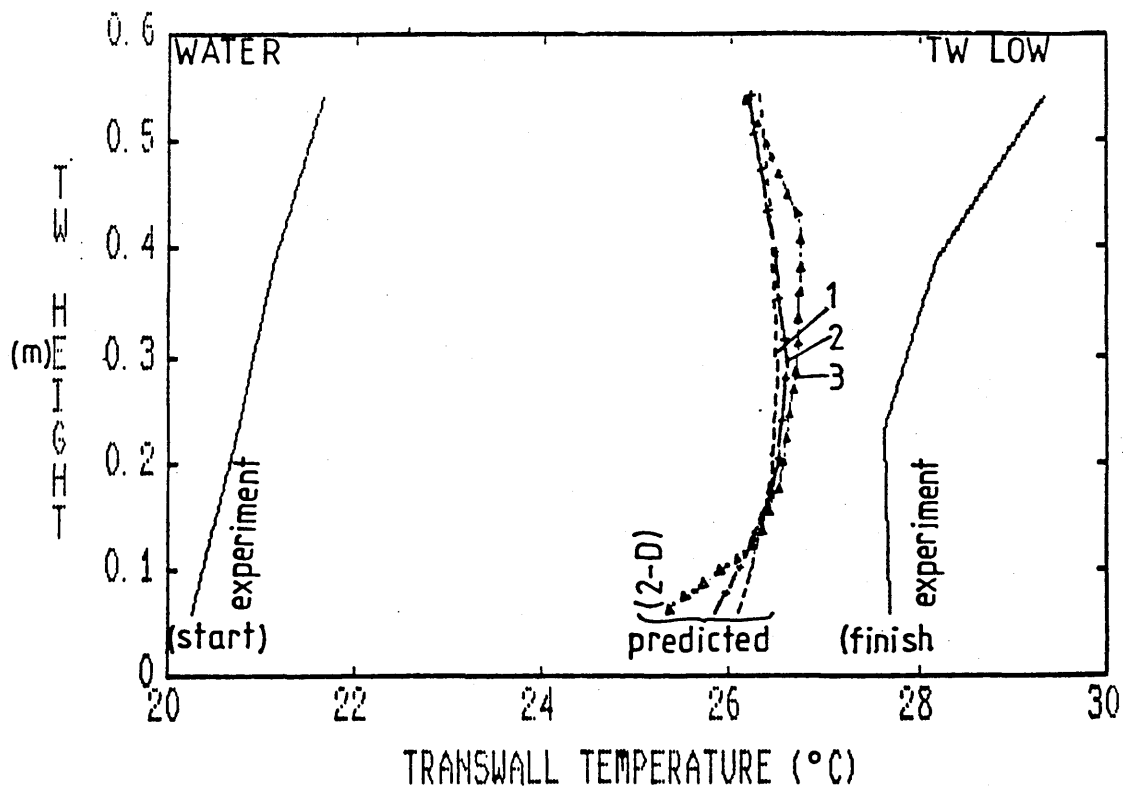


Figure 3.16(d) The transwall vertical temperature profiles. Transwall surface temperature is LOWER than the surroundings. Vertical effective conductivity factor equals 1, Curve (1); 0.5, Curve (2), and 0.1, Curve (3).

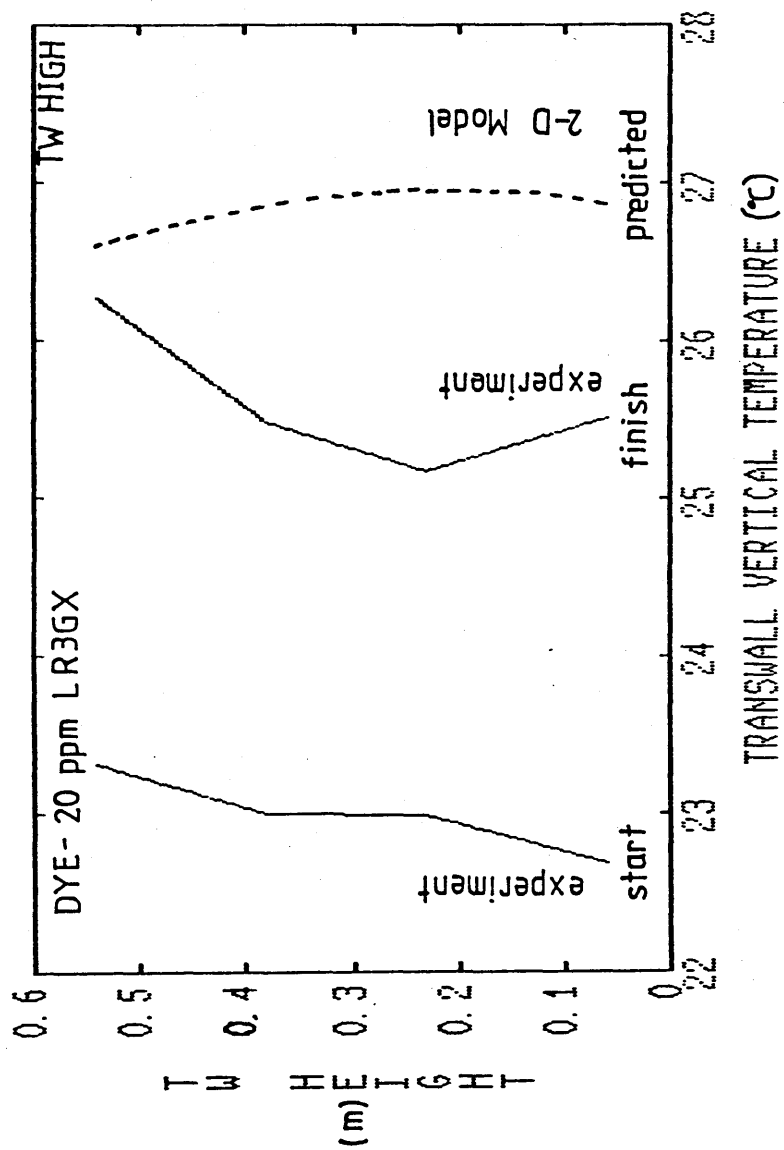


Figure 3.16(e) Transwall vertical temperature profiles. Surface temperatures of transwall higher than the surroundings, Vertical effective conductivity factor, r , equals unity.

3.8 Conclusions.

The two-dimensional computer model of the transwall employing the concept of "effective conductivity", and using the explicit finite difference method has been developed to predict the temperature distribution within the transwall. The computer predicted results have been compared with those measured experimentally, and the following is concluded.

- 1) The one-dimensional model performs fairly well bearing in mind its limitations. The maximum prediction error is only 18%, and with water alone this reduces to 5%. These figures are based on mid plane temperatures.
- 2) The two-dimensional model is less satisfactory. The vertical variation of temperature makes a simple representation of error rather meaningless, but based on mid plane temperatures this method cannot predict temperature rises to better than 35%. This figure is reduced to 18% for water alone with lower volumetric absorption.
- 3) The two-dimensional model is not sensitive to variations vertically in the surface/air heat transfer coefficients, and apparently insensitive to up to a 50% variation in the magnitude of these

coefficients. It is recognized that the modest 3-4°C temperature differences between surface and air may mask the latter observation.

- 4) The thermal conductivity approach cannot by itself adequately represent the two-dimensional temperature variations in a transwall subject to free circulation, i.e. in the absence of a gelling agent.
- 5) The computer program for the two-dimensional model is 4 times the length of the one-dimensional treatment, and it is recommended that this be used until the suggestions for improvement, chapter 5, are tested and possibly implemented.

Chapter 4

Chapter 4

Application of the Transwall Models.

4.1 Introduction.

This chapter is concerned with the application of a transwall simulation model to determine the optimum parameters for the transwall when constructed in a house located in the west of Scotland.

The house is described and the heat load program outlined. The simulation model is specified and the equations are developed for calculating the necessary data, e.g. glazing and air gap temperatures. The optimum water thickness and dye concentration are determined. The simulation model is then used to compare the performance of the Ames transwall module with that of MERA. The effects of free and forced circulation over the transwall, and the 'quenched' mode, are quantified. The performance of the superior MERA transwall is shown monthly over a year and the benefits of operating in a sunnier climate, specifically Nice, illustrated.

4.2 The House

The transwall is taken to be located in a house designed on passive solar principles, viz large south facing windows, a clerestory to transmit irradiation into the centre of the building, light airy open plan,

gallery etc. Photographs of the house are shown in Figures 4.1(a,b,c) and elevation and plan in Figures 4.1(d,e). The house was the subject of an honours project [46] and a specification of the house is given in Appendix F. Briefly it is the size of a typical suburban detached house, plan area 9 m x 9 m, with a high level of insulation in the walls, ceiling, and under the floor. It is fitted with a heat recovery system which uses extract air to heat inducted air. It has two large double glazed windows facing south, of which one is in the roof forming the clerestory, and only a small window to the north. The windows on non south facing walls are taken to be of Kappafloat construction.

The transwall is located as shown in Figures 4.1(a,b,c) and is built 5 modules high by 7 modules long giving a surface area of 25 m² and a building volume to transwall surface ratio of 20 m³/m². This is quite high, and, for example, it does not compare well with a single story roof pond building which might have a ratio of closer to 5m³/m² aperture area. Provision can be made to install a low 10 module transwall on the balcony which would increase the transwall area by 30% to 32 m². The balcony transwall will have lower heat losses than the main walls but this is counter balanced by partial roof aperture shading early and late in the day.

A possible method of constructing the wall is to



Figure 4.1(a) The House - Front View (South)

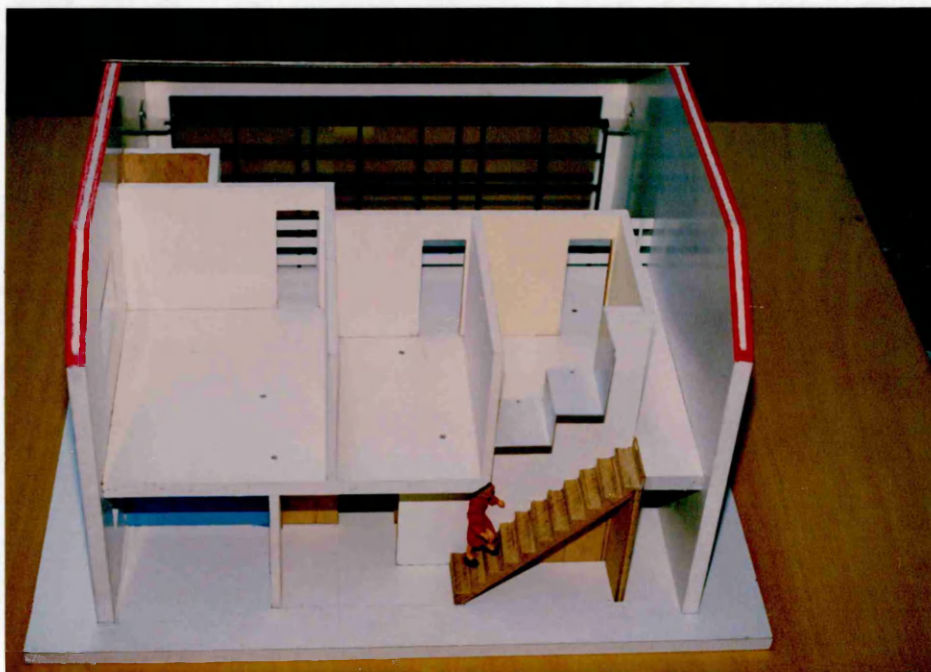


Figure 4.1(b) The House - North, showing the plan view. The transwall modules can be clearly seen in the background.

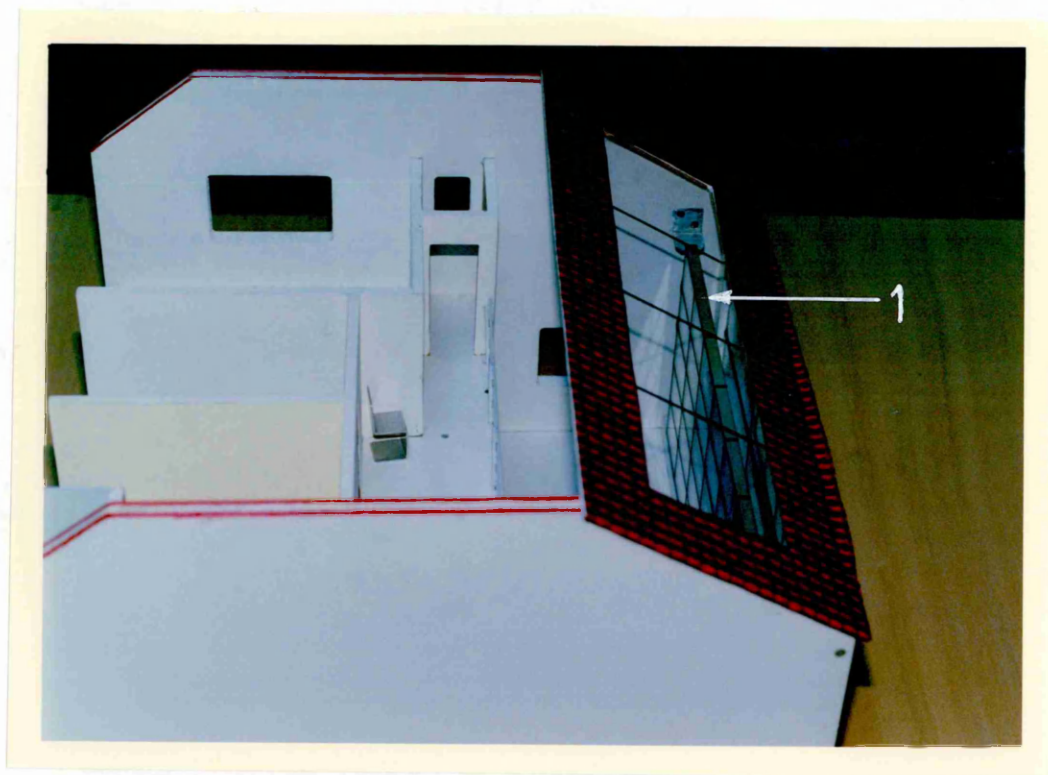


Figure 4.1(c) The House - End View, showing the thicknes of the modules as seen through the sun roof (see 1).

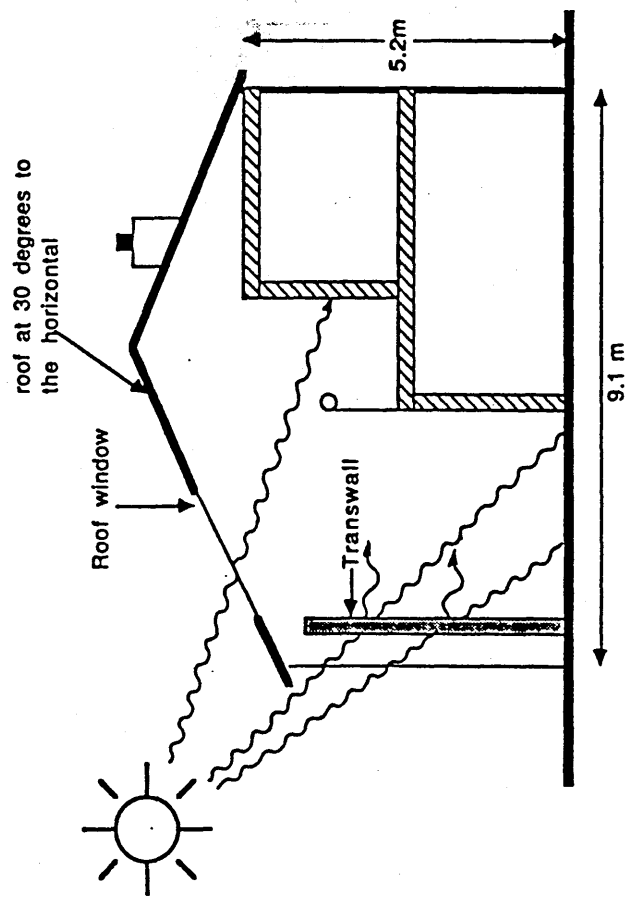


Figure 4.1(d) Section through the House Design,
[Ham, 1988].

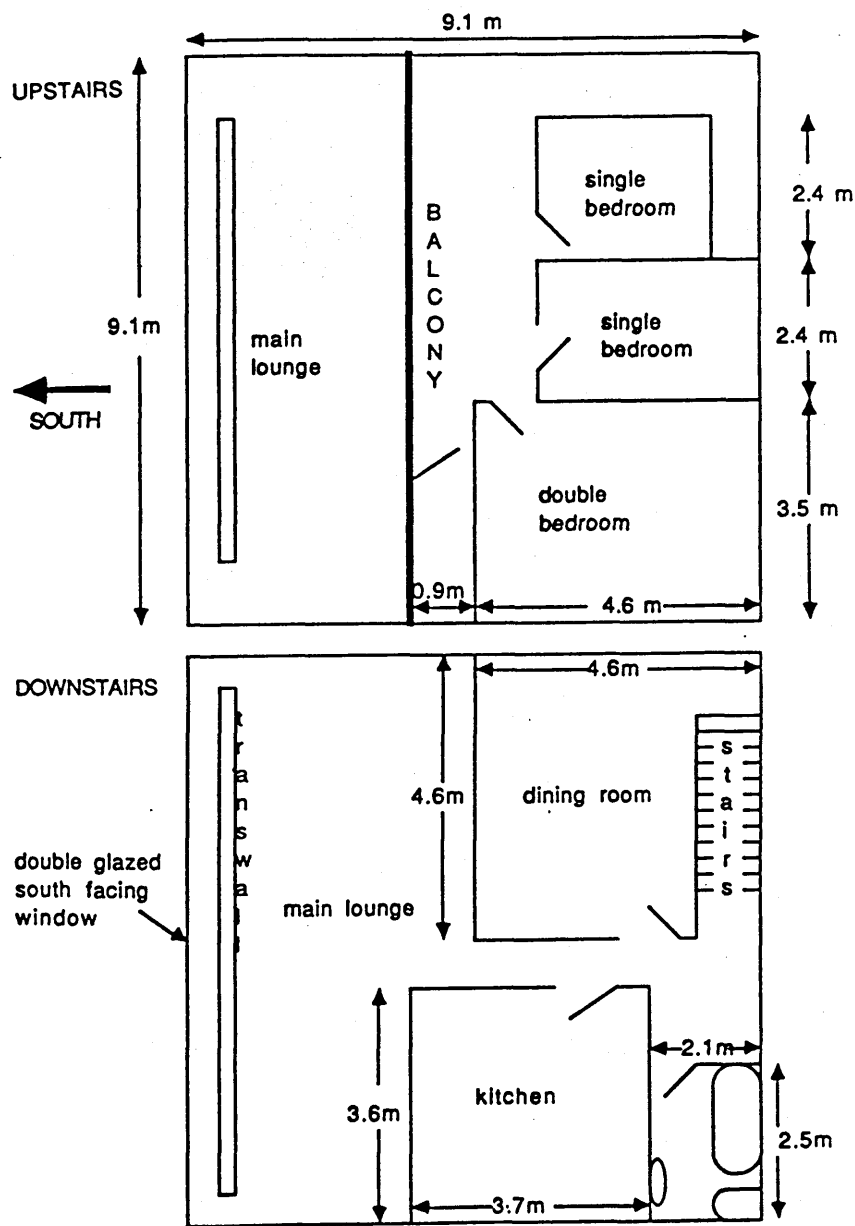


Figure 4.1(e) The Plan of House Design,[Ham,1988].

locate the modules in a standard steel shelving system such as Link 51 Handy Tube. This system is versatile, easy assembled on site, visually acceptable, and available in a cut to length option. A 3 x 6 module framework was stressed [47] using a plane frame stress analysis, program PL Frame 15. All joints were taken as rigid, except at ground level where they were pinned. The two largest stresses, bending and axial, were found to be within the maximum values permitted for the frame section. The cost of the frame, piping valves, etc came to £40/module, similar to the cost of the module itself. It is clear that efforts to reduce the cost of the transwall are best directed towards reducing the frame cost. In fact, the link 51 Handy Tube framework is probably inadequate for the 5 x 7 modules wall proposed in this model, and if the frame is constructed from more robust standard 40 x 40 x 3 mm m.s. hollow square section, and with some parts pre-welded, then the frame and piping cost falls to £23/module. This figure excludes painting.

A photograph of a module held in a Link Handy Tube frame is shown in Appendix A. The aluminium facing is 75 mm width and secured by box bands to the frame. The general appearance is plain, neat and efficient. The copper tube used to fill and syphon out the contents is seen at 1 and this is connected to a pipe system seen at the back of the facing at 2. A valve system concealed within the transwall base has been designed [47] which

allows the modules to be filled from, and drained into, a 4 m³ tank. The module, Appendix A, is constructed from 10 mm clear glass and joined by standard silicon aquarium adhesive. The modules are supplied by a local aquarium manufacturer [48]. The module has an upper strengthening rib which also serves to support a plastic lid with a cut out for the filling/syphon tube. The cut out is sealed by foam which permits air to enter but excludes algae spores.

4.3 The Heat Load.

The heat load on the house was found from a computer program, written in BASIC, which was part of an honours project [46]. The thermal capacity of the light weight construction is ignored, and it is assumed that the heating systems maintain a constant house temperature of 20°C. The ambient temperature is allowed to vary in a skewed sine wave given by C.I.B.S.E. Vol A [49]. Solar gains are obtained from the Angstrom - Page/Collares - Pereira - Rabl [2] methods to predict the hourly beam and diffuse irradiation using regression constants for Aldergrove. This site in Ulster is the nearest appropriate to the West of Scotland. A subroutine calculates the glazing transmission from first principles for a variety of window types. The ventilation heat exchanger subroutine permits a variety of systems to be tested illustrating the effects of air change rates, effectiveness etc. When the combined

direct gain and transwall energy release exceeds the heat load then this excess energy is assumed to be dumped.

4.4 The Simulation Model.

The one-dimensional model described in Section 2.2.2 was used, viz half glass slabs, 5 water slabs with two half slabs, floating glass/water surface heat transfer coefficient, and floating effective conductivity. The equations providing the irradiation absorption in the slabs are those of Section 2.2.1 modified by the term

$$(1-\rho_g)^4 \tau_g^2$$

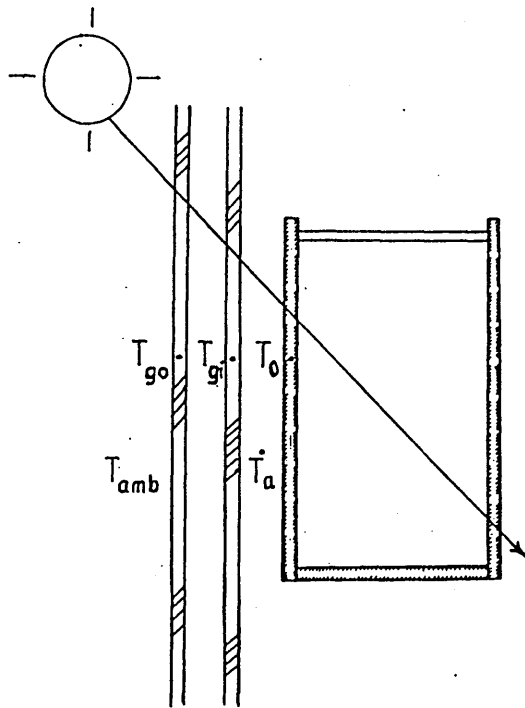
to account for the double glazing. The reflectance at the glass/air interface is ρ_g , and τ_g is the transmission through the glazing. The slab absorptances are calculated for each hour, 8 wavebands are used over the range 0.3 - 4.1 μm , and polarization components are combined on the exit of a ray. Beam and diffuse irradiation are treated separately.

The one-dimensional model was chosen in preference to the potentially more accurate two-dimensional model for two reasons. The major reason was a question of time. The heat load program for the solar house, coupled with the one-dimensional transwall and absorption programs took 4 1/2 hours on a P.C. in order to simulate 48 hours of real time operation. The run has to simulate two days in order to produce a 24 hour cycle, i.e. the start and finish temperatures must be

similar. Thus the run representing a year required 10 days allowing for data preparation. On balance it was felt better to tolerate this excessive running time than to rewrite the heat load program and incorporate the much longer two-dimensional transwall and absorption programs into it. Secondly, essentially a comparison is being made, e.g. between Ames and MERA systems, and consequently inaccuracies of the one-dimensional approach will tend to cancel.

4.5 Derivation of the Glazing and Air Gap Temperatures.

The transwall is taken to be situated behind a double glazed window.



T_o = one-dimensional transwall surface temperature

T_{gi}, T_{go} = inner and outer glazing temperatures

T_a	= temperature in air gap between transwall and glazing at midpoint of wall
T_{amb}	= ambient temperature
h_{ga}	= convective heat transfer coefficient between air and transwall and glazing surfaces with air circulation
h_k	= convective heat transfer coefficient across air gap without air circulation based on temperature difference $(T_o - T_{gi})$
h_{kg}	= as h_k but between glazing sheets
h_r	= linearised radiation heat transfer coefficient transwall to glazing
h_{rg}	= as h_r but between glazing sheets
h_{amb}	= combined convection and radiation heat transfer coefficient outer glazing to ambient.
$(I_{\odot})_{gi,go}$	= solar irradiation absorbed in inner and outer glazing sheets per unit area of transwall surface.

The first case considered is where there is no air circulation between the transwall and the glazing, i.e. what Ames refers to as the 'quenched' wall.

Energy balances on the two glazing sheets:-

$$(I\alpha)_{gi} + h_r(T_0 - T_{gi}) + h_k(T_0 - T_{gi}) - h_k(T_{gi} - T_{go})$$

$$-h_{rg}(T_{gi} - T_{go}) = 0$$

$$(I\alpha)_{go} - h_{rg}(T_{gi} - T_{go}) + h_{kg}(T_{gi} - T_{go})$$

$$-h_{amb}(T_{go} - T_{amb}) = 0$$

Solving for T_{gi} gives

$$\begin{aligned} T_{gi} = [c_2 c_4 T_0 + c_3 \{(I\alpha)_{go} + h_{amb} \cdot T_{amb}\} \\ + c_4 (I\alpha)_{gi}] / (c_4 c_1 - c_3^2) \\ \dots\dots\dots (4.1) \end{aligned}$$

$$\text{where } c_1 = c_2 + c_3$$

$$c_2 = h_r + h_k$$

$$c_3 = h_{rg} + h_{kg}$$

$$c_4 = c_3 + h_{amb}$$

If air circulation is permitted then similar energy balances on the glazing give:-

$$\begin{aligned} T_{gi} = [c_4 h_r T_0 + c_3 \{(I\alpha)_{go} + h_{amb} T_{amb}\} + c_4 (I\alpha)_{gi} \\ + c_4 h_{ga} T_a] / (c_1 c_4 - c_3^2) \\ \dots\dots\dots (4.2) \end{aligned}$$

$$\text{where } c_2 = h_r + h_{ga}$$

The radiation absorbed in the windows glazing $(I\alpha)_{gi}$, $(I\alpha)_{go}$ is calculated on the assumption that double reflected rays are second order and can be

ignored. The irradiation is split into beam and diffuse, predicted by the Angstrom-Page method and taken to be constant over an hour. The $(I\alpha)_{gi}$, $(I\alpha)_{go}$ terms are small in themselves, and it is safe to neglect window glass absorption from back reflected irradiation from within the transwall and to assume mean values for the window glass transmission and absorption. The window absorption terms are:-

$$(I\alpha)_{gi} = (I_b \cos i + 0.5 I_d) [\tau_g(1-\rho_g)^2 \{1 - \tau_g^2 \rho_g - \tau_g(1-\rho_g) + \tau(1-\tau)\rho(1-\rho)\}] \dots (4.3)$$

$$(I\alpha)_{go} = (I_b \cos i + 0.5 I_d) [(1-\rho_g)[1 - \tau_g^2 \rho_g - \tau_g(1-\rho_g) + \tau_g(1-\tau_g)\rho_g(1-\rho_g)\{1 + (1-\rho_g)^2 \tau_g^2 + (1-\rho_g)^2 \tau_g^2\}]] \dots (4.4)$$

The introduction of air circulation requires that the mean air gap temperature, T_a , be found. This is calculated at a point half way up the wall of height L. An energy balance on the air flow in the gap gives:-

$$T_a = \{m_a c_p T_r + 0.5 h_{ga} L (T_o - T_{gi})\} / (m_a c_p + h_{ga} L)$$

where m_a = air mass flow in gap/unit width

T_r = room temperature and inlet temperature of air into gap

c_p = specific heat capacity of air at constant pressure.

$$m_a = \rho_a w \left[\frac{2gL}{8(A_g/A_v)^2 + 2} \right]^{\frac{1}{2}} \left[\frac{T_a - T_r}{T_a} \right]^{\frac{1}{2}} \quad [1],$$

where p_a = is the air density halfway up the duct

w = width of air gap

A_g/A_v = area ratio air gap to top and
bottom vent area/m run of wall.

When forced convection is considered the mass flow rate, m_a , per metre run of wall is specified, and the convective heat transfer coefficient found from Akbarzadeh et al. [50] who developed it for a Trombe wall situation.

$$Nu = 0.090 \quad Ra^{1/3}$$

An obvious constraint in choosing a value for m_a is the fan power required. The value taken was 0.18 kg/s. m which will give a mean air velocity of about 1 m/s and a fan power consumption of 63 W/m run of wall. This value is based on data for a R.S. long life tangential fan, and it is too large to ignore relative to the heat release from the wall.

4.6 Results of the Computer Simulation.

4.6.1 Optimum Dye Concentration and Water Thickness.

Figure 4.2 (a) shows plots of heat release/ $\text{m}^2/24$ hours and the irradiation absorbed in the transwall as a percentage of a 45° incident beam of irradiation/ m^2 wall against the concentration in ppm of Lissamine Red 3GX dye. The curves are for the mean mid month day of March chosen because it represents the mean performance of the wall over the year. The two curves are similar, which suggest that it is sufficient to optimise the dye concentration on the absorption of a single beam rather than having to run the complete heat load program over a day, or over 12 mean month days. There seems little point in using a concentration for this dye of greater than 10-20 ppm. The former value could be used for duller winter days, the latter in brighter seasons.

The plot of transwall heat release/24 hours against water thickness, Figure 4.2 (b), shows that there is little to be gained in having a water thickness in excess of 20 cm and a minimum of at least 10 cm is required. The 'optimum' is taken as 15 cm, which is in agreement with Ames findings.

The optimum value of 20 ppm LR3GX dye and 15 cm water thickness are similar to those found by Nisbet and Kwan [7] for a transwall in a horticultural glass house.

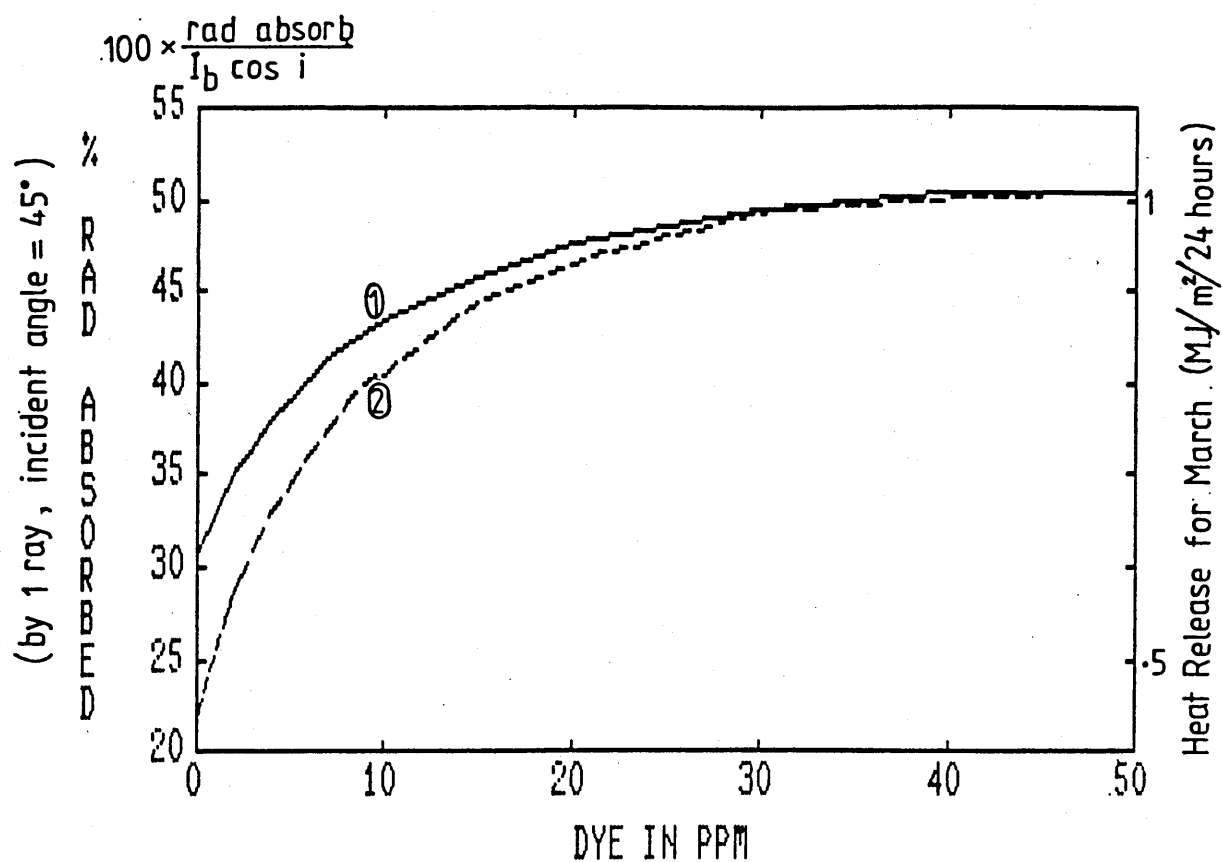


Figure 4.2 (a) Optimum dye concentration (Lissamine Red 3GX).
Curve (1) is from single ray absorption, and Curve (2) from Heat Release/24 hrs.

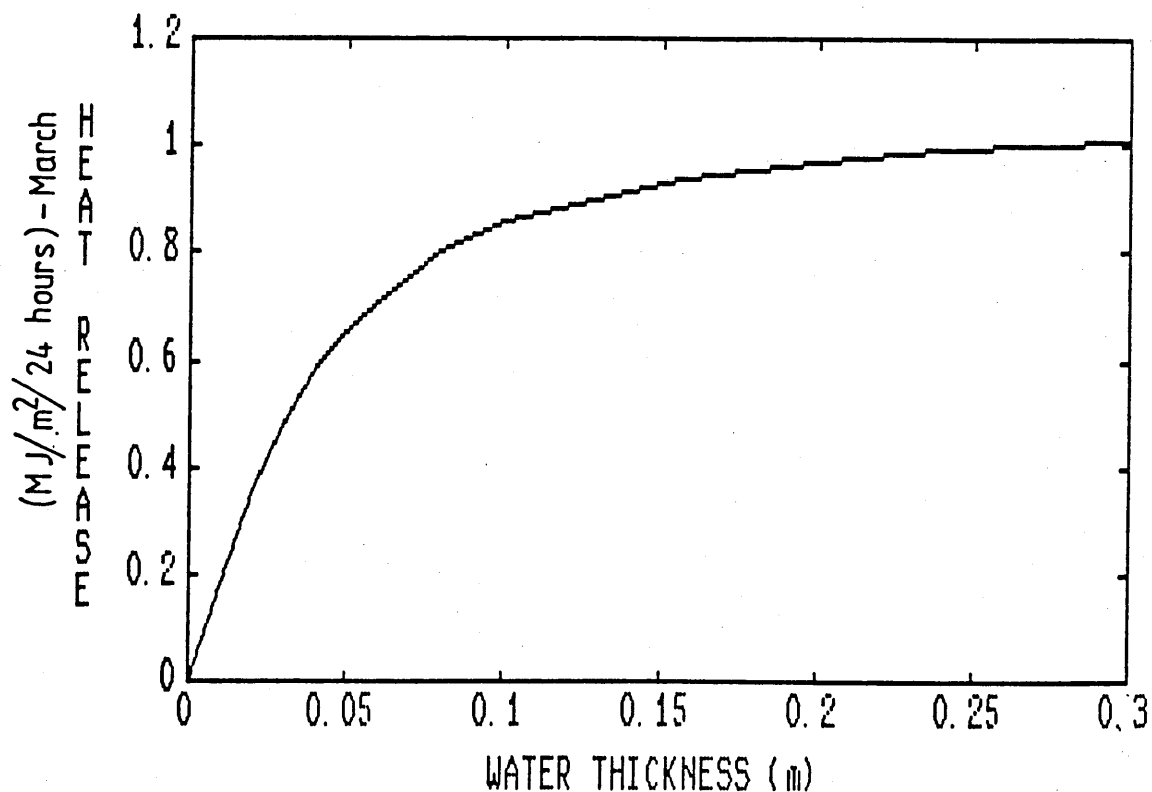


Figure 4.2(b) Optimum water thickness (20 ppm Lissamine Red 3GX).

The computer simulations were run to compare the performance of the MERA transwall using LR3GX dye and the Ames transwall which was taken to contain a gel which inhibits water circulation, without increasing absorption, and had the rear face made from Pilkington glass, Antisun Grey 41/60. This gives the same transmission as that reported by Ames. A dye concentration of 40 ppm was chosen in order that the transmissions of the two modules are equal. The Ames module was taken to have the same water thickness, 15 cm, as the MERA module and the same glass thickness, 10 mm. The latter is thicker than the 6 mm glass used by Ames because the author regards their glass thickness as unsafe. In deference to the Ames method of operation air circulation between the transwall and the window was prevented.

The plot of transwall heat release/ $\text{m}^2\cdot\text{h}$ against time of day is shown in Figure 4.3(a) and for the mean ^{day} month of March. At first sight it may appear that the Ames module is the superior because the MERA module gives 14% less heat release over the day. However, it is contended by the author that the heat release during the evening is the crucial index of performance, and Figure 4.3(a) illustrates the marked superiority of the MERA module over the hours 1700-2300 hrs. In fact, the MERA module gives a higher heat release over the time

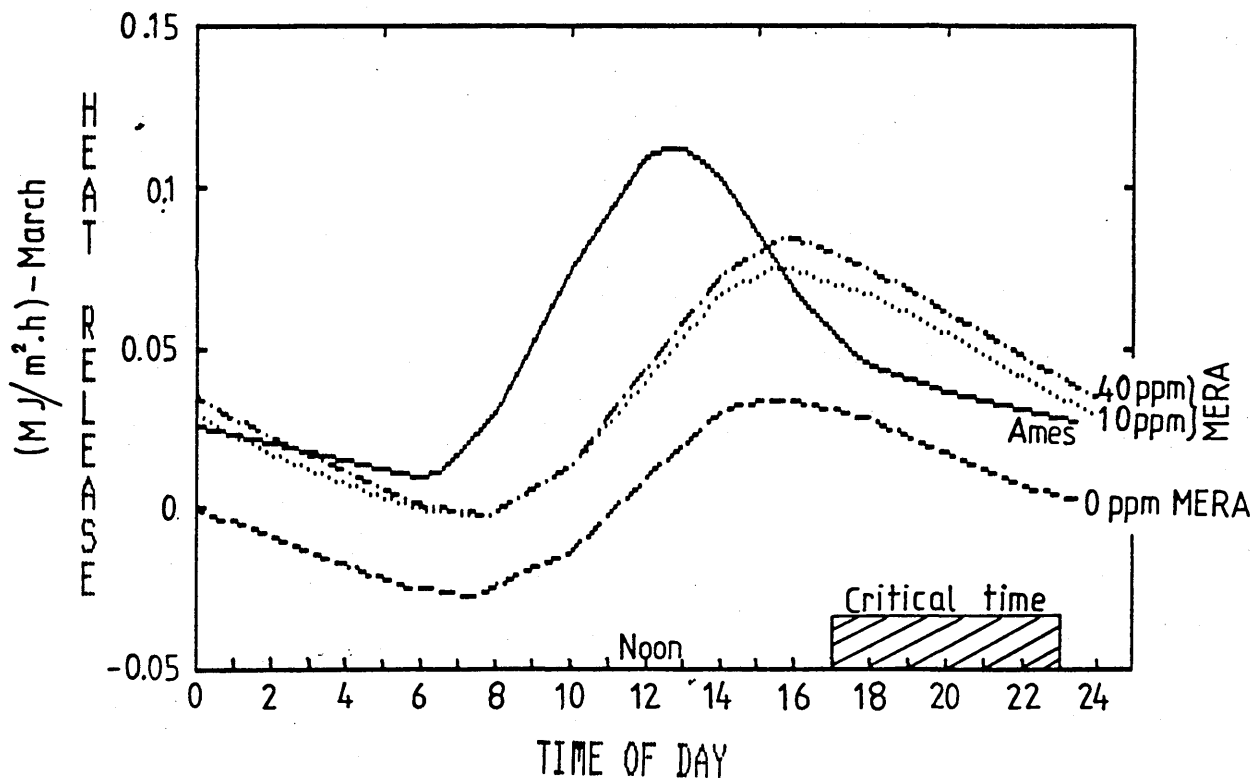


Figure 4.3(a) Effect of water circulation — Ames vs MERA.

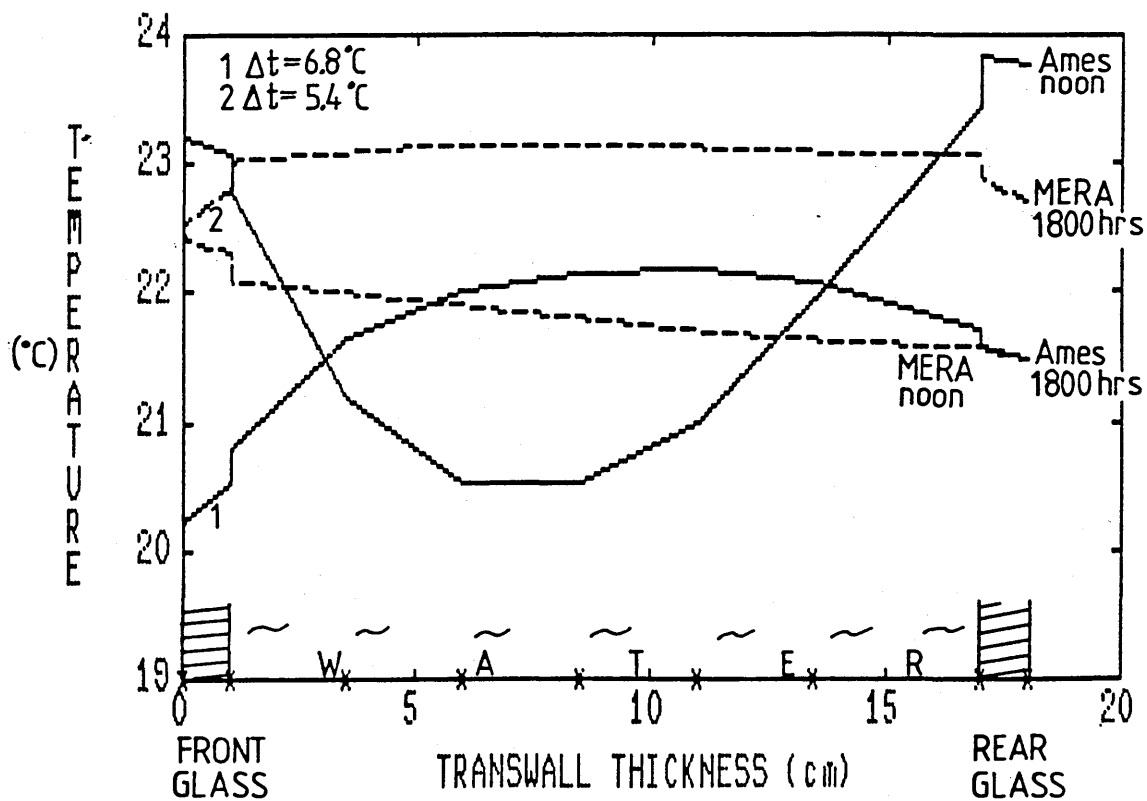



Figure 4.3(b) Transwall temperatures 1200, 1800 hrs MERA & Ames modules.

1500 - 0200 hrs, while the Ames module peaks at 1230 hrs when the direct gain is close to its maximum. Note that the MERA module with a "pale" 10 ppm dye is still markedly the superior, and even 3ppm of dye will match the performance of the Ames module. A view through a transwall with different dye concentrations is shown in Figures 4.3 (d-h), pp 140 c-d.

The reason for the inferior performance of the Ames module can be seen in Figure 4.3(b) which shows a plot of the  transwall temperature distribution at noon and 1800 hrs for both systems. At noon the outer surface temperature of the inner wall of the Ames module is, as designed, higher than the MERA version, but ironically the outer wall surface temperature is also higher because of the high water absorption. The Ames module gives a rapid heat release when irradiated because of the high absorption in the inner glass and the lower effective conductivity of the gel, i.e. the effective conductivity factor* (ECF) is unity. At 1800 hrs, without irradiation, the inner surface temperature quickly falls again because of the lower internal thermal conductivity. On the other hand the high circulation of the MERA module, ECF 26, minimised heat losses at noon, and at 1800 hrs the ECF is still

$$* \text{ effective conductivity factor} = \frac{\text{effective conductivity}}{\text{thermal conductivity}}$$

15 so that the inner wall surface temperature is relatively high. Note that the transwall-glass outer surface temperature difference at 1800 hrs is higher, 6.8°C , for the Ames module compared with that of the MERA version, 5.4°C .

The validity of the one-dimensional computer model when representing the Ames transwall module was checked by constructing a small module, of the same dimensions of those of Chapter 2, except that the rear face consisted of 4 mm Pilkington Antisun 41/60 Grey glass. The module was filled with water gelled by the addition of 0.05% Carbopol 941. The predicted and experimental temperature curves, Figure 4.3(c), are similar in shape although there is a degree of underprediction. The predicted temperatures are sensitive to the accuracy of the measured transmission through the module because it is used to calculate the incident irradiation from the simulator. The extinction coefficients were taken to be that of water [26]. However, a 6 week old water-gel solution was used, and later visual inspection suggested that it was not as clear as expected. Possible explanations are either some separation of the water and gelling agent or more likely, contamination by dust. The sensitivity of the temperature prediction to a reduction in the transmission of 5% is shown Figure 4.3(c). In this case the match is good except for some over prediction at the rear face which is probably due to uncertainty in the heat transfer coefficient at that

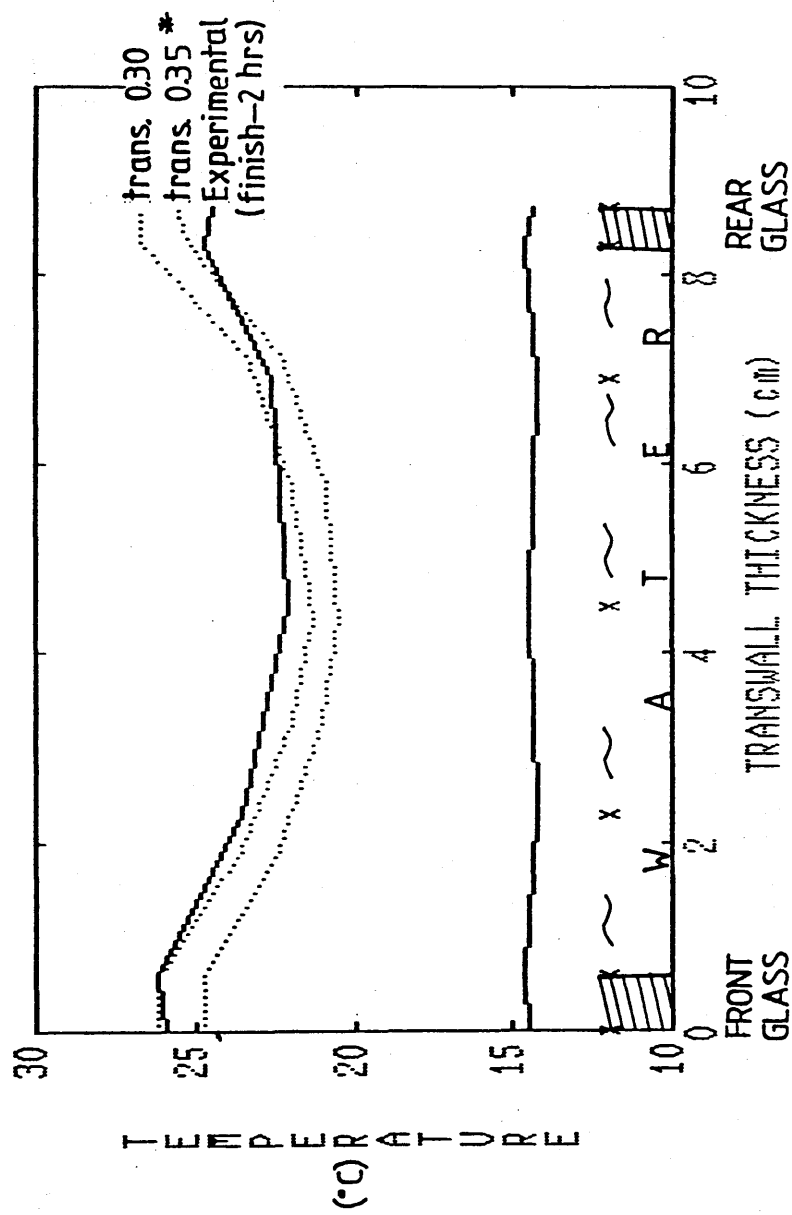


Figure 4.3(c) Temperature distribution of Ames system.

*correct value



Figure 4.3(d) A view through a transwall filled with clear water.



Figure 4.3(e) A view through a clear water filled transwall with Antisun Grey forming the rear plate of the transwall.

Figure 4.3 (f)



5 ppm Lissamine Red 3GX

Figure 4.3 (g)



10 ppm Lissamine Red 3GX

Figure 4.3 (h)



20 ppm Lissamine Red 3GX

face.

4.6.3 Effect of Air Circulation.

The effect of air circulation between the transwall and the window was examined for the MERA module for the three cases; no circulation (Ames 'quenched' wall), free convection, forced convection. The plot of heat release/m².h against time, Figure 4.4 shows that there is little practical difference between no air circulation and free convection over the key time interval 1700-2300 hrs. This is scarcely surprising because the transwall surface temperature driving the free convection is low relative, say, to a Trombe wall. There is a slight trend for free convection to give a higher output at mid afternoon and lower during the early hours of the morning. A decision to circulate or not is likely to be based on more mundane considerations such as the prevention of air circulation will avoid cleaning the glass surface of the air gap.

If forced circulation is employed to boost the thermal output of the transwall then clearly it cannot be allowed to operate continually otherwise the window will act as a substantial heat sink. Figure 4.4 shows the effect of forced convection over the time period 1700-2300 hrs at a rate such that the mean air velocity is 1 m/s. The plot shows that the window is already acting as a heat sink. Couple this with a fan energy consumption of 63 w/m run of the wall then clearly

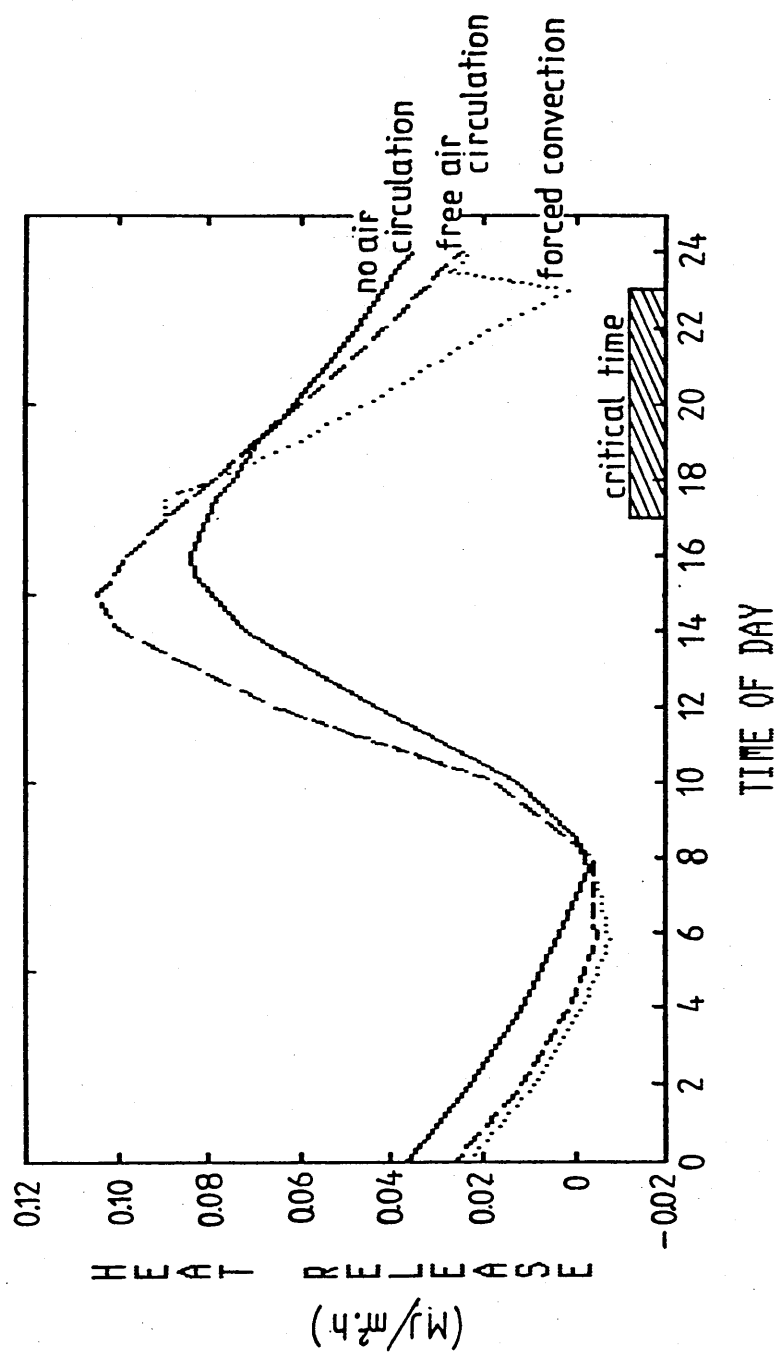


Figure 4.4 Effect of air circulation between window & Transwall, March, 40 ppm Lissamine Red 3GX.

forced convection is not recommended for a transwall.

4.6.4 Annual Energy Savings.

The contribution of the transwall, and the direct gain through the transwall, to meeting the mean heat load for each mean month day is shown in Figure 4.5(a). The direct gain through the transwall is shown separately because this is not available to an opaque storage wall. The site is the West of Scotland and the heating season is taken as September to May inclusive.

It is fair to say that at first sight the fractional saving is unimpressive. Little saving can be expected in a winter maritime climate, 5% transwall, 12% transwall plus direct gain, but the spring and autumn savings of 17% transwall only, 30% transwall plus direct gain through the wall are more impressive. Nevertheless it was thought that the transwall would perform better at around 25%. The author believes there are two main reasons for this, the low level of mean irradiation in the West of Scotland and the high building volume/m² transwall used in the design. Taking the latter reason first, if a low 2 x 5 module transwall is located on the balcony then the spring/autumn transwall contribution would rise from 16% to about 23% allowing for the improved efficiency, i.e. lower heat losses.

The effect of locating in a sunnier climate, specifically for a site in Nice, is shown in Figure 4.5(b). Here the heat release/m².h is shown for April

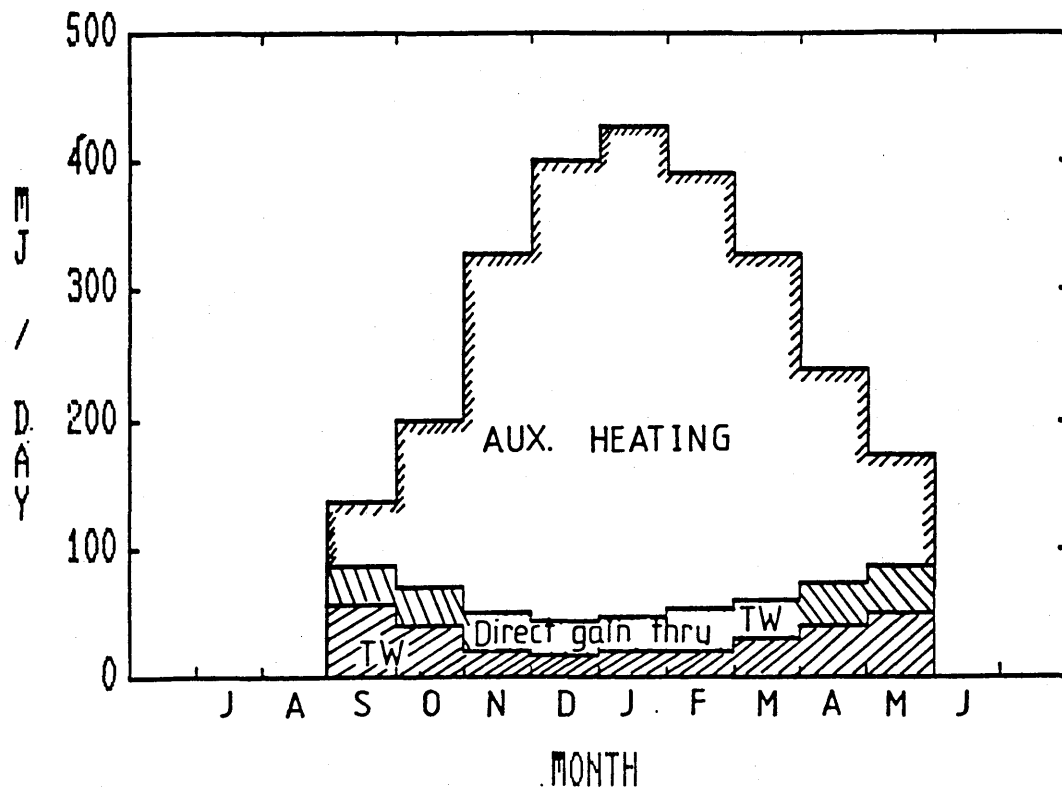


Figure 4.5(a) Contribution of the Transwall, & the direct gain through the transwall, to meeting the mean heat load for each mean month day.

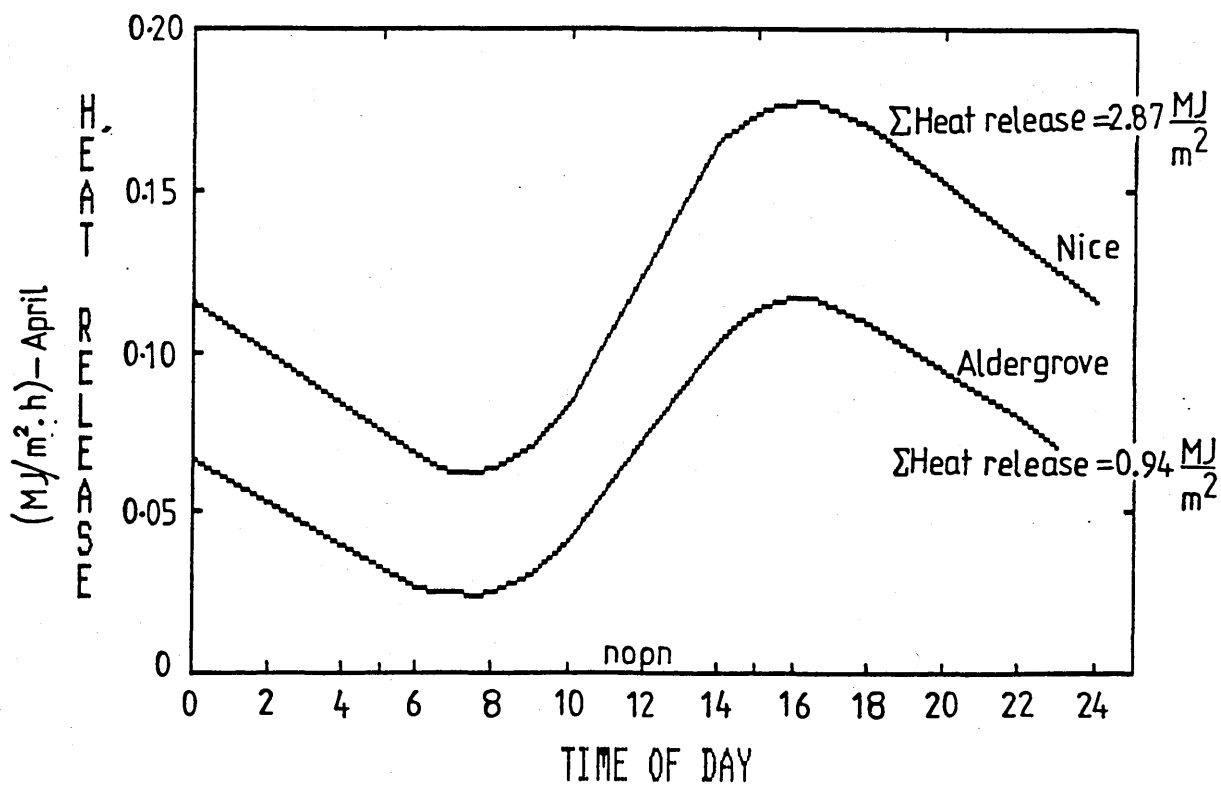


Figure 4.5(b) Nice vs Aldergrove.

for two sites. The difference in heat release is startling, an increase of 300% for the site in Nice, which means that the transwall provides 58% of the heat load. In addition, the heat load in Nice is much reduced. Over a year, the transwall provides 43% of the heat load, and 18% direct gain through the transwall, Figure 4.5(c), for Nice. Figure 4.5(d) shows a plot of the big difference in solar irradiation for the two sites, and a plot of the cosine of the incidence angle is given because the higher irradiation is modified by the higher altitude angle.

It is concluded from this that the transwall is a valid thermal proposition for sunnier locations, e.g. the east of the U.K. rather than the west. Improvements can be made. The house can be redesigned to increase the transwall area per unit building volume, and the irradiation can be boosted by an exterior reflective coating of, say, marble chips or a water surface. Finally, the other benefits of a transwall must not be ignored, i.e. light open aspect with protection against UV degradation and excessive temperature swings.

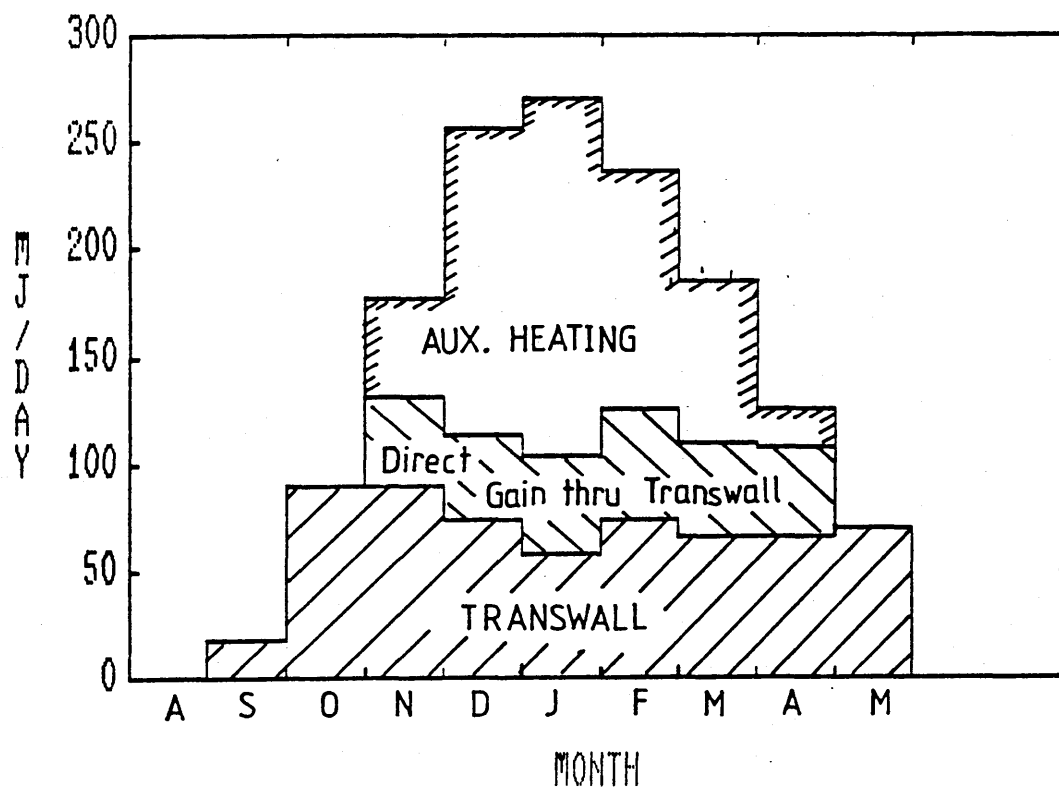


Figure 4.5(c) Contribution of the Transwall and Direct Gain through the transwall to meeting the annual heat load for a site in Nice.

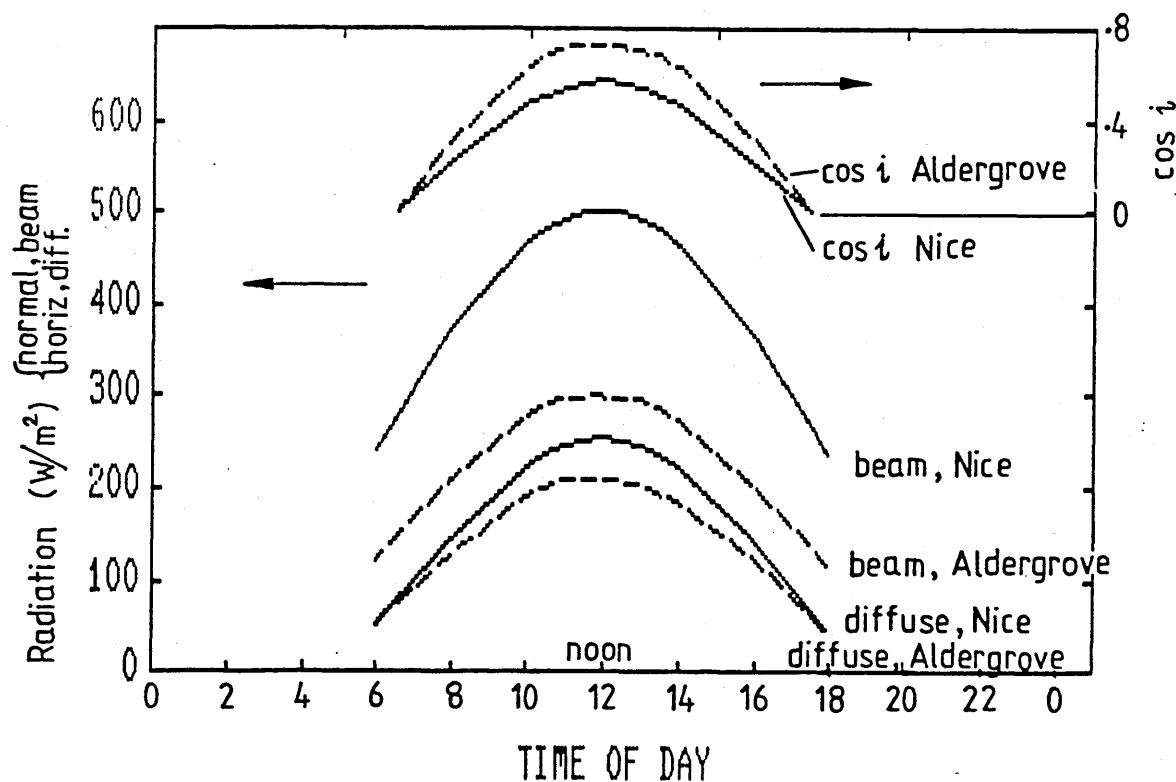


Figure 4.5(d) Solar Irradiation in April, Nice vs Aldergrove.

4.7 Conclusions.

The following conclusions resulting from the simulation runs are summarised:-

- (1) The MERA transwall system using a water/dye is superior to the Ames system using a gel and a solar absorbing glass wall.
- (2) The optimum dye concentration range of Lissamine Red 3GX is 10-20 ppm.
- (3) The optimum water thickness is 15 cm.
- (4) The difference in performance of a transwall without air circulation between the wall and the window, and with free convection, is insignificant. Forced convection should not be used.
- (5) The transwall system is well suited to sunnier climates, and consequently it is not seen at its best in the West of Scotland.

Chapter 5.

Future Work, Summary and Conclusions.

5.1 Introduction.

The concluding chapter suggests future work that could be done to improve further the performance of the computer simulation of the passive solar system. It also gives the summary and conclusions on the work that has been presented in this thesis.

5.2 Future Work.

The computer model of the one-dimensional transwall temperature distribution is believed to perform reasonably well bearing in mind the fundamental limitations on the method and substantial improvement is unlikely. The two-dimensional model has not performed as well as was originally thought likely because of the difficulty in accounting for stratification. If it is thought that an improvement over the one-dimensional model is required then the thrust of any future computer modelling should be directed towards better accounting for this phenomenon. However, due regard should be paid to a prerequisite that any such changes should retain the relative simplicity of the current approach when compared to the method of the volumetric balancing of mass, momentum, energy, with its long computer running time.

On the basis of 'further work' two possibilities are

suggested to account for temperature stratification in the two-dimensional model, namely,

- 1) To allow a partial redistribution of the enthalpy rise in the first water 1/2 slab to the upper 1 1/2 slabs using the two-dimensional analysis.
- 2) To split the transwall into two halves, the upper and the lower, and then apply the one-dimensional analysis to both halves, and make vertical temperature adjustments between the two halves using dimensionless correlations.

5.2.1 Concept: The Partial Redistribution Of the Enthalpy Rise In The Transwall.

It has been demonstrated herein that the concept of effective conductivity can represent adequately the effects of circulation in a horizontal plane. In order to do so in the vertical direction it needs to be boosted by transferring some of the enthalpy rise from the circulation boundary layer adjacent to the outer wall to the upper volumes. Which volumes and the fraction of energy removed is a matter of trial and error. On the basis of five volumetric slabs vertical, with half slabs top and bottom, the upper half slab, 6, will have a depth of 6 cm, and evidence suggests that the vertical slab, 5, will also have to be involved. By day the enthalpy involved could be a function of the irradiation absorbed in the first water half slabs, and by night the enthalpy removal would be a function of the

enthalpy rise of the water slabs above mean room ambient as datum. The former argument is justified by the observed, and reported [51], fact that temperature stratification increases with increasing horizontal heat flux. It may be necessary to superimpose the two enthalpy removals by day. Clearly the energy transport must balance within the transwall.

Consider a simple model shown in Figure 5.1

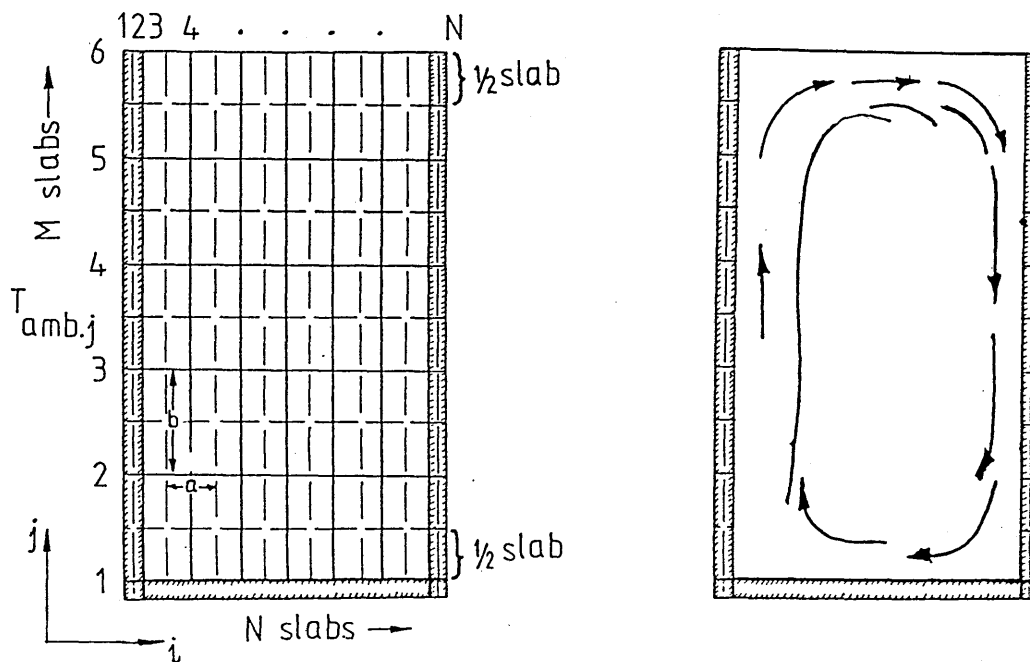


Figure 5.1(a) Transwall Slab Arrangement Figure 5.1(b) Circulation

Let $(I\alpha)_3,j$ = irradiation absorbed in first water slab

F_s = stratification parameter, which might be a constant or a function of the irradiation and/or transmission through the transwall.

Then energy removed from
first water 1/2-slabs

$$= \sum_{j=1}^{(M-1)} (I\alpha)_{3,j} \left(1 - \frac{j}{M} F_s\right)$$

Energy gain
slabs

$$\left\{ \begin{array}{l} i=3, j=6 \\ i=(N-2), j=6 \end{array} \right\} = \frac{1}{2(N-5)} \sum_{j=0}^{(M-1)} (I\alpha)_{3,j} \left(1 - \frac{j}{M} F_s\right)$$

Energy gain
for each slab

$$\left\{ i=4 \rightarrow (N-3), j=6 \right\} = \frac{1}{N-5} \sum_{j=1}^{(M-1)} (I\alpha)_{3,j} \left(1 - \frac{j}{M} F_s\right)$$

An initial trial value of F_s would be 0.05.

If this energy redistribution proved inadequate to the task of reproducing the temperature stratification gradient then it might be necessary to redistribute some energy to the slabs in horizontal row (M-1). These slabs have twice the volume of slabs of horizontal row M, and therefore an equal distribution to rows M and (M-1) would make sense.

When irradiation ceases the $(I\alpha)_{3,j}$ term could be replaced by

$$\left[\rho_w \left(\frac{ab}{2} \right) c_{pw} (T_j - T_{amb.j}) \right] \text{ for } T_j > T_{amb.j}$$

where $T_{amb.j}$ is the ambient temperature at station j.

5.2.2 Correlation Factors for Stratification.

If the energy redistribution method cannot adequately reproduce the vertical temperature gradients then an alternative would be to treat the transwall module as a series of tiers of one-dimensional systems, and with the mid slab water temperatures linked by a dimensionless correlation. The number of tiers envisaged is three at most, and two might well suffice. Clearly the adjustment of the temperature must be such that the overall energy balance of the transwall is maintained.

There appears to be a dearth of papers published which enables the vertical temperature gradient to be predicted in the precise situation of the transwall, i.e. side induced irradiation of a water filled enclosure. In fact there does not appear to be many which deals with the vertical gradient in a salt-free water filled enclosure without an inflow and outflow.

In an interesting paper on stratification in a large tank (3.5 m high, Gr_L-10^{13}) Purslow et al. [52] plotted

$$\frac{y}{H} \text{ vs } \frac{T(y) - T_c}{2(\bar{T} - T_c)}$$

where y = vertical distance

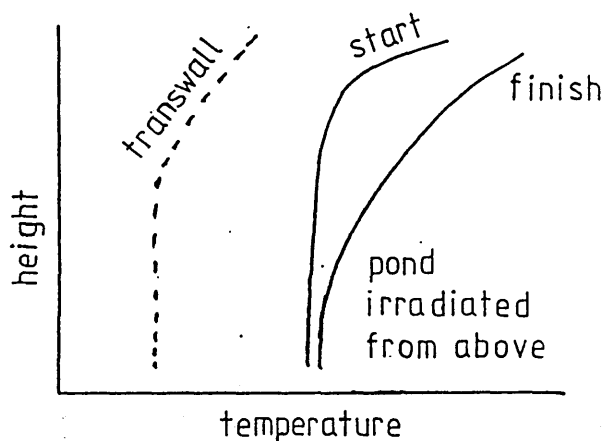
H = height enclosure

T_c = temperature cold face

\bar{T} = mean enclosure temperature

However, it was clear that a simple relationship does not exist and the temperature gradient is a function of the heat transfer rate from the hot to the cooler face. The view was expressed that the situation in an enclosure is sufficiently complex for simple scaling laws to be invalid, and that the heat transfer across a cavity is affected by stratification.

Snider and Viskanta [51] irradiated water from above in a plexiglass tank and the temperature distribution shows a marked difference to the transwall.



The temperature gradients at the start and finish of the vertical irradiation are markedly different, whereas the transwall vertical temperature gradient seems reasonably independent of time for a given constant irradiation flux. However, they also comment that the temperature distribution strongly depends on the volumetric absorption of radiation. It is conceded that the transwall and vertical irradiation cases are not similar.

Kutateladze et al. [53] noted that the turbulent free convection flow in a vertical slot produced a central core of fluid which was stably stratified, and provided a simple correlation to give the gradient:

$$\frac{H}{\Delta T_m} \frac{dT_m}{dx} = 0.35$$

where H = height of slot

ΔT_m = ^{mean} wall temperature difference.

However, the correlation gives a gradient 1/3 that of the transwall, which is not surprising considering the physical difference of their experimental system and the transwall situation.

Bergholz [54] investigated natural convection in an enclosure but without irradiation. Unfortunately, the work seems to imply a preknowledge of the vertical temperature gradient, but it can be reworked to provide an expression,

$$\gamma = \left\{ \frac{1}{4} \left(\frac{SD}{\Delta T} \right) Ra_D \right\}^{\frac{1}{4}}$$

where S = vertical temperature gradient

D = distance between vertical walls

ΔT = wall temperature difference

Curves are given for the critical Grashof number vs γ and thus if Gr_c is known S can be found. But this is not particularly helpful because Gr_c is the Grashof

number at which boundary layer flow becomes unstable and for the transwall case $Gr_{\bar{c}} \gamma$ did not lie in the field plotted.

It might be possible to correlate a vertical temperature gradient term with the Rayleigh number, Ra_L ,

$$\text{e.g. ratio} = \frac{\text{radiation absorbed}}{\text{energy conducted}}$$

and call it say, the stratification number, S_t .

$$\text{Therefore, } S_t = \frac{q_{\alpha} L^2}{k_e \Delta t} = \frac{q_{\alpha} L}{k_e t_g}$$

where q_{α} = radiation absorbed/unit volume
 L = depth water, (m)
 k_e = effective conductivity in vertical direction, (W/m.K)
 Δt = vertical temperature difference over length L , (K)

t_g = temperature gradient, $\Delta t/L$

Then $S_t = a Ra_L^b$

where a = constant to be determined

b = another constant, possible 1/4 for laminar flow.

5.2.3. Summary of Improvements to the Experimental Apparatus

Some of the experimental errors and uncertainties could be reduced by improving the experimental set up. The following ideas are suggested.

- 1) Confining the simulator behind the glass partition.
- 2) Proportional temperature control system in the laboratory.
- 3) More lamps for the simulator, perhaps 5 working lamps.
- 4) Better cooling system for the solar test cell that does not involve air blasting over the transwall.
- 5) More thermocouples to give glass temperatures in the vertical plane.

5.3 Summary of the Achievements of this Programme of Work

This thesis presents a unique water-dye version of the transwall passive solar system which the author has demonstrated superior to the established Ames system. The general superiority of the transwall system over rival passive systems has been argued. Specific conclusions are presented in the next section.

The author has developed and validated a one-dimensional computer model of the transwall which is a valuable design tool capable of running on an IBM PS Computer or a suitable mainframe. No other program is known which can reproduce as well the phenomena within the transwall, and account for the actual or predicted variation of solar input, and yet run on a personal computer. The temperature distribution within the transwall, and its heat storage and release, given by

the program agrees well with experiment subject to the limitations of the one-dimensional approach. Spectral extinction coefficients for a dye, LR3GX, various glasses and a gelling agent are presented. The spectral problems of a tungsten-halogen solar simulator are extensively reported, and the manner in which they were overcome to give good agreement between predicted and experimental values is detailed.

An existing two-dimensional solar absorption program in BASIC has been completely converted into FORTRAN 77 and extensively modified to adapt to changes in program modelling the temperature distribution. The error in using a one-dimensional solar absorption model, rather than two-dimensional is quantified, and good agreement is obtained between predicted and measured transmissions.

The author has developed a computer program which gives the two-dimensional temperature distribution within the transwall. Experimental verification shows that the program works reasonably well in horizontal direction, but the effective conductivity approach of itself cannot accurately reproduce the stratified vertical temperature distribution. The author contends that quantifying this deficiency provides valuable knowledge. Suggestions are made for further work to improve the prediction of the vertical temperature gradients.

Finally, the one-dimensional computer model of the

transwall has been applied to the crucial comparison between the MERA water-dye version of the transwall and the solar absorbing glass/gelling agent version of Ames. The author has shown that the MERA module has the superior performance, lower cost, and is more robust in construction. The application of the computer model to a solar house design has established essential optimum parameters, i.e. dye concentration, water thickness, and the insensitivity of the system to free air circulation between the transwall and the window. The energy saving produced by the transwall is unfortunately typical of what might be expected of passive solar systems in the West of Scotland with its poor record of sunshine. The benefit of operating in a sunnier climate, the South of France, has been quantified.

The author contends that the work reported herein will advance the cause of the transwall passive solar system, and the essential materials is worthy of publication.

5.4 Conclusions.

The work reported herein gives rise to the following conclusions:-

- 1) The computer model of the one-dimensional temperature distribution in the transwall gives a distribution whose shape is a reasonable match to that produced by experiment. The temperature rise

predicted is to within 18% of measured values for the transwall module irradiated by the solar simulator, and to within 18% for the full size module under solar irradiation. The comparable figure is 10% for a small transwall module filled with a gelling agent and having one wall of solar absorbing glass.

- 2) The one-dimensional computer prediction of transmission through the small transwall module agrees with experiment to within 6%, and to within 10% for the full size module.
- 3) The transmission through a transwall module irradiated by a solar simulator is liable to an error of up to 13% if the energy levels of the spectral wavebands are assumed to be those of air mass 2. The variation of the waveband energy levels with voltage should be taken into account.
- 4) The shape of the predicted two-dimensional temperature plots is broadly in agreement with experiment, aside from the expected fundamental inability to reproduce the experimental slight vee configuration. The accuracy of the predicted temperature rise is more difficult to assess for multiple horizontal planes, but taking the extreme case it is no better than 35%.

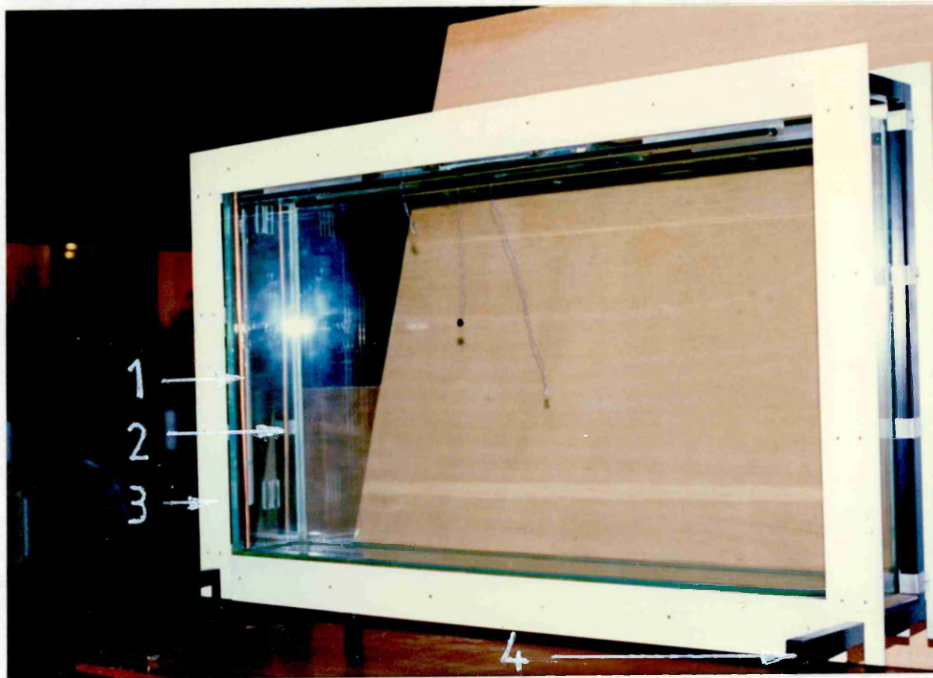
- 5) The one-dimensional treatment of volumetric absorption will under predict the absorption of the inner water and glass slabs by 10% when compared to the two -dimensional approach.
- 6) The concept of effective conductivity can be applied with confidence to the one-dimensional treatment of the transwall, but it is demonstrated that it cannot, by itself, reproduce accurately the vertical temperature distribution. The error will increase with increasing volumetric irradiation absorption.
- 7) The MERA version of the transwall module with 3 ppm of LR3GX dye gives the same heat release over the period 1700-2300 hrs as the Ames version, and 44% more with a pale 10 ppm LR3GX dye concentration. The cost of the MERA module is 80% less than the Ames version.
- 8) The performance of a transwall is insensitive to whether or not there is free air circulation between the transwall and the window. Forced convection should not be used.
- 9) The optimum dye concentration of Lissamine Red 3GX is in the range 10-20 ppm. The optimum water thickness is in the region of 150 mm.

10) The energy savings for a transwall equipped solar house in the West of Scotland are 30% in Spring and Autumn, 12% in winter, based on energy release plus transmitted direct gain. The figure for the heat release only are 17%, 5% respectively. The Spring/Autumn figure for a location in Nice is 58%.

Appendices

APPENDIX A

The Glasgow University Transwall Design.



Glass Type : 10 mm clear glass

Size : 1.2 m \times 0.6 m \times 0.18 m

Locations 1 & 2 : copper tube for filling
and syphoning out the
contents.

Location 3 : 75 mm width aluminium facing

Location 4 : Link 51 Handy Tube

Appendix B

B.1. Procedure for the alignment of the Solar Simulator

The solar simulator was aligned with the transwall module so that uniformity of the level of irradiation over it was maximised. Failure to do this is likely to lead to abnormal water circulation patterns. This was achieved by making a rotating traverse of a 50 mm diameter silicon cell. The diameter of the traverse was 190 mm. The silicon^{cell} was mounted on a disk as shown in Figure B1.1. The irradiation levels were recorded at each quarter of a revolution, 90°.

Table B1 shows the sets of readings recorded and they were found to agree to within $\pm 4.5\%$ with each other. A closer look at Table B1 shows that the simulator irradiance formed a somewhat stronger horizontal band, which accounts for higher values registered by the silicon cell at positions A and C. The average values of irradiance at these positions agree to about 2%. On the other hand, the irradiance band seemed to weaken as one moves either way vertically from the centre as verified by lower values of irradiance at positions B and D. The average values of irradiance at positions B and D agree to about 0.5%.

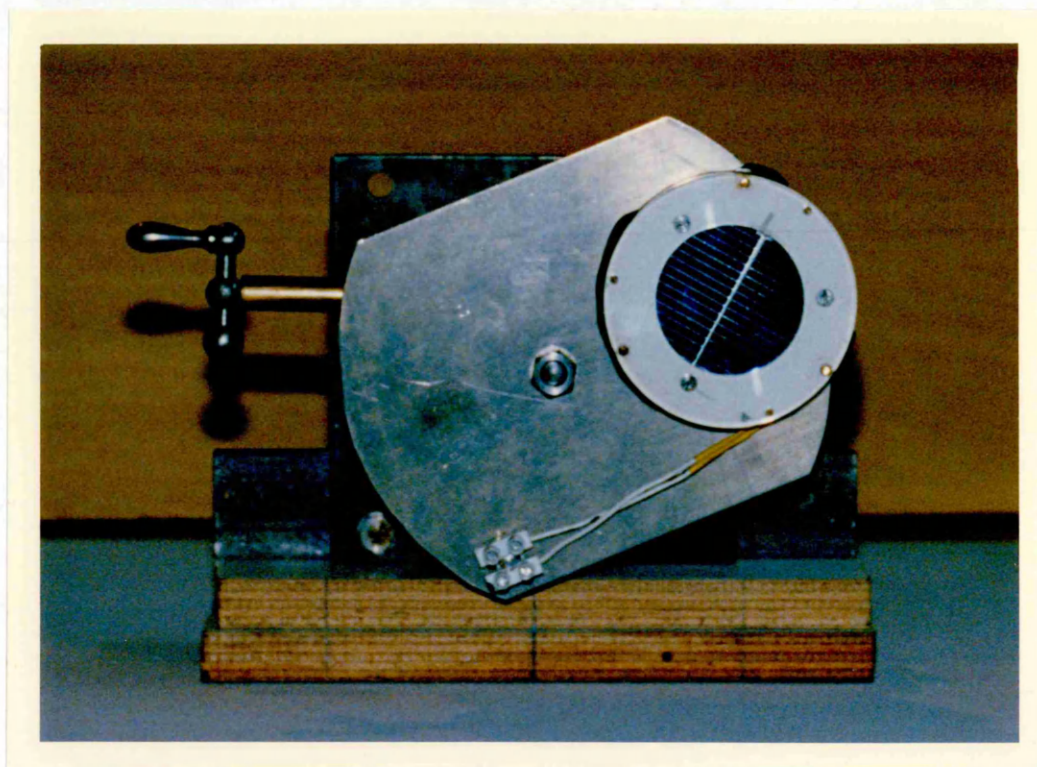
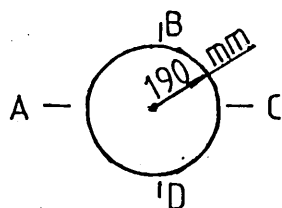


Figure B1.1 The Silicon Cell mounted on a manually operated rotating disk.

Table B1. Solar Silicon Cell readings for the alignment of the Solar Simulator.



Set No.	Solar Silicon Cell Positions			
	A mV	B mV	C mV	D mV
1	99.58	91.75	97.13	91.86
2	98.82	90.56	97.03	91.97
3	99.09	91.76	96.55	91.71
Average	99.16	91.36	96.90	91.85

However, the working section of the simulator is formed by the centre 3 lamps/lenses, the other 9 serve as guard lamps/lenses. Thus the true uniform area is not a rectangle as one might be tempted to believe, but an equilateral triangle (see Section 2.3.1(c)).

The simulator angle of incidence was 5° .

Appendix C

Experiments With The Small Transwall Module:

Investigating the 13% Discrepancy in Transmission.

C.1.1 Introduction

A discrepancy of 13% was found between the measured and predicted values of simulator irradiance transmitted through the small transwall cell. Possible reasons could be that the methods of measurement and calculations were incorrect; the glass of the small transwall module was not Pilkington float glass as specified; and that the spectrum of ^{the} solar simulator was not A.M.2 as assumed and consequently the fractional energies of the wavebands were incorrect.

C.1.2 Measurement and Calculations

The method of transmission measurement and calculations were tested by irradiating the small module by a solar beam. The module was contained in a collimator box in order eliminate sky diffuse irradiation. The box contained two compartments in parallel with a Kipp and Zonen solarimeter at the back of each compartment. The small transwall module was placed in one compartment and the other left empty to act as a monitor of the constancy of irradiation. The results of this test in Table C1, gave 50% transmission against 45% predicted, yielding a discrepancy of 10%. The two tests, one performed with the small transwall

Table C1. The Absorption of Solar Irradiation through a 6 mm Small Transwall Module irradiated by Solar Beam Radiation at Air Mass 2.

Set No.	Solarimeter "C.M.5" Model Only mV	Solarimeter "C.M.3" Model Only mV	Solarimeter "C.M.3" Model Empty TW mV	Solarimeter "C.M.3" Model TW + Water mV	% Transmission
1	{10.53 10.53 10.52	9.91	6.19	4.82	48.6
2	{10.61 10.66 10.88	9.89	6.28	5.01	50.7
Average	10.62	9.90	6.24	4.91	49.6

Note: The Solarimeter Model "C.M.5" was used to monitor the constancy of irradiation, and was placed in an empty compartment of a collimator box.

module illuminated by the solar simulator, and this one under discussion in which the solar beam irradiated the small transwall module, are in good agreement with each other, a mere 2% difference. The spectral energy bands used for the simulator covered the range 0.3-4.1 μm , divided into 8 wavebands. Therefore, it is evident that the methods of measurement and their calculations cannot be blamed for the discrepancy in question.

C1.3 Transwall Glass Type

The possibility arose that the small transwall module might have not been constructed from Pilkington float glass as requested. A new small transwall module was constructed from 6 mm Pilkington float glass with a sample retained to measure the dependancy of transmission on wavelength. It was irradiated with the solar simulator to determine the absorption of solar irradiation within the new module. The test results shown in Table C2, indicate that 52% transmission was obtained, which is in excellent agreement with the two previous tests.

The internal transmission of solar irradiation through a small piece of 5.1 cm by 5.1 cm by 0.6 cm new Pilkington glass (off-cuts) was also measured using both a solar beam and the solar simulator to irradiate the glass piece. The values of the internal transmission measured using different solarimeters are shown in

Table C2. Transmission of Solar Irradiation through the NEW 6 mm Small Transwall Module irradiated by Solar Simulator at 120 Volts.

Set No.	Simulator Voltage	Kipp Only	Kipp +		Kipp+ Full TW	% Transmission	
			Empty TW	mV		Empty TW	Full TW
	V	mV	mV	mV			
1	120	8.780	5.632	4.675	64.4	53.2	
		8.770	5.605	4.608	63.9	52.5	
2	120	8.601	5.547	4.525	64.4	52.6	
		8.564	5.513	4.506	64.3	52.6	
3	120	8.594	5.476	4.447	63.7	51.7	
		8.571	5.433	4.426	63.3	51.6	
AVERAGE = 52.4							

Tables C3, C4, and C6. Table C3 is of particular interest here because the solarimeter used was the Kipp and Zonen solarimeter which is more accurate than the silicon cells. The results of Table C3 give 80% measured transmission when the sheet of glass was irradiated by the solar simulator, against 81% transmission shown in Table C4 for a case in which the same sheet of glass was irradiated by solar beam - a perfect match. An approximate estimate of the internal transmission yielded 83% as shown in Table C5. The measured transmission is boosted by about 3% by internally reflected irradiation.

C1.4 Extinction Coefficients

The extinction coefficients of sample of the glass of a 6 mm small transwall module, a 10 mm glass obtained from Coral Reef, aquaria manufacturers, and a 10 mm sheet of Pilkington glass were calculated over 8 wavebands from the runs of transmission curves made in the Department of Chemistry at Glasgow University, for an 0.3-3.2 micron range. A Perkin-Elmer Lambda 9, UV/VIS/NIR Spectrophotometer was used to obtain the transmission curves. Table C6 shows the extinction coefficients of the three types of glass mentioned above. The transmission charts for the small transwall module glass (new), Coral Reef and Pilkington glass are shown in Figure C1.4, superimposed on one another.

When the absorption of irradiation within the small

Table C3. Transmission of Solar Irradiation through
a 5.1 cm × 5.1 cm × 0.6 cm sheet of Pilkington
Glass irradiated by Solar Simulator at 120 Volts

Set No.	Simulator Voltage V	Kipp Only mV	Kipp+ Glass mV	% Transmission
1	120	8.624	6.898	80.0
		8.608	6.883	80.0
2	120	9.667	7.764	80.3
		9.658	7.750	80.2

Average % Transmission = 80.1

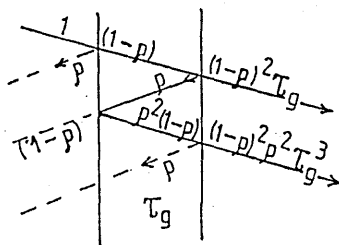
Table C4. Transmission of Solar Irradiation through
a 5.1 cm × 5.1 cm × 0.6 cm sheet of Pilkington Glass
irradiated by Solar Beam Radiation at Air Mass 2.

Set No.	Kipp Only mV	Kipp Glass mV	% Transmission	
1	10.70	8.40	78.5	} Average = 81.2
2	10.17	8.26	81.2	
3	10.65	8.67	81.4	
4	10.40	8.42	80.9	

Table C5. An approximate estimate of the internal transmission through a 6mm Small Transwall Module

Waveband μm	Extinction Coeff. m^{-1}	e^{-KL}	f_{wb} (Simulator)	$f_{wb} \times e^{-KL}$
0.3 - 0.35	116.5	0.4971	0.001	0.0005
0.35 - 0.4	21.07	0.8812	0.008	0.007
0.4 - 0.6	11.75	0.9319	0.265	0.247
0.6 - 0.75	15.47	0.9114	0.349	0.3181
0.75 - 0.9	23.86	0.8666	0.162	0.1404
0.9 - 1.2	30.48	0.8329	0.098	0.0816
1.2 - 2.1	19.78	0.8881	0.117	0.1039
2.1 - 4.1	52.09	0.7316	0	0.0
				0.8985

To obtain the internal transmission for 1 normal ray with two reflections (internally) from the measurement of total transmission,



$$(1-p)^2 T_{g_{int.}} (1+p^2 T_{g_{int.}}^2) = 80.1$$

$$0.96^2 T_g (1+0.04^2 \times 0.9^2) = 80.1$$

$$T_g = \frac{80.1}{0.96 \times 1.0013}$$

$$= 83\%$$

Table C6. The Extinction Coefficients calculated from the Transmission Curves produced by a Perkin-Elmer Lambda.9 Spectrophotometer.

Waveband μm	Small ⁽¹⁾ Transwall 6 mm m^{-1}	Coral ⁽¹⁾ Reef 10 mm m^{-1}	Pilkington ⁽¹⁾ Glass 10 mm m^{-1}	Fraction ⁽²⁾ Energy A.M.2
0.3 - 0.35	116.5	84.3	87.45	0.00489
0.35 - 0.4	21.07	15.46	14.77	0.01893
0.4 - 0.6	11.75	7.89	8.55	0.02685
0.6 - 0.75	15.47	11.94	12.79	0.19923
0.75 - 0.9	23.86	21.29	22.97	0.16848
0.9 - 1.2	30.47	27.61	29.8	0.14036
1.2 - 2.1	19.78	17.26	18.44	0.17548
2.1 - 4.1	52.09	38.17	39.06	0.02103

1) Extinction Coefficients calculated from transmission charts

2) Fractional Energies in waveband for Air Mass 2 obtained by differencing the accumulated fractional energies in each waveband (Table B5, Greveniotis, 1986)

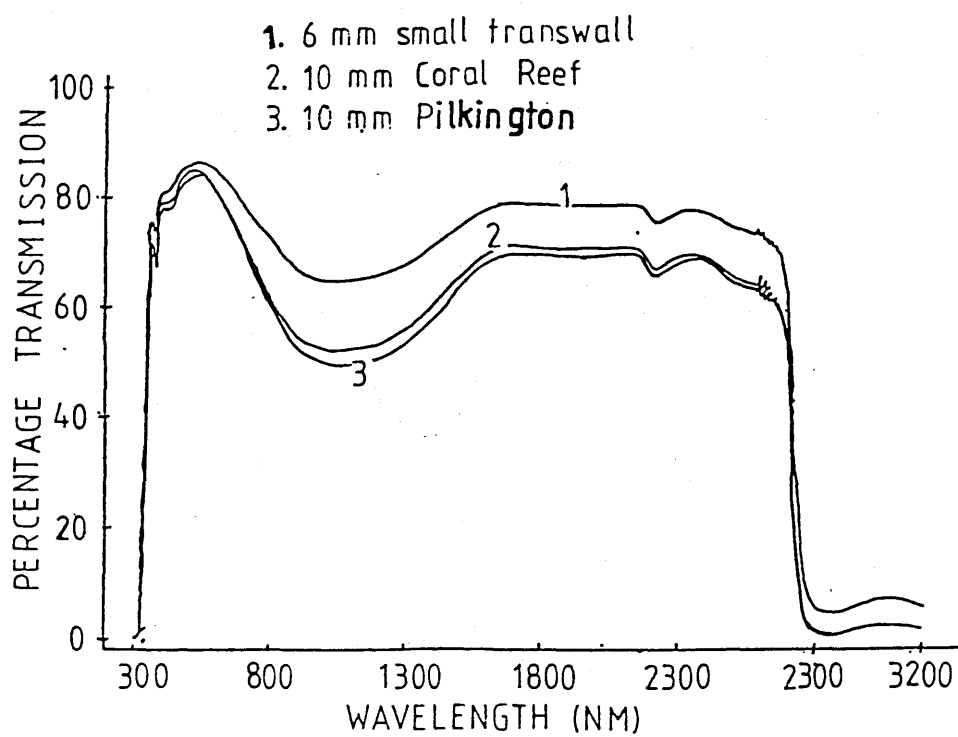


Figure C14 Transmission curves for the small transwall, Coral Reef and Pilkington glass superimposed on one another.

transwall module was calculated using the new values of extinction coefficients thus obtained and A.M.2 fractional energies from literature [Paparsenos, 1983, Greveniotis, 1986], 41% and 41.5% transmission were obtained respectively, worse than when the Pilkington float glass extinction coefficients Paparsenos, 1983] were used earlier giving 45% transmission. However, because the new extinction coefficients thus used were calculated from experiment using basic principles, the extinction coefficients were exonerated as a probable source of this aggravating discrepancy. Only the spectrum of the solar simulator and the corresponding fractional energies of the wavebands remained to be examined as a potential source for the discrepancy in question. A treatise on the fractional energies is already given in the text, Section 2.5.2(c).

Appendix D

The Calibration of the Transwall Thermocouples

D.1.1 Introduction

The thermocouples used to measured the water temperatures in the transwall modules were calibrated against a platinum resistance thermometer (PRT). It was necessary to recheck the R_0 value of the PRT before the thermocouple calibration was carried out.

D.1.2 The Platinum Resistance Thermometer.

The PRT used was a Tinsley High Precision (No 207260) with a NPL calibration certificate No. ST 6533 (c).

The α and S constants were

$$\alpha = 0.00393665$$

$$S = 1.4926$$

where

$$t_c = \frac{R_t - R_0}{\alpha R_0} + \delta \left(\frac{t}{100} - 1 \right) \frac{t}{100}$$

The resistance was measured with an ASL 6 decade AC Bridge and the R_0 value was obtained using a NPL certificated triple point cell. The R_0 value was found to be 24.5517Ω , which showed a drift from the NPL value

of only $\pm 0.1\%$

D1.3 The Transwall Thermocouples.

Chromel vs alumel thermocouples (type K) were used to measure water and glass temperatures for the small and the full size transwall modules, ambient air and solar test cell temperatures. The wire diameter selected was 0.2 mm in order to minimise any disturbance and consequently the strength and stiffness of the wire is important. It is for this reason that type K thermocouples were chosen rather than the more stable type T, copper-constantan.

Thermocouples for measuring water temperatures, 15 for the small transwall module and 20 for the full size transwall module, were calibrated against the PRT and were connected to the Solartron-Schlumberger 3530 Orion Data Logger via cold junctions to record the water and glass temperatures. A good external cold junction gives better accuracy than the internal reference in the logger.

The cold junctions consist of pairs of 1 cm by 40 cm glass tubes down which run thermocouple wires together with a corresponding wire from a pair of insulated copper wires. The thermocouple wire is split, one wire running down each tube and gently twisted with a copper wire at the lower end of the tube. The twisted pair is immersed in about a 4 cm column of mercury to give good electrical and thermal contact. The mercury column is

sealed by pouring melted paraffin wax down each tube. The copper wires are joined on the other end to the data logger or to a heavy duty thermocouple switch. The cold junctions were immersed in a crushed ice/water mixture held in large Dewar flasks. The composition of the ice/water mixture was given the standard column test, i.e. a 1/2" core of ice/water was extracted and tested to see if it stood without collapsing. The ice/water was handled with gloves and the water was air saturated.

The thermocouples were immersed in a 39.7 cm by 29.5 cm by 23.6 cm stainless steel water bath equipped with a Gallenkampf Thermo Stirrer 100 to control the water temperature. The calibration temperature range was 15-40°C raised at 5°C intervals to the next temperature after each 1/2 hour. Small plastic balls, about 15 mm o.d. were placed on top of the water level in the bath to act as an insulation, primarily aimed at preventing evaporation and subsequent excess heat loss from the bath.

D1.4 The Small Transwall Module Thermocouples-

The small transwall thermocouples were held in a grid support and arranged in three horizontal planes of five thermocouple rows from the front to the rear end of the support. The positions of the thermocouples from the front to the rear end of the small transwall are shown in Figure D1.4. A second order polynomial curve fit was made to obtain the calibration correlation

NOTE : All dimensions are in millimetres.

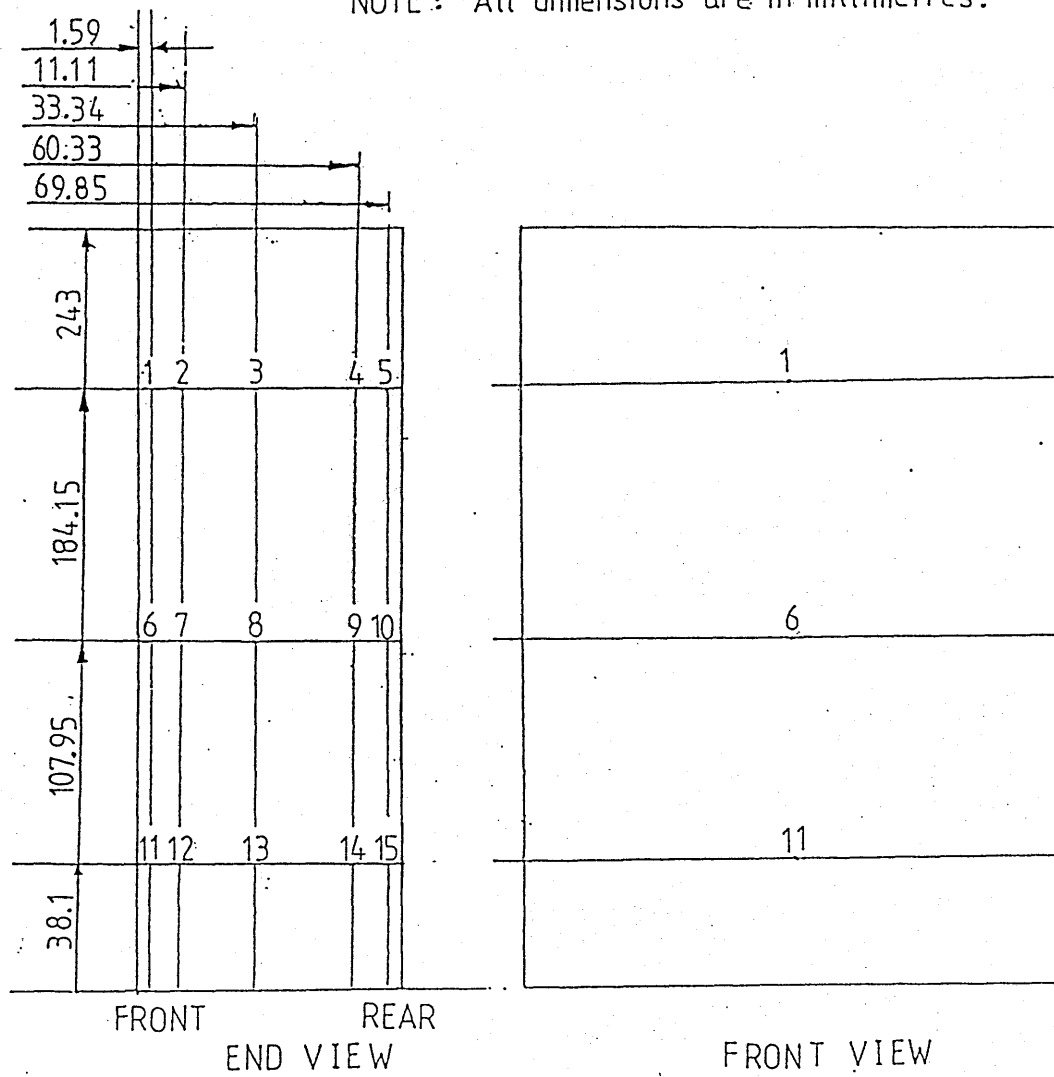


Figure D1.4 The positions of the small transwall module thermocouples in a grid support.

Table D1. Correlation Equations for the Small Transwall
Module Thermocouples.

Thermocouple No.	Correlation Equation $t_0 = at^2 + bt + c$
1	$(-3.6558E-4)t^2 + (0.99905)t - 0.01946$
2	$(6.9412E-4)t^2 + (0.95544)t + 0.58329$
3	$(-4.3107E-4)t^2 + (1.00752)t + 0.14551$
4	$(-6.5555E-4)t^2 + (1.03437)t - 0.86893$
5	$(-4.4389E-4)t^2 + (1.03874)t - 0.66927$
6	$(-3.0377E-4)t^2 + (0.99371)t - 0.16193$
7	$(2.9229E-4)t^2 + (0.87716)t + 0.67489$
8	$(-3.4928E-4)t^2 + (1.01903)t + 8.39643E-3$
9	$(2.4805E-4)t^2 + (0.97975)t + 0.31222$
10	$(2.4161E-4)t^2 + (1.00019)t - 0.63863$
11	$(-4.1308E-4)t^2 + (0.99541)t - 0.40675$
12	$(-3.2950E-4)t^2 + (1.01504)t - 0.35189$
13	$(-1.9114E-3)t^2 + (1.07654)t - 1.21536$
14	$(-2.0868E-3)t^2 + (1.12945)t - 2.68164$
15	$(-2.0601E-3)t^2 + (0.86264)t + 2.08696$

equations for the small transwall thermocouples. Table D1 shows the correlation equations for individual thermocouples. These correlations give the deviation from the standard tables rather than the true form.

$$t = a_0 + a_1 \text{ (mV)} + a_2 \text{ (mV)}^2$$

where mV is the millivolt reading.

D1.5 The Full Size Transwall Module Thermocouples

The thermocouples of the full size transwall module, sometimes referred to as the thermocouple "fingers", were used to measure the temperatures of a full size transwall module placed in the solar test cell at the Mechanical Engineering Research Annex.

The thermocouples are arranged in pairs of five thermocouple "fingers", each set of five lying on a horizontal plane. Each "finger" is formed by a length of hypodermic tubing with the thermocouple wires protruding 20 mm. The "fingers", are attached to vertical hypodermic tubes that can be raised, lowered or rotated by clamps inside the water bath or the full size transwall module.

The thermocouple fingers were interlaced with each other in pairs, with one set of five fingers, chosen arbitrarily as a reference and then moved to the second set of five. Twenty full size transwall thermocouples in the sets of (1-5), (5-10), (11-15) and (16-20) were interlaced randomly with each other. Figure D1.5 shows on the far left corner a vertical orientation of the

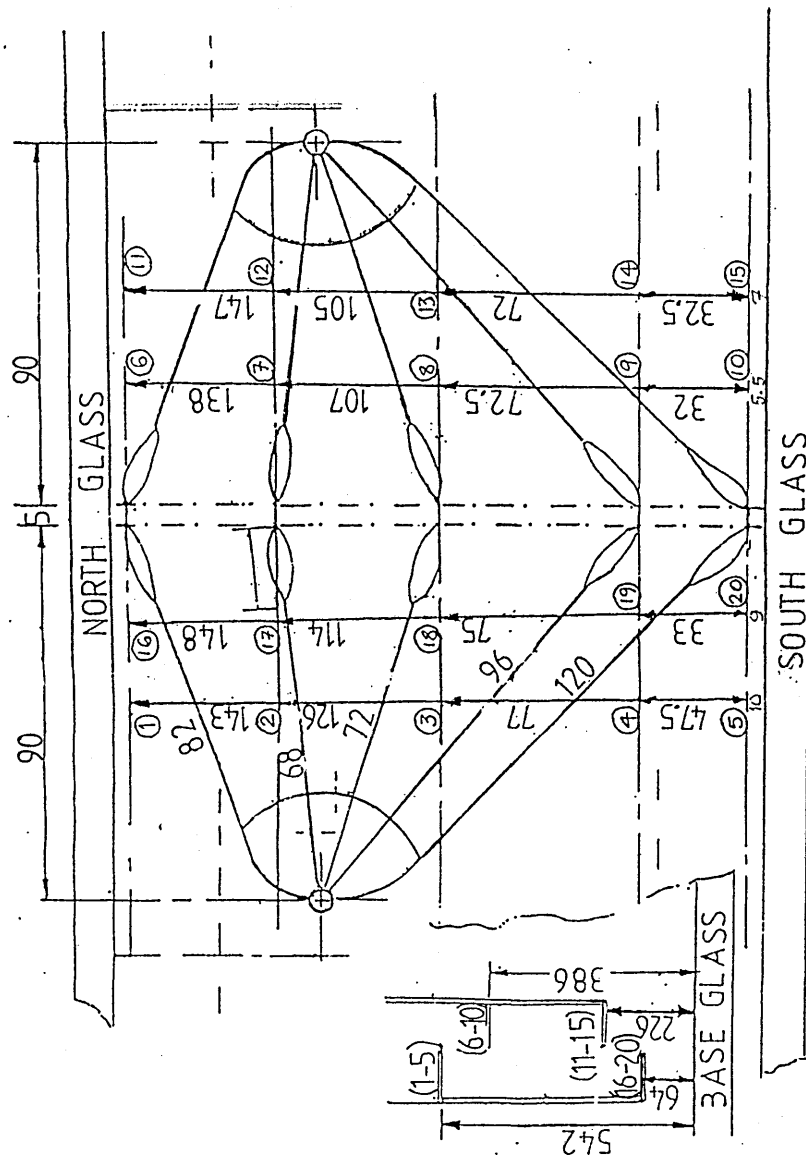


Figure D1.5 The plan view of the thermocouple 'fingers'. All dimensions in mm.

Table D2. Correlation Equations For the Full Size Transwall
Module Thermocouples.

Thermocouple No.	Correlation Equation $t_0 = at^2 + bt + c$
1	$(-1.5466E-3)t^2 + (1.09856)t - 1.60859$
2	$(1.0045E-4)t^2 + (0.99408)t + 0.19186$
3	$(-1.6946E-3)t^2 + (1.10549)t - 1.68121$
4	$(-8.2708E-5)t^2 + (1.00593)t + 0.04829$
5	$(-1.7327E-3)t^2 + (1.10706)t - 1.59158$
6	$(-3.6819E-4)t^2 + (1.01929)t - 0.21150$
7	$(-5.2282E-4)t^2 + (1.03126)t - 0.56831$
8	$(-1.6543E-4)t^2 + (1.00341)t - 0.02997$
9	$(-5.7233E-4)t^2 + (1.03293)t - 0.62875$
10	$(-2.1245E-4)t^2 + (1.00731)t - 0.10699$
11	$(-1.1732E-3)t^2 + (1.06617)t - 1.18862$
12	$(-4.0426E-4)t^2 + (1.01702)t + 0.21917$
13	$(-1.1172E-3)t^2 + (1.06312)t - 1.03507$
14	$(-2.6585E-4)t^2 + (1.00808)t - 0.03507$
15	$(-9.4186E-4)t^2 + (1.05204)t - 0.86612$
16	$(1.5637E-4)t^2 + (0.98701)t + 0.35636$
17	$(-4.2427E-4)t^2 + (1.02492)t - 0.36279$
18	$(2.9733E-4)t^2 + (0.97824)t + 0.52423$
19	$(-2.2522E-4)t^2 + (1.01145)t - 0.12148$
20	$(4.4831E-4)t^2 + (0.96779)t + 0.74428$

pairs of thermocouple fingers from the base glass, as well as the plan view of the interlaced thermocouple probes as they appear during the normal test operation of the full size transwall module. Figure D1.5 also shows the actual distances in centimeters, of the individual thermocouples from the south facing glass, or front face of the transwall glass tank.

A second order polynomial curve fit was also made to obtain the calibration correlation equations for a full size transwall module. Table D2 shows the correlation equations for each thermocouple. Similarly, as with the small transwall module, these equations only give the deviation from the standard tables, rather than the true temperature which would have the form:-

$$t = a_0 + a_1 \text{ (mV)} + a_2 \text{ (mV)}^2$$

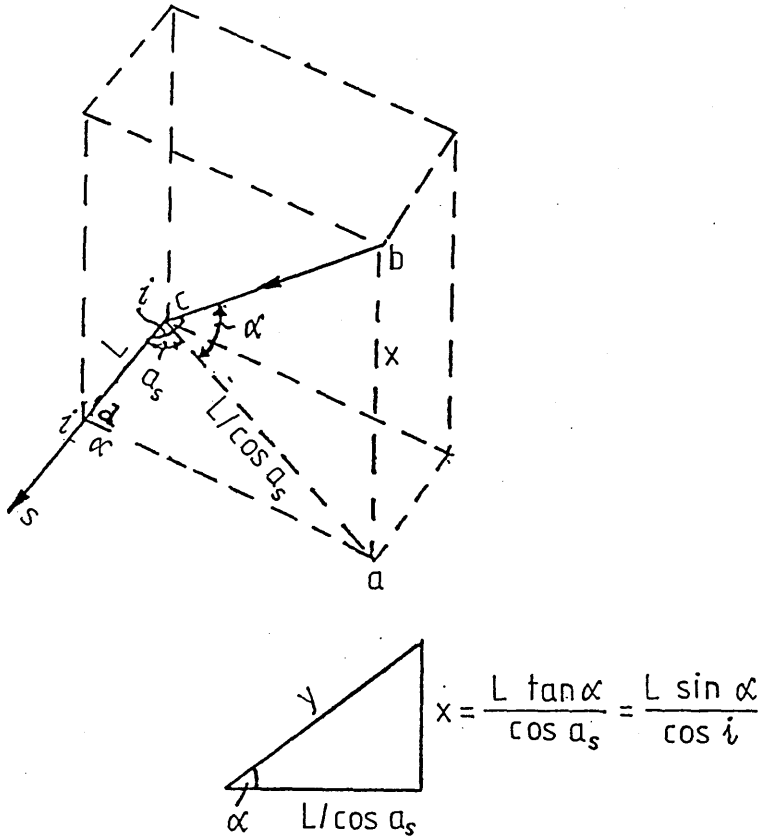
where mV is the millivolt reading.

D1.6 The Radiation Flux Correction.

Paparsenos [26] investigated the radiation correction for the thermocouples in the small module irradiated by the solar simulator. He found that a correction of 0.5°C was required for thermocouples on the outer glass surface, 0.25°C for the thermocouples on the inner glass surface (glass/water interface) and no correction was necessary for the water temperature measuring thermocouples more than 5 mm from the latter surface.

Appendix E.

E.1 Refractive Altitude and Azimuth Angles.



When calculating shadow factors it is essential to find where the limiting beam strikes the horizontal and vertical planes of the various slabs. This is easily done using the altitude, α , and solar azimuth angles, a_s , angles.

Consider any ray $b \rightarrow c$ on the Figure above. It is required to find the distances x and y , i.e. ab and bc . From the triangles acd , acb it is seen that:

$$x = \frac{L \tan \alpha}{\cos a_s}$$

$$\text{or} \quad x = \frac{L \sin \alpha}{\cos \alpha \cos a_s} = \frac{L \sin \alpha}{\cos i}$$

where i = angle of incidence

$$\text{equally} \quad y = \frac{L}{\cos a_s \cos \alpha} = \frac{L}{\cos i}$$

Unfortunately in a transwall the incident ray is bent and the altitude and solar azimuth angles calculated in air do not apply. It is essential, therefore, to calculate effective altitude and azimuth angles for each material of different refractive index. It is important to note that the incident and refracted rays lie in the same plane

Consider the incident beam BO striking a south facing receiving plane.

OS = normal,

$\triangle ABC$ is parallel to the receiving plane,

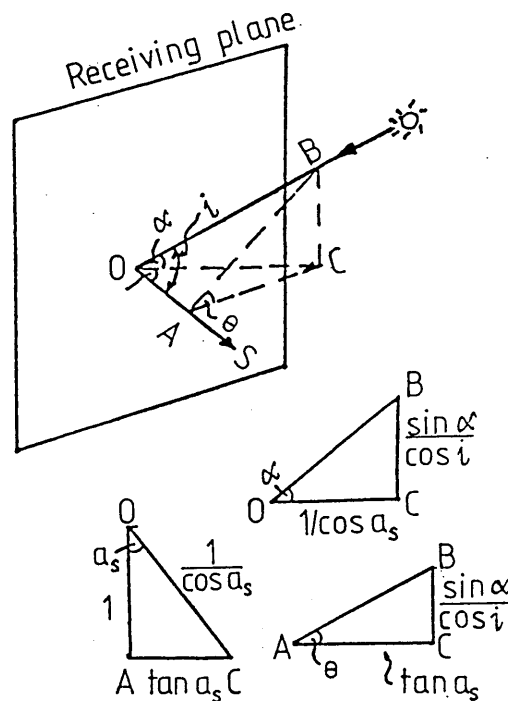
OA is of unit length,

i = incident angle,

r = refractive angle,

α_r = altitude of refracted ray,

a_{sr} = solar azimuth angle of refracted ray.



The angle of inclination of the incident plane, θ , will be the same as the angle of inclination, θ , of the refractive plane.

The angle θ is given by ΔABC :

$$\theta = \tan^{-1} \left(\frac{\sin \alpha}{\cos i \tan a_s} \right)$$

$$= \tan^{-1} \left(\frac{\tan \alpha}{\sin a_s} \right) \dots (1)$$

The refracted solar azimuth angle, a_{sr1} , from $\Delta O'FD$:

$$a_{sr} = \tan^{-1}(\tan r \cos \theta) \dots (2)$$

The refracted angle, α_r , from $\Delta O'OD$:-

$$\alpha_r = \sin^{-1} \left(\frac{\tan r \sin \theta}{1/\cos r} \right)$$

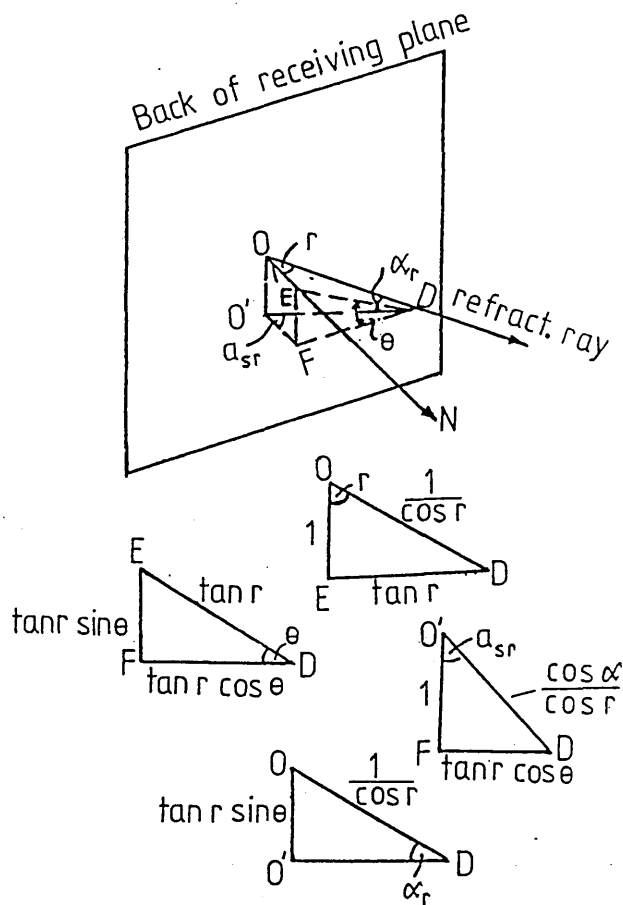
$$= \sin^{-1}(\sin r \sin \theta) \dots (3)$$

When the ray passes from glass to water it will be bent again, but it will still lie in the same incident plane inclined at the same angle θ to the horizontal.

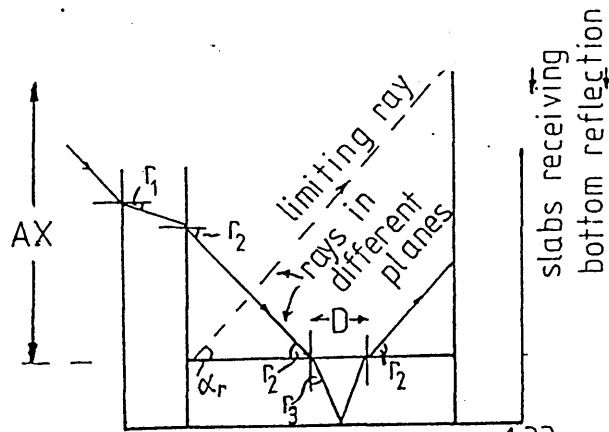
α_{r2} = second refracted angle
 a_{sr2} = second azimuth angle

$$\alpha_{r2} = \sin^{-1}(\sin r_2 \sin \theta) \dots (4)$$

$$a_{sr2} = \tan^{-1}(\tan r_2 \cos \theta) \dots (5)$$

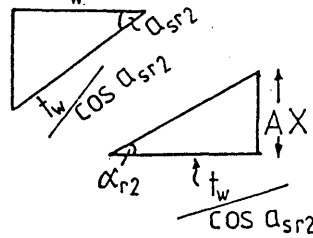


E2. Reflections at the Bottom Glass (Base).



$$\sin r_3 = \sin(90^\circ - \frac{r}{2}) \times \frac{1.33}{1.51}$$

- NB (i) the full line ray (in one plane) is different plane to limiting ray
(ii) both rays inclined to paper



The limiting ray to receive irradiation reflected from glass/air interface at the bottom = AX,

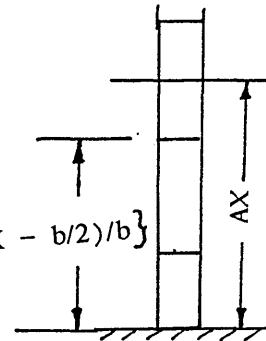
$$\text{where } AX = t_w \frac{\tan \alpha_{r2}}{\cos a_{sr2}}$$

An acceptance factor is defined AF(J), so that for slabs above the limiting ray (ht. > AX)

$$AF(J) = 0$$

For the slab hit by the limiting ray,

$$AF(J) = \frac{AX - \{b/2 + b \text{ INT}((AX - b/2)/b)\}}{b}$$



E3. Beam Irradiation.

E3.1 Beam Irradiation, Outer Glass.

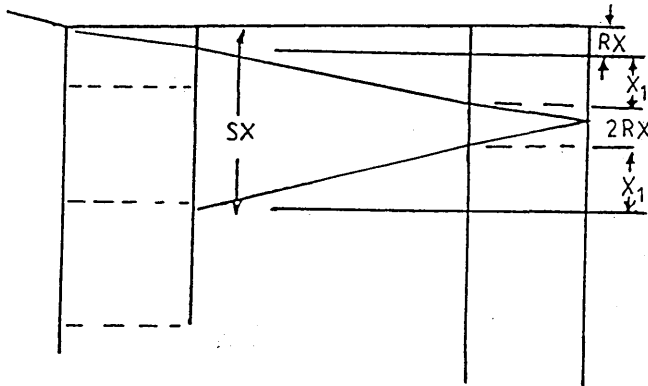
E3.1.1 The Shadow Factor, SF_+ .

$SF_1(J) = 0$ if the slab does not receive
any reflected irradiation.

$SF_1(J) = 1$ if all of the slab receives
reflected irradiation.

$SF_1(J) = 0 \rightarrow 1$ part of the slab receives
irradiation.

Shadow Factor.



RX = displacement of beam through glass.

$$RX = t_g \frac{\tan \alpha_{r1}}{\cos a_{sr1}} \quad (\text{see Appendix E1})$$

$$X1 = t_w \frac{\tan \alpha_{r2}}{\cos a_{sr2}}$$

$$Y = SX - \frac{1}{2}b$$

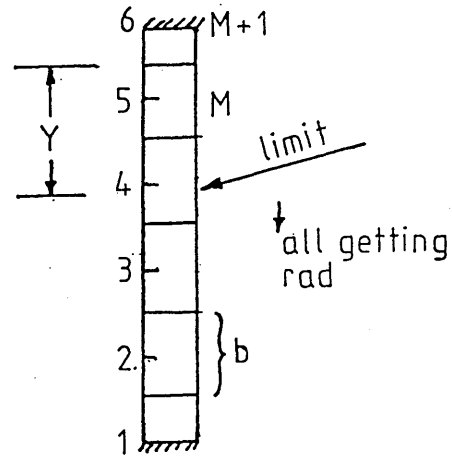
(i) slabs getting full
reflected irradiation
= $(M-1) - \text{INT}(Y/b)$

(ii) slab number getting
part irradiation
= $M - \text{INT}(Y/b)$

(iii) shadow factor of slab
hit by boundary ray
$$b - (Y - \text{INT}(Y/b)) \times b$$

= $\frac{\quad}{b}$

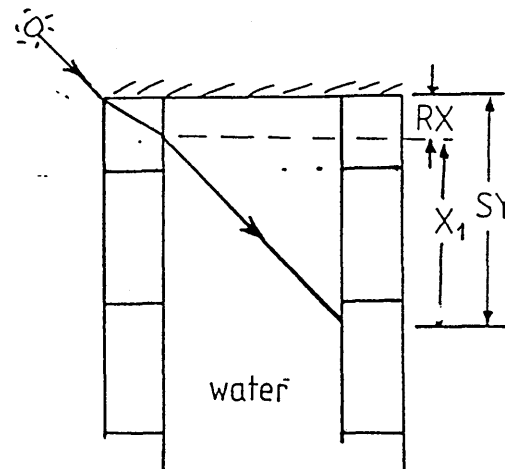
$$\therefore SF_1(J) = 1 - Y/b + \text{INT}(Y/b)$$



E3.2 Beam Irradiation, Inner Glass.

The inner glass slabs will in addition to receiving beam irradiation directly, have its upper slabs shaded by the lid and its lower slabs irradiated by reflected irradiation from above.

Note; For 5 vertical slabs of the MERA transwall only the top $1\frac{1}{2}$ slabs will be in shadow for latitude 56° .



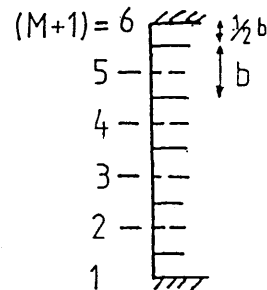
$$SY = RX + X_1$$

$$= t_g \frac{\tan \alpha_{r1}}{\cos a_{sr1}} + t_w \frac{\tan \alpha_{r2}}{\cos a_{sr2}}$$

where α_{r1} , a_{sr1} = refracted altitude
and azimuth angles
in glass.

α_{r2} , a_{sr2} = refracted altitude
and azimuth angles
in water

t_g , t_w = glass and water
thicknesses.



$$\text{If } SY < b/2, \text{ then } SF_2(M+1) = \frac{b/2 - SY}{b/2} = \frac{b - 2SY}{b}$$

$$\text{If } SY \geq b/2, \text{ then } SF_2(M+1) = 0$$

$$SF_2(M) = (1.5b - SY)/b$$

$$\text{Slabs 1-4 included } SF_2(J) = 1$$

Note: If substantially more than 5 slabs are used, say, 7 and over, then the last $2\frac{1}{2}$ slabs are liable to shading.

E4. Diffuse Irradiation.

E4.1 Summing Diffuse Irradiation over Waveband Interval.

This is achieved by fixing a ratio between beam and diffuse irradiation, call it the weighted waveband beam/diffuse ratio (W.W.B.D. for short).

$$IR_{\lambda} = \frac{I_{mb} \times {}_{\lambda}I_{fb}}{I_{md} \times {}_{\lambda}I_{fd}}$$

where I_{mb} = measured beam irradiation (m^2 normal).

$${}_{\lambda}I_{fb} = \text{fractional beam energy in waveband } \left(\sum_{0-\lambda}^{\infty} I_{fb} = 1 \right)$$

I_{md} = measured diffuse irradiation

$${}_{\lambda}I_{fd} = \text{fractional diffuse energy in waveband } \left(\sum_{0-\lambda}^{\infty} I_{fd} = 1 \right)$$

Then diffuse irradiation γ ∞

$$\text{striking vertical surface} \quad J = \left(\sum_{0-\lambda}^{\infty} I_{md} \times I_{fd\lambda} \right) \times ((1 + \cos \beta)/2)$$

$$+ \left\{ \left(\sum_{0-\lambda}^{\infty} I_{md} \times I_{fd\lambda} \right) + \left(\sum_{0-\lambda}^{\infty} I_{mb} \times I_{fb\lambda} \right) \right\} \rho/2 *$$

$$= \frac{1}{2} \left(\sum_{0-\lambda}^{\infty} I_{md} \times I_{fd\lambda} \right) \{1 + \cos \beta + (1 + IR_{\lambda})\rho\}$$

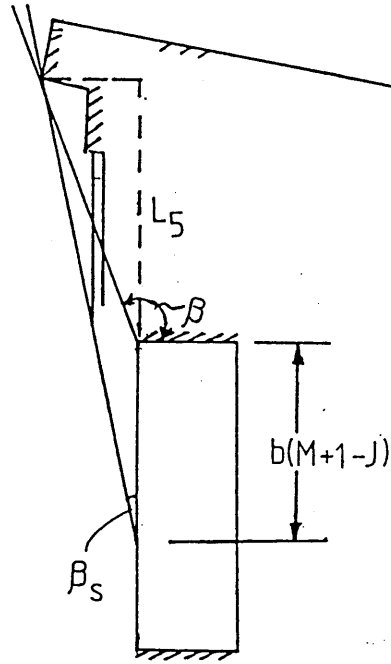
$$= \frac{1}{2} I_{md} (1 + \cos \beta + (1 + IR_{\lambda})\rho)$$

*Note: the ground reflected irradiation view factor will be $\frac{1}{2}$ not $((1 - \cos \beta)/2)$ because β is an artificial plane for sky irradiation only.

E4.2 Effective Sky Dome Angle, β .

The transwall will not see a complete quarter-sphere of the sky dome because of (slight) shading of the roof.

The maximum effective sky dome angle, β , measures 101° for the transwall under test.



The effect is : $((1 + \cos 101^\circ)/2) = 0.404$ instead of 0.5.
(assuming window is long in relation to length $L5$)

The effective sky dome angle, β_s , for a slab will be given by:

$$\beta_s = \tan^{-1} \left\{ \frac{L5 \tan (\beta - 90^\circ)}{[L5 + b(M+1-J)]} \right\}$$

The view factor for each slab, $VF_1(J)$, will be given by

$$VF_1(J) = \frac{1}{2} \{ 1 + \cos \beta_s + (1 + IR_\lambda) \rho \}$$

*

*

*

*

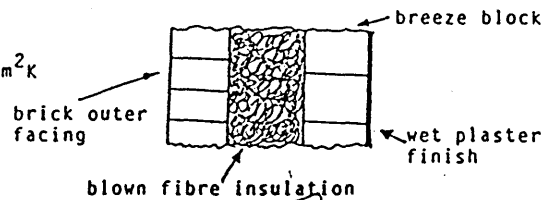
APPENDIX F

The Specification of the House, [Ham, 1988].

HOUSE CONSTRUCTION MATERIALS

(A) EXTERNAL WALLS

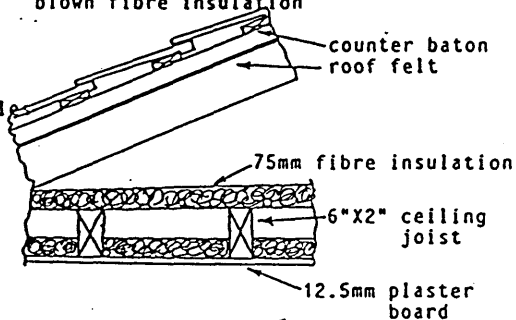
U-Value $0.29 \text{ W/m}^2\text{K}$



(B) ROOF AND CEILING

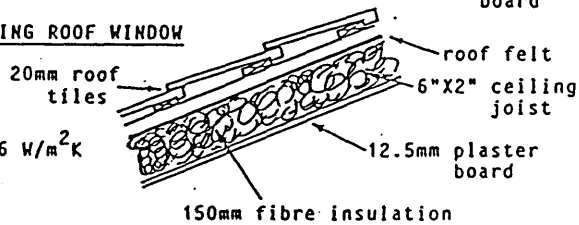
20mm roof tile

U-Value $0.23 \text{ W/m}^2\text{K}$



(C) ROOF SURROUNDING ROOF WINDOW

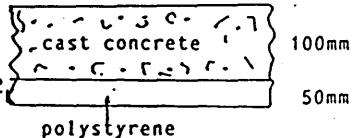
U-Value $0.26 \text{ W/m}^2\text{K}$



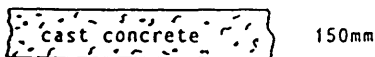
(D) FLOORS

GROUND FLOOR

U-Value $0.48 \text{ W/m}^2\text{K}$



FIRST FLOOR



(E) WINDOWS

WINDOW	KAPPAFLOAT		DOUBLE GLAZING	
	no curtains	curtains	curtains	no curtains
U-VALUE $\text{W/m}^2\text{K}$	1.6	1.2	2.5	3.3

APPENDIX G.

Spectral Extinction Coefficients of Lissamine Red 3GX dye and
of water with fractional energy for AM2 [Nisbet and Kwan, 1987].

Waveband μm	Ext.coef. m^{-1}		Fract. energy waveband
	Water	LR3GX	
.3 -.35	.04428	0	.006
.35-.4	.01773	$.176 \times 10^9$.022
.4 -.6	.01483	$.315 \times 10^9$.279
.6 -.75	.3895	$.010 \times 10^9$.215
.75-.9	2.583	0	.142
.9 -1.2	71.06	0	.146
1.2-2.1	7114	0	.150
2.1-4.1	2×10^6	0	.040

References

References

- 1 Duffie, J.A. & Beckman, W.A.
Solar Engineering of Thermal Processes.
John Wiley & Sons, New York, (1980).
- 2 Kreith, F. & Kreider, J.F.
Principles of Solar Engineering.
Hemisphere & McGraw-Hill, New York,
(1978).
- 3 Twidell, J. & Weir, T.
Renewable Energy Resources. E. & T.N.
Spoon, London, (1986).
- 4 Commission of the European Communities.
"Project Monitor", Issue No.4, (June
1987), pp.1-8.
- 5 Commission of the European Communities.
"Project Monitor", Issue No.36, (February
1989), pp.1-8.
- 6 Commission of the European Communities.
"Project Monitor", Issue No.42, (February
1989), pp.1-8.
- 7 Nisbet, S.K. & Kwan, C.M.
"The application of the Transwall to
Horticultural Glasshouses", Solar Energy,
Vol.39, No.6. Pergamon Press, U.S.A.
(1987), pp.473-482.
- 8 McDaniels, D.K.
The Sun. Our Future Energy Source. John
Wiley & Sons, New York, (1979).
- 9 Bainbridge, D.A.
"Water Wall Passive Systems for New and
Retrofit Construction". Proceedings of
the 3rd National Passive Solar Energy
Conference. San Jose, California, (1979),
pp.473-478.
- 10 Arasteh, D., Nall, D.H., Harrje, D.T. & Settles,
G.S.
"Performance of a Selective Surfaced Water
Wall Retrofit". Proceedings of the 5th
National Passive Solar Energy Conference.
American Section of I.S.E.S. Amherst,
Massachusetts, (October 22-26, 1980),
pp.287-291.

- 11 Monsen, W.A., Klein, S.A., Beckman, W.A. & Utzinger, D.M.
"The Resistance Network Design Method for Passive Solar Systems". Proceedings of the 5th National Passive Solar Conference. Amherst, MA., (October 22-26, 1980), pp.119-123.
- 12 Fraker, H. & Lindsay, L.
"Preliminary Performance Results for a Focusing Roof Aperture; Water Wall, and Direct Gain Combination Passive Solar Heating System - Geisel Residence". Proceedings of the 3rd National Passive Solar Energy Conference. San Jose, California, (1979), pp.659-665.
- 13 Van der Mersch, P.L., Burns, P.J. & Winn, C.B.
"Solar Radiation Analyses and Effects for Performance Prediction of Cylinder Water Walls". Proceedings of the 5th National Passive Solar Conference. Amherst, MA., (October 22-26, 1980), pp.224-228.
- 14 Maloney, T.
"Comparative Performance Data from Side by Side of Various Waterwalls in a Low Sun Climate". Proceedings of the 3rd National Passive Solar Energy Conference. San Jose, California, (1979), pp.479-480.
- 15 Cabelli, A.
"Storage Tanks - A Numerical Experiment". Solar Energy, Vol.19. Pergamon Press, U.K. (1979), pp.45-54.
- 16 Crowther, K.
"Cooling From An Evaporating Thermosiphoning Roof Pond". Proceedings of the 4th National Passive Solar Energy Conference, Kansas City, Missouri, pp.499-503. (1979)
- 17 Crowther, K. & Metzger, B.
"The Thermosiphoning Cool Pool. A Natural Cooling System". Proceedings of the 3rd National Passive Solar Energy Conference. San Jose, California, (1979), pp.448-451.
- 18 Mitchell Jr., C.P. & Hausen, D.G.
"A Comparison Study of Roof Pond Solar Energy Collectors". Proceedings of the 4th National Passive Solar Energy Conference, Kansas City, Missouri, pp.733-735. (1979).

- 19 Fate, R.E. & Mancini, T.R.
 "The Performance of a Roof-Pond Solar House". Proceedings of the 4th National Passive Solar Energy Conference, Kansas City, Missouri, pp.728-732. (1979).
- 20 Greveniotis, K.
 Absorption of Radiation in the Transwall. M.Sc. Thesis, Department of Mechanical Engineering, University of Glasgow, (1986).
- 21 Hull, J.R., McClelland, J.F., Hodges, L., Huang, J.L., Fuchs, R. & Block, D.A.
 "Effect of Design Parameter Changes on the Thermal Performance of a Transwall Passive Solar Heating System". Proceedings of the 5th National Passive Solar Conference. Amherst, MA., (October 22-26, 1980), pp.349-398.
- 22 Fuchs, R. & McClelland, J.F.
 "Passive Solar Heating of Buildings Using a Transwall Structure". Solar Energy, 23. (1979), pp.123-128.
- 23 McClelland, J.F. & Fuchs, R.
 "A Preliminary Study of Passive Solar Heating Performance and Visual Clarity for a Transwall Structure". Proceedings of 3rd National Passive Solar Conference. San Jose, CA. (1979), pp.107-113.
- 24 Hull, J.R., McClelland, J.F., Hodges, L., Fuchs, R. & Block, D.A.
 "Solar Heating Performance Results for a Transwall Test-Prototype System". Proceedings of the Annual Meeting of the American Section of I.S.E.S. Phoenix, Arizona, (1980), pp.923-927.
- 25 McClelland, J.F., Mercer, R.W., Hodges, L., Szydlowski, R.F., Sidles, P.H., Struss, R.G., Hull, J.R. & Block, D.A.
 "Transwall - A Modular Visually Transmitting Thermal Storage Wall - Status Report". Solar World Forum, Vol.3. Brighton, U.K. Pergamon Press, Oxford, (1981), pp.1881-1888.
- 26 Paparsenos, G.F.
 The Analysis of the Transwall Passive Solar System. Ph.D. Thesis. Department of Mechanical Engineering, University of Glasgow, (1983).

- 27 Sodha, M.S., Bansal, N.K. & Sant, Ram.
"Periodic Analysis of a Transwall: A Passive Heating Concept". Applied Energy, 14. (1983), pp.33-48.
- 28 Commission of the European Communities.
"Project Monitor". Issue No.9. (December 1987), pp.1-8.
- 29 Holman, J.P.
Heat Transfer. McGraw-Hill, New York, (1981).
- 30 MacGregor, R.K. & Emery, A.F.
"Free Convection Through Vertical Plane Layers - Moderate and High Prandtl Number Fluids". Journal of Heat Transfer, Transactions of the ASME. New York, (August 1969), pp.391-403.
- 31 Newell, M.E. & Schmidt, F.W.
"Heat Transfer by Laminar Natural Convection within Rectangular Enclosures". Journal of Heat Transfer, Trans. of ASME. New York. (February 1970), pp.159-168.
- 32 White, F.M.
Heat Transfer, Addison-Wesley, Reading, MA. (1984).
- 33 Dropkin, D. & Somerscales, E.
"Heat Transfer by Natural Convection in Liquids Confined by Two Parallel Plates which are Inclined at Various Angles with Respect to the Horizontal". Journal of Heat Transfer, Trans. of the ASME. New York. (February 1965), pp.77-84.
- 34 Emery, A. & Chu, N.C.
"Heat Transfer Across Vertical Layers". Journal of Heat Transfer, Trans. ASME. NY. (February 1965), pp.110-116
- 35 Lankhorst, A.M., Henkes, R.A.W.M. & Hoogendoorn, C.J.
"Natural Convection in Cavities at High Rayleigh Numbers, Computation and Validation". 2nd U.K. Conference, Heat Transfer. University of Strathclyde, Glasgow, (September 1988), pp.353-364.

- 36 Webb, B.W. & Viskanta, R.
"Radiation - Induced Buoyancy - Driven Flow in Rectangular Enclosures: Experiment and Analysis". Journal Heat Transfer. Trans. ASME. New York. (May 1987), pp.427-433.
- 37 Patankar, S.V.
Numerical Heat Transfer and Fluid Flow. McGraw-Hill, New York, (1980).
- 38 Lauriat, G.
"Combined Radiation - Convection in Gray Fluids Enclosed in Vertical Cavities". Journal Heat Transfer. Trans. ASME. New York. (November 1982), pp.609-615.
- 39 Özisik, M.N.
Heat Transfer, A Basic Approach. McGraw-Hill, St.Louis, MO. (1985).
- 40 Croft, D.R. & Lilley, D.G.
Heat Transfer Calculations Using Finite Difference Equations. Applied Science, London, (1977).
- 41 Bayley, T.F., Owen, J.M. & Turner, A.B.
Heat Transfer. Nelson, London, (1972).
- 42 Rohsenow, W.M., Hartnett, J.P. & Ganic, E.N.
Handbook of Heat Transfer Fundamentals. McGraw-Hill, New York, (1985).
- 43 Yass, K. & Curtis, H.B.
"Low-Cost, Air Mass 2 Solar Simulator". NASA Report N74-27719, NASA Research, Lewis Centre, Cleveland, OH. (June 1974), pp.1-23.
- 44 Li, S.C.
Honours Project Report. "Solar Roof Pond". Department of Mechanical Engineering, University of Glasgow. (1987).
- 45 Brandemeuhl, M.J. & Beckman, W.A.
"Transmissions of Diffuse Radiation Through CPC and Flat Plate Collector Glazings". Solar Energy, 24. (1980), pp.511-513.
- 46 Ham, I.M.
Honours Project Report. "An Evaluation of a Transwall for Domestic Heating". Department of Mechanical Engineering, University of Glasgow. (1988).

- 47 Francis, L.
Honours Project Report. "Design of a Transwall System". Department of Mechanical Engineering, University of Glasgow. (1987).
- 48 Coral Reef Aquaria
Paisley Road West, Glasgow.
- 49 Chartered Institution of Building Service Engineers.
CIBSE Guide, Vol.A, Design Data, CIBSE, London, (1986).
- 50 Akbarzadeh, A., Charters, W.W.S. & Lesslie, D.A.
"Thermocirculation Characteristics of a Trombe Wall Passive Test Cell". Solar Energy, Vol.28, No.6. (December 1981), pp.461-468.
- 51 Snider, D.M. & Viskanta, R.
"Radiation Induced Thermal Stratification in Surface Layers of Stagnant Water". Journal of Heat Transfer. Trans. ASME, New York. (February 1975), pp.35-40.
- 52 Purslow, B., Quarini, G., Lovegrove, P. & Cowan, G.
"Natural Convection Experiment in a Large Water Filled Cavity". 2nd U.K. National Conference on Heat Transfer, University of Strathclyde, Glasgow, (September 1988), pp.109-102.
- 53 Kutateladze, S.S., Ivakin, V.P., Kirdyashkin, A.G. & Kekalov, A.N.
:Thermal Free Convection in a Liquid in a Vertical Slot Under Turbulent Flow Conditions". Heat Transfer - Soviet Research, Vol.10, No.5, (September/October 1978), pp.118-125.
- 54 Bergholz, R.F.
"Instability of Steady Natural Convection in a Vertical Fluid Layer". Journal of Fluid Mechanics, Vol.84, Part 4, U.K. (1978), pp.743-768.

